STRUCTURAL BEHAVIOUR OF TWINWALLS

by

Jaylina Rana

Thesis submitted to the Department of Civil, Environmental & Geomatic Engineering in partial fulfilment of the requirements for the degree of

EngD Urban Sustainability and Resilience

Declaration

‘I, **Jaylina Rana**, confirm that the work presented in this thesis is my own. Where information has been derived from other sources, I confirm that this has been indicated in the thesis.'

Signature: ……..

Abstract

The construction industry is relentlessly aiming to achieve inventive methods for more economic and sustainable construction. This quest has resulted in the development of hybrid concrete construction (HCC) which combines the benefits of in-situ and precast concrete. Twinwall panels are a relatively new form of HCC consisting of two reinforced precast concrete biscuits which are connected by shear connectors in the form of 3-dimensional triangular steel lattices, partially embedded in the inner faces of the biscuits. The void between the biscuits is then filled with in-situ concrete. Thus, the overall aim of this project was to develop a deeper understanding of the structural behaviour of twinwall panels.

Push-out tests were performed on twinwall specimens to investigate the effect of (1) surface roughness (2) strength of concrete and (3) embedment depth of connectors on interface shear strength. It was found that the interface shear strength increases with increasing surface roughness and the strength of the concrete used in the outer biscuits but was unaffected by the strength of the concrete used in the core. Shear strength also initially increased with increasing embedment depth of connectors but then levelled off. The results further showed that the provisions of clause 6.2.5 of Eurocode 2 can be used to make conservative estimates of the interface shear strength of twinwall elements.

The twinwall panels were also subjected to four point bending flexural tests. Results confirmed that using lattice shear connectors, increasing the depth of the lattice shear connectors and introducing a concrete core increased the flexural failure load, stiffness and degree of composite action of the twinwall test specimens. All twinwall test specimens also behaved in a partially composite manner.

A Finite Element (FE) model was also developed using the ABAQUS software. Comparison of the experimental and FE results confirmed the FE model developed can be used to simulate the behaviour of twinwall panels. As the diameter of the dowel bar increased, the failure load, stiffness and degree composite action increased. The FE results suggest that single trusses can be used instead of double trusses in twinwalls. The failure load and stiffness increased as the overall thickness of the specimens increased but the degree of composite action decreased with increasing thickness.

Acknowledgement

First and foremost, I would like to thank Dr Chankya Arya for his guidance, support and patience throughout my research. Without his insight and direction, this research would not have been possible. My gratitude also goes to Dr John Stehle from Laing O'Rourke for providing me with the platform to pursue my research on concrete twinwalls. I am also grateful to Warren Gaynor, the technician in the Concrete Laboratory of University College London (UCL) who assisted me immensely during my experimental work. Moreover, I am thankful to the Centre for Urban Sustainability and Resilience (UCL), Laing O'Rourke and the Engineering Council UK to give me the opportunity to carry out my Engineering Doctorate degree.

My deepest gratitude goes to my husband, Anil, who has been my rock for all these years. His support and encouragement have always inspired me to challenge myself during my research. I also thank to my mum, dad, sister Shalina, Amar, Aayush and Rohan immensely for their continuous belief in my aspirations. Last but not least, a special mention goes to my beautiful baby daughter, Alinah, for being a wonderful blessing in our lives.

Table of Contents

List of Figures

List of Tables

List of Equations

Chapter 1

Introduction

1.1 Background

The continuous attempt of the construction industry to achieve inventive methods of decreasing the cost and time of construction projects while providing competitive, buildable and high quality that address client demand for better value construction, has led to the development of precast concrete methods which combine the various advantages of concrete (flexibility, cost-effectiveness, durability and sustainability) with the benefits of a controlled off-site production environment (excellent finishes and consistency).

In fact, the UK precast concrete industry is estimated to produce over 38 million tonnes of products annually, worth in excess of £2.5 billion and provides direct employment to over 22,000 people in around 800 precast factories located around the UK (British Precast, 2015). However, the inherent limitations precast construction such as lack of flexibility and design restrictions have resulted in the development of hybrid concrete

systems which combine the benefits in economy and high quality finish of precast concrete with the added flexibility and inherent robustness of in-situ concrete. Hybrid concrete construction meets the industry requirements for increased off-site manufacture, reduced construction costs and time, safer and faster construction and consistent performance (Goodchild and Glass, 2004).

Twinwalls or twinwall panels are a relatively new form of Hybrid Concrete Construction (HCC) which combines the advantages of precast and in-situ concrete. A typical twinwall consists of two precast concrete biscuits, reinforced with longitudinal and transverse reinforcement, which are connected by shear connectors in the form of 3-dimensional triangular steel lattices, partially embedded in the inner faces of the biscuits. The precast twinwall panel is fabricated off-site and the void between the biscuits is filled with in-situ concrete on site as shown in Figure 1.1.

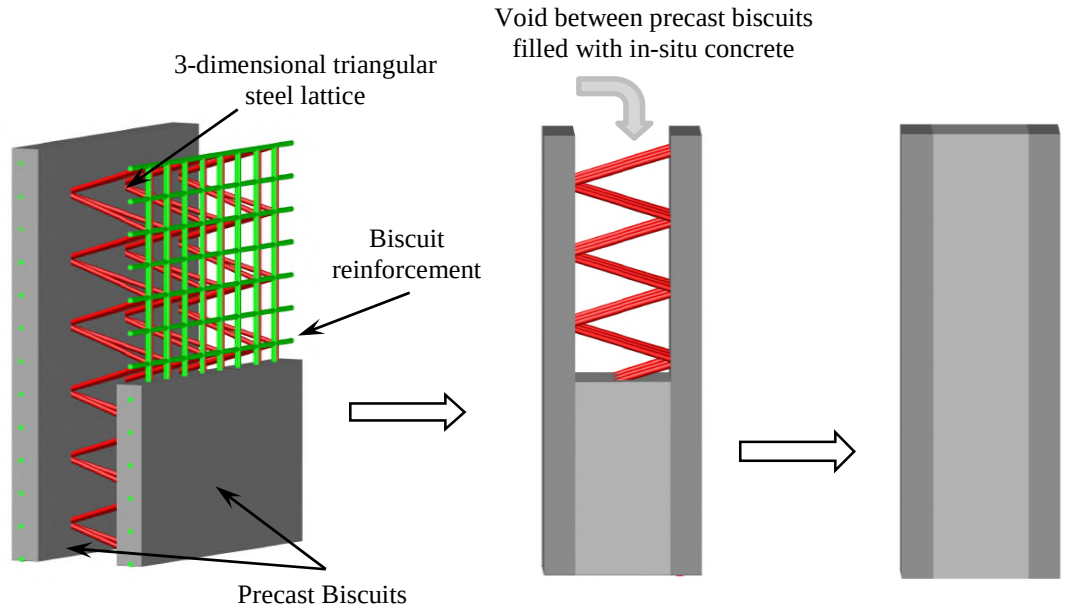

a) Precast twinwall fabricated off-site **b) Void filled with in-situ concrete to form concrete core** **c) Typical twinwall after core is filled**

Figure 1.1- Details of Typical Twinwall Panel

The optimum use of the precast biscuits and the in-situ core in twinwalls leads to significant cost savings, increased speed of construction, greater buildability and improved health and safety. Even though the cost of the hybrid twinwalls is generally comparable that of similar precast concrete units (Laing O'Rourke, 2010), major buildability savings are achieved as a result of reduced erection times and less labour-intensive construction on site.

Twinwalls are most beneficial when it comes to speed. A study by the Concrete Centre (2006) concluded that the lead-in time for a typical hybrid twinwall is 6 weeks with the construction process taking slightly above one week per 1000 m^2 per crane. Furthermore, off-site fabrication of the precast components of twinwalls decreases the duration of critical operations on site which may have otherwise been restricted by site progress or conditions. Twinwalls also have health and safety benefits since the majority of the twinwall components is fabricated in the controlled environment of a factory thereby reducing the number of potential accidents on site. In addition, twinwalls offer durability benefits by virtue of their in-situ concrete core which provides resistance to water penetration resulting in low maintenance costs.

Similar to other structural systems, twinwalls also have a few disadvantages. Propping of the precast biscuits is required prior to the pouring the in-situ concrete but is removed once the in-situ concrete core gains sufficient strength. Typical twinwall panels are also usually restricted to a maximum height of 3.6 m and the positioning and details of the construction joints require careful design in order to prevent adverse effects on the structural efficiency and serviceability performance. Continuity is usually provided at the horizontal and vertical joints using one or two layers of splice reinforcement.

1.2 Research Significance

Twinwalls have traditionally been used as compression elements including shear walls, bearing/non-bearing walls and cladding panels. Concrete manufacturers are now seeking to extend the range of applications of the twinwalls to other forms of structure, in particular the walls of water retaining structures (e.g. water tanks). In this situation the walls act as cantilevers and are subject to combined bending and shear with maximum bending moments and shear forces occurring at the base of the walls.

For design purposes, the flexural strength of the twinwalls is based on the strength of the outer biscuits which is a function of the strength of the concrete and the longitudinal and transverse reinforcement provided. This is a sensible assumption to make since the precast biscuits behave as cantilever walls subjected to bending forces resulting in one portion of the wall being in compression and the other in tension. The compressive stresses are resisted by the concrete and the tensile stresses are resisted by the longitudinal reinforcement provided in the biscuits. The transverse reinforcement is provided to prevent splitting cracks from developing in the concrete biscuits. However, in order for adequate flexural strength to be provided in twinwall panels, both precast concrete biscuits must act together so that the forces applied can be transferred from one biscuit to the other. Thus, the degree of composite action taking place in twinwalls is fundamental to their structural behaviour. It is therefore important to determine the effect of various parameters on the degree of composite action in twinwalls.

The shear strength is based on the strength of the lattice shear connectors which resist the applied shear forces by developing longitudinal shear forces across the biscuit/core

interface. This is the area where most of the ambiguity lies. Firstly, the lattice shear connectors used in twinwalls are not conventional in comparison with more traditional studs or ribbed shear connectors. The role of the lattice shear connector and its interaction with the non-linear concrete is therefore unclear. Additionally, the contribution of the in-situ concrete core to the overall strength of the twinwall and the structural actions taking place at the precast/in-situ (biscuit/core) interfaces are not well understood.

There is therefore a need to determine whether the actual structural performance of twinwall panels corresponds to theoretical predictions used for design purposes. The current level of understanding and prediction of structural behaviour of twinwall panels are very limited. This is due to the complex interactions between the non-linear materials in twinwall panels, the difficulty in the fabrication of small scaled and large scaled specimens for testing as well as the reluctance of manufacturers to share information with competitors.

Additionally, there is no documented or published research on the behaviour of twinwall panels. Thus, this research is unique in its own right and of immense value in providing a better understanding of structural actions taking place in twinwall panels.

1.3 Aim and Objectives

In view of the above, the main aim of this research is ***to provide an understanding of the structural behaviour of twinwalls***.

The key objectives are as follows:

- To develop a deeper understanding of the structural behaviour of twinwalls.
- To investigate the effect of different variables on the interface shear behaviour of twinwalls
- To investigate the effect of different variables on the flexural behaviour twinwalls.
- To develop a Finite Element model to simulate the behaviour of twinwalls and to predict the effect of different variables on their behaviour.
- To provide recommendations for the design of twinwalls.

1.4 Thesis Outline

The outline of this thesis is summarised below:

Chapter 2 provides a critical analysis of a wide range of published material relevant to this study. As discussed, no documented research was found on twinwalls. Therefore, literature related to sandwich panels (PCSPs) which are similar to twinwalls were reviewed. The background, variations, structural behaviour and mechanisms as well as testing methods are discussed.

Chapter 3 describes the experimental (laboratory) push-out tests carried out on twinwall test specimens. The effects of specimen size (size effects), base restraints, surface roughness, concrete strength, embedment depth and dowel bar diameter on the interface shear strength of twinwalls were investigated in Phase I.

Chapter 4 presents and discusses the findings from Phase I of the experimental work.

Chapter 5 describes the experimental flexural tests carried out on twinwall test specimens. The roles of the concrete biscuits, the concrete core and the lattice shear connectors were investigated in Phase II.

Chapter 6 presents and discusses the findings from Phase II of the experimental work.

Chapter 7 presents the Finite Element (FE) analysis work carried out to further investigate the structural behaviour of twinwalls. The FE model was first validated with

experimental results from the flexural tests in Chapters 5-6. The effect of varying the dowel bar diameter, the type of connector and the overall thickness of actual sized twinwall specimens was investigated. This chapter also presents and discusses the results from the FE analysis.

Chapter 8 summarises the findings from the experimental, theoretical and numerical (FE) analyses and provides recommendations for the design of twinwalls. Recommendations for future work to be carried out on the structural behaviour of twinwall panels are also made in this chapter.

Chapter 2

Literature Review

2.1 Introduction

Twinwalls are a variation of the well-established form of the concrete construction component known as Precast Concrete Sandwich Panels (PCSP). PCSPs consist of two reinforced concrete biscuits (wythes) which are separated by an insulation core. The concrete biscuits are usually connected through the insulation core by shear connectors as shown in Figure 2.1.

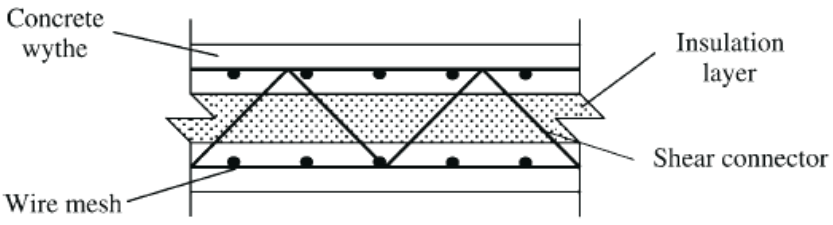

Figure 2.1- Components of typical PCSP

The thickness of each concrete biscuit is dependent on its structural function, concrete cover, anchorage of connectors, stripping and finish. Although over the years,

recommendations have been made with respect to the thickness of the concrete biscuits, PCSP manufacturers often determine the appropriate thicknesses for their own sandwich panel product.

Concrete biscuits can be grouped as structural and non-structural. A biscuit is considered structural if it provides a significant contribution to the load resistance of the panel. In fully or partially composite panels, both concrete biscuits are structural. In non-composite panels, either one of the biscuits is structural and the other non-structural; or both wythes are structural and independently resist the applied loads in proportion to their relative stiffness. On the other hand, a non-structural biscuit has negligible contribution to the structural strength of the panel. Hence, such biscuits are often used for cladding and aesthetical purposes as well as to encase the insulation provided between the biscuits.

PCSPs have been favoured for use as wall panels over other construction materials due to their superior thermal and structural efficiency. The thermal efficiency is provided by the properties of the insulation material while the structural efficiency is dependent on the interaction of the concrete biscuits and the shear connectors.

PCSPs are a perfect example of precast concrete construction where the structural component is manufactured offsite. However, in twinwalls, the concrete biscuits connected by the shear connectors are manufactured off-site and the void between the concrete biscuits is filled with in-situ concrete on site. In fact, twinwalls can be categorised as a hybrid concrete construction component. Hybrid Concrete Construction (HCC) is a method of construction which integrates precast and cast in-situ concrete to

take best advantage of their different inherent qualities. Hence, the accuracy, speed and high quality finish of precast components can be combined with the flexibility and economy of in-situ concrete to produce an aesthetically pleasing and effective form of structure.

Although the PCI committee was unable to determine the first use of precast concrete sandwich panels it is generally accepted that this type of insulated twinwall panel has been in use for more than 40 years in North America (Benayoune, 2007). Variations of the PCSPs have been developed and used in many countries across the world, including America, Germany and the UAE. Initially, PCSPs were designed to act non-compositely with a thicker structural concrete biscuit, a non-structural concrete biscuit, an insulation core and shear connectors. During the past few decades, extensive research has been carried out to optimise the components of PCSPs in order to increase the degree of composite action taking place.

2.1.1 Variations of Sandwich Panels

Various forms of sandwich panels have been investigated previously with different combinations of biscuit, core and shear connector properties (materials, types, orientation etc). The biscuits or wythes used in sandwich panels are made up of thin but high strength material in order to resist the applied loads. This can partly be attributed to the use of less dense materials in the core which are designed as non-structural components. A wide range of materials has therefore been used to form the biscuits, core and shear connectors. The combination of the varying properties of the sandwich

panel component therefore results in the optimum design of the sandwich panels for particular applications.

Paik et al. (1999) carried out an experimental and theoretical investigation of the strength of sandwich panels formed with aluminium biscuits and an aluminium honeycomb core. The study showed that the strength of the aluminium honeycomb panel was satisfactory and ideal for use in weight significant structures to provide lighter weight components in comparison to other more traditional materials. Additionally, the weight saving advantage of this panel resulted in lower fabrication costs.

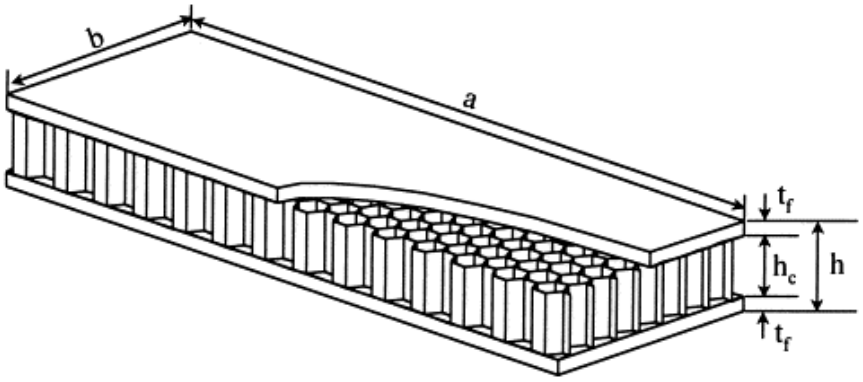

Figure 2.2- Honeycomb-cored sandwich panel (Paik et al, 1999)

Stoll et al. (2004) investigated the effect of using different core filling such as Fibre reinforced composites (FRC), PVC foam and balsa wood on the properties of sandwich panels. Results confirmed that FRC increased the shear and compressive strength of sandwich panels. The PVC core improved the density of the panels and the balsa wood core had very good compressive strengths.

Lee et al. (2006) investigated the performance of expanded polystyrene (EPS) panels with cementitious coatings. The study showed that the EPS sandwich panels were structurally satisfactory when subjected to wind, snow and seismic loads. In addition, results confirmed that the panels were structurally efficient, durable and fire resistant. Hence, it was recommended that EPS sandwich panels could be used for the construction affordable houses in developing countries.

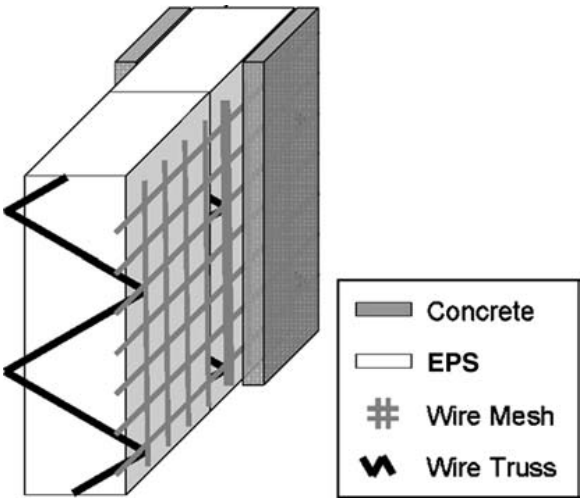

Figure 2.3 - EPS sandwich panel (Lee et al, 2006)

Naito et al (2009) evaluated the performance of shear ties to understand the failure modes of sandwich wall panels conducted on the performance of shear ties. Direct shear experiments were conducted on a variety of commercially-available connectors from the United States as shown in Figure 2.4. These included carbon steel, stainless steel, galvanized carbon steel, carbon fibre reinforced polymers (CFRP), glass fibre reinforced polymer (GFRP), and basalt fibre reinforced polymer (BFRP).

The experimental results indicate that shear ties used in sandwich wall panels had considerable variations in strength, stiffness, and deformability. The FRP truss type connections exhibited an elastic brittle response while the steel wire truss exhibited an elastic plastic behaviour. The steel M-clip (I) and the C-clip (H) with adequate embedment exhibited elastic-plastic behaviour at low shear deformations. Thus, results confirmed that different types of connectors resulted in variations in the structural behaviour of the panels.

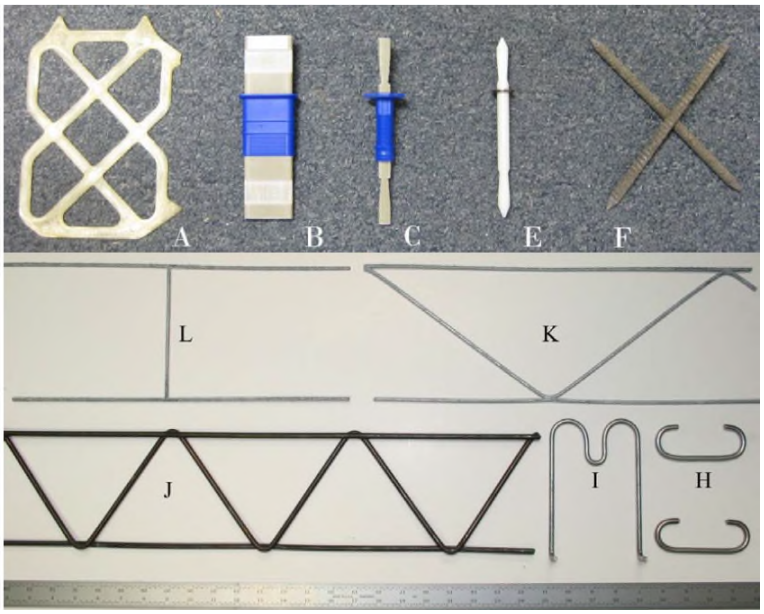

Figure 2.4 – Types of shear ties (Naito et al, 2009)

In light of the above, several other investigations have been carried out by researchers on the mechanical properties of sandwich panels comprising different materials and types of connectors. For instance, Case and Lakes (1997) investigated the performance of glass fibre honeycomb core sandwich panels and Scudamore et al (2002) carried out tests on sandwich panels consisting of foam, balsa wood and honeycomb cores. Hence, a good knowledge of the structural actions taking place in sandwich panels is required

in order to understand the complex interactions occurring between the various components of sandwich panels.

2.2 Structural Behaviour of Sandwich Panels

2.2.1 Structural Behaviour of Twinwalls

As discussed previously, twinwalls are a variation of traditional PCSPs. As well as their traditional use as load-bearing or non load-bearing walls, twinwalls can also be used as retaining walls for water retaining structures. In such applications, twinwalls behave as cantilever walls and are subjected to combined bending and shear with maximum bending moment and shear forces occurring at the base of the walls. For design purposes, the flexural strength of the twinwalls is based on the strength of the outer biscuits which is a function of the strength of the concrete and the longitudinal and transverse reinforcement provided. The shear strength is based on the strength of the lattice shear connectors which resist the applied shear forces by developing longitudinal shear forces across the biscuit/core interface as shown in Figure 2.5.

Before slip occurs at the biscuit/core interface, the longitudinal shear forces are resisted by the diagonal bars of the lattice girder which develop compressive and tensile forces. Hence, only half of the bars of the lattice girder are in tension and act as structural ties to prevent any cracks from forming in the concrete. The bars also cause friction to occur at the interface between the core and the biscuit. As the applied forces increase, slip occurs at the core/biscuit interface. After slip occurs, dowel action occurs in the lattice

bars which develop tensile forces. Additionally, the lattice bars which were initially in compression develop tensile forces across the core/biscuit interface.

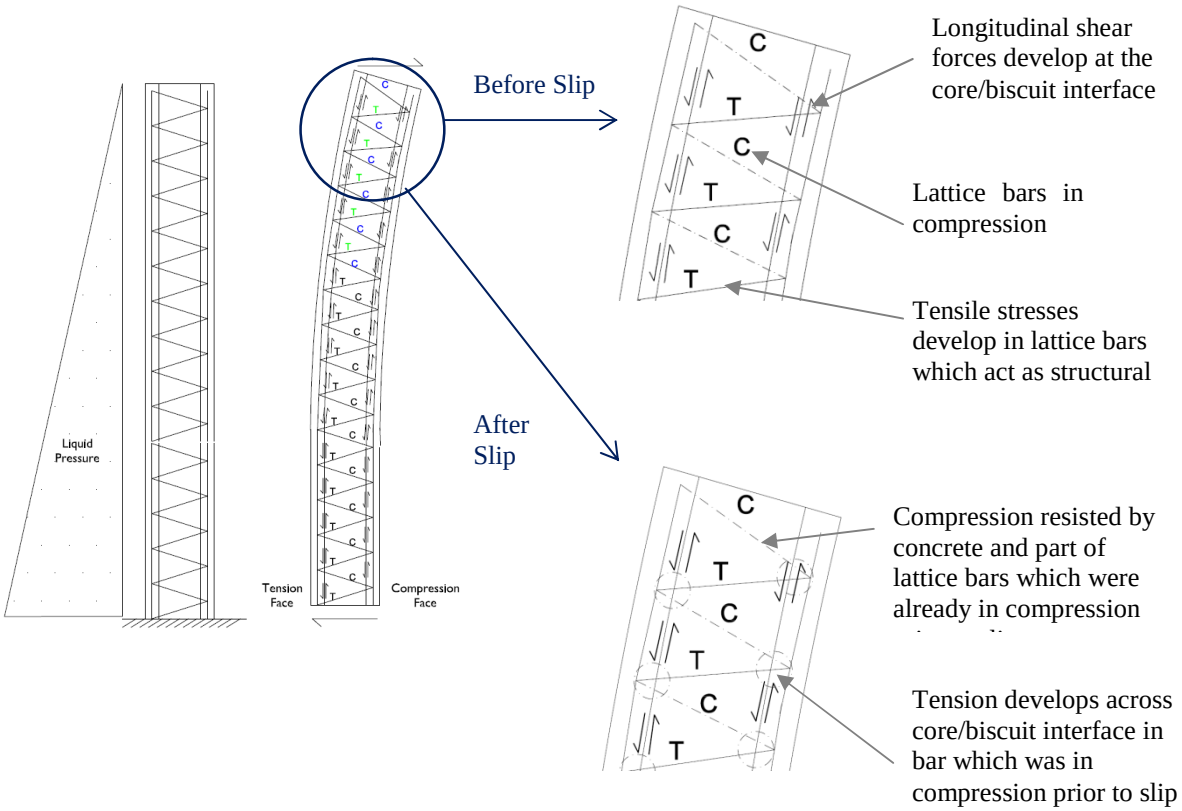

Figure 2.5 - Forces developed in twinwall in water tank application

Thus, the structural actions taking place in the lattice girder under combined shear and bending is rather complex and not well understood. This can be attributed to the fact that twinwalls are a fairly new hybrid concrete construction component but can also be partly due to the high cost of full-scale specimens and the reluctance of manufacturers to share propriety information with their competitors. Hence, an understanding of the basic principles of longitudinal shear and flexural behaviour of sandwich walls can provide valuable information on the structural performance of twinwalls in water tank applications

2.2.2 Longitudinal Shear Behaviour

2.2.2.1 Overview of Longitudinal Shear

In twinwalls, the outer concrete biscuits are cast off-site (precast). The in-situ concrete is then poured to fill the void between the concrete biscuits on-site. As the in-situ concrete cures, a bond if formed between the precast and cast-in-place concrete thereby enabling the twinwall composite panel to behave as a continuous and efficient monolithic member.

The interface bond between the two concrete layers is fundamental in ensuring that the composite sections behave as purely monolithic. It the interface bond is strong, the composite panel will deform as a single monolithic section when subjected to loading. The fully bonded interface will allow for forces to be transferred across the concrete interface. However, if the interface bond is weak, the concrete interfaces begin to slip relative to each other resulting in the concrete sections to behave as two separate members under loading. This is shown in Figure 2.6.

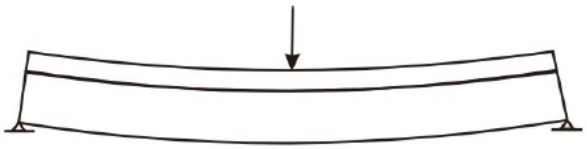

(a) Fully Composite section

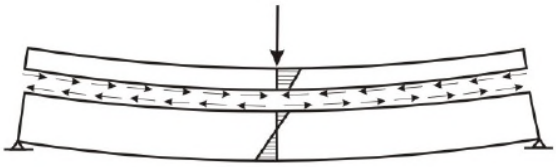

(b) Shear transfer of Composite Section

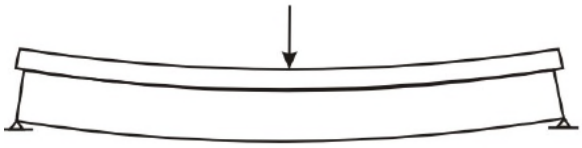

(c) Horizontal slip occurs at interface

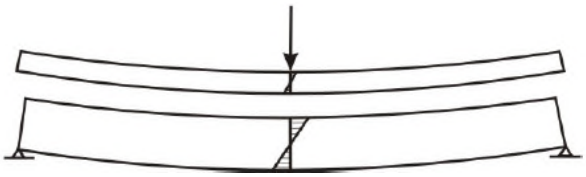

Shear transfer of Non-composite section

Figure 2.6 – Overview of interface shear transfer at concrete interfaces

It must therefore be ensured that the concrete sections transfer all the applied unbalanced forces, without any slip taking place at the interface. When load is applied to composite sections such as twinwall panels, the longitudinal shear forces are transferred across the interface by virtue of the cohesion or interface bond and aggregate interlock of the two concrete layers. If the system loading exceeds the horizontal shear stress capacity, the bond is compromised and the elements will begin to slide relative to one another. Horizontal shear connectors extending across the interface are then engaged to resist further slip from occurring at the concrete interfaces. Such shear connectors are typically an extension of the shear reinforcement of the composite sections and are usually in the form of shear studs, dowel bars, lattice girders etc.

2.2.2.2 Longitudinal Shear in Sandwich Panels

The type, configuration and spacing of shear connectors are highly dependent on the final degree of composite action desired (Bush, 1994). Other factors include the magnitude of the applied load, the length of the biscuits and the nature of the shear connector used. The structural performance (in terms of degree of composite action taking place in sandwich panels) is also significantly dependent on the strength and stiffness of the shear connectors used. Hence, a sandwich panel can exhibit fully composite, non-composite or partially composite behaviour based on the degree of composite action taking place. The definition of composite action differs between that defined under service loads and that defined at ultimate load.

1. Under service load conditions, the degree of composite action is defined as:

- A sandwich panel is considered fully composite if its biscuits are connected in such a way that they resist the applied load as an integrated structure. The connectors must transfer all of the required longitudinal shear force to produce bending stress distribution over the cross section of the panel.

- A sandwich panel is considered partially composite if its connectors can transfer between 0-100% of the longitudinal shear required for a fully composite panel.

- A sandwich is considered non-composite if its concrete biscuits are connected with elements (connectors) that have no capacity for longitudinal shear transfer. In this

case, if the two concrete biscuits are of equal stiffness and reinforcement, each biscuit resists 50 % of the load.

2. At the ultimate strength, the composite action is defined as:

- A sandwich is considered fully composite at ultimate strength if it fails with an identical failure mode as do solid reinforced concrete beams, i.e. if the failure occurs by either concrete crushing at the exterior compression surface of the panel or by yielding of the steel reinforcement of the other biscuit in tension. Either of these modes of failure occurs only if the connecting system has equal or greater strength in shear than is required to transfer the maximum forces occurring in the biscuits.

- A sandwich panel is considered partially composite at ultimate strength if the connectors possess shear strength less than is required for fully composite action. In this case, the connectors fail before concrete crushing at the compression surface of the panel and before tensile yielding of the reinforcement of the other biscuit.

- A sandwich panel is considered non-composite at ultimate strength if the connectors can transfer no shear between the concrete biscuit.

Hence, for composite panels, the strains remain linear across the depth of the panel thickness; for non-composite panels, the strain variation is completely separate for each biscuit; and for partially composite panels, the strain distribution of the partially composite behaviour as an intermediate between the fully composite and non-composite limits as shown in Figure 2.7.

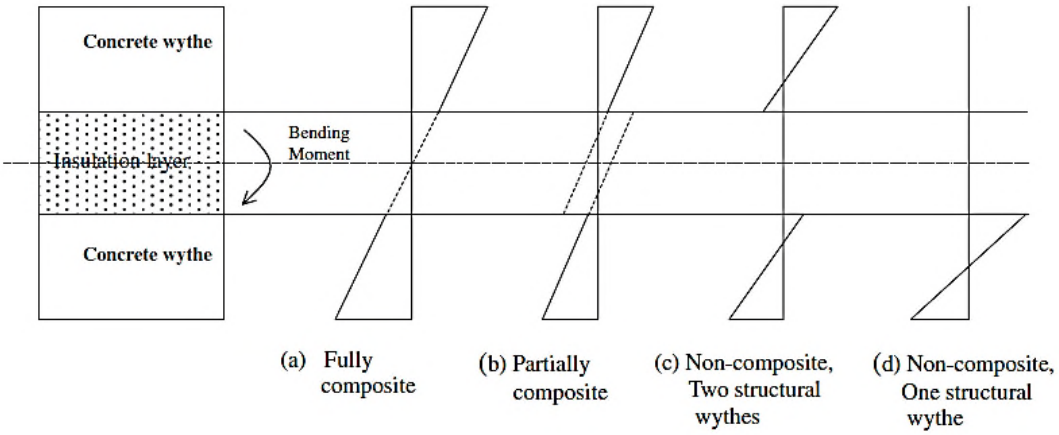

Figure 2.7- Strain distribution in PCSPs under flexure (Benayoune et al, 2008)

Thus, variation in the properties of the components of sandwich panels such as twinwalls results in differences in their structural behaviour

2.2.2.3 Mechanism of Longitudinal Shear

The load transfer mechanism of shear forces between two concrete layers is usually described in terms of the shear-friction theory. According to this theory, interface shear is depended on (1) the degree of interaction between shear friction parameters across the sliding or shear plane, e.g. widening across the sliding plane and/or slip along the sliding plane; and (2) the normal stress to the sliding plane. The main parameters influencing the interface shear are (a) the cohesion or adhesion between particles at the concrete interface, (b) the friction occurring at the concrete interface and (c) the shear reinforcement crossing the interface.

The shear-friction theory is used to predict the behaviour of concrete-to-concrete interfaces subjected to longitudinal shear stresses. Developed in the 1960s, this theory has been adopted by a variety of design codes including CEB-FIP Model Code 1990

(1990), BS 8110- (1997), Eurocode 2 (2004) and ACI 318 (2008). The shear-friction theory assumes that the transfer mechanism of shear forces at a concrete-to-concrete interface subjected simultaneously to shear and compression forces is ensured by friction only. A simple saw-tooth model shown in Figure 2.8 is generally adopted to show the basic principles of the shear-friction model.

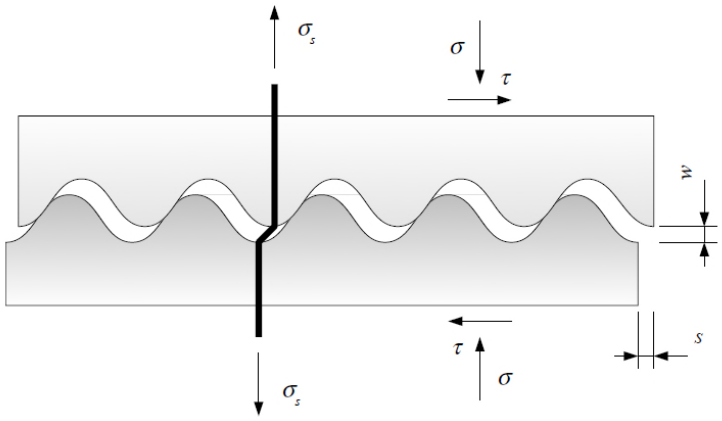

Figure 2.8 - Shear Friction Model (Adapted from Oehlers and Bradford, 1995)

When longitudinal shear is transferred at a concrete interface or joint, two scenarios can occur: (1) the shear is transferred across an initially cracked plane and (2) the shear is transferred across an initially uncracked plane. The shear friction theory considers the first scenario where (a) adhesion or cohesion, (b) shear-friction and (c) shear reinforcement or dowel action influence the transfer of the longitudinal shear forces across the interface.

Mattock et al (1972) investigated the magnitude of the maximum shear stress transferred across either uncracked or initially cracked (pre-cracked by splitting) shear

planes under compressive or tensile normal forces. The shear strength in initially uncracked elements is dependent on (1) the strength of the transverse and (2) the strength of the concrete. In initially uncracked elements when the shear force is applied, diagonal tensile stresses develop in the concrete and lead to the formation of the herringbone parallel diagonal cracks. As the shear force increases, the rotation of the concrete element induces tensile stresses in the transverse reinforcement.

In initially cracked elements, the shear forces caused the cracks to slip relative to each other and the shear distortion is resisted along the line of the crack by three mechanisms (1) dowel action, (2) aggregate interlock and (3) friction.

A. Aggregate Interlock

At the crack front, the shear stress is transferred by a mechanism known as aggregate interlock or shear-friction. It must be noted that shear-friction can only occur if (1) the crack surface is held together by transverse reinforcement (i.e., δ_{normal} =0) or (2) an external active normal stress, δ_{normal} if applied to the element.

When a crack is held by transverse reinforcement, under shear, crack faces displace relative to each other and projections of aggregate on opposing crack faces bear against each other thereby transferring shear stresses (Haskett et al, 2010). As slip increases across the crack interface, the cracks widen. This causes tension to develop in the transverse reinforcement which resists the widening of the crack by virtue of its axial stiffness, ρE_s. Hence, to maintain equilibrium, compressive forces normal to the cracked

face develop. One component of this compressive normal force is the axial strength of the transverse reinforcement often referred to as passive friction.

B. Dowel Action

The slip at the crack faces or the concrete interface is resisted by bending of the transverse reinforcement across the crack, referred to as dowel action. This is analogous to the behaviour of mechanical shear connectors where the slip induced by the flexural forces applied to composite members is resisted by deformation or bending of the connectors. Hence, the shear connectors only resist the longitudinal shear after slip occurs.

The dowel strength is therefore primarily dependent on the shear strength of the reinforcing bars, i.e. ρf_{yr} where ρ is area of reinforcement crossing the shear plan as a proportion of the shear plane. However, as Oehlers and Bradford (1995) suggests, the dowel strength is also influenced by the compressive strength of the concrete and the concrete modulus.

C. Friction

When external active normal forces, δ_{normal} are applied, the shear-friction resistance depends on whether the forces applied are compressive or tensile. When normal compressive forces are applied, shear stresses are distributed in the same manner as the transverse reinforcement described above. Hence, compressive forces develop the aggregate interlock mechanism thereby increasing the shear-friction resistance. On the

other hand, tensile forces decrease the shear-friction resistance by allowing the crack to widen which reduces the amount of interlock and the development of passive compressive forces and passive friction.

Thus, the aggregate interlock strength is dependent on (1) the passive restraint of the transverse reinforcement ρE_s (fracture of the protruding aggregates at the interface) and (2) the passive friction across the crack interface.

The active frictional resistance, $v_{friction}$ is also defined by Mattock and Hawkins (1972) as:

$$\mathbf{v_{friction} = 0.8\ \delta_{normal}}$$

Equation 2.1- Frictional resistance: Mattock and Hawkins (1972)

The above mechanisms for a headed stud across a cracked plane are illustrated below:

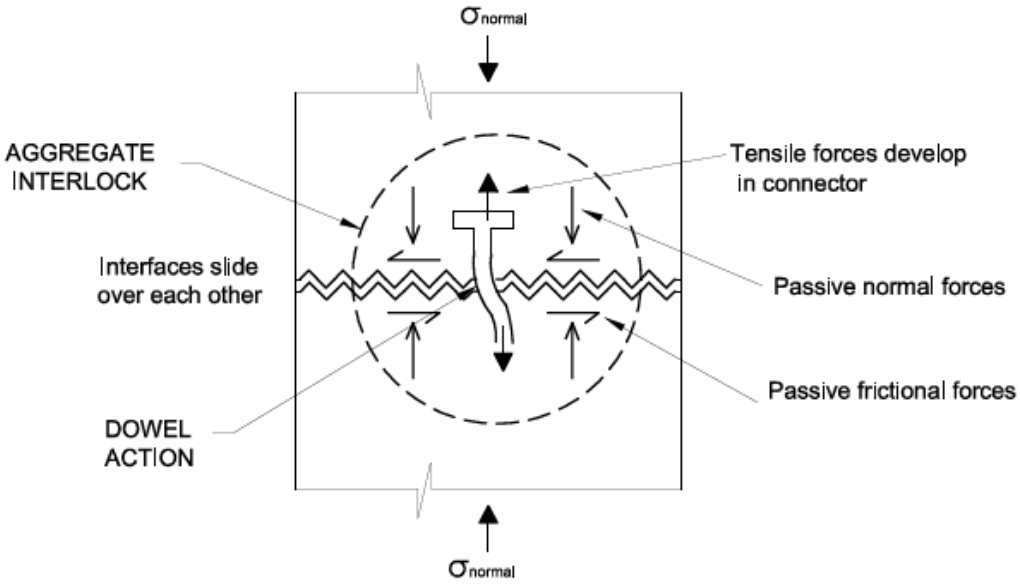

Figure 2.9 - Mechanisms of aggregate interlock, dowel action and friction

D. Longitudinal/Interface shear

The interface shear is therefore the sum of the dowel strength, aggregate interlock resistance and frictional resistance.

$$v_{interface\ shear} = v_{lock} + v_{dowel} + + v_{friction}$$

Mattock and Hawkins (1972) propose a lower bound solution to the shear strength of a cracked shear plane as follows:

$$v_{interface\ shear} = 1.4 + 0.8\ \rho f_{yr} + 0.8\ \delta_{normal}$$

Equation 2.2- Interface shear: Mattock and Hawkins (1972)

Based on the findings of Mattock and Hawkins (1972), Oehlers and Bradford (1995) also quantified the dowel strength as:

$$v_{dowel} = \left(3.4 \left[E_c / E_s\right]^{0.40} \left[f_c / f_y\right]^{0.35}\right) \rho f_{yr}$$

Equation 2.3- Dowel Strength: Mattock and Hawkins (1972) and Oehlers and Bradford (1995)

where,

- E_c is the modulus of elasticity of concrete,
- E_s is the modulus of elasticity of steel,
- f_c is the compressive cylinder strength of concrete,
- f_y is the yield strength of steel,
- f_{yr} is the yield strength of the reinforcing bars and
- ρ is the area of reinforcement crossing the shear plan as a proportion of the shear plane.

Oehlers and Bradford (1995) suggest that the terms inside the above brackets were equal to the 0.8 value suggested by Mattock and Hawkins (1972).

Mattock and Hawkins (1972) also propose an upper limit to the shear capacity as 0.3 f_c. In addition, Oehlers and Bradford (1995) support that the aggregate interlock forces were mostly influenced by the tensile strength of the concrete. The Mattock and Hawkins (1972) equation was therefore revised to the following:

$$\mathbf{v_{interface\ shear} = 0.66\ f_{ct} + 0.8\ \rho f_{yr} + 0.8\ \delta_{normal} < 0.3\ f_c}$$

Equation 2.4- Interface shear- Revised: Mattock and Hawkins (1972)

where, f_{ct} is the direct tensile strength of the concrete.

According to more recent study by Reinecke and Zilch (2001), the shear stress developing at a concrete-to-concrete interface, t(s) for a given crack with a longitudinal displacement between the concrete part, s, is given by:

$$\mathbf{\tau_{(s)} = \tau_{adh(s)} + \tau_{sf(s)} + \tau_{sr(s)}}$$

Equation 2.5- Interface shear: Reinecke and Zilch (2001)

where $\tau_{adh(s)}$ is the contribution of the adhesion, $\tau_{sf(s)}$ is the contribution of the shear and $\tau_{sr(s)}$ is the contribution of the shear reinforcement for the shear stresses as shown in Figure 2.10.

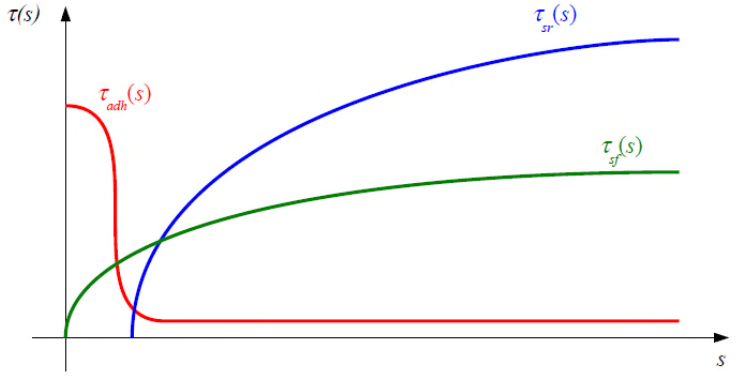

Figure 2.10 - Contribution of adhesion, shear-friction and shear reinforcement (Reinecke and Zilch, 2001)

The above figure shows that at early stages of loading, the shear stress is mainly provided by the adhesion forces at the concrete to concrete interface. At this stage the crack (longitudinal displacement) is very small. As the load is increased, the adhesion forces are overcome resulting in further cracking. This causes the development of shear-friction and shear reinforcement (dowel action) to occur. Thus, the total interface shear is a function of the adhesion, shear-friction as well as shear-reinforcement forces.

E. Interface Shear in Design Standards

i. CEB-FIP Model Code (1990)

According to the CEB-FIP Model Code 1990 (1990), the design shear stress at the concrete-to-concrete interface v_u is given by:

$$\mathbf{v_u = c\, f_{ctd} + \mu\, (\sigma_n + \rho\, f_y) \leq 0.25\, f_{cd}}$$

Equation 2.6- Interface shear: CEB-FIP Model Code 1990

where,

- c and μ are factors that depend on the roughness of the interface as summarised in **Table 2.1** below.
- f_{ctd} is the design tensile strength of the weakest concrete
- σ_n is the external normal stress acting on the interface
- ρ is the reinforcement ratio (> 0.1%)
- f_y is the yield strength of the reinforcement
- f_{cd} is the design compressive strength of concrete.

If the shear stress at the interface is negligible so that no shear reinforcement is necessary, then the design shear stress at the concrete-to-concrete interface v_u is given by:

$$\mathbf{v_u = c\, f_{ctd}}$$

The CEB-FIP Model Code 1990 also takes into account the orientation of the shear reinforcement that crosses the interface. For plain interfaces, the design shear stress at the interface v_u is given by:

$$\mathbf{v_u = \mu\, [\sigma_n + \rho\, f_y\, (\sin \alpha + \cos \alpha)\,] \leq 0.30\, f_{cd}}$$

where, α is the angle between the shear reinforcement and the shear plane.

Type of surface		Coefficient of cohesion c	Coefficient of friction μ
Category	**Description**		
Type 1 (Smooth)	I : a smooth surface, as obtained by casting a steel or timber shutter	0.2	0.6
	II : a surface which lies between trowelled or floated to a degree, which is effectively as smooth as (I)		
	III : a surface which as been trowelled or tamped in such a way that small ridges, indentations or undulations have been left		
	IV : a surface achieved by slip forming or vibro-beam screeding		
	V : a surface achieved by extrusion		
	VI : a surface, which has been deliberated textured by lightly brushing the concrete when wet		
Type 2 (Rough)	VII : as for (IV), but with more pronounced texturing, as obtained by brushing, by a transverse screeder, by combining with a steel rake or with an expanded metal	0.4	0.9
	VIII : a surface which has been thoroughly compacted, but no attempt has been made to smooth, tamp or texture the surface in any way, having a rough surface with coarse aggregate protruding, but firmly fixed in the matrix		
	IX : where the concrete has been sprayed when wet, to expose the coarse aggregate without disturbing it		
	X : a surface which has been provided with mechanical shear keys		

Table 2.1- Coefficients of cohesion and friction: CEB-FIP Model Code 1990 (1990)

ii. BS 8110-1 (1997)

Part 1 of the British Standards BS 8110-1:1997 refers to the interface shear as horizontal shear. According to Clause 5.4.7.2, the design horizontal shear stress should be less than the upper bound limits provided in Table 5.5. For instance, a precast unit without links and an as-cast surface at the concrete interface has an upper limit of 0.65

N/mm^2 while that treated with a retarder (to increase the surface roughness) has an upper limit of 0.80 N/mm^2.

When the shear reinforcement crossing the interface has to resist to the entire acting shear force, the ultimate longitudinal shear stress at the interface v_u is given by:

$$\mathbf{v_u = 0.6\ F_b\ \rho\ \tan\alpha}$$

Equation 2.7- Interface shear: BS 8110-1

where,

- F_b is the minimum value between 0.95 f_y A_s and the anchorage value of the reinforcement where,
    - f_y is the yield strength of the reinforcement
    - A_s is the area of the shear reinforcement crossing the interface
- ρ is the reinforcement ratio
- α is the angle of internal friction between the faces of the joint.

According to BS 8110-1, the angle of friction, α, is dependent on the finish of the surface as summarised in Table 2.2.

Type of surface	tan α
Smooth interface, as in untreated concrete	0.7
Roughened or castellated joint without continuous in-situ strips across the ends of joints	1.4
Roughened or castellated joint with continuous in-situ strips across the ends of joints	1.7

Table 2.2- Angle of internal friction: BS 8110-1 (1997)

Precast unit	Type of Surface	In-situ Concrete Strength		
		25MPa	30MPa	> 40MPa
Without shear reinforcement crossing the interface	As-cast or as-extruded	0.40	0.55	0.65
	Brushed, screeded or rough-tamped	0.60	0.65	0.75
	Washed to remove laitance or treated with retarder and cleaned	0.70	0.75	0.80
With shear reinforcement crossing the interface	As-cast or as-extruded	1.20	1.80	2.00
	Brushed, screeded or rough-tamped	1.80	2.00	2.20
	Washed to remove laitance or treated with retarder and cleaned	2.10	2.20	2.50

Table 2.3- Design ultimate longitudinal shear stress: BS 8110-1 (1997)

For the ultimate limit state, the design longitudinal shear stress at the interface is dependent on 1) the preparation of the substrate surface; 2) the strength of the in-situ concrete; and 3) the existence of shear reinforcement crossing the interface. The recommendations provided by BS 8110-1 (1997) is given in Table 2.3.

iii. Eurocode 2 (2004)

In Eurocode 2, BS EN 1992-1-1:2004, the interface shear is referred to as the design shear interface resistance. Section 6.2.5 defines the design shear interface resistance as follows:

$$v_{Rdi} = c\, f_{ctd} + \rho\, f_{yd}\, (\mu \sin\alpha + \cos\alpha) + \mu\, \sigma_n + \leq 0.5\, v\, f_{cd}$$

Equation 2.8- Interface shear: Eurocode 2

where,

- v_{Rdi} is the design shear resistance at the interface

- c and μ depend on roughness of the interface
- f_{ctd} is the design tensile strength of the concrete
- σ_n is the stress per unit area caused by minimum external normal force across interface
- ρ is equal to A_s/A_i where, A_s is the area of reinforcement (including shear reinforcement) crossing the interface and A_i is the area of joint
- α is the angle defined in Figure 6.9 of Eurocode 2: BS EN 1992-1-1:2004. This is provided in Figure 2.11.
- v is the reduction factor obtained from 6.2.2 (6)
- f_{cd} is the design compressive strength of concrete.

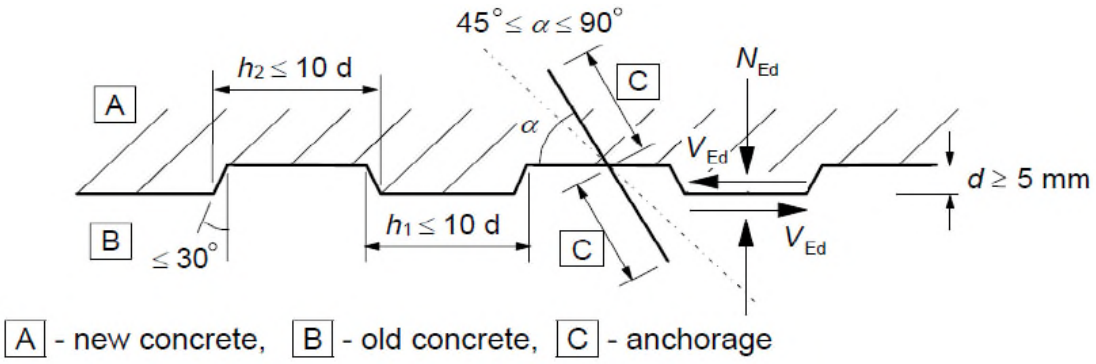

Figure 2.11 – Angle α: EC2

The first term in the above equation relates to the bond between the surfaces and any mechanical interlock provided by indenting the surface. The second term relates to the mechanical resistance of the reinforcement across the interface and the third term accounts for the friction across the interface as a result of the action of compressive stress, σ_n.

For each type of surface (i.e. very smooth, smooth, rough and indented), cohesion and fiction coefficients ae used to determine the shear at the interface between concretes cast as different times. The corrigendum to EC2 (2004), effective since 16th January 2008, presents significant modifications to the coefficient of cohesion, in particular, for the very smooth surface. This is shown in Table 2.4.

Type of Surface	Coefficient of cohesion, c		Coefficient of friction, μ	
	EC 2 (2004)	Corrigendum (2008)	EC 2 (2004)	Corrigendum (2008)
Very smooth	0.25	0.025-0.010	0.50	0.50
Smooth	0.35	0.20	0.60	0.60
Rough	0.45	0.40	0.70	0.70
Indented	0.50	0.50	0.90	0.90

Table 2.4- Design ultimate longitudinal shear stress: BS 8110-1 (1997)

According to EC2, the design shear interface resistance v_{Rdi} must be greater than the design value of the shear stress at the interface, v_{Ei}., i.e $v_{Ei} \leq v_{Rdi}$.

The design value of the shear stress at the interface, v_{Ei} is given by:

$$\mathbf{v_{Ei} = \beta V_{Ed} / zb_i}$$

Equation 2.9- Design Interface shear: Eurocode 2

where,

- β is the ratio of longitudinal force in new concrete and the total longitudinal force. β is conservatively taken as 1.
- z is the lever arm of the composite section.
- B_i is the width of the width of the interface shear plane.

The above equation assumes that all loads are carried on the composite section thus making it compatible with the design approach adopted for ultimate flexure. The basic shear stress for design at the interface is therefore related to the maximum longitudinal shear stress at the junction between compression and tension zones given by $V_{Ed} / zb_{i.}$

As mentioned above, EC4 defines z as being the lever arm of the composite section which should be derived from the stress block of the loaded beam considered. However, since determining the value of z for each loading is time-consuming and rather difficult, Hendy and Smith (1997) suggest that it would be reasonable to use the same value as obtained from the ultimate bending resistance analysis.

F. Methods of Testing Interface Shear

i. Bond Strength

The shear at the interface between two layers of concrete is dependent on the bond strength at the interfaces. Bond strength tests are usually carried out during concrete rehabilitation works for repairing or strenghteinig structures involving adding new concrete to existing concrete substrates. Thus, determining the bonding of the new material to the old material by an appropriate method of laboratory testing is fundamental in order to determine the interfce shear.

Hindo (1990) describes the three common for testing concrete boinding anf therfore interface shear as (1) Slant test, (2) Direct tension and (3) Direct shear tests as illustrated in the figure below.

The specimens for the slant test are prepared and bonded under laboratory conditions due to the slanted bonding interface. The direct shear and direct tension tests use samples cored from site or produced in the laboratory. It must be noted that all three tests must be carried out under laboratory conditions.

The pull-off or pull-out test is another means of testing the bond strength at the interface of two concrete layers. The pull-out tests is a modified version of the Direct Tension test described by Hindo (1990) and is the most common and accurate of all bond strength testing methods.

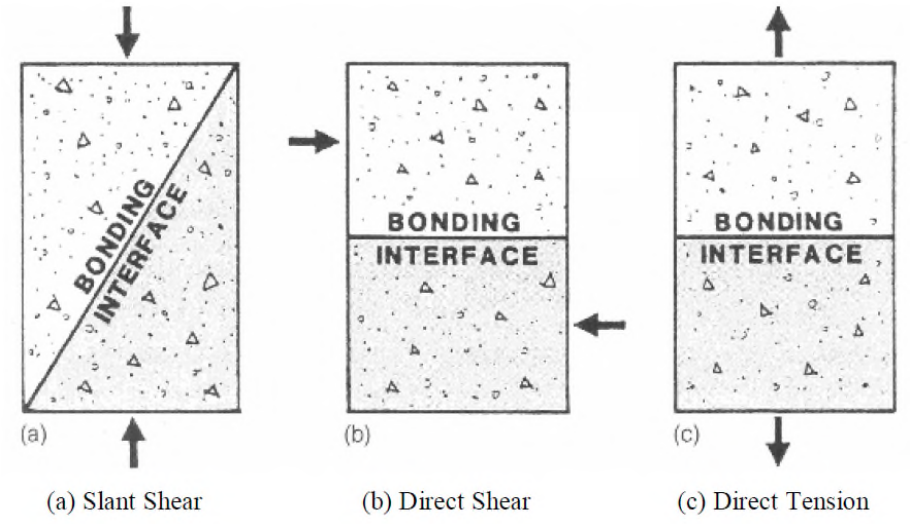

Figure 2.12 - Laboratory Bond Strength Tests (Hindo, 1990)

Julio et al (2004) carried out tests on specimens using slant tests and pull-out tests and proved that the bond strengths from the slant tests is over five times that of the pull-out tests (based on a correlation factor of 0.1855 between both tests). In addition, the pull-out test evaluates the bond strength in tension at the interface of the concrete layers and can be carried in-situ.

ii. Push-out Tests

a) Description of Push-out Test

The pull-out test is only applicable in cases the bond strength at the concrete interface is critical. In composite construction where concrete and steel interact with each other; the deformation, stress distributions and modes of failure primarily depend on the behaviour of the shear connection between the steel and the concrete elements. For instance, in L-shaped rib shear connectors used profiled sheeting construction, separation between the concrete and the steel is prevented which ensures that most of the longitudinal shear is transferred. Such connectors exhibit almost infinite slip before failure and the pull-out strength of the concrete dictates the connection strength. On the other hand, mechanical shear connectors such as headed studs impose very high concentrations of load onto the concrete element. These loads are transferred from the steel to the concrete by dowel action of the connectors. Due to the complexity of this dowel action and the large variety of mechanical shear connectors used in composite construction, the strength and ductility of such connectors are always determined experimentally.

It is almost impossible to determine the shear behaviour of connectors from composite beams. In such tests, the connectors are indirectly loaded from the flexural forces applied to the composite beam and as Oehlers and Bradford (1995) state the force in the connector is not directly proportional to the load applied to the beam and primarily depends on the stiffness of the individual components. In addition, composite beam

tests are expensive which would hinder the development of shear connectors in industry.

Instead of full scale beam tests, small-scale push or push-out tests have been used extensively to directly determine the strength of shear connectors from as early as the 1930s (Ernst et al, 2010). In a standard push-out test, the shear connectors are first attached to the flanges of a short length of steel I-section and two small concrete slabs are then cast around the shear connectors. The specimens are bedded onto a lower platen of a compression-testing machine/ frame and load is applied to the upper end of the steel section. Various adaptations of this set-up have been used. For instance, *Liew and Sohel (2009)* tested 12 (steel/concrete core/steel) sandwich beam specimens consisting of a concrete core, sandwiched between two relatively thin steel plates, connected to the concrete by J-hook shear connectors. *Naito et al (2009)* investigated the efficiency of various commercially available steel ties by carrying out push-out tests on specimens in which the ties were attached to a layer of insulation and concrete was cast around the insulation and in the inner core (concrete-insulation/concrete core/insulation-concrete).

Eurocode 4, BS EN 1991-1:2004 (E) Annex B sets out the requirements for a typical push out test illustrated below. Flanges of a short length of steel I-section are connected to two small concrete slabs using shear studs and the load is applied to the upper end of the steel section in increments.

The load is applied in four stages: (1) up to 40 % of expected failure load, (2) 25 times between 5% and 40% of the expected failure load, (3) up to failure load ensuring that

failure does not occur in less than 15 minutes and (4) beyond failure until the load has dropped to 20% below maximum load. The deflection or slip between the steel member and the two concrete slabs is measured at several points and the average deflection is plotted against the load to obtain load-deflection profiles. The shear resistance of the studs and the average slip is then derived from the experimental results.

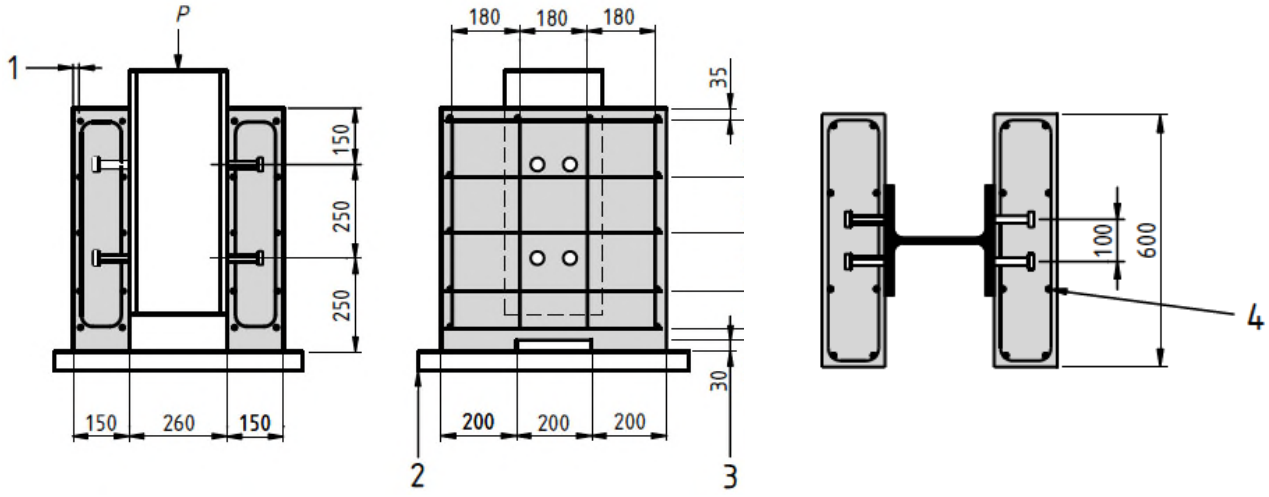

Figure 2.13 - Test specimen for standard Push-out test (EC4, p111)

b) Limitations of Push-out Tests

As previously discussed, the determination of the strength of the shear connectors from full-scale composite beam tests is expensive, complex and subject to modelling inaccuracies. Although push-out tests are comparatively inexpensive and easily carried out, the forces induced in the shear connectors in push specimens are different from those in composite beams.

The shear strengths obtained from push specimens are influenced by four main factors including (1) the restraints at the base of the specimens (2) the number of connectors per

concrete section, (3) the reinforcement in the concrete and (4) direction of concrete placing.

1) Restraints at base

In standard push-out tests, the base of the test specimen is usually restrained by the reaction (testing) frame or floor. This causes frictional forces to develop between the base of the specimen and the reaction frame which in turn induces a horizontal force to resist against horizontal movement. This causes additional compressive forces to develop in the shear connectors which do not occur in a composite beam, thereby increasing the shear strength observed during push-out tests shown in Figure 2.14.

Teraszkiewicz (1965) determined that the shear strength of headed studs decreased by a third when the base of one biscuit was free to slide and by almost half when those of both concrete biscuits were free to slide. Other studies (Hicks and McConnel, 1996 and Al-deen et al, 2011) have also concluded that the use of roller bearings which reduces friction by allowing the base to slide, significantly reduces the shear connection strength.

Most recently, researchers (Topkaya et al, 2004 and Ernst et al, 2010) have circumvented the need of anchoring the base of the test specimens to a reaction floor by developing horizontal push-out tests rigs where the specimens are mounted and tested horizontally as shown in Figure 2.15.

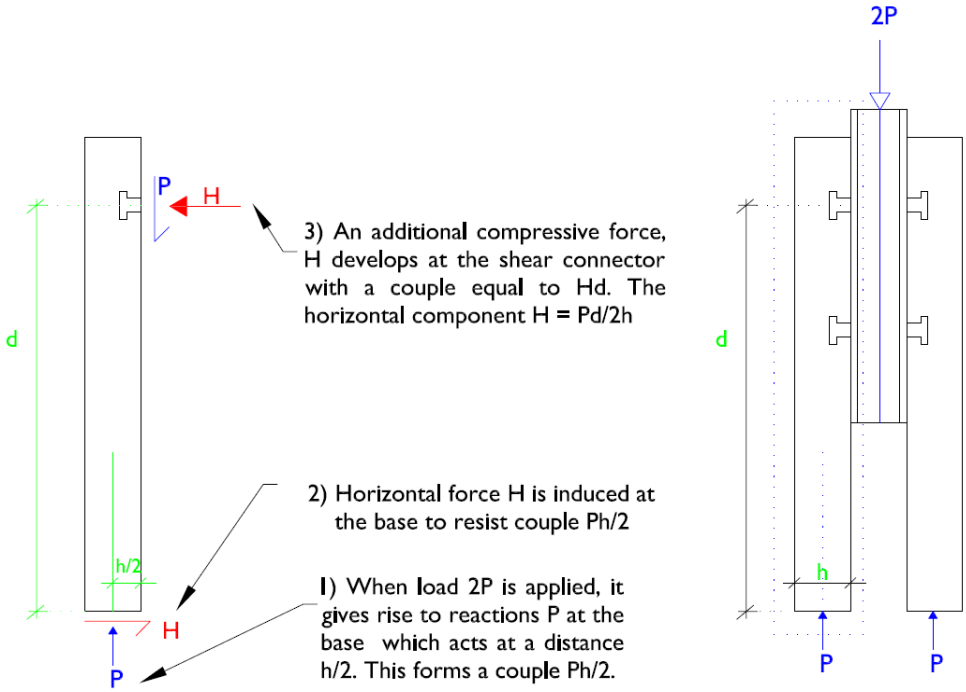

a) Forces in left biscuit with connector *b) Push-out test specimen*

Figure 2.14 – Additional horizontal force due to fixed bases

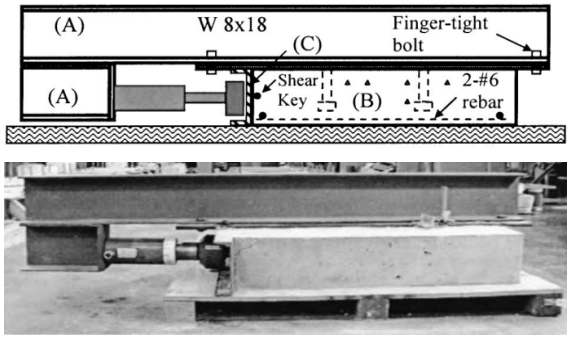

Topkaya et al: 2004, p 954

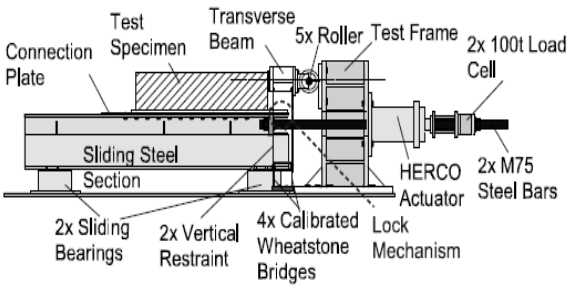

Ernst et al: 2010, p189

Figure 2.15 - Horizontal push-out test set-up

In light of the above, the friction at the base of push-out tests an important parameter to be considered in the determination of the shear strength of shear connectors in push-out tests.

2) Number shear connectors per concrete slab

In the past, the standard push-out test set-up was based on the requirements of in in BS 5400-5 (1979, 2005) consisting of only one level of shear connectors. Previous studies showed that the number of levels or rows of studs resulted in no significant changes in the shear connection strength of behaviour of push out specimens (Ollgaard et al, 1971 and Jayas & Hosain, 1988). However, in push-out tests, the concrete slabs are cast on separate days and it is essential that load redistribution occurs between the weaker and the stronger sides so that failure occurs at the mean strength.

An analysis on the mechanism of failure in push specimens by Oehlers and Johnson (1987) showed that the mean strength when one level of shear connector was used was only 86% of the strength obtained with push-out specimens consisting of two levels of shear connectors. It was concluded that two levels of shear connectors are required to ensure that the connectors have good rotational stiffness to redistribute the forces between the connectors in the two concrete slabs so that the push-out specimens fail at the mean strength in both sides. This has been implemented in EC4 where it is recommended that two rows of shear connectors are used in standard push-out test specimens.

3) Reinforcement in concrete slabs

The lack of transverse reinforcement in the concrete slabs of push-out tests carried out by earlier researchers (Slutter and Driscoll, 1965 and Hawkins, 1973) resulted in concrete splitting failures and lower shear connections strengths and deformation

capacities. A study by Johnson and Oehlers (1981) concluded that the presence of transverse reinforcement in push specimens prevented the propagation of longitudinal splitting cracks resulting in higher shear connector strengths and improve ductility. Oehlers and Park (1992) carried out push-out tests on 25 specimens and determined that the transverse reinforcement provides confinement to the concrete in the vicinity of the shear connectors and that the strength of the shear connectors is hence affected by the stiffness of the transverse reinforcement but not by its strength.

Further research by Lloyd and Wright (1989) confirms that the variation in size and position of reinforcement in the transverse concrete slab has no discernible effect on the ultimate connection resistance. It must therefore be ensured that adequate transverse reinforcement is provided in the concrete slabs of push-out test specimens to prevent any splitting cracks from occurring in the concrete.

4) Direction of concrete placing

The direction of concrete placing during the preparation of push-out test specimens affects the development of the strength of the shear connectors and the composite action between the concrete and steel. A study by Yukio et al (1983) concluded that casting the specimens in an upright position significantly increase the deformations and overestimates the slip observed in push-out test specimens. Kuhn and Buckner (1986) investigated the effect of concrete placement on the shear strength of headed studs on twelve push-out specimens and observed that a shear strength reduction of about 30 % occurred in specimens where the concrete was cast beneath the stud in comparison with those where the concrete was cast above or to the side of the steel concrete interface.

This reduction in shear strength can be due to bleeding of the concrete in the bearing zone of the shear connectors or to the formation of void at the connector-concrete interface. Hence, particular attention must therefore be given to the direction of concrete placing when the push-out test specimens are prepared and cast.

2.3 Previous Research

2.3.1 Interface Shear Strength

Revesz (1953) was amongst the first researchers to investigate the shear strength occurring at concrete-to-concrete interfaces. Three point loading tests were carried out on five composite beams. Four of the beams were prestressed with high tensile strength wire and one was reinforced with mild steel. For all the beams, the roughness of the web surface was smooth, and there were no shear ties across the interface as shown in Figure 2.16.

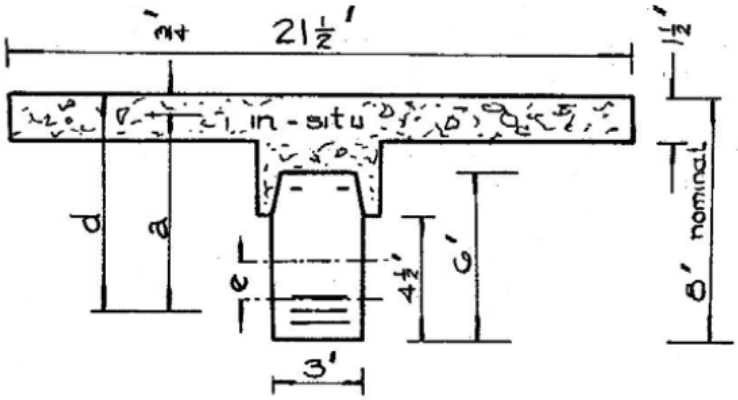

Figure 2.16 – Cross Section of Test Specimen (Revesz, 1953)

At the time of the test, the concrete cylinder strength was 2480 psi (17 N/mm^2) for the cast-in-place flange and 5225 psi (36 N/mm^2) for the precast web. The age of the concrete at the time of the test was 4 days for the cast-in-place flange and 85 days for the precast web. Further to the tests, it was recommended the contact surfaces of the precast web and cast-in-place concrete of composite beams should be roughened in order to prevent failure by horizontal shear.

Hanson (1960) studied the effect of interface roughness, keys and stirrups crossing the interface on the horizontal shear transfer at connection between precast girders and in-situ cast slab. The shear-deflection curves and shear-slip curves for the girder tests are shown in **Figure 2.17**.

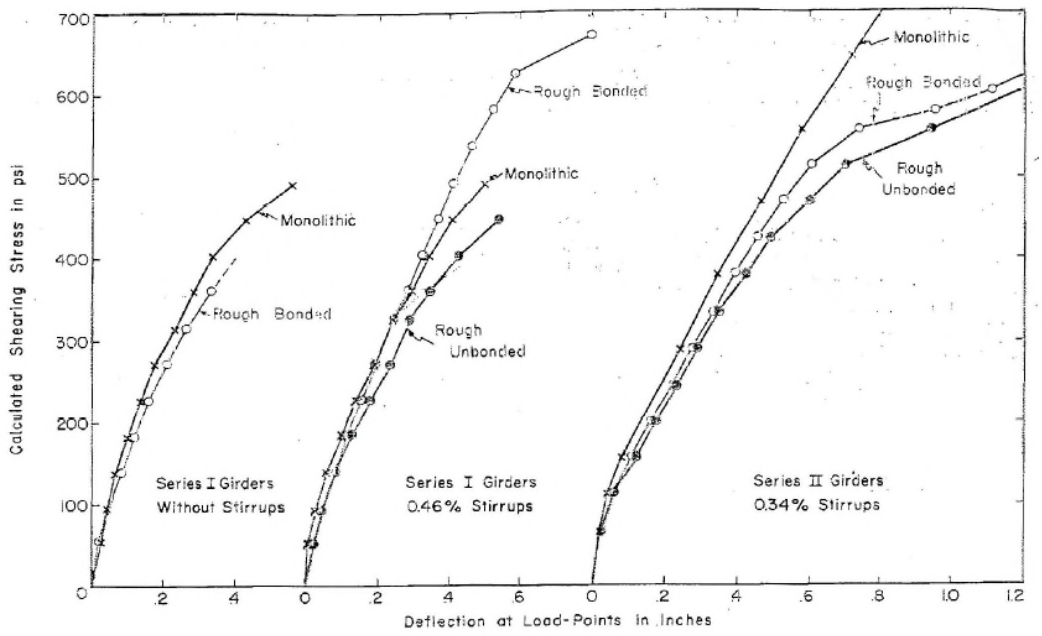

Figure 2.17 - Load-deflection and Load-slip curves: Hanson, 1960

It was observed that as the interface roughness and keys and stirrups crossing the interface increased, the interface horizontal shear stress improved. Additionally, the shear-deflection and shear-slip profiles indicated that the composite action decreases at

a slip of 0.005 inches (0.13 mm) in the test specimens. Thus, a slip value of 0.005 inches was considered to be critical to the composite behaviour of the test specimens.

Bryson et al (1965) carried out three point bending tests on prestressed split beams consisting of varying depths of precast and prestressed tension portions of the web, and cast-in-place compression section. Shear connectors were provided across the interface of the two concrete layers and the surface roughness was applied with a stiff wire hand brush so that the largest size aggregate was exposed. All the specimens failed in flexural compression due to crushing of the concrete. The strains in the concrete were linear indicating composite action occurred at the interface. The authors concluded that the precast and cast insitu concrete sections of the split beams had developed sufficient bond to act monothically during the tests.

Patnaik (1999) tested nine composite beams with an as-placed surface finish and no shear ties across the interface. The concrete strengths for the flange and web along with the interface width were varied for the beams. The study suggested that the strength of the concrete of the web or slab (the lowest value, f'_c can be related to the horizontal shear stress, v_{uf0} by: $\mathbf{v_{uf0} = 0.35\sqrt{f'_c}}$

The horizontal shear stress from the Patnaik (1990) equation also provided strength predictions which were well over two times of that of most design standards and codes.

Choi et al (1999) carried out push-off tests on 76 specimens to evaluate the use of special powder-driven mechanical fasteners (nails) for shear transfer in bonded concrete overlays for bridge deck or payment rehabilitation. The roughness at the interface and interface shea reinforcement were varied. The contact surfaces of overlay specimens

were shotblasted to varying degrees of roughness and were designated as light, medium and heavy shotblasting.

Test results showed that slip occurred at failry low shear stresses when the interface was lightly shotblasted, but the resistance of nails in shear-friction in overlay specimens was mobilized as soon as adhesion was lost and interface slip occurred. It was also noted that overlay specimens with 0.38 % interface shear reinforcement had 10 to 16 % higher interface strength than those without nails with the same contact area.

Gonhert (2003) carried out push-off tests on 90 concrete composite members to determine the horizontal shear strength along the interface of a roughened surface. The cross section of the test specimen used as well as the test set up is shown in Figure 2.18.

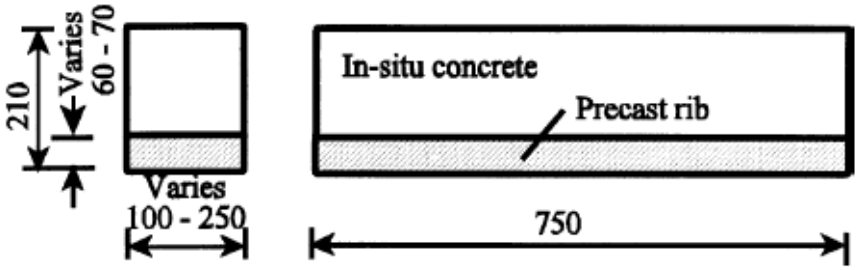

(a) Test specimen

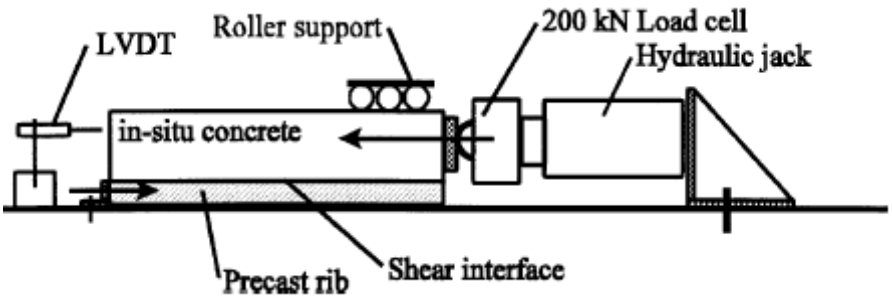

(b) Test set-up

Figure 2.18 – Test specimen and set-up: Gonhert, 2003

Results indicated that there was a poor correlation between the horizontal shear strength and the compressive strength of the concrete. However, the horizontal shear capacity of the specimens increased as the concrete strength increased. It was also observed that there was a significant increase in the shear capacity as the roughness increased.

Julio et al (2010) an experimental study was performed to evaluate the shear strength between a sandblasted concrete substrate and a concrete overlay, for different amounts of transverse reinforcement. The results showed that the reinforcement crossing the interface did not significantly increase the interface debonding stress. In addition, the interface shear strength increased with the increase of reinforcement crossing the interface. It was also noted that higher shear strength of the interface was achieved with sandblasted surfaces than with surfaces cast against steel formwork. Further to the experimental tests, it was recommended that a roughness parameter assessed with suitable equipment should be used to quantify the surface roughness at the concrete interfaces. Additionally, the cohesion and the friction coefficient should be calculated based on this roughness parameter, instead of being linked to the finishing treatment of the surface. It was also suggested that the design value of the shear stress at the interface should first be compared with the shear strength of the interface provided by adhesion only.

2.3.2 Push-out Tests on Sandwich Panels

Bush et al (1994) carried out push-out tests on two series of composite concrete sandwich panels. The first series consisted of solid concrete zones which formed around the trussed connectors while in the second series the solid concrete zone was eliminated.

Results confirmed that the concrete zones forming around the trussed connectors in the first series significantly affected both the shear stiffness and strength of the interface. The panels with the solid concrete zones resisted 70% more load and were 350% stiffer than those without the sold concrete zones.

Amin et al (1994) investigated the structural performance of fibre reinforced polymer bent bar (FRPBB) shear connectors in PCSPs using push-out tests. Results confirmed that the strength of the specimens was governed by the axial strength of the connectors. It was also observed that the majority of the FRPBB shear connectors failed at the portion of the diagonals falling within the insulation layer due to axial compression, flexural combined with axial compression, and flexural combined with axial tension. Additionally, the friction between the concrete and the insulation contributes to almost 10 percent of shear capacity of the specimen.

Pong et al (2005) investigated the use of glass fibre-reinforced polymer (GFRP) as a shear transfer connectors in PCSPs consisting of three concrete biscuits and two insulation layers. 30 push-out specimens with difference types of shear connectors were tested. Results showed that failure of the test specimens occurred due to brittle failure as a result of shear and flexural. At failure, a sudden drop in the applied load was observed followed by the failure of all the connectors.

The experimental results were then compared with the theoretical predictions of the shear capacity as defined by ACI 318-02. It was noted that the experimental ultimate failure loads obtained from the push-out tests were much lower than the ACI 318002

values. Thus, the study concluded that the ACI methodology should not be used to determine the horizontal shear occurring in PCSPs with GFRP shear connectors.

Hany et al. (2007) carried out push-out tests on 30 PCSPs comprising three concrete wythes and two insulation wythes. The shear transfer capacity of three different shapes of NU-Tie (five specimens for each type) was determined experimentally. Results were compared with other commercially available shear connectors including lattice fibre glass polymer and welded wire fabric connectors. The push-out tests showed that the behaviour of the panels with the NU-Tie was very similar to the commercially available shear connectors. The shear capacity of the NU Ties was also greater than the commercially available lattice fibre glass polymer.

Naito et al (2009) investigated the shear strength of different shear ties in sandwich panels using push-out tests. The shear ties used included carbon steel, stainless steel, galvanized carbon steel, carbon fibre reinforced polymers (CFRP), glass fibre reinforced polymer (GFRP), and basalt fibre reinforced polymer (BFRP). The push-out specimens are shown in Figure 2.19.

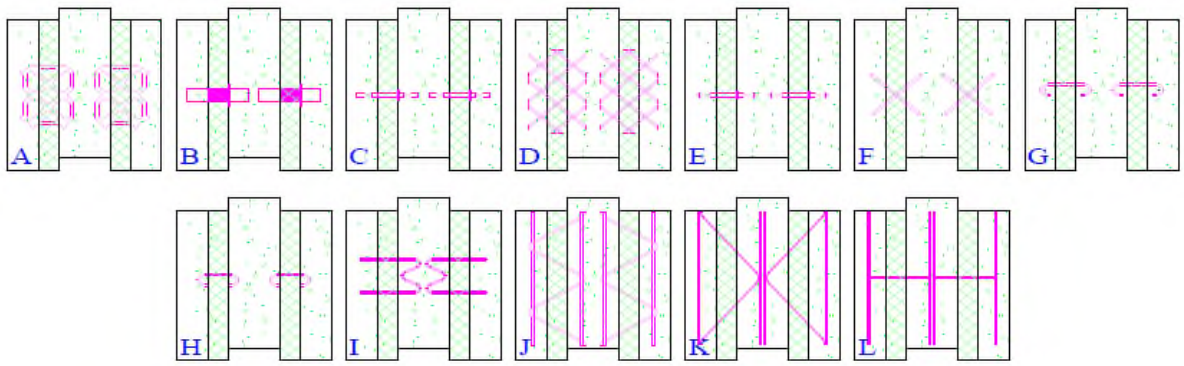

Figure 2.19 – Details of push-out specimens (Naito et al, 2009)

The experimental results indicate that shear ties used in sandwich wall panels had considerable variations in strength, stiffness, and deformability. The FRP truss type connections (A and D) exhibited an elastic brittle response, because the shear behaviour was dominated by FRP in tension. The steel wire truss (K) exhibited an elastic plastic behaviour, because the shear behaviour was dominated by steel in tension. The steel M-clip (I) and the C-clip with adequate embedment (G) exhibited elastic-plastic behaviour at low shear deformations, because the leg of the connection is subjected to dowel action. The FRP non-composite pins (C and E) exhibited an elastic-plastic response with minor hardening.

Aziz (2010) carried out an investigation to verify the methodology recommended by ACI 318-08 for the calculation of the shear transfer capacity at the interface between the concrete wythes. 16 push-out specimens with varying surface conditions (smooth or rough) and presence of shear reinforcement between the interfaces were tested. Details of the push-out specimens are shown in Figure 2.20. Results confirmed that the rough concrete interfaces increased the shear capacity of the concrete at the interface between the old and new concrete. It was also observed the use of shear reinforcement across the concrete interface improved the shear resistance of the test specimens provided that the shear reinforcement were adequately embedded in the concrete wythes.

The comparison between the experimental push-out tests results and the theoretical predictions defined by ACI 318-02 showed that the ACI values was significantly higher than the experimental results. Hence, the study recommended that further experimental tests are required in order to validate the use of the ACI code for the determination of the shear capacity of PCSPs.

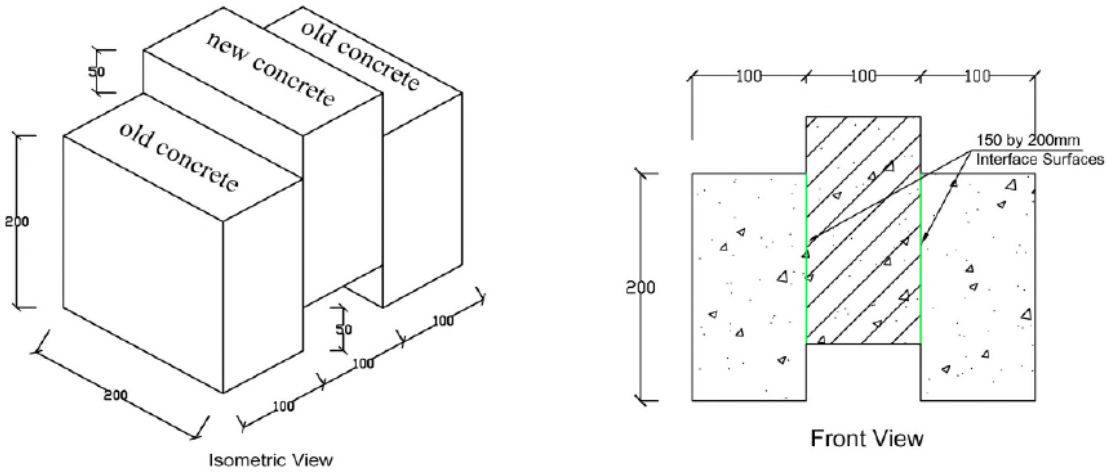

Figure 2.20- Isometric and Front Views of the Tested Specimens (Aziz, 2010)

2.3.3 Flexural Behaviour of Sandwich Panels

Pfeifer and Hanson (1965) investigated the effects of the type of insulation, thickness of panel and type of the connectors on the capacity of sandwich panels. Flexural tests were carried out on fifty 900 mm x 1500 mm sandwich panels with thicknesses ranging from 57 mm to 152 mm. the shear connectors used in this study included expanded metal connectors, commercial truss connectors, welded fibre fabric connectors and concrete edge ribbed connectors. Five different types of light weight insulation cores were also used. Results from the moment-deflection profiles confirmed that the variation in flexural stiffness is generally reduced for panels containing plastic or glass fibre insulation while panels with cellular or formed glass cores showed a relatively high value of moment resistance. The flexural tests also confirmed that the metal connectors with diagonal members such as commercially available welded wire trusses were more effective in transferring shear than those without diagonal members.

Einea et al. (1994) compared the results from the experiment and finite element analysis of sandwich panels with hybrid truss connectors where the diagonals were fibre reinforced plastic bars and the chords were pre-stressed steel strands. Two small scale and full scale specimens were tested under flexure. Results confirmed that the full scale panels were significantly stiffer than the small scale specimens. Moreover, the FE investigation indicated that longer panels with the same stiffness and number of shear connectors exhibited more composite behaviour than shorter panels.

Bush and Stine (1994) carried out flexural tests on composite sandwich panels to investigate the effect of the number and spacing of the connectors on their flexural behaviour. Two series of composite concrete sandwich panels were tested. The first series consisted of three panels fabricated in the same manner as commercial panels with solid concrete zones. The second series were cast as idealised panels were extraneous paths at shear transfer (solid concrete zone) were eliminated through modification of certain construction details. The test specimens were made of two 76 mm x 2440 mm x 4880 mm concrete wythes (concrete biscuit) separated by a 51 mm thick insulation material (expended polystyrene). Results showed that a high degree of composite stiffness and composite flexural capacity were attained with truss girder connectors oriented longitudinally in the panels. Test results also showed that construction details can have a significant impact on the distribution of shear in elements crossing the interface.

Salmon et. al. (1997) investigated the effect of using fibre reinforced plastic (FRP) and steel truss connectors on the flexural strength and composite behaviour of PCSPs. Two full scale panels (9140 mm long x 2440 mm wide x 203 mm thick) with each connector

type were tested under bending. The results obtained were compared with theoretical principles. It was observed that the strength of each PCSP was almost equal to the theoretical determined fully-composite strength of the panel. The results also showed that the stresses in the elements of the FRP bars were in agreement with the predictions of the linear elastic structural analysis performed. It was therefore confirmed that the linear analysis model can be used to determine the degree of composite behaviour of PCSP panel as follows:

$$\mathbf{I_e = Mh / (f_b - f_t)}$$

Equation 2.10 – Degree of composite action: Salmon et al, 1997

where,

- I_e is the panel effective moment of inertia including shear deformation I_g is the moment of inertia of gross cross section
- f_b is the stress at bottom face of the panel
- f_t is the stress at top face of the panel
- M is the moment capacity of the panel below the crooking moment at the load corresponding to f_c and f_b
- h is thickness of the panel

From the above equation, the panels containing the FRP shear connectors were 82 % composite while the panels containing the steel connectors were 88% composite.

Bush and Zhiqi (1998) adopted a close for elastic continuum approach to estimate service load deflections and bending stresses of non-loadbearing semi-composite prestressed sandwich panels with truss connectors. The close form solution used originally derived by Allen (1970) was modified to meet the specifications of the

sandwich panels used. Flexural tests were carried out on prestressed sandwich panels and the experimental maximum deflections and bending stresses were then compared to those obtained from Finite Element Modelling (FEM) predictions. The differences in between the experimental and FE predicted values were attributed to (1) differences between the actual and assumed material properties, (2) the presence of extraneous stress paths and (3) differences in the restraints conditions of the panel. However, the researchers still maintained that theoretical predictions can be used for the design and understanding of the behaviour of semi-composite sandwich panels.

Pessiki and Mlynarczyk (2003) carried out flexural tests on four full scale prestressed and precast sandwich panels. The control panels comprised two two 76 mm concrete wythes, a 51 mm insulation core and metal wythe connectors (M-ties). The degree of composite action developed by each shear transfer mechanism (regions of solid concrete, wythe connectors, and bond) was then evaluated by testing three additional panels that included only one mechanism each.

The degree of composite action (K) was determined from the following equation:

$$\mathbf{K = \frac{I_e - I_{nc}}{I_c - I_{nc}} \times 100}$$

Equation 2.11 – Degree of composite action: Pessiki and Mlynarczyk, 2003

where,

- I_c and I_{nc} are the theoretical values of the fully composite and non-composite moment of inertia for the panel.
- I_{exp} is experimental value of moment of Inertia determined from the deflection as:

$$I_{exp} = \frac{5wl^4}{384\partial E_c}$$

Equation 2.12 – Experimental moment of inertia: Pessiki and Mlynarczyk, 2003

where,

- L is the length of the panel.
- W is the uniformly distributed load applied.
- ∂ is the experimental deflection.
- E_c is the modulus of elasticity of concrete.

Results confirmed that the control, the concrete region, wythe connector and the bond specimens attained 100%, 92%, 10% and 5% of the full composite action respectively. It was therefore recommended that the solid concrete regions should be proportioned adequately in order to provide maximum composite action in PCSPs.

Kabir (2005) investigated the mechanical characteristics of 3-dimensional wall panels under static shear and bending loads. Four point bending tests were carried out on six 3000 mm long x 160 mm wide sandwich panels comprising top and bottom wythes, a polystyrene isolated core and steel diagonal shear connectors. FE analysis was then carried out using the ANSYS software to evaluate the flexural behaviour of the sandwich panels.

Results confirmed that the stiffness of the FE panels was lower than that of the experimental panels. This was attributed to the deficiency in the quality of concrete and the welded wire fabric used. The displacements at midspan of the panels were plotted against the applied load. Results confirmed that the panels behaved like fully composite

sections during the elastic stage and in a partially composite manner in the non-linear stage. The geometry of the panels tested and the load-deflection profiles obtained are shown in Figure 2.21.

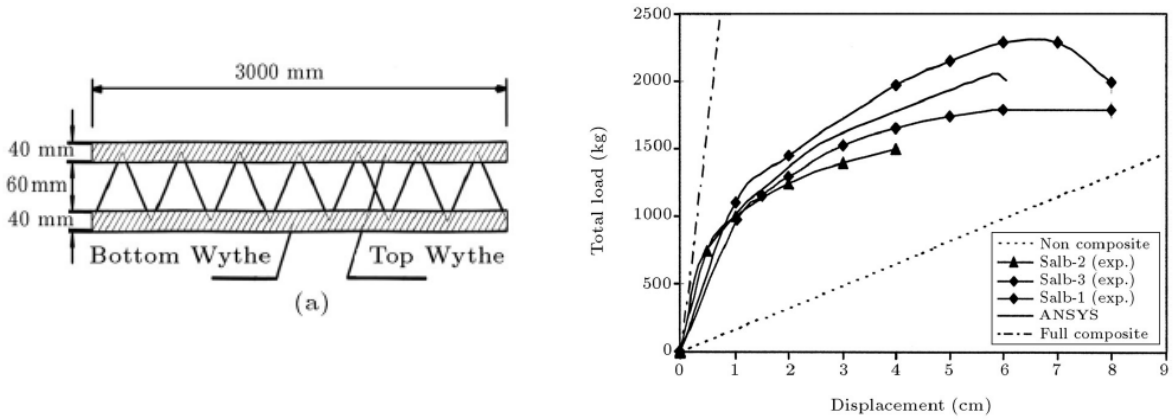

(a) Geometry of panel *(b) Load-displacement profile*

Figure 2.21- Geometry and Load-displacement profiles of sandwich panels (Kabir, 2005)

Pong et.al in 2005 determined the thermal and structural resistance of PCSPs with glass fibre reinforced polymer (GFRP) shear connectors. Three point bending tests were carried out on xix full scale panels (top and bottom wythes thickness of 76 mm and insulation core thickness of 304 mm) connected by V-shaped GFRP shear connectors were tested under three point bending. The mode of shear transfer, degree of composite action and the flexural capacity from the experiment were compared with theoretical prediction of ACI 318-02.

It was determined that the experimental ultimate failure load was lower the ACI predicted value which assumes that the panels behave in a fully composite manner. The ratio of the experimental failure load to the theoretical fully composite load was

calculated. Results confirmed that the panels with (GFRP) shear connectors reached approximately 75% of the fully composite strength It was recommended that the number of GFRP connectors should be increased in order to achieve full composite action.

Benayoune et al. (2006) investigated the ultimate strength and behaviour of PCSPs with steel truss shear connectors. Six (2400 mm long x 1200 mm wide) full-scale sandwich panels with variable aspect ratios and slenderness ratios were cast and tested under eccentric loads. The deflections, strains across the insulation layer and shear connectors as well as crack propagation under the applied load were observed. Results indicated that all panels behaved in a fully composite manner under eccentric load till failure. It was also observed that as the slenderness ration increased, the ultimate strength decreased non-linearly.

Finite Element Analysis (FEA) was also carried out to estimate the strength of the panels. The experimental and FE results were compared with values based on the ACI design practice. A semi-empirical formula relating to the area of the concrete and steel, strength of the steel and thickness and height of the panel was developed to better fit the experimental and FE results.

Maximos et al. (2007) carried out tests on PCSPs with different shapes of GFRP shear connectors referred to as NU-Ties. Three point bending tests were carried out on 14 test specimens with different types of shear connectors as well as the amount of transverse reinforcement. Results confirmed that transverse reinforcement has almost no effect on the structural behaviour of the panels. In addition, the experimental failure load was

lower than the theoretical fully composite predictions. The experimental deflections observed were also much larger than the theoretical predictions. This was attributed to the flexibility of the NU-Tie connectors in comparison with other solid concrete connectors.

Lee and Pessiki (2007) provided recommendations on the design and analysis of three-wythes sandwich panels. It was shown that the panels could be designed as per the recommendations of the ACI design codes but needed to take into account the transverse bending stresses developing at the ends of the panels. Several approaches to reduce the transverse bending were introduced and evaluated, including the use of partially debonded strands and shear connectors. It was concluded that three-wythe panel could be treated as composite panels, suitable for longer spans.

Lee and Pessiki (2008) extended their research on the structural behaviour of three-wythe concrete sandwich panels experimentally and numerically using FE analysis. Two panels consisting of three 50 mm thick wythes separated by two 25 mm insulation cores and connected by M-tie metal shear connectors were teste under flexure. The first panel was used as a control and the second panel comprised an additional concrete rib. The Load-Deflection profile showed that the panels exhibited linear behaviour until the formation of the first crack, beyond which a reduction in the flexural stiffness of the panels was observed. It was also observed that the second panel was stronger and stiffer than the first panel suggesting that the presence of the concrete rib decreased shear-log effects.

The equations suggested by Mlynorezyle and Pessiki (2003) were then used to determine the degree of composite action of both panels. Results showed that the first and second panel exhibited 79% and 94% of composite action respectively. It was also concluded that the three-wythes panels showed ductile flexural behaviour as a result of flexural cracking and yielding of the reinforcement. It was noted that no horizontal shear failure had occurred in the test panels. The experimental results (in terms of the load-deflection profiles, degree and composite action, flexural strength and horizontal shear) were also in agreement with the FE results.

Benayoune et al (2008) carried out experimental and numerical (FE) investigation on PCSPs with truss shaped shear connectors. Six samples consisting of 40 mm thick reinforced concrete biscuits with a 40 mm thick insulation core and truss shear connectors were tested. The panels had aspect ratios (length /width) ranging from 2.6 to 1.0.

Experimental results confirmed that the mode of failure and crack patterns of the PCSP two way spanning specimen with an aspect ratio of 2.67 were very similar to those of solid slabs. The load-deflection profiles showed that the first cracks occurred at the load where there was a shift from elastic to plastic behaviour in the test specimens. Failure occurred as a result of buckling of the lattice, concrete crushing and yielding of the reinforcement in the bottom biscuit. It was therefore concluded that the specimens behaved in a partially composite manner.

The degree of composite action occurring at elastic and ultimate stages was also calculated. For the elastic stage, the variation of stresses occurring in the top and bottom

concrete biscuits at each load increment was plotted. The distribution of stresses were then used to evaluate the effective moment of inertia, I_e as follows:

$$\mathbf{I_e = \frac{Mh}{\sigma_b - \sigma_t}}$$

Equation 2.13 – Degree of composite action at elastic stage: Benayoune, 2008

where,

- M is the applied bending moment
- h is the depth of the panel
- σ_t and σ_b are the stresses occurring in the top and bottom biscuits respectively.

The ratio I_e/I_g was then used to provide an indication of the degree of composite action taking place during the elastic stage, where I_g is the moment of inertia of PCSP assuming the biscuits and the core behave in a fully composite manner.

The degree of composite action occurring at the ultimate stage, i.e. at failure was taken as the ratio of the experimental failure load to that of the theoretical fully composite load. The non-composite and fully composite loads were calculated by deriving the forces in the concrete and steel using the stress block analogy. The stress blocks used for the non-composite and fully composite extremes are showed in *Figure 2.22.*

At ultimate stage,

Degree of composite action = Experimental Failure Load / Theoretical Failure Load

Equation 2.14 – Degree of composite action at ultimate stage: Benayoune, 2008

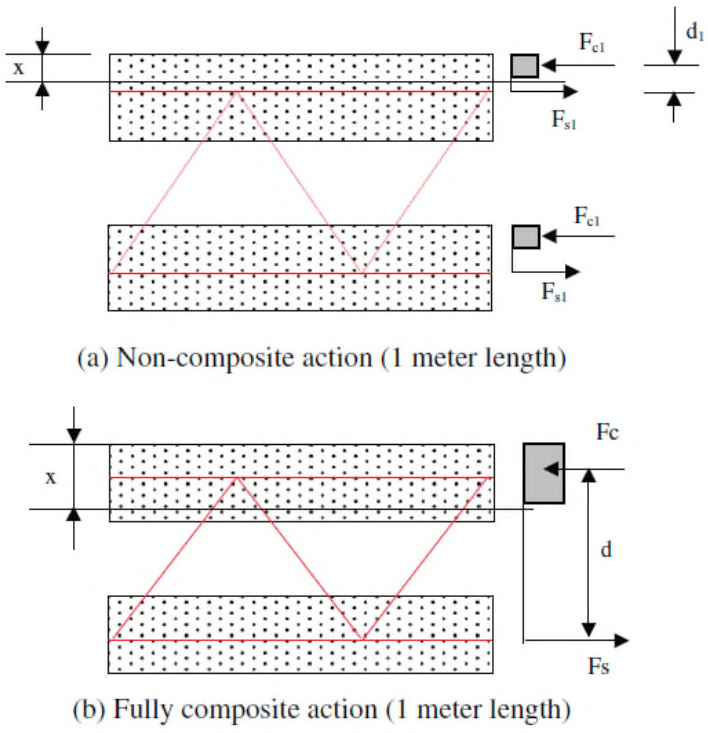

Figure 2.22- Stress blocks for non composite and fully composite panels (Benayoune et al, 2008)

Results confirmed that the degree of composite action of panels was mainly dependent on the stiffness of shear connectors. The comparison between the results from the FE analysis, the theoretical predictions and the experiment showed a good correlation.

Rizcolla et al (2009) investigated the structural performance of PCSPs, reinforced with carbon fibre reinforced polymer (CFP) in order to maximise composite action. Six full scale sandwich panels (6100 mm long x 3700 mm wide) consisting of two 51 mm thick prestressed wythes and a 120 mm thick insulation layer were subjected to a combination of vertical and lateral flexural loads. Four main parameters were varied including the type of foam (expanded polystyrene foam, EPS or extruded polystyrene foam, XPS); presence of solid concrete zone; panel configuration variation in wythes thickness and shear grid reinforcement ratio; the midspan deflection; the relative displacement

between the wythes and strain across the thickness of the panel were measured to predict the degree of composite action between the wythes.

Results showed that the panel stiffness was significantly influenced by the type and the configuration of the shear transfer mechanism. The solid concrete zones resulted in more composite action than the other types of shear mechanisms. In addition, the experimental results confirmed that the XPS foam did not contribute to the shear transfer mechanism between the wythes. The study also proposed a simplified design chart to calculate the nominal moment capacity of EPS and XPS foam core panels at different degree of composite interaction. However, the chart was only limited to the configuration, geometry, material and reinforcement used in the investigation.

2.4 Finite Element Analysis

In the past few decades, global research has been endeavouring in finding efficient ways to simulate reinforced concrete structures, and analyse their behaviour non-linearly. One of the methods used to achieve this goal is the development of computer numerical modelling techniques to reproduce realistic engineering models with a non-linear finite element analysis approach.

The complex nature of sandwich panels makes them difficult to analyse by conventional methods. It is not feasible to prepare full-scale samples varying a range of characteristics i.e. size, shape, type of shear connectors etc. as it will need a huge amount of valuable time and cost. Moreover, due to nonlinearity of panel components and the structural correlations between them, it is difficult to predict its behaviour.

Hence, Finite Element (FE) analysis is an effective tool to simulate the behaviour of sandwich panels with varying properties of biscuit, core and shear connector properties under different loading and boundary conditions.

Hoigard et al (1993) used FE analysis methods to investigate the behaviour of thin stone veneers on insulated partially composite PCSPs. The results from experimental tests were first used to validate the FE model. The FE modelling of a 7.92 m long pre-cast concrete column cover was analysed. The study showed that the FE and experimental results were in agreement with each other and that the structural response of composite precast concrete building panels can be predicted by finite element methods.

Attard et al. (1996) investigated the out-of-plane buckling of reinforced concrete walls using FE analysis. The concrete was modelled as non-linear and orthotropic plate bending element and the reinforcing steel was modelled as elastic-plastic beam elements. The FE results were compared with the experimental results from 24 simply supported reinforced concrete panels tested by the Attard et al (1994) and Swartz et al (1974) as shown in Figure 2.23. Comparison between the FE results and the experimental results showed good agreement.

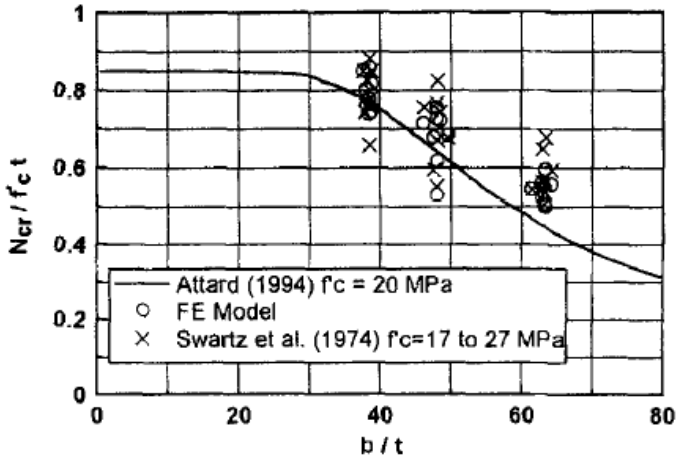

Figure 2.23 - Comparison of FE results with experimental results (Attard, 1994)

Pokharel and Mahendran (2004) evaluated the local bucking behaviour of foam supported steel plate sandwich element experimentally using the finite element program, ABAQUS. The finite element model was based on the application of compressive load to one end of the steel face with all four sides of the plate being simply supported. Figure 2.24 shows the model geometry, mesh size and the loading pattern for half-length models.

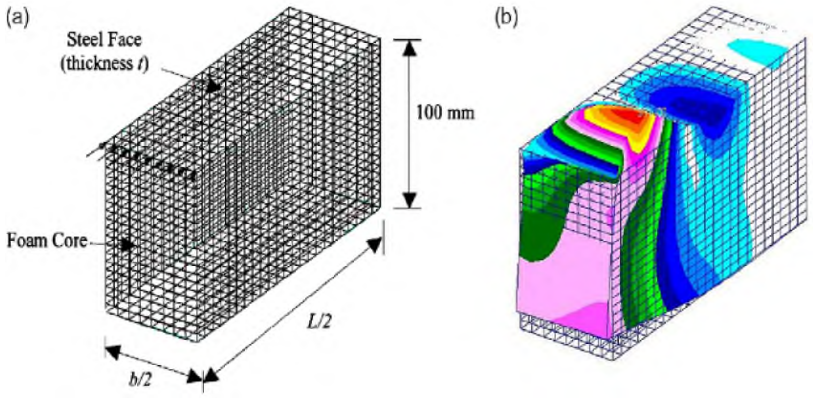

Figure 2.24 - Half-length FEA model simulating experimental steel plates supported by foam core (a) Model; (b) Buckle shape (Pokharel and Mahendran, 2004)

The FE model was validated using the experimental results and then used to review the current design rules. Results confirmed that the design rule used cannot be applied for slender plates. Based on the results from this study, an improved design equation was developed to consider the local buckling and post-buckling behaviour of sandwich panels for a large range of b/t (breadth/thickness) ratios (<600) for design purposes.

Kabir (2005) used the FE analysis software ANSYS to investigate the structural properties of lightweight shotcrete sandwich panels under shear and bending loads. The numerical model was also validated with experimental results as shown in Figure 2.25. It was observed that the load-displacement curves for the FE and experimental results

were very similar. The effect of using three different sizes of steel wire shear connectors on the rigidity of the panel was devaluated using the FE analysis. Results showed that the panel with the biggest size of shear connectors (4mm) achieved higher degree of composite behaviour.

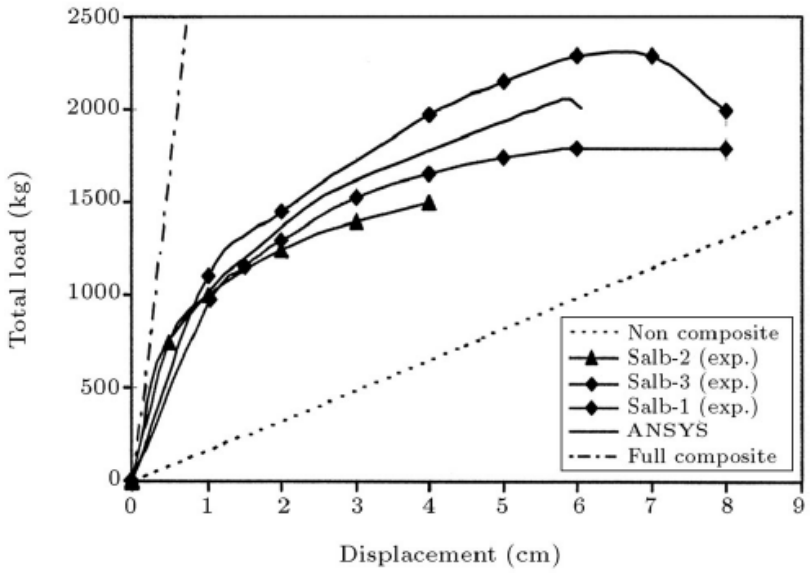

Figure 2.25 - Load deflection curves for horizontal slab bending test (Kabir, 2005)

Benayoune et al. (2006, 2007) conducted two studies on the behaviour of PCSP with steel truss shear connectors under axial and eccentric load. Experimental tests and FE analysis suing the LUSAS software were undertaken. Load deformation response, variation of strains across the insulation layer, strains in shear connectors, crack appearance and propagation under increasing load were recorded and analysed. The outcomes from the FE analysis are verified as they closely match the experimental data. The FE model was also able to successfully predict the ultimate strength of panels.

Mousa and Udin (2012) carried out FE analysis using the ANSYS software in order to model the response of Composite Structural Insulated Panels (CSIP) walls under in-

plane loading. Experimental results were validated using the proposed analytical models and FE modelling (Figure 2.26), and were observed to be in good agreement. Furthermore, a parametric FE study was conducted to investigate the influence of key design parameters on the behaviour of CSIPs. The study showed that span-to-depth ratio and core density have a significant effect on the structural performance of CSIP wall panels.

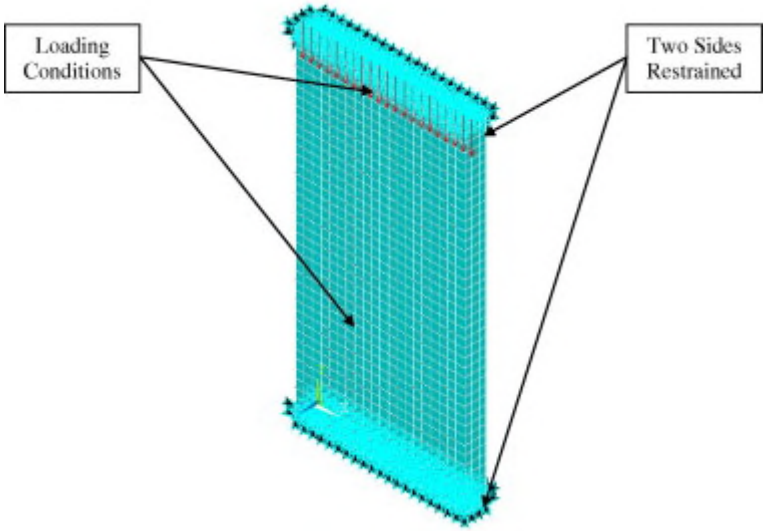

Figure 2.26 - Structural CSIP wall panel with loading and boundary conditions: Mousa and Udin, 2012

Kang (2015) developed a FE models using the general-purpose FE analysis package, ABAQUS to simulate the shear resistance of connectors in foam-insulated concrete sandwich panels. The concrete damaged plasticity (CDP) model provided by ABAQUS was used to model the concrete biscuits. The CDP model takes into account the degradation of the elastic stiffness caused by plastic straining both in tension and compression. It also assumes that the two main failure mechanisms are tensile cracking and compressive crushing of the concrete material. The material properties for the CDP model is summarised in Table 2.5. The sandwich panels before and after the shear loading are shown in Figure 2.27.

Concrete Parameters	
E, modulus of elasticity GPa	24.8
ν, Poisson's ratio	0.18
Density kg/m^3	2403
Compressive strength MPa	28–34
Tensile strength MPa	2.8

CPD Model Parameters	
ψ, dilation angle	30°
ε, flow potential eccentricity	0.1
σ_{b0}/σ_{c0}	1.16
K_c	0.667
μ, viscosity parameter	0

Concrete Compression Hardening	
Yield stress, MPa	***Crushing strain***
24	0
28–34	0.002
17	0.003

Concrete Tension Stiffening	
Remaining stress after cracking, MPa	***Cracking strain***
2	0
0	0.002
–	–

Table 2.5- ABAQUS Concrete Parameters (Kang, 2015)

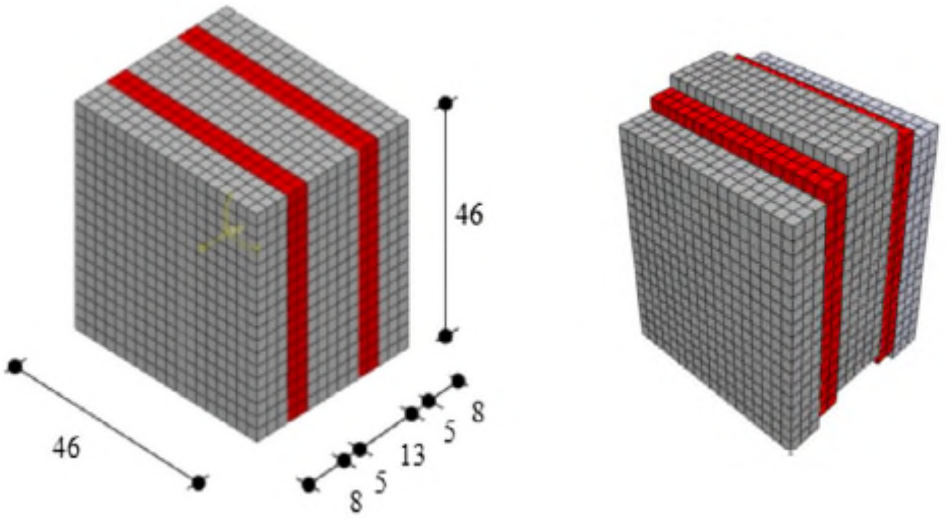

a) Sandwich panel for shear test *b) Deformed sandwich panel for shear test*

Figure 2.27- Sandwich test panels using ABAQUS (Kang, 2015)

The models were then validated using data from static tests performed at the University of Missouri. The modelling approach used was compatible with the American Concrete Institute (ACI) Code and existing design practices. The results of this study would

therefore provide improved methodology for the analysis and design of foam-insulated sandwich panels under both static and blast loadings.

The pressure–displacement curve of the experimental test data and the FE model showed good agreement due to the satisfactory simulation of the compression hardening and tension stiffening of concrete. It was also concluded that the FE model satisfactorily simulated the detailed structural behaviours of concrete, rebar, foam and ties during all loading stages (elastic, yielding, ultimate and post-failure).

2.5 Summary

Twinwalls are a variation of the long established PCSPs. Other variations of the PCSPs have been investigated by many researchers with different compositions of the biscuits, core and shear connectors. The combinations of the various material properties used result in different structural behaviour of the PCSPs.

Under flexural loads, PCSPs and therefore twinwalls can behave as fully composite, non-composite and partially composite panels. In fully-composite panels, the shear connectors must transfer all of the required longitudinal shear force. In non-composite panels, the shear connectors have no capacity for longitudinal shear transfer. In partially composite panels, the shear connectors transfer between 0-100% of the longitudinal shear required for a fully composite panel.

In twinwalls, the interface between the precast concrete in the biscuits and the in-situ concrete in the core give rise to longitudinal/interface shear forces. The load transfer

mechanism of shear forces between two concrete layers is primarily influenced by three main factors (1) the cohesion or adhesion between particles at the concrete interface, (2) the friction occurring at the concrete interface and (3) the shear reinforcement crossing the interface. These factors have been taken into account in codes such as CEB-FIP Model Code (1990), BS 8110-1 (1997) and Eurocode 2 for the design of interface shear between two concrete layers.

The cohesion or adhesion gives rise to aggregate interlock which is dependent on the roughness of the surface between the two concrete layers. The friction occurring at the concrete interface is caused by the presence of external active normal forces. The shear reinforcement crossing the interface dictates the dowel strength of the reinforcing bars. The dowel strength is influenced by the area of the area and the yield strength of the reinforcement crossing the shear plan as a proportion of the shear plane.

The interface shear between two concrete interfaces can be determined by (1) the bond strength tests which include the slant, direct shear and direct tension tests or (2) the push-out tests. The push-out test is most common for concrete interfaces with more than two reinforcement bars crossing at the interface.

The push-out tests are influenced by four main factors including (1) the restraints at the base of the specimens (2) the number of connectors per concrete section, (3) the reinforcement in the concrete and (4) direction of concrete placing.

Various researches have investigated the interface shear developing between two concrete interfaces with different surface roughnesses, reinforcement bars or shear

connectors crossing the interface and external friction forces applied. All results confirm that push-out tests are an effective way of determining the interface shear capacity between two concrete layers as well as the longitudinal shear capacity of shear connectors crossing the concrete interfaces.

The flexural behaviour of PCSPs has been studied by various researchers. Three point or four point bending tests have most commonly been used to determine the deflection occurring in the biscuits at ever load increment.

During the linear elastic stage, the degree of composite action of PCSPs can be calculated from the ratio I_e/I_g where I_g is the moment of inertia of PCSP assuming the biscuits and the core behave in a fully composite manner; and $I_e = \frac{Mh}{\sigma_b - \sigma_t}$. At ultimate stage, the degree of composite action can be calculated as the ratio of the experimental failure load to the theoretical failure load.

Finite Element analysis an effective tool in simulating the behaviour of PCSPs. FE software such as ANSYS, LUSAS and ABAQUS have been used by many researchers to investigate the behaviour of PCSPs with different material properties, loading and boundary conditions. The Damaged Plasticy Model (DPM) provided by ABAQUS is most commonly used to model the behaviour of the non-linear concrete in PCSPs.

In view of the above, the following gaps in the current understanding of twinwalls have been identified:

- As mentioned previously, twinwalls are a variation of PCSPs. Though different material properties of the biscuits, core and shear connectors exist, no documental literature was available on twinwall panels with concrete precast biscuit, concrete insitu core and 3-D truss shear connectors.

- Push-out tests are commonly used to determine the interface shear behaviour of PCSPs. However, twinwalls are fundamentally different from standard push-out specimens since they are made up of a concrete core instead of the commonly used steel I-section.

- Although a wide range of shear connectors (including 2-D lattice girders) used in PCSPs have been investigated, there is no documented work on the use of 3 dimensional lattice shear connectors used in twinwalls.

- The interaction at the interface between the biscuit and the core in twinwall panels has not been investigated in terms of aggregate interlock, dowel action or friction.

- It has been noted that the embedment failure in PCSPs has not been investigated in most of the previous studies on PCSPs.

- There is a lot of documented literature on the degree of composite action in various types of PCSPs but the degree of composite action for twinwalls has not been investigated previously.

- Review of the literature on PSCPs and twinwalls confirmed that there is no published work that has been carried out the structural behaviour of twinwalls in terms of stiffness, deformation and failure mechanism.

- Additionally, no literature was found on the FE analysis has been carried out to validate experimental results of twinwall panels.

Chapter 3

Phase I: Experimental Procedure

Push-out Tests

3.1 Introduction

As discussed in Chapter 2, in retaining wall applications, twinwalls behave as cantilever walls and are subjected to combined bending and shear with maximum bending moment and shear forces occurring at the base of the walls. For design purposes, the flexural strength of the twinwalls is based on the strength of the outer biscuits which is a function of the strength of the concrete and the longitudinal and transverse reinforcement provided. The shear strength is based on the strength of the lattice shear connectors which resist the applied shear forces by developing longitudinal shear forces across the biscuit/core interface.

The structural actions taking place in the lattice girder under combined shear and bending is not well understood. There is also a clear lack of documented work in this field. This can be attributed to the fact that twinwalls are a fairly new hybrid concrete

construction component but can also be partly due to the high cost of full-scale specimens and the reluctance of manufacturers to share propriety information with their competitors. Hence, small scale tests were carried out under laboratory conditions in order to provide a better understanding of the structural behaviour of twinwalls.

In Phase I, push-out tests were carried out to investigate the effect of different variables on the shear behaviour of twinwalls. The methodologies adopted, mix designs, sample preparation and test procedures are presented in the following section.

3.2 Push-out Tests

3.2.1 Background

Push-out tests were used to investigate the behaviour of individual shear connectors experimentally. As discussed in the literature review, the standard method used is set out in Eurocode 4, BS EN 1991-1:2004 (E) Annex B where flanges of a short length of steel I-section are connected to two concrete slabs using shear studs. The test specimen is conventionally bedded down on mortar directly onto the reaction floor with load being applied to the upper end of the steel member. Load is then applied to the I-beam and the deflection or slip between the steel member and the two concrete slabs is measured at each load increment. The average deflection is plotted against the load to obtain load-deflection profiles. The structural behaviour of twinwalls can in fact be simulated under laboratory conditions using push-out tests as shown in Figure 3.1.

In the push-out test, when the load P is applied to the top of the core, longitudinal shear forces develop along the interface between the biscuit and the core. The core and biscuit interfaces slide over each other giving rise to friction forces which are resisted by normal compressive forces in the concrete. This is known as aggregate interlock and occurs because the biscuit interfaces are effectively held together by the lattice bars across the core/biscuit interface. The shear is effectively resisted at the by the interlocking of the aggregate particles which protrude from each concrete biscuit. The shear resistance through the interface interlock is a function of the tensile strength of the concrete and the passive restraint provided by the steel which is dependent on its stiffness and area (Oehlers and Bradford: 1995). In addition, load P causes compressive struts to develop in the concrete and in some of the lattice bars in a similar manner to the structural actions taking place in twinwalls in water tank applications shown in Figure 3.1(a).

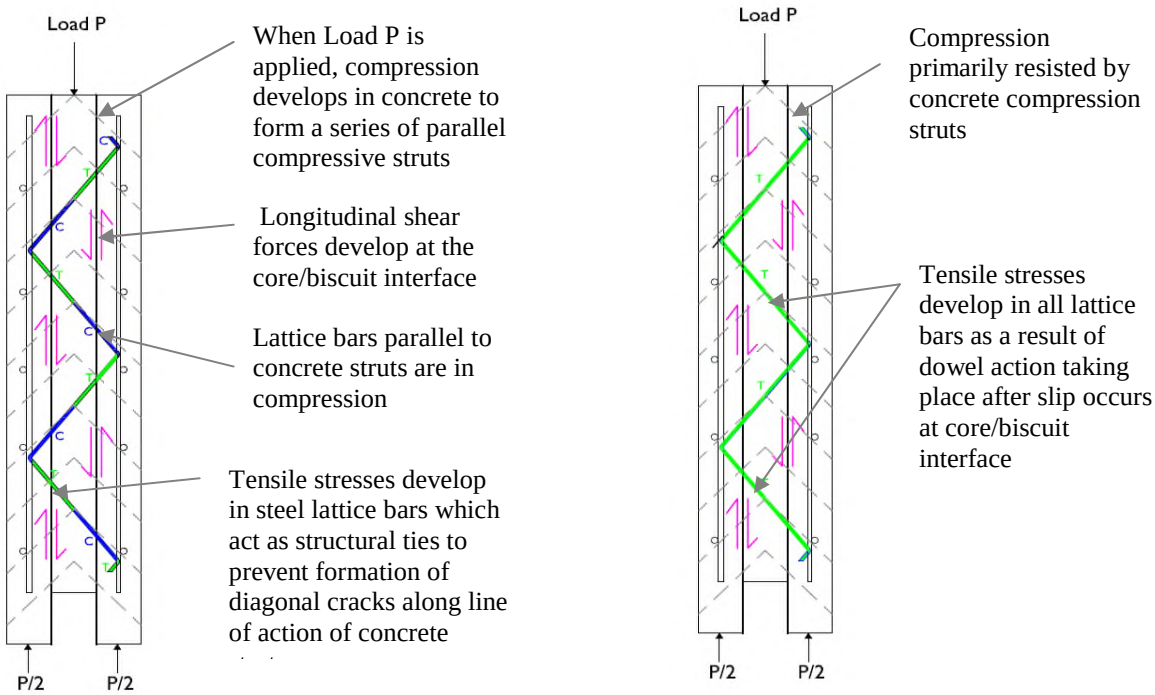

a) Prior to slip

b) After slip occurs

Figure 3.1 - Forces developing in twinwall in push-out test

Tensile forces develop in some of the lattice bars which act as structural ties to prevent the formation of diagonal cracks along the line of action of the compressive struts as shown in Figure 3.1(b). As the load P continues to increase, slip occurs at the core/biscuit interface. At this point, tensile forces develop in all the lattice bars and the slip is resisted by bending of the lattice bars at the core/biscuit interface (dowel action). The dowel strength of the shear connector is a function of four main parameters including the cross-sectional area of the dowel, the tensile strength of the dowel, the compressive strength of the concrete and the concrete modulus (Oehlers and Bradford:1995).

The push-out test therefore closely replicates the structural actions taking place in twinwalls in water tank applications and can be used to determine the shear behaviour of the twinwalls.

However, the twinwall is also fundamentally different from standard push-out specimens since it is made up of a concrete core instead of the commonly used steel I-section. Additionally, the shear connector used twinwalls is a three-dimensional lattice girder which is fully embedded in the concrete biscuits and core in comparison with shear connectors (e.g. studs) use in standard push-out tests which do not extend to the full width of the push-out tests specimens. Hence, the structural behaviour of the twinwalls under push-out tests may be significantly different from that observed in standard push-out tests.

It was also highlighted in the literature review that the experimental data obtained from the push-out test can be significantly influenced by several parameters including the

friction at the base of the concrete slabs, the number of shear connectors per concrete slab, the reinforcement in concrete slabs and the direction of concrete placing. The lattice girder used is three-dimensional and in order to satisfy the general geometric requirements of Annex B, EC4 and 480 mm long lattice girder was used in experimental tests. This ensured that a minimum of two nodes and eight diagonal bars were provided in each concrete biscuit so that good rotational stiffness and redistribution of forces was achieved. Adequate transverse reinforcement was also provided in the concrete biscuits in order to prevent the formation of longitudinal splitting cracks. Particular attention was given to the direction of concrete placing by casting all specimens in a horizontal position so that no voids or bleeding occurred at the lattice/concrete interface. In addition, the friction at the base of the specimens was be investigated by varying the restraints in the push-out test specimens. This ascertained that the push-out test data obtained are not overestimated thereby providing more conservative estimates of the shear strength values.

3.2.2 Test Details

In light of the above, two sets of tests were carried out:

a) Set 1: **Influence of Size Effects**

The first set was used to determine the correct test methodology in terms of test specimen geometry, test method and loading regime. This was carried out in order to determine the influence of size effects on the behaviour of twinwalls as well as to optimise the efficiency of the testing regime and improve the reliability of the results

obtained. Results from ‘large-scale specimens’ were compared with those from ‘small-scale specimens’.

b) Set 2: Investigation of the parameters influencing the interface shear strength

Further to the tests in Set 1, consequent tests were carried out to determine the effect of varying several parameters on the behaviour of twinwalls. The following key parameters were investigated:

1. *Restraints* at the base of the test specimens
2. *Surface roughness* of the concrete at the core/biscuit interface
3. *Compressive strength of the concrete* in the core and biscuits
4. *Embedment depth* of the lattice shear connector
5. *Dowel bar diameter* (i.e. diameter of the diagonal bars of the lattice girder)

3.3 Set 1

3.3.1 Introduction

As discussed previously, the main aim of this test was to determine the influence of size effects in order to optimise the test methodology to be adopted for Set 2 tests.

In the first set, the behaviour of large scale specimens was compared with that of smaller scale specimens. Large scale specimens were based on the actual geometry of twinwalls whereas small-scale specimens comprised proportionally smaller thicknesses

of the concrete biscuits and lattice bar diameters. This was undertaken in order to verify whether small scale specimens replicated the behaviour of large scale specimens. The use of small scale specimens would facilitate the preparation, casting, manoeuvring, instrumentation and testing of the test specimens thereby resulting reducing errors and increasing the accuracy of the test measurements.

3.3.2 Details of test specimens

Details of the test specimens used for the push-out tests are shown in Figures 3.2 and 3.3. In the large scale specimens referred to as Type P1, the outer biscuits (1 and 2) (530mm long x 200mm wide x 80mm deep) were reinforced with three 12 mm diameter and five 16 mm diameter steel bars steel bars placed mid-depth at 60 mm centres in the longitudinal direction and 75 mm and 100 mm centres in the transverse direction. The lattice girder was 300 mm deep. The diagonals and bottom bars were 8 mm diameter and the top bar 10 mm diameter.

In the small scale specimens referred to as Type P2, the two outer biscuits (1 and 2) (530mm long x 100mm wide x 40 mm deep) were reinforced with 4 mm diameter mild steel bars placed mid-depth at 40 mm centres in the longitudinal direction and 75 mm and 100 mm centres in the transverse direction. The lattice girder was 80 mm deep. The diagonals and bottom bars were 3 mm diameter and the top bar 5 mm diameter.

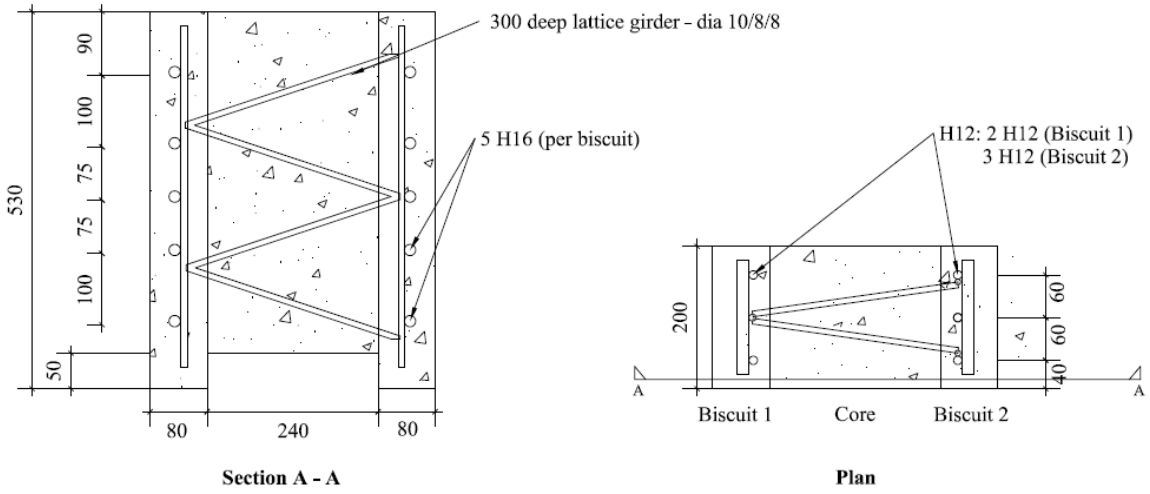

Figure 3.2 - Details of Large Scale Push-out Test Specimens: P1

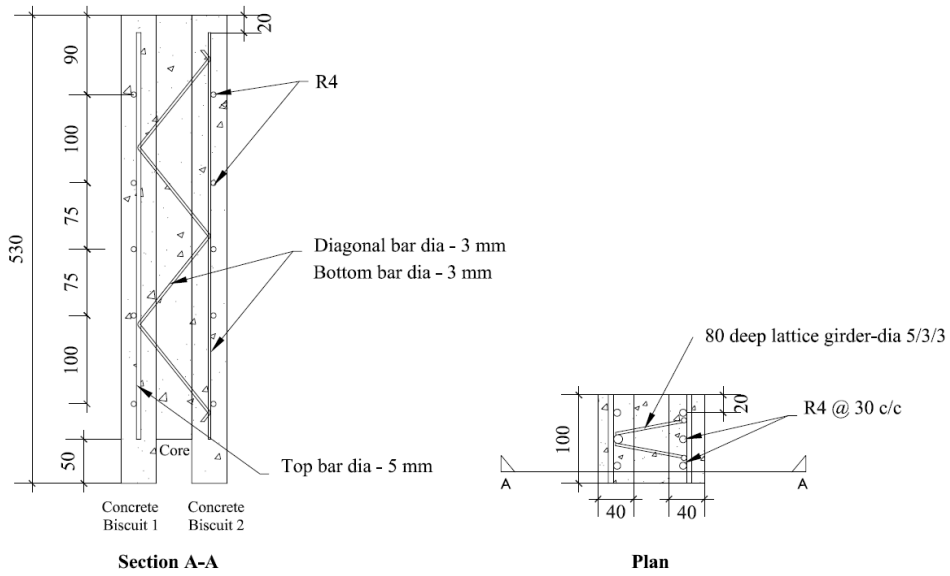

Figure 3.3 - Details of Push-out Test Specimens: P2

3.3.3 Materials

Details of the concrete mix for the target 28-day strength of 50 N/mm^2 are provided in Table 3.1. The concrete was designed assuming water/cement ratios of 0.50. Portland Cement (CEM1, Class 42.5/52.5), fine aggregates (0/4 natural sand with 60% of fine

particles passing the 0.6 mm sieve), coarse aggregates (4/10 graded uncrushed aggregate) and tap water were used where applicable.

Tensile tests were carried out on the reinforcement and lattice diagonal bars to determine the yield strength of the steel for types P1 and P2. Five bars were tested in each case and the average stresses and strains were calculated. The yield stress was taken as the proof stress occurring at 0.2% strain as summarised in Table 3.2 and Figure 3.4.

Materials	Type	
	P1	P2
Cement	0.450	0.770
Fine Aggregate	0.650	1.110
Coarse Aggregate	0.935	-
Water	0.225	0.385

Table 3.1 – Batch Weights of Concrete – P1 and P2

Type	Yield strength, f_y (N/mm^2)	
	Reinforcement	Lattice Leg
P1	576	620
P2	267	280

Table 3.2 – Yield Strength of steel bars – P1 and P2

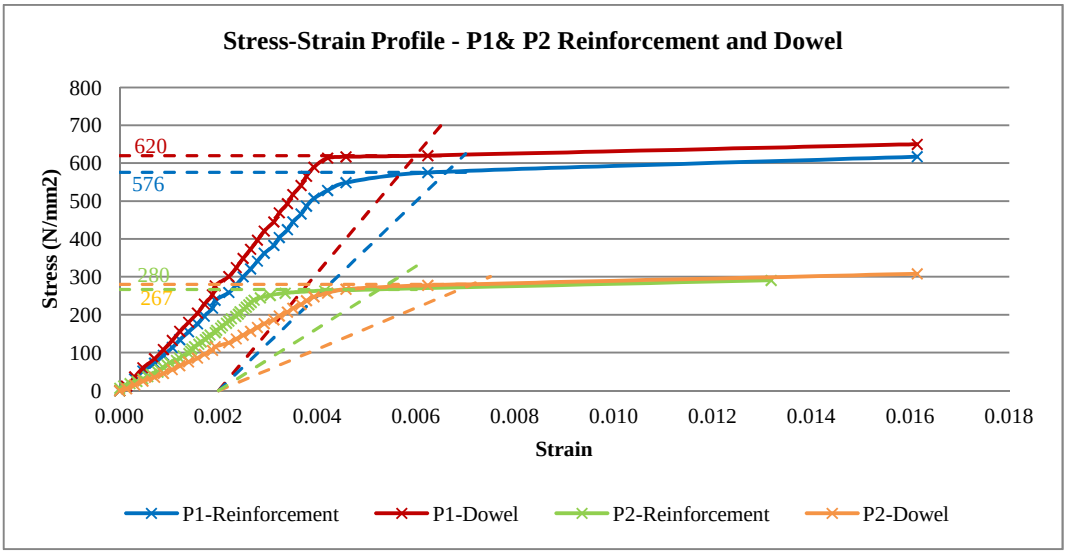

Figure 3.4 – Stress-Strain profile: P1& P2 Reinforcement and Dowel

3.3.4 Casting Procedure

The casting procedure for the specimens in Types P1 and P2 occurred in three main stages as shown in Figures 3.5 and 3.6. The bottom half of the reinforcement cage was placed in a clean timber mould and supported on spacers. Sufficient concrete was poured and compacted by vibration form Biscuit 1. The shaded area in Figure 3.5 represents the 'new' concrete poured on each day of casting. In P1 and P2, the lattices were embedded 40 mm and 20 mm into the concrete respectively.

After curing for 24 hours, the specimens were inverted and the upper half of the cage was supported on spacers to achieve the required embedment. The assembly was positioned in a second timber mould and concreted to form Biscuit 2. After curing the concrete in Biscuit 2 for 24 hours, the two sets of moulds were removed. Shuttering was then attached to the outside face and 50mm from the base of the specimens, and the core was cast. The shuttering was removed after 24 hours and the specimen air conditioned for a further seven days. Three cubes were also cast from each batch of concrete and cured and conditioned in the same way as the concrete in the test specimen.

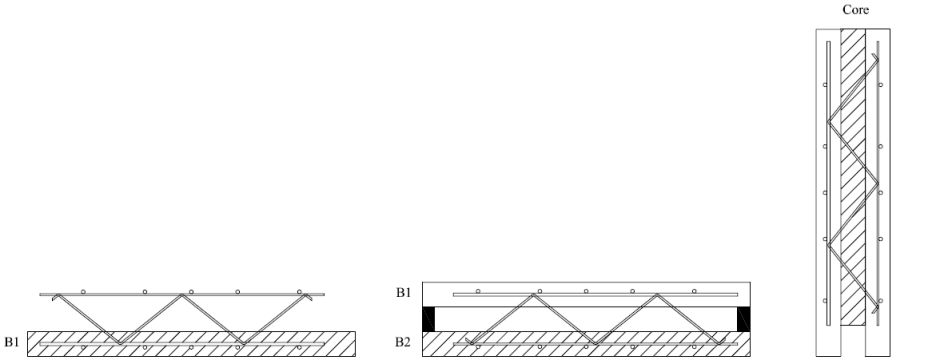

Figure 3.5 - Casting Procedure – P2

After a total of six days after the core was cast, the specimens were tested. The specimens were painted white to help monitor crack development during testing as shown in Figure 3.6. A total of five specimens were cast and tested for each specimen type.

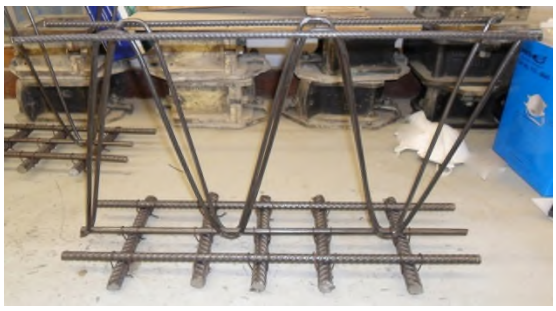

1) Lattice girder and reinforcement

2) Lattice and reinforcement placed in timber formwork and spacers used to achieve correct embedment depth

3) Biscuit 1 is cast on Day 1

4) Biscuit 1 24 hours after casting

5) Concrete poured to form Biscuit 2 on Day 2

6) Biscuit 2 24 hours after casting

8) New formwork mounted and core is cast on Day 3

9) Specimen painted white and steel plate mounted on top of core

Figure 3.6 - Casting Procedure – P1

3.3.5 Test Set-up

The push-out tests on P1 and P2 test specimens were carried out with reference to the recommendations made in Annex B of Eurocode 4 (BS EN 1991-1:2004). This requires the load to be applied in four distinct stages: up to 40 % of expected failure load, 25 times between 5% and 40% of the expected failure load, up to failure load ensuring that failure does not occur in less than 15 minutes and beyond failure until the load has dropped to 20% below maximum load. Hence, the failure load had to be predicted prior to the tests.

Ignoring any effects at the core-biscuit interface of the test specimens, failure was assumed to occur as a result of the yielding of the diagonal bars in the lattice girder. Hence, the predicted failure load was calculated as: Failure load = Number of diagonal bars x Area of diagonal bars x Yield stress (Table 3.3). The results for P1 and P2 are summarised in Table 3.3.

Properties	**Type**	
	P1	**P2**
Bar Diameter (mm)	8	3
Yield Strength	680	280
Failure Load (kN)	273	35

Table 3.3 – Calculated Failure Load – P1 and P2

From the above table, the failure loads for P1 and P2 were conservatively taken as 300 kN and 40 kN respectively. For P1, the load was therefore first increased to 120 kN (40 % of predicted failure load), then 25 times between 15 kN (5 % of predicted failure load) and 120 kN (40 % of predicted failure load), up to the failure load and beyond failure until the load dropped to approximately 240 kN (20 % below predicted failure

load). For P2, the load was first increased to 10 kN, then 25 times between 2 kN and 10 kN, up to the failure load and beyond failure until the load dropped to approximately 32 kN.

All test specimens were correctly positioned in a universal testing machine with a capacity of 500 kN and load was applied to the core according to the loading pattern discussed above. Failure was taken as the maximum load attained by the specimen. Figure 3.7 shows the test set-up for P1 and P2 specimens. At each load increment, the deflection at the bottom of the core was measured using dial gauges. The general behaviour of the specimens was also observed with particular attention to crack formation and propagation.

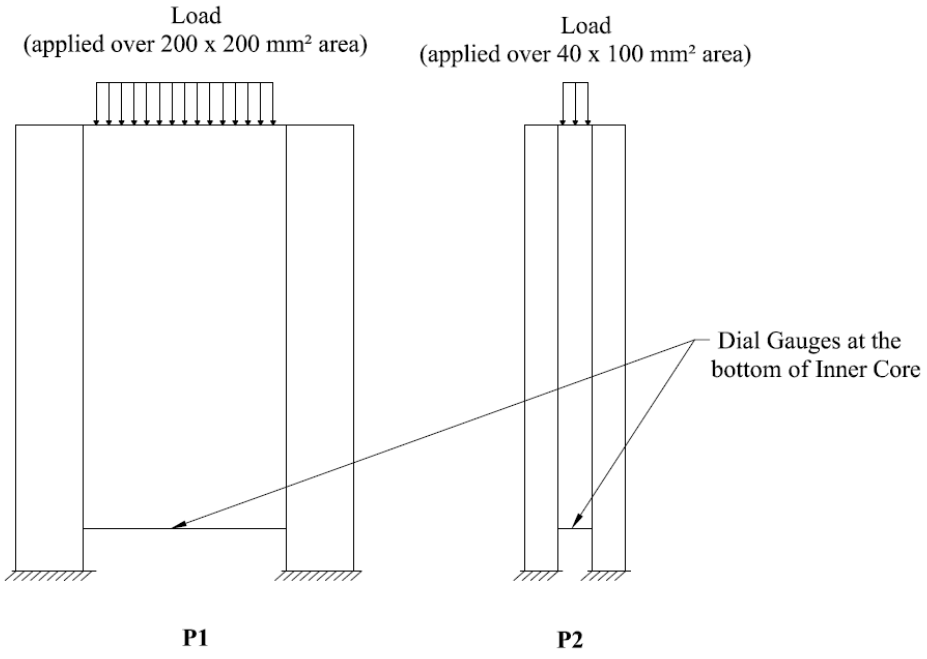

Figure 3.7 – Test set-up: P1 and P2

3.4 Set 2

Further to the preliminary test, further push-out tests were carried out to determine the effect of varying the following parameters on the shear strength of twinwall specimens:

1) Restraints at the base of the test specimens
2) Surface roughness of the concrete at the core/biscuit interface
3) Compressive strength of the concrete in the core and biscuits
4) Embedment depth of the lattice shear connector
5) Diameter of the lattice bars.

3.4.1 Details of Test Specimens

A total of 12 sets of tests were carried out on the small scale specimens. Five specimens were tested for each specimen type A1-K1. Type A1 acted as the control specimen with a smooth surface roughness, an embedment depth of 20 mm, 28-day concrete strength of biscuits and core of 50 N/mm^2, top lattice bar diameter of 5 mm, diagonal lattice bar diameter of 3 mm, bottom bar diameter of 3 mm and with fixed base restraints. The geometry of type A1 specimen is shown in Figure 3.8.

In the other specimens, the surface roughness at the inner face of the biscuits, embedment depth of the lattice in the biscuits, the strength of the concrete used for the biscuits and core and restraints at the supports of Biscuits 1 and 2 was varied as summarised in Table 3.4 and Figure 3.9.

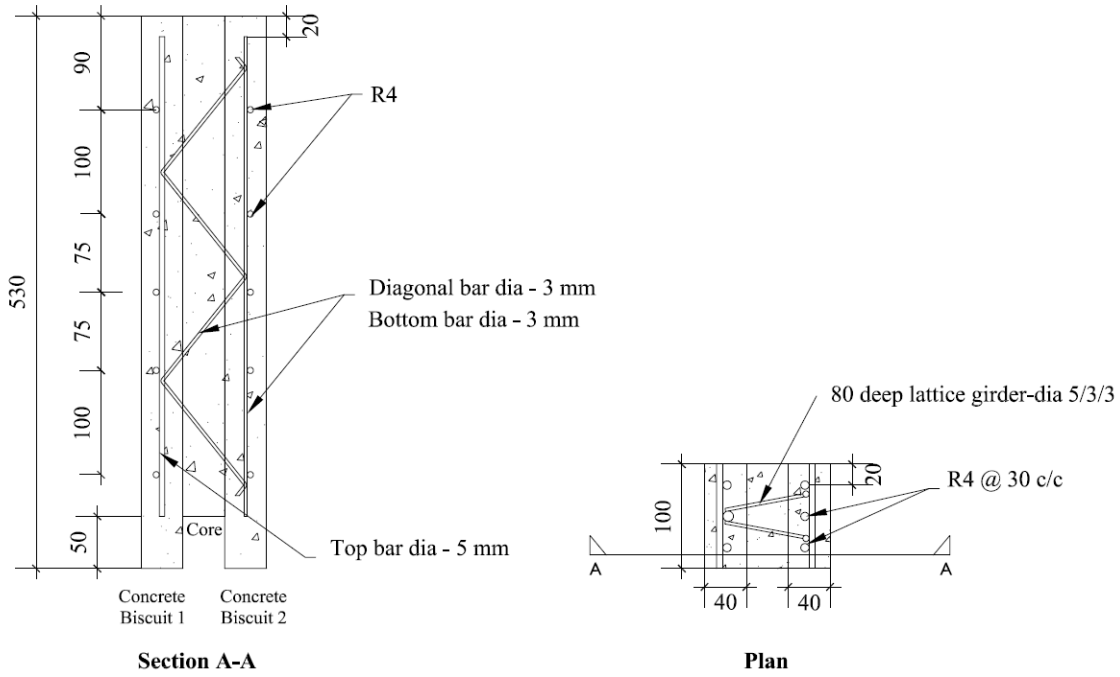

Figure 3.8 - Details of Push-out Test Specimens: A1

Type	Surface Roughness	Embedment Depth	Concrete Strength	Diameter of Lattice bars	Base Restraints
A1	Smooth	20mm	50N/mm^2 – Biscuit 1 50 N/mm^2 – Core 50N/mm^2 – Biscuit 2	Top – 5 mm Diagonal – 3 mm Bottom - 3 mm	Fixed/Fixed
B1	"	"	"	"	PTFE/PTFE
C1	"	"	"	"	Fixed/Roller
D1	"	"	"	"	Roller/Roller
E1	Very	"	"	"	Fixed/Fixed
F1	Rough	"	"	"	"
G1	Smooth	"	50N/mm^2 – Biscuit 1 10 N/mm^2 – Core 50N/mm^2 – Biscuit 2	"	"
H1	"	"	10N/mm^2 – Biscuit 1 50 N/mm^2 – Core 10N/mm^2 – Biscuit 2	"	"
I1	"	15 mm	50N/mm^2 – Biscuit 1 50 N/mm^2 – Core 50N/mm^2 – Biscuit 2	"	"
J1	"	25 mm	"	"	"
K1		20 mm	"	Top – 8 mm Diagonal – 6 mm Bottom – 6 mm	"

Table 3.4 – Test Details – Types A1-K1

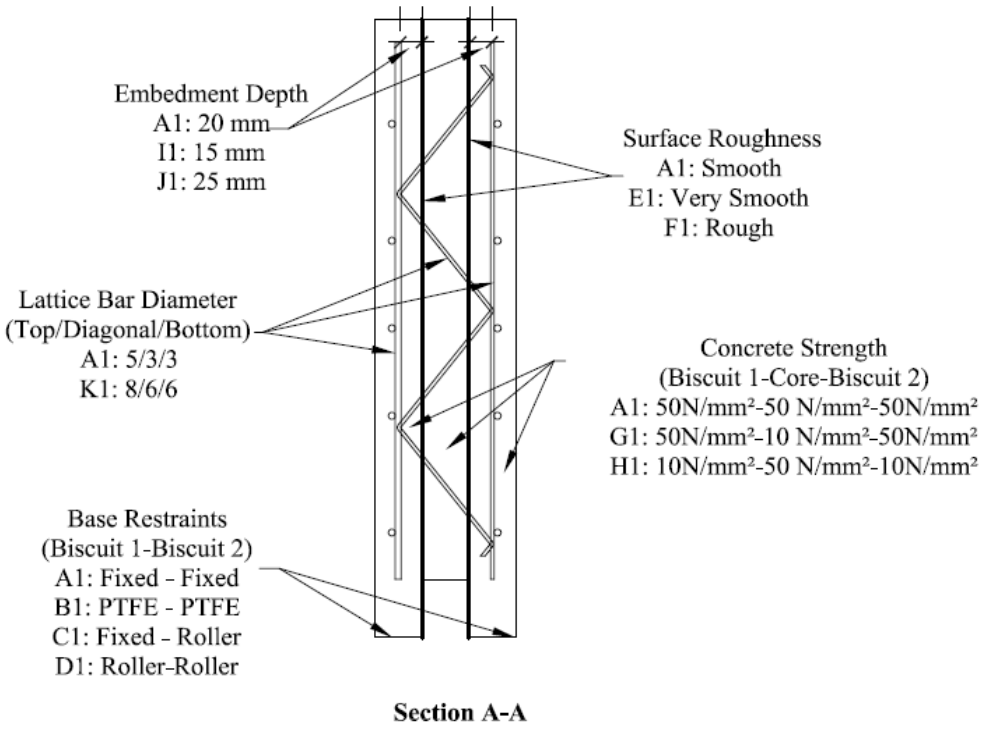

Figure 3.9 - Details of Push-out Test Specimens: Parameters varied – Types A1-K1

3.4.2 Materials

Details of the concrete mix for the target 28-day strength of 50 N/mm^2 and 10 N/mm^2 (Ref. G1/H1, Table 3.4) are provided in Tables 3.5 and 3.6. The concrete was designed assuming water/cement ratios of 0.50 and 0.90 for target strengths of 50 N/mm^2 and 10 N/mm^2 respectively. Portland Cement (CEM1, Class 42.5/52.5), fine aggregates (0/4 natural sand with 60% of fine particles passing the 0.6 mm sieve), coarse aggregates (4/10 graded uncrushed aggregate) and tap water were used where applicable.

Tensile tests were carried out on the reinforcement and lattice diagonal bars to determine the yield strength of the steel for types P2, A1-J1 (lattice bar diameter: 3 mm) and K1 (diagonal bar diameter: 6 mm). Five bars were tested in each case and the

average stresses and strains were calculated. The yield stress was taken as the proof stress occurring at 0.2% strain. For type A1-J1, the yield strength for the reinforcement and lattice bars were 267 N/mm^2 and 280 N/mm^2 respectively. For type K1, the yield strength for the reinforcement and lattice bars were 267 N/mm^2 and 240 N/mm^2 respectively.

Materials	**Batch Weights (kg/litre of concrete)**
	50 N/mm^2
	A1-F1, I1-K1
Cement	0.770
Fine Aggregate	1.110
Coarse Aggregate	-
Water	0.385

Table 3.5 – Batch Weights of Concrete: 50N/mm^2 mix

Materials	**Batch Weights (kg/litre of concrete)**
	10 N/mm^2
	G1-H1
Cement	0.610
Fine Aggregate	1.220
Coarse Aggregate	-
Water	0.550

Table 3.6 – Batch Weights of Concrete: 10N/mm^2 mix

3.4.3 Casting Procedure

A total of five specimens were cast and tested for each specimen type. The casting procedure for the control specimens for type A1 occurred in three main stages as shown in Figure 3.5 as discussed previously. Three cubes were also cast from each batch of concrete and cured and conditioned in the same way as the concrete in the test specimen.

3.4.4 Specific Test Details

Further details of the parameters varied in the push-out tests are provided below.

3.4.4.1 Base Restraints

In the case of specimen type A1, the bases of Biscuit 1 and Biscuit 2 were restrained by the base of the test frame. For type B1 specimens, a 10 mm thick PTFE (polytetrafluoroethylene) was placed between the bases of Biscuits 1 and 2 and the base of the testing machine to reduce friction. For type C1 specimens, the base of Biscuit 1 was restrained by a steel plate acting as a fixed support and Biscuit 2 was restrained a 10 mm thick steel plate supported over three 16 mm diameter steel bars to act as a roller support. For type D1 specimens, Biscuits 1 and 2 were restrained by the roller supports used for specimen type C1. The restraints at the base of Biscuits 1 and 2 are shown in Figure 3.10.

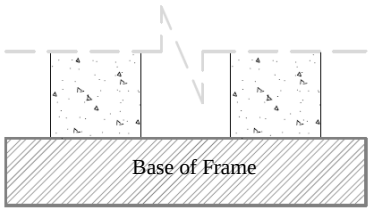

Type A1: Fixed/Fixed
Biscuits 1 and 2 restrained by base of frame

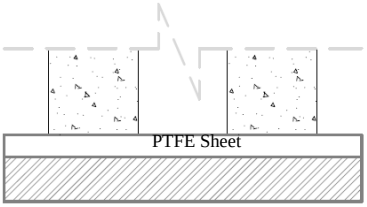

Type B1: PTFE/PTFE
Biscuits 1 and 2 restrained by 10 mm thick PTFE sheet

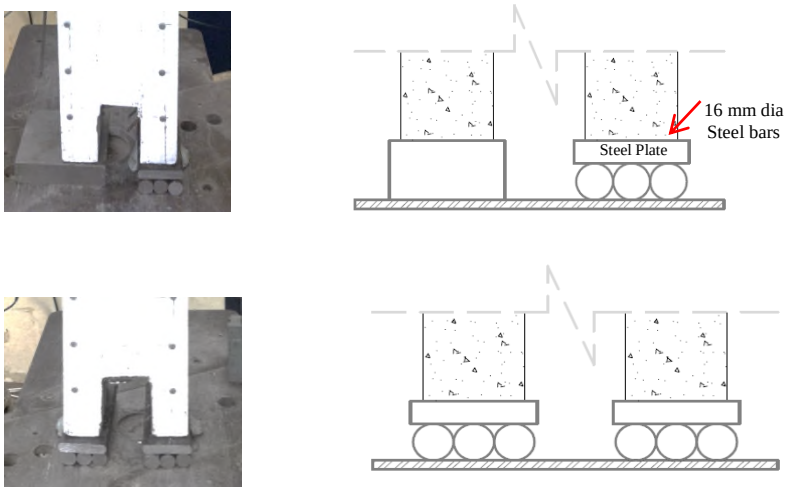

Type C1: Fixed/Roller
Biscuits 1 restrained by steel plate and Biscuit 2 restrained by steel plate and bars

Type D1: Roller/Roller
Biscuits 1 and 2 restrained by steel plates and bars

Figure 3.10 - Restraints at Base of Biscuits

3.4.4.2 Surface Roughness

In the case of type A1 specimens, the inner faces of each biscuit were left as cast which were designed to produce a finish corresponding to the "smooth" category in Section 6.2.5 of Eurocode 2 (EC2): Part1.1 (BS EN 1992-1-1:2004).

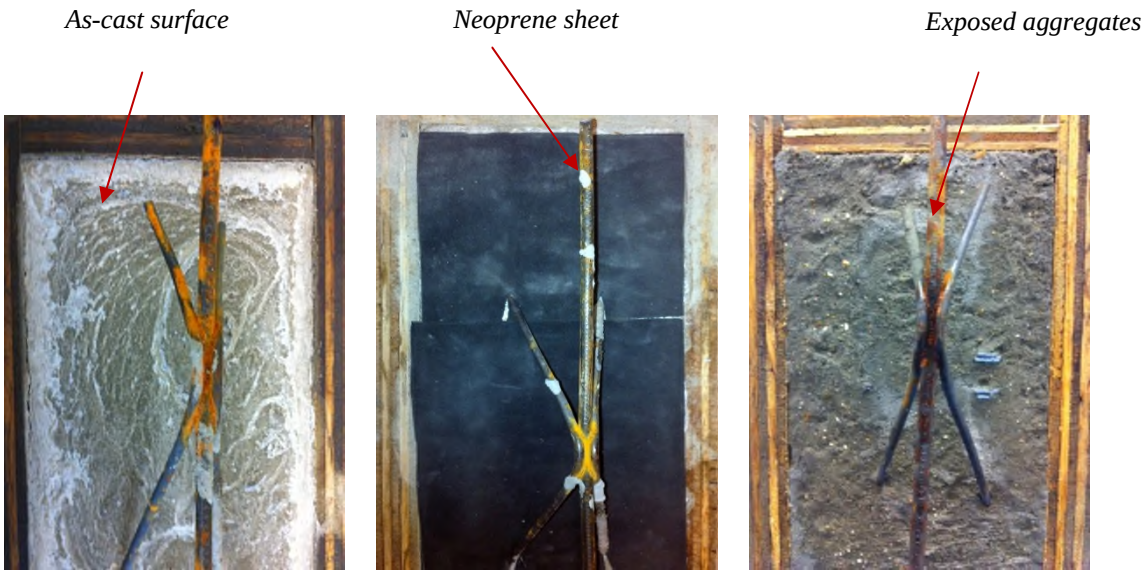

Type A - Smooth ***Type E – Very Smooth*** ***Type F - Rough***

Figure 3.11 – Surface Roughness: Finish of Biscuit Surfaces

For type E1 specimens a 3mm thick neoprene sheet was attached to the inner face of each biscuit prior to casting the core to correspond to the “very smooth” category in EC2. The exposed aggregate finish in type F1 specimens was achieved by painting the inner face of the biscuits with a retarder and pressure washing prior to removing cement particles. This finish was designed to accord with the “rough” category in EC2. The finishes for types A1, E1 and F1 specimens are shown in Figure 3.11.

3.4.4.3 Concrete Strength

In the case of specimen type A1, the target 28-day strength of concrete for both biscuits and the core was 50 N/mm^2. For specimen type G1, the target 28-day strength of the core only was decreased to 10 N/mm^2 and for specimen type H1, the target 28-day strengths for both biscuits only was decreased to 10 N/mm^2.

3.4.4.4 Embedment Depth

For specimen types A1, I1 and J1 specimens, 20 mm, 25 mm and 15 mm spacers were used to achieve embedment depths of 20 mm, 15 mm and 25 mm respectively. These values were based on the critical embedment depth of the test specimens.

The critical embedment depth was calculated in accordance with Clause 6.3.3 of Eurocode 4: BS EN 1994-1-1:2004 (EC4). The EC4 design resistance of shear connectors are derived from the following equations:

$P_{Rd} = (0.8\, f_u\, \pi\, d^2/4)\, /\gamma_v$ or: $P_{Rd} = (0.29\alpha d^2\, \sqrt{f_{ck} E_{cm}})\, /\gamma_v$

With: $\alpha = 0.2\ (h_{sc}/d + 1)$ for $3 \leq h_{sc}/d \leq 4$ and $\alpha = 1$ for $h_{sc}/d > 4$

where:

γ_v is the partial factor,

d is the diameter the shear connector,

f_u is the specified ultimate tensile strength of the material of the shear connector ,

f_{ck} is the characteristic cylinder compressive strength of the concrete,

h_{sc} is the overall nominal height of the connector.

Based on the above, the embedded depth of the lattice in the twinwall can be obtained by calculating the value of h_{sc}. In the case of the push-out test specimens,

- $f_u = 430 N/mm^2$ based on $f_y = 280\ N/mm^2$
- d = 4.24 mm (diameter equivalent to 2 no. lattice bars embedded in the concrete, $d = \sqrt{(2x\ л\ x\ 3^2\ /4)}$
- $f_{ck,cube} = 35\ N/mm^2$ (concrete target strength)
    - From EC2, Table 3.1, $f_{ck} = 28\ N/mm^2$ and $E_{cm} = 32{,}308\ N/mm^2$
- If it is assumed that $3 \leq h_{sc}/d \leq 4$, then $\alpha = 0.2\ (h_{sc}/d + 1)$

Thus:

$P_{Rd} = (0.8\ f_u\ л\ d^2/4)\ /\gamma_v = (0.29\alpha d^2\ \sqrt{f_{ck}E_{cm}}\ )\ /\gamma_v$

$\rightarrow 0.8\ f_u\ л\ d^2/4 = 0.29\alpha d^2\ \sqrt{f_{ck}E_{cm}} = 0.29\ x\ 0.2\ (h_{sc}/d + 1)\ x\ d^2\ \sqrt{f_{ck}E_{cm}}$

$\rightarrow 0.8\ f_u\ л\ /4 = 0.29\ x\ 0.2\ (h_{sc}/d + 1)\ x\ \sqrt{f_{ck}E_{cm}}$

$\rightarrow 0.8\ x\ 280\ x\ л\ /4 = 0.29\ x\ 0.2\ (h_{sc}/4.24 + 1)\ x\ \sqrt{28x32{,}308} \rightarrow$ ***$h_{sc} = 16.5\ mm$***

Thus, the critical embedment depth of the test specimens is 16.5 mm.

3.4.4.5 Diameter of Lattice Bars

In the case of specimen type A1, the diameters of the top, diagonal and bottom bars of the lattice were 5 mm, 3 mm and 3 mm respectively. For specimen type K1, the diameters of the top, diagonal and bottom bars of the lattice were increased to 8 mm, 6 mm and 6 mm respectively.

3.4.5 Test Set-Up

Figure 3.12 shows the test set-up for specimen types A1-K1. The push-out tests carried out were derived from the recommendations made in Annex B of Eurocode 4 (BS EN 1991-1:2004). Firstly, the cyclic loading and unloading phase (5% to 40% - 25 cycles) was not carried out during the tests. Based on the results of Set 1, it was determined that the cyclic loading and unloading phase resulted in an increase of up to 1% of the total deflection. Additionally, the last unloading phase of the EC4 where the deflections should be measured beyond the failure load was not carried out. This is because the testing machine used was not sensitive enough to capture the decrease in the load and increase in the deflections beyond the failure load.

The test specimens were correctly positioned in a universal testing machine with a capacity of 500 kN as shown in Figure 3.12. Load was applied to the core in 2 kN increments until failure. Failure was taken as the maximum load attained by the specimen. At each load increment, the deflection at the bottom of the core was measured using dial gauges and the lateral displacement of the test specimen was measured using DEMEC studs positioned at 100 mm centres on the two outer biscuits.

The general behaviour of the specimens was also observed with particular attention to crack formation and propagation.

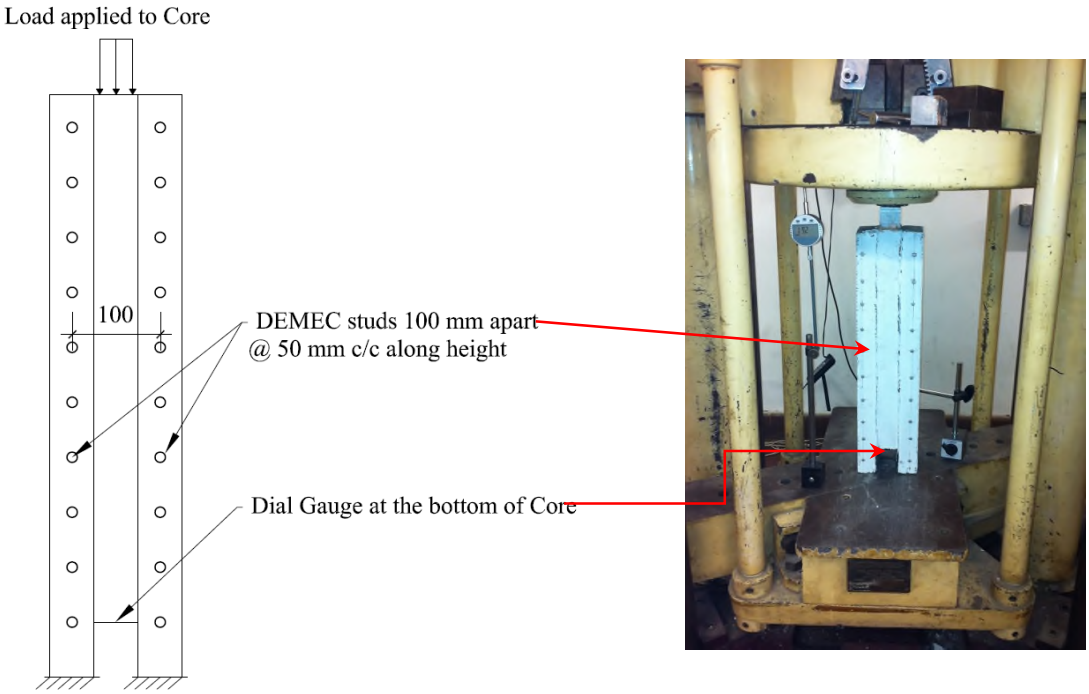

Figure 3.12 – Typical Push-out Test Set-up

3.4.6 Comparison with Theoretical Approach

The failure load obtained from the experimental push-out tests was compared with the theoretical approach adopted by EC2. In Chapter 2, it was discussed that longitudinal shear stress at the (precast/in-situ) concrete interface, v_{Rdi}, can be theoretically calculated using Section 6.2.5 of Eurocode 2 (EC2): Part1.1 (BS EN 1992-1-1:2004). This is given by:

$$v_{Rdi} = c\, f_{ctd} + \mu\sigma_n + \rho\, f_{yd}\,(\mu \sin\alpha + \cos\alpha) \leq 0.5\, v\, f_{cd}$$

Equation 3.1 – EC2 Interface Shear

where, f_{ctd} is the design tensile strength of concrete; f_{yd} is the design yield strength of reinforcement; σ_n is the stress per unit area caused by an external normal force across the interface; $\rho = A_s/A_i$; A_s is the area of reinforcement crossing the interface, with adequate anchorage at both sides of the interface; A_i is the area of the joint; α is the angle between reinforcement and slip surface, but $45^0 < \alpha < 90^0$; c is the coefficient of cohesion; and μ is the coefficient of friction.

According to the above, the interface shear is dependent on the roughness of the concrete at the core/biscuit interface, compressive strength of the concrete and the embedment depth of the shear connectors. The theoretical failure load for the push-out specimens was therefore calculated and compared with the experimental results. The following assumptions were made:

- It was assumed that there are no external normal forces, i.e. $\sigma_n = 0$,
- A_i = 48,000 mm^2 [= 480 mm (lever arm) x 100 (width)] , A_s = 57 mm^2 (= $8\times\pi 3mm^2/4$)
- f_{ctd} was taken as the lowest experimental cube compressive strength of the concrete
- f_{yd} was taken as 280 N/mm^2 and 340 N/mm^2 for types A1-J1 and K1 respectively
- EC2 equation imposes a limit of $45^0 \leq \alpha \leq 90^0$ for the angle of inclination of the dowel, α. For the lattice girders used in the push-out tests, the angle $\alpha = 38^0$ [$\tan^{-1}$ (80/100)] which lies outside the EC2 limits. Thus, the failure load is calculated for an inclination angle of $\alpha = 38^0$ (actual) and $\alpha = 45^0$ (EC2 limit).

Experimental and theoretical results of the push-out tests in Phase I are presented and discussed in Chapter 4.

Chapter 4

Phase I: Results and Discussion

Push-out Tests

4.1 Introduction

As discussed in Chapter 3, two sets of push-out tests were carried out: Set 1 and Set 2. Set 1 aimed at improving the push-out test methodology in terms of specimen size and testing regime while Set 2 was carried out to investigate the effects of several parameters influencing the interface shear behaviour of twinwalls.

In Set 1, the influence of size effects (i.e. large scale vs. small scale test specimens) was investigated. In Set 2, push-out tests were carried out using the small scale specimen from Set 1 to determine the influence of the following parameters on the interface shear behaviour of twinwalls: (1) restraints at the base of the test specimens, (2) roughness at the biscuit/core interface, (3) compressive strength of the concrete in the biscuits and the core, (4) embedment depth of the lattice girder in the biscuits and (5) dowel bar diameter (i.e. diameter of the lattice diagonal bars).

The results from the experimental tests from both Set 1 and Set 2 are presented and discussed in terms of the following:

1) *Compressive strength of concrete*: 7-day cube compressive strength of the concrete in Biscuit 1, Biscuit 2 and the core.
2) *Failure Load*: Maximum load applied to the test specimens
3) *Deflection at failure*: Maximum deflection at the bottom of the core of the test specimens
4) *First Crack Load*: Load at which the first crack occurs in the test specimens, expressed as a percentage of the failure load
5) *Load-Deflection Profile*: Deflection observed at the bottom of the core in test specimens plotted for each load increment
6) *Variation of Lateral Deflection*: Readings from the DEMEC gauges at each load increment plotted against the (1) load and (2) height from the bottom of the test specimens
7) *Failure Mechanism*: General behaviour of the test specimens in terms of cracking and failure mechanism observed

4.2 Set 1

4.2.1 Concrete compressive strength

4.2.1.1 Results

The specimens were tested on the seventh day from the day when the core was cast. Thus, a 7-day compressive strength of approximately 70 % of the target 28-day

compressive strength was expected. The target 7-day strength was 35 N/mm^2 for the 50 N/mm^2 mix. The compressive strengths are based on the strengths of three concrete cubes cast on the day of each concrete pour. Results are summarised in Table 4.1.

Compressive Strengths (N/mm^2)	P1			P2		
	B1	**B2**	**Core**	**B1**	**B2**	**Core**
Cube 1	39.65	39.05	40.50	39.30	36.70	35.00
Cube 2	39.20	40.65	39.75	36.80	36.30	35.00
Cube 3	38.45	38.10	39.05	36.90	36.00	36.20
Mean	37.67	36.33	35.40	39.75	37.80	36.43
Standard Deviation	1.42	0.35	0.69	0.64	0.53	0.40

Table 4.1 – P1 and P2 : Compressive Strengths

4.2.1.2 Discussion

From Table 4.1, it is observed that the average compressive strengths of the concrete for the core and biscuits of P1 and P2 are greater than the target strength of 35 N/mm^2. The standard deviations of the concrete ranged from 0.35 N/mm^2 to 1.42 N/mm^2 which accounted for 1.00 % - 4.06 % of the target 35 N/mm^2 concrete strength. Hence, the compressive strengths obtained were deemed as being satisfactory.

4.2.2 Failure Load

4.2.2.1 Results

The loads of all test specimens at failure are given in Table 4.2. The average values are based on the results from the five specimens tested for each set.

Specimen No.	Failure Load	
	P1	P2
1	260	40
2	256	42
3	260	40
4	258	42
5	260	42
Average	258	41

Table 4.2 – P1 and P2: Load at Failure

4.2.2.2 Discussion

From Table 4.2, it is observed that the failure load of the large scale specimen in P1 is approximately 6.5 times greater than that in P2 with the small scale specimens. This is expected since the greater diameters of the lattice girder bars and the concrete biscuits increase the shear strength of the test specimens in P1.

4.2.3 Deflection at Failure

4.2.3.1 Results

The deflections at the bottom of the core (bottom deflection) for all specimens are given in Table 4.3. The deflections for each test specimen are the average values of two dial gauge readings recorded at each load increment.

Specimen No.	Bottom Deflection	
	P1	P2
1	3.46	0.90
2	3.11	1.08
3	3.07	0.87
4	3.33	1.01
5	3.00	1.37
Average	3.19	1.05

Table 4.3 – P1 and P2: Bottom Deflections at Failure

4.2.3.2 Discussion

The average deflections at the bottom of the core for P1 and P2 are 3.19 mm, 1.05 mm respectively. The increase in the bottom deflection in P1 can be attributed to the significantly higher failure loads in the test specimens in comparison with those in P2.

4.2.4 Change in Bottom Deflection due to Cyclic Unloading/Loading

4.2.4.1 Results

The changes in the bottom deflection at 40% of the failure load before and after the cyclic unloading (5% of failure load) and loading (40% of failure load) in P1 and P2 specimens are presented in Table 4.4.

Specimen No.	Bottom deflection before and after cyclic unloading/loading at 40% of failure load (mm)					
	P1			P2		
	Before	After	Change	Before	After	Change
1	0.82	0.85	0.02	0.00	0.00	0.00
2	0.58	0.58	0.00	0.06	0.07	0.01
3	0.69	0.71	0.02	0.09	0.09	0.00
4	0.40	0.41	0.01	0.00	0.00	0.00
5	0.75	0.77	0.02	0.11	0.12	0.01

Table 4.4 – P1 and P2: Changes in bottom deflection due to cyclic unloading/loading

4.2.4.2 Discussion

From the above results, it can be seen that cyclic unloading and loading leads to maximum increases of 0.02 mm for P1 and 0.01 mm for P2. This accounts for approximately 0.63% and 0.43% of the average bottom deflections (Table 4.3) recorded for P1 and P2 respectively. The increase in deflection may be attributed to the decrease (unloading) and increase (loading) in aggregate interlock action which occurs at the interfaces between the biscuit and the core due to the aggregates at the interface sliding over each other. However, since no cracking was observed at the core/biscuit interface during the cyclic unloading/loading phase, it can be concluded that the effect of the cyclic unloading and loading is not critical to the failure and shear strength of the push-out test specimens.

4.2.5 First Crack Load

4.2.5.1 Results

The first crack in the test specimens occurred at the core/biscuit interface. The crack either occurred across the core/biscuit 2 interface with a second crack occurring shortly

afterwards at the core/biscuit 1 interface or it occurred simultaneously at both core/biscuit interfaces. The loads at which the first crack occurred for each type are given in Table 4.5.

Specimen No.	Load at which first crack occurs (kN)			
	P1		P2	
	Load	% Failure Load	Load	% Failure Load
1	200	77%	32	76%
2	210	82%	30	75%
3	200	77%	34	81%
4	190	74%	34	85%
5	200	77%	34	81%

Table 4.5 – P1 & P2: First Crack Load

4.2.5.2 Discussion

The first crack occurs at a minimum of 74 % and 75 % of the failure load for P1 and P2 specimens respectively. The results show that the load at which the first crack forms does not depend on the geometry of the test specimens used. The first crack load could therefore be interpreted as the point at which the aggregate interlock forces are overcome causing the core/biscuit interface to slip relative to each other. Additionally, the first crack load could be taken as the serviceability limit for design purposes under which cracking would not be expected in twinwalls. It can be concluded that in twinwalls where lattice girders are used as shear connectors, cracking is not expected under serviceability loads of approximately 70%.

4.2.6 Load-Bottom Deflection Profile

4.2.6.1 Results

The strength of shear connectors depends on their ability to redistribute shear forces among themselves which is determined by their load/deflection characteristics. The load-bottom deflection profile obtained from push-out tests gives an indication of the stiffness and ductility of the shear connectors used. The load-bottom deflection curves for all specimens of P1 and P2 are plotted in Figures 4.1-4.2.

The load-bottom deflection profiles both P1 and P2 are also plotted relative to each other in Figure 4.3 to obtain a direct comparison between the results. The average bottom deflection for the five specimens tested for each test type is plotted for each load increment.

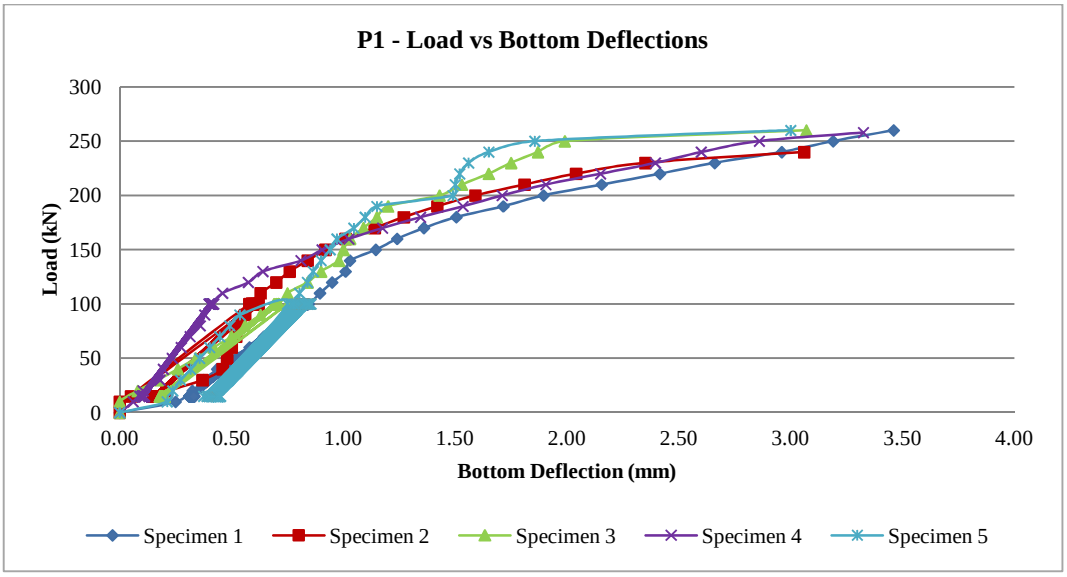

Figure 4.1 - Load v/s Bottom Deflection: P1

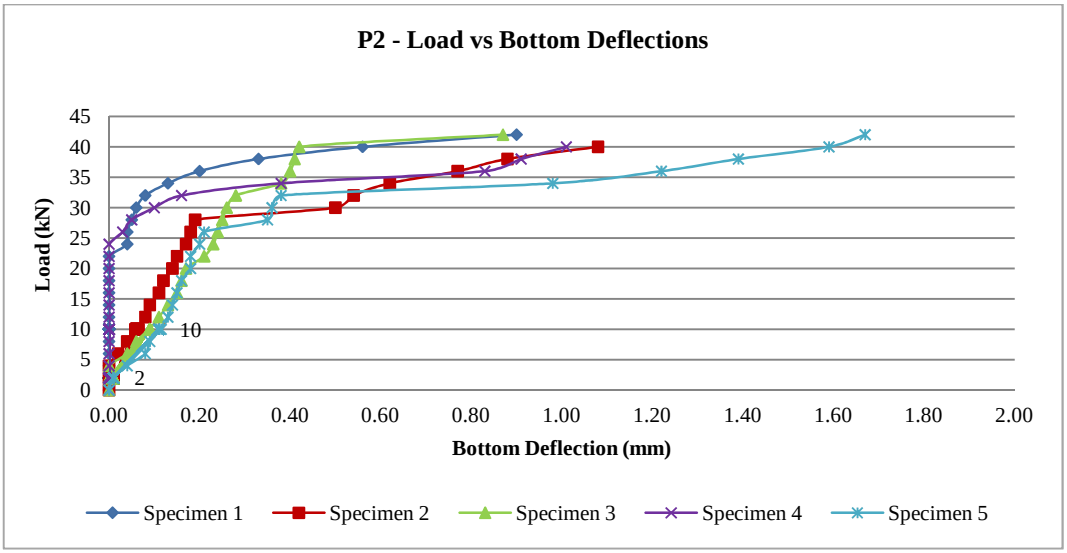

Figure 4.2 - Load v/s Bottom Deflection: P2

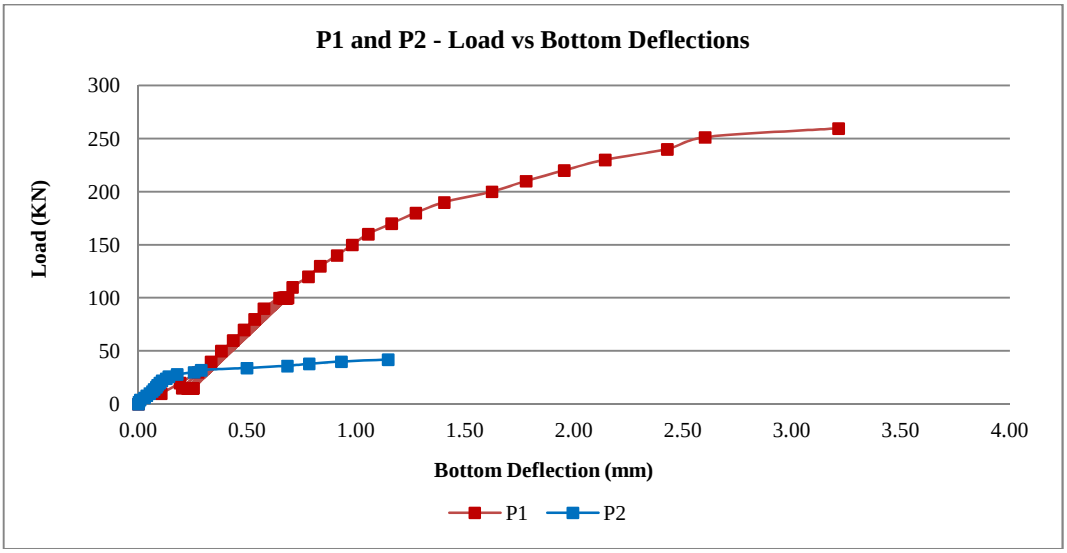

Figure 4.3 - Load v/s Bottom Deflection: Comparison between P1 and P2

4.2.6.2 Discussion

From Figures 4.1 and 4.2, it can be seen that all test specimens deform in three stages:

1. Firstly, the specimens deform elastically before the first crack appears with the load-deflection profiles being approximately linear. The cyclic loading/unloading

procedure results in an increase in deflection thereby shifting the load-deflection plots slightly to the right.

2. Cracking occurs at the core/biscuit interface which leads to a sharp increase in the bottom deflection. This is reflected by the horizontal shift observed in the load-deflection profiles at loads where the cracking occurs. When the load is applied, aggregate interlock takes place and the interfaces between the core and the biscuits slide against one another. As the load increases, slip occurs at the core/biscuit interface resulting in a crack being formed and an increase in bottom deflection is observed.

3. After cracking at the core/biscuit interface occurs, the specimens exhibit a non-linear load-deflection relationship until failure. At this stage, the aggregate interlock forces at the core/biscuit interface have been overcome and dowel action begins to occur in the lattice bars. Tensile forces are induced in the bars and the slip is resisted by bending of the lattice bars at the core/biscuit interface. This explains the non-linear behaviour in the load-deflection profiles.

All specimens also undergo significant deformations prior to failure. This shows that the lattice girder has good ductility and is effective in its use as a shear connector in twinwalls. The load-deflection plots for P1 and P2 in Figure 4.3 confirm that the specimens in both sets behave in the same manner. It can be concluded that the smaller scale specimens in P2 can be used to carry out subsequent push-out tests instead of the larger specimens in P1. This will facilitate the preparation, casting, manoeuvring,

instrumentation and testing of the test specimens thereby resulting reducing errors and increasing the accuracy of the test measurements.

4.2.7 Failure Mechanism

4.2.7.1 Results

The general behaviour of the test specimens was observed with particular attention to the formation of cracks during the push-out tests. In fact, the general behaviour of the test specimens of P1 and P2 was very similar.

When the load was increased, the first crack either occurred along the interface between the core and biscuit 2 which was closely followed by another crack along the core/biscuit 1 interface; or simultaneously along both interfaces. The first and second cracks occurred between 74 % and 82% of the failure load in P1 and between 75 % and 85 % of the failure load in P2.

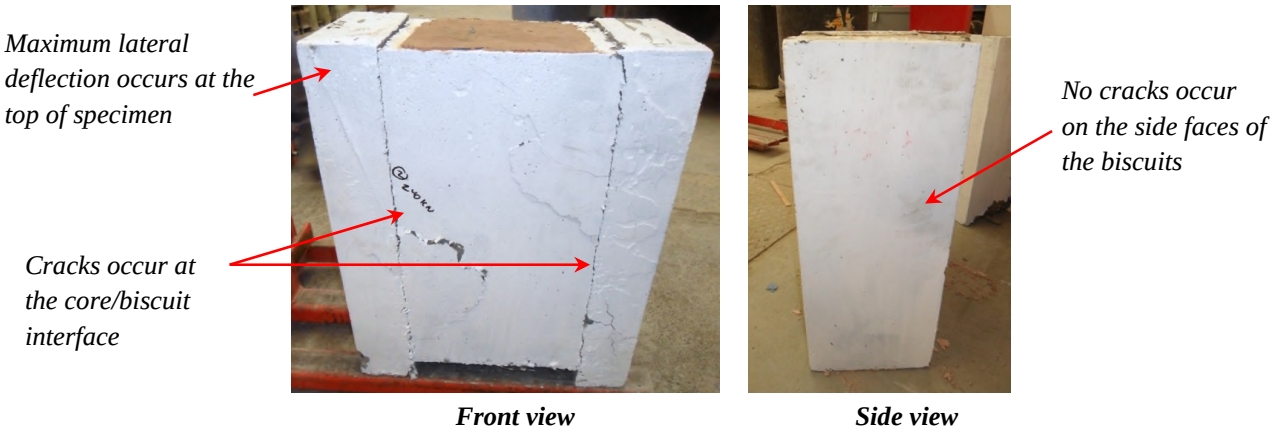

Figure 4.4 - General Behaviour of test specimens: P1

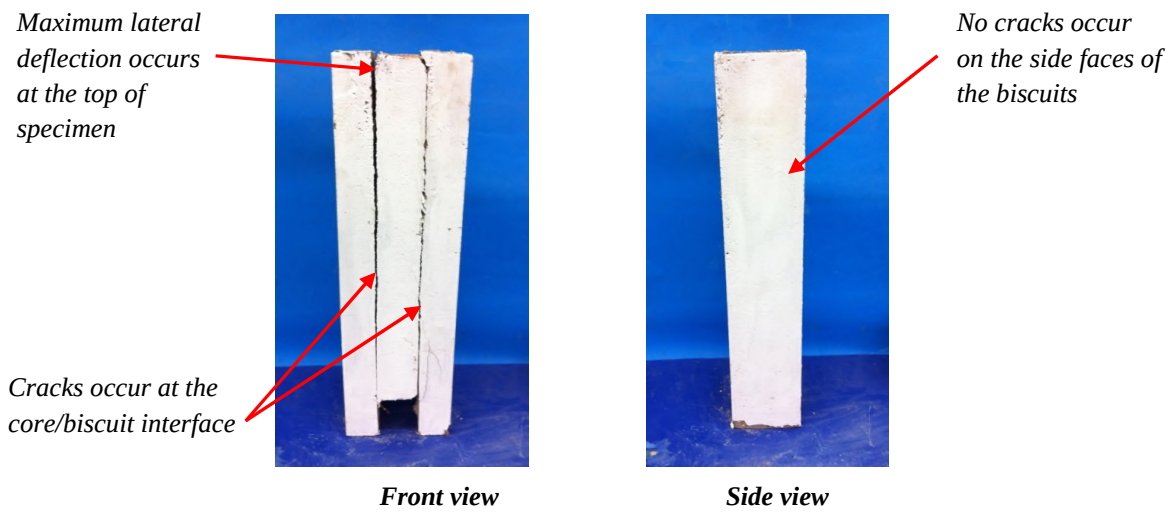

Figure 4.5 - General Behaviour of test specimens: P2

As the load continued to increase, the interface cracks deepened and further smaller cracks began to develop on the surface of the test specimens. This was closely followed by 'bang' noises suggesting the fracture of the lattice bars and excessive lateral and bottom deflections until the load began to drop beyond its maximum. It was also observed that the maximum lateral deflection occurred at the top of the specimens. No cracks occurred on the side faces of the biscuits. Figures 4.4 and 4.5 show typical push-out test specimens for P1 and P2 after failure.

The core was also removed after the tests to expose the lattice bars and to gain a better understanding of the failure mechanism of the test specimens as shown in Figures 4.6 and 4.7.

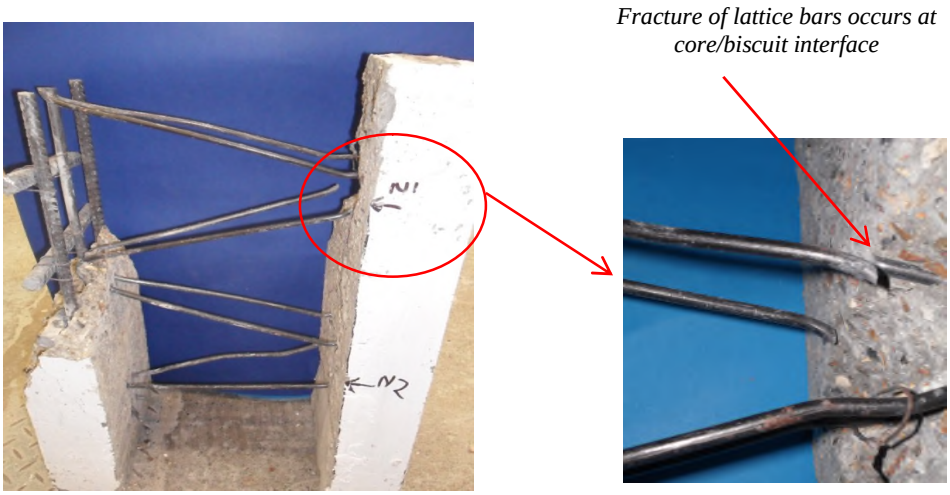

Figure 4.6 - Behaviour of specimens with core removed – P1

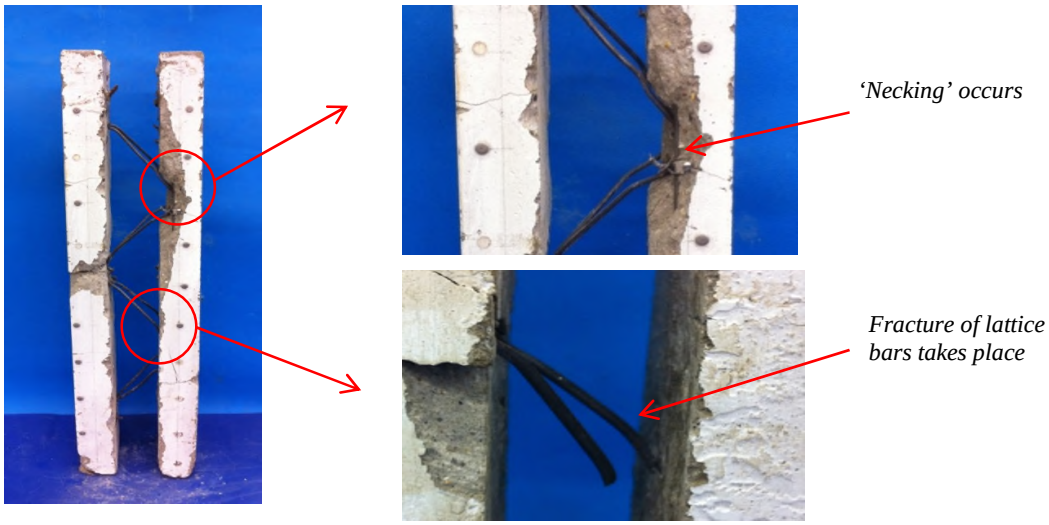

Figure 4.7 - Behaviour of specimens with core removed: P2

4.2.7.2 Discussion

The general behaviour gives an indication of the failure mechanism of the test specimens. As explained previously, when the load is applied, longitudinal shear forces develop along he interfaces between the core and the biscuits which are resisted by the aggregate interlock mechanism. As the load is increased further, cracking occurred at

the core/biscuit interface and dowel action was induced in the lattice bars which are subjected to tensile forces. This is confirmed by the necking and fracture observed in the diagonal bars. In addition, it can be concluded that failure of the test specimens is caused by steel yielding.

Another important observation was that no cracks were observed on the sides of the specimen. This confirms that the transverse reinforcement provided in the biscuits were adequate in preventing the formation of splitting cracks in the outer biscuits.

It was also observed that maximum lateral deflections occurred at the top of all test specimens. This can be partly due to the additional horizontal force induced at the shear connectors as a result of the friction at the base of the specimens as discussed previously. Hence, the lateral deflections need to be monitored and recorded in consequent push-out test in order to provide a better understanding of the behaviour of the test specimens.

It can also be seen that the specimens in P1 and P2 fail by steel yielding. Hence, the failure mechanism is not altered when small or large scale specimens are used. This confirms that the small scale specimens closely replicate the failure mechanism of large scale specimens. It can be concluded that small scale specimens can be used instead to large scale specimens to carry out subsequent push-out tests.

4.3 Set 2

This section presents the results of the push-out tests carried out on the twinwall specimens. As discussed previously, the effect of varying the following parameters on the shear strength of twinwall specimens was investigated:

a) *Restraints* at the base of the test specimens: Fixed/Fixed, PTFE/PTFE, Fixed/Roller and Roller/Roller.
b) *Surface roughness* of the concrete at the core/biscuit interface: 'very smooth', 'smooth' and 'rough'.
c) *Compressive strength* of the concrete in the core and biscuits: 50/50/50, 50/10/50n and 10/50/10.
d) *Embedment depth* of the lattice shear connector: 15 mm, 20 mm and 25 mm.
e) *Dowel bar diameter* of the lattice bars: 3 mm and 6 mm.

4.3.1 Compressive Strength of Concrete

All specimens were tested on the seventh day from the day when the core was cast. Thus, a 7-day cube compressive strength of approximately 70% of the target 28-day compressive strength was expected. The 7-day strength was 35 N/mm^2 and 7 N/mm^2 for the 50 N/mm^2 mix and 10 N/mm^2 mix respectively.

4.3.1.1 Results

The cube compressive strengths of the three cubes tested for Biscuit 1, Biscuit 2 and the Core for each specimen type (A1-K1) are summarised in Tables 4.6-4.10. Table 4.11 provides the average cube compressive strengths and the standard deviations for each specimen type.

Cube Compressive Strengths (N/mm^2)	A1: Fixed/Fixed			B1: PTFE/PTFE			C1: Fixed/Roller			D1: Roller/Roller		
	B1	B2	Core	B1	B2	Core	B1	B2	Core	B1	B2	Core
Cube 1	39.3	36.7	35	39.9	37.2	36.8	36.59	40.27	38.72	36.68	39.27	37.75
Cube 2	36.8	36.3	35	40.3	38.2	36.5	40.83	43.23	38.34	39.31	42.15	37.38
Cube 3	36.9	36	36.2	39.05	38	36	37.18	39.95	36.35	37.25	38.95	35.44
Mean	37.67	36.33	35.40	39.75	37.80	36.43	38.20	41.15	37.80	37.75	40.12	36.86
Standard Deviation	1.42	0.35	0.69	0.64	0.53	0.40	2.30	1.81	1.27	1.38	1.76	1.24

Table 4.6- Compressive strength – Base Restraints

Cube Compressive Strengths (N/mm^2)	A1: Smooth			E1: Very smooth			F1: Rough		
	B1	E1	Core	B1	E1	Core	B1	E1	Core
Cube 1	39.3	36.7	35	37.6	37.7	39.3	38.34	37.8	36.48
Cube 2	36.8	36.3	35	35.9	38.5	37.2	35.82	34.58	38.16
Cube 3	36.9	36	36.2	37.6	38.4	35.8	34.98	36.24	36.42
Mean	37.67	36.33	35.4	37.03	38.2	37.43	36.38	36.21	37.02
Standard Deviation	1.42	0.35	0.69	0.98	0.44	1.76	1.75	1.61	0.99

Table 4.7- Compressive strength - Surface Roughness

Cube Compressive Strengths (N/mm^2)	A1: 50/50/50			G1: 50/10/50			H1: 10/50/10		
	B1	E1	Core	B1	E1	Core	B1	E1	Core
Cube 1	39.3	36.7	35	38.38	37.12	7.02	9.36	35.00	9.44
Cube 2	36.8	36.3	35	35.44	36.12	7.74	10.14	32.48	8.92
Cube 3	36.9	36	36.2	37.54	38.38	6.6	8.86	37.76	7.72
Mean	37.67	36.33	35.4	37.12	37.21	7.12	9.45	34.08	8.69
Standard Deviation	1.42	0.35	0.69	1.51	1.13	0.58	0.65	2.64	0.88

Table 4.8- Compressive strength – Concrete Strength

Compressive Strengths (N/mm^2)	A1: Emb 20			I1: Emb 15			J1: Emb 25		
	B1	E1	Core	B1	E1	Core	B1	E1	Core
Cube 1	39.3	36.7	35	35.92	36.31	35.39	38.96	39.12	40.52
Cube 2	36.8	36.3	35	38.03	34.73	36.24	40.8	37.4	38.98
Cube 3	36.9	36	36.2	35.27	36.15	35.63	38.38	38.56	38.58
Mean	37.67	36.33	35.4	36.41	35.73	35.75	39.38	38.36	39.36
Standard Deviation	1.42	0.35	0.69	1.44	0.87	0.44	1.26	0.88	1.02

Table 4.9- Compressive strength – Embedment Depth

Compressive Strengths (N/mm^2)	A1: 3 mm dia			K1:6 mm dia		
	B1	E1	Core	B1	E1	Core
Cube 1	39.3	36.7	35	40.4	38.84	37.82
Cube 2	36.8	36.3	35	39.25	39.09	38.38
Cube 3	36.9	36	36.2	40.16	37.73	38.15
Average	37.67	36.33	35.4	39.94	38.55	38.12
Standard Deviation	1.42	0.35	0.69	0.61	0.72	0.28

Table 4.10- Compressive strength – Dowel bar diameter

Type	Parameter varied	Cube compressive Strength (N/mm^2)					
		Biscuit 1		Biscuit 2		Core	
		Average	Std Dev	Average	Std Dev	Average	Std Dev
A1	Control	37.67	1.42	36.33	0.35	35.40	0.69
B1	Restraints: PTFE/PTFE	39.75	0.64	37.80	0.53	36.43	0.40
C1	Restraints: Fixed/Roller	38.20	2.30	41.15	1.81	37.80	1.27
D1	Restraints: Roller/Roller	37.75	1.38	40.12	1.76	36.86	1.24
E1	Roughness: Very smooth	37.03	0.98	38.20	0.44	37.43	1.76
F1	Roughness: Rough	36.38	1.75	36.21	1.61	37.02	0.99
G1	Concrete Strength: 50/10/50	37.12	1.51	37.21	1.13	7.12	0.58
H1	Concrete Strength: 10/50/10	9.45	0.65	34.08	2.64	8.69	0.88
I1	Embedment: 15mm	36.41	1.44	35.73	0.87	35.75	0.44
J1	Embedment: 25mm	39.38	1.26	38.36	0.88	39.36	1.02
K1	Dowel bar dia: 6 mm	39.94	0.61	38.55	0.72	38.12	0.28

Table 4.11- Compressive strength: A1-K1

4.3.1.2 Discussion

Results show that the average cube compressive strengths of the concrete for the core and the biscuits for all specimen types A1-K1 were greater than the target strength of 35N/mm^2. The standard deviation of the concrete for all specimen types ranged between 0.28 N/mm^2 to 2.64 N/mm^2 which accounted for 0.80% - 7.55% of the target cube compressive strength of 35N/mm^2. Hence, the cube compressive strengths for all test specimens were deemed as being satisfactory.

4.3.2 Experimental Failure Load

The loads at which the test specimens failed (i.e. the maximum load attained by the specimens) are provided in Table 4.6. The average value of the failure load for each of the five test specimens tested for types A1-K1 are calculated.

4.3.2.1 Results

The loads of all test specimens at failure are given in Table 4.12. The average values of the failure loads for the five specimens tested for each set of test is also summarised.

Type	Parameter varied	Experimental Failure Load (kN)					Failure Load (Average, kN)
		S1	S2	S3	S4	S5	
A1	Control	42	40	42	40	42	41.20
B1	Restraints: PTFE/PTFE	42	40	42	42	40	41.20
C1	Restraints: Fixed/Roller	38	40	38	38	38	38.40
D1	Restraints: Roller/Roller	36	36	38	36	38	36.80
E1	Roughness: Very smooth	30	28	30	28	30	29.20
F1	Roughness: Rough	68	74	70	74	70	71.20
G1	Concrete Strength: 50/10/50	40	42	40	42	40	40.80
H1	Concrete Strength: 10/50/10	30	32	30	30	32	30.80
I1	Embedment: 15mm	34	34	32	34	32	33.20
J1	Embedment: 25mm	40	42	42	40	40	40.80
K1	Dowel bar dia: 6 mm	118	122	122	118	122	120.40

Table 4.12- Experimental Failure Load: A1-K1

A. Reduction in Failure Load due to Base Restraints

The above results show that varying the restraint at the base of the test specimens directly influences the failure load. When the PTFE sheet is used, no change in the failure load is observed. This confirms that the PTFE sheets are not very effective in reducing friction at the base of the specimens. In contrast, the introduction of a roller support in type C1 at the base of one biscuit causes the failure load to decrease by 6%. The failure load in type D1 reduces further by 5% compared to type C1 and by 12 % compared to types A1 and B1 (where no roller supports are used at the base of both biscuits). The results are in agreement with the findings of previous studies (Teraszkiewicz, 1965; Hicks and McConnell, 1996 and Al-deen et al, 2011) and confirm that the use of roller supports reduce the friction at the base of the test specimens as well as the shear strengths obtained from push-out tests.

It must be underlined that using the roller supports did pose problems when positioning and instrumenting the test specimens prior to the start of the loading procedure. This was due to the limited space around the testing frame which resulted in difficulty in manoeuvring the test specimens.

It was therefore impracticable to use the roller supports for consequent push-out tests and thus, it was agreed that the specimens would be positioned directly on the base of the testing frame as in type A1. A reduction in the failure loads of 12 % (corresponding to type D1 where roller supports are used at the base of the biscuits) was applied to the failure loads of subsequent push out tests in order to account for the additional forces induced in the test specimens due to friction between the base and the reaction frame.

B. Failure Load after Reduction due to Restraints

As discussed above, since fixed supports were used for types A1, E1-K1, a reduction factor of 12% was applied to the failure loads observed to account for the friction at the base of the test specimens. The reduced failure loads are summarised in the table below.

Type	Parameter varied	Failure Load (Average, kN)	Failure Load (Reduced, kN)
A1	Control	41.20	36.26
E1	Roughness: Very smooth	29.20	25.70
F1	Roughness: Rough	71.20	62.66
G1	Concrete Strength: 50/10/50	40.80	35.90
H1	Concrete Strength: 10/50/10	30.80	27.10
I1	Embedment: 15mm	33.20	29.22
J1	Embedment: 25mm	40.80	35.90
K1	Dowel bar dia: 6 mm	120.40	105.95

Table 4.13-Reduced Experimental Failure Load: A1-K1

4.3.2.2 Discussion

A. Effect of Surface Roughness

Results show that varying the surface roughness at the core/biscuit interface directly influences the failure load. Using the neoprene sheet to achieve a 'very smooth' surface roughness in type E1 decreases the failure load by 29% compared to the 'smooth' surface in type A1. On the other hand, increasing the surface roughness to a 'rough' surface increases the failure load by 73% and 144% compared to the 'smooth' and 'very smooth' surfaces. From the push-out tests, it can be concluded that $P_{very\ smooth} \approx 1.4\ P_{smooth} \approx 1.7\ P_{rough}$. Hence, as the surface roughness at the core/biscuit interface increases, the failure load also increases as a result of the increase in aggregate interlock that takes place. These results are in agreement with the work carried out by Hanson (1960) who observed that as interface roughness crossing the interface increased, the interface horizontal shear stress improved. It is also confirmed that the interface finishes produced without special effort under laboratory conditions can develop adequate shear resistance.

B. Effect of Concrete Strength

From Table 4.13, it can be seen that the failure load increases by 25% when the strength of the concrete in the biscuits is increased from 28-day strength of 10N/mm^2 to 50 N/mm^2. However, the failure load does not change significantly when the strength of the core is increased from 10N/mm^2 to 50 N/mm^2. This confirms that the failure load

increases with increasing strength of the concrete in the biscuits but is not affected by the strength of the concrete in the core as shown in Figure 4.8.

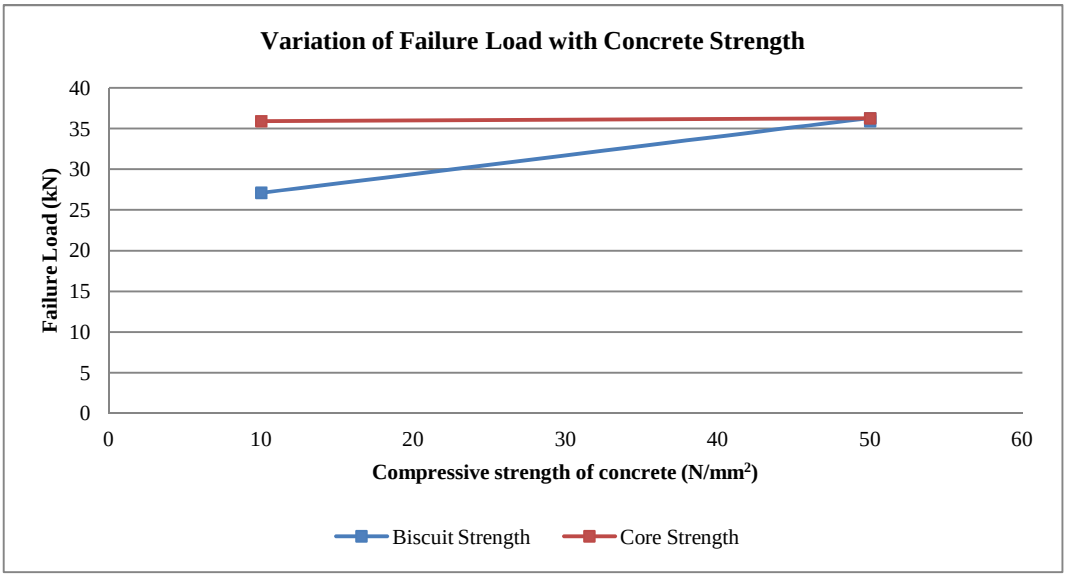

Figure 4.8- Effect of Concrete Strength on Failure Load

C. Effect of Embedment Depth

From the results in Table 4.13, it is noted that the failure load increases by 19% when the embedment depth is increased from 15 mm to 20 mm. However, when the embedment depth is increased from 20 mm to 25 mm, there is almost no change in the failure load. This suggests that the lattice is fully anchored at an embedment depth of 20 mm as shown in Figure 4.9.

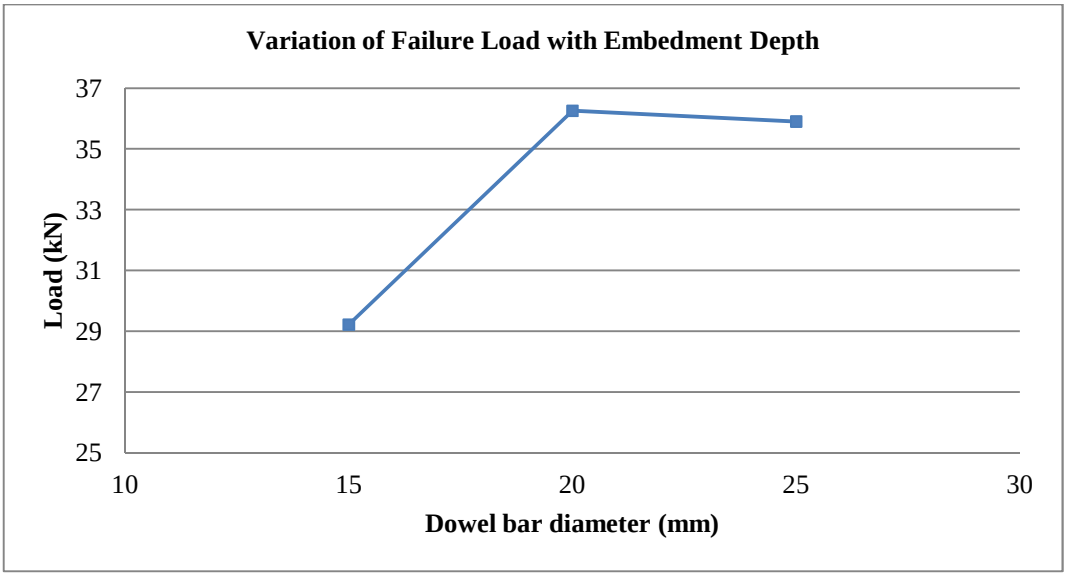

Figure 4.9- Effect of Embedment Depth on Failure Load

As discussed previously, the minimum theoretical embedment depth was calculated as 16.5 mm in accordance with the recommendation Clause 6.3.3 of Eurocode 4. The results therefore suggest that Eurocode 4 can be applied for the determination of the critical embedment depth required for the design of twinwall applications.

D. Effect of Dowel Bar Diameter

The experimental failure loads observed confirm that varying the dowel bar diameter directly influences the failure load. Increasing the diameter of the dowel bar from 3 mm to 6 mm leads to an increase in the failure load of type A1 by almost three times, i.e. $P_{3mm} \approx 3\ P_{6mm}$. As the diameter of the bar increases, the dowel action taking place in the bar also increases, thereby resulting in a higher failure load in type K1.

4.3.3 EC2 Theoretical Failure Load

As discussed in previous chapters, the shear stress at the core/biscuit interface can be theoretically calculated using Clause 6.2.5 of Eurocode 2. On this basis, it can be assumed that there are no external normal forces, i.e. $\sigma_n = 0$ and $A_i = 48{,}000$ mm^2 [480 mm (lever arm) x 100 mm (width)].

The EC2 equation imposes a limit of $45^0 \leq \alpha \leq 90^0$ for the angle of inclination of the dowel, α. In this test, the angle $\alpha = 38^0$ [tan-1 (80/100)] which lies outside the EC2 limits. Thus, the failure load is calculated for an inclination angle of $\alpha = 38^0$ (actual) and $\alpha = 45^0$ (EC2 limit) and the results are compared.

Further particulars relating to the various parameters investigated are provided below:

A. Surface Roughness

The interface shear strength also depends on the cohesion and friction coefficients which in turn are influenced by the roughness at the core/biscuit interfaces. Hence, the theoretical values for types A1, E1 and F1 with varying roughnesses can be determined by assuming different values of c and μ values as shown in Table 4.14.

B. Concrete Strength

The values of f_{ctd} for each specimen type can be conservatively determined from the average experimental cube compressive strength as summarised in Table 4.11.

C. Embedment Depth

The EC2 equation assumes that assumes that the dowels (i.e. lattice diagonal bars) are fully anchored on both sides of the concrete interfaces. According to previously calculations, this value has been determined as 16.5 mm. Since Clause 6.2.5 of EC2 does not account for specific embedment depths, the theoretical results are therefore unaffected by the varying embedment depths.

D. Dowel Bar Diameter

For all specimen types except type K1, A_s = 57 mm^2 (=8x π 3^2/4) and the yield strength of the diagonal lattice bars is taken as 280 N/mm^2 as determined from previous tensile tests. For type K1 (6 mm dowel bars), A_s = 226 mm^2 (=8x π 6^2/4) and the yield strength of the diagonal lattice bars is taken as 340 N/mm^2.

4.3.3.1 Results

The theoretical EC2 failure loads calculated for types A1, E1-K1 are summarised in Table 4.14. Note that the EC2 theoretical values were not calculated for types B1-D1 since the base restraints is a function of the test method only.

Type	Parameters varied	Theoretical EC2 FL (kN)							Exp. FL (kN)
		c	μ	$f_{ck,cube}$ (N/mm^2)	f_{ctd} (N/mm^2)	ρ	V_{Ed} (kN, 38^o)	V_{Ed} (kN, 45^o)	
A1	Control	0.2	0.6	35.40	1.95	0.001	37.05	36.64	36.26
E1	Roughness: Very smooth	0.03	0.5	37.03	2.01	0.001	20.24	19.69	25.70
F1	Roughness: Rough	0.4	0.7	36.21	1.98	0.001	57.33	57.06	62.66
G1	Concrete Strength: 50/10/50	0.2	0.6	7.12	0.67	0.001	24.75	24.34	35.90
H1	Concrete Strength: 10/50/10	0.2	0.6	8.69	0.76	0.001	25.67	25.26	27.10
I1	Embedment : 15mm	0.2	0.6	35.73	1.96	0.001	37.17	36.76	29.22
J1	Embedment : 25mm	0.2	0.6	38.36	2.06	0.001	38.08	37.67	35.90
K1	Dowel bar dia: 6 mm	0.2	0.6	38.12	2.05	0.005	92.97	91.33	105.95

Table 4.14- Theoretical EC2 Failure Load: A1-K1

4.3.3.2 Discussion

A. Effect of Surface Roughness

From Table 4.14, it can be seen that the experimental and theoretical and experimental failure loads increase as the surface roughness increases from ‘very smooth’ to ‘smooth’ and to ‘rough’. This trend is also presented in Figure 4.10.

Results indicate show that the EC2 theoretical values obtained by using the actual angle of inclination $\alpha = 38^0$ and the EC2 limit of $\alpha = 45^0$ are almost equal. This suggests that although the actual angle of inclination $\alpha = 38^0$ lies outside the EC2 limitation of $45^0 \leq$

$\alpha \leq 90^0$, the EC2 equation is still valid. Thus, the validity of the EC2 equation can be extended to take into account a smaller angle of inclination of $\alpha = 38^0$.

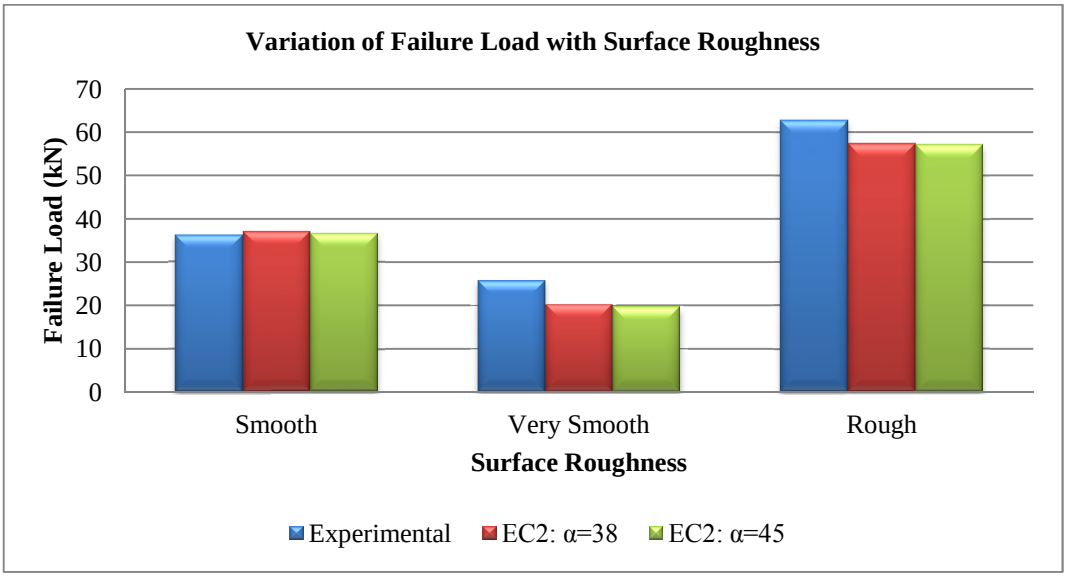

Figure 4.10- Effect of Surface Roughness on Failure Load

Figure 4.10 also shows that the experimental failure load for types E1 and F1 specimens with the 'very smooth' and 'rough' surfaces respectively are significantly higher than the EC2 theoretical predictions. However, the EC2 theoretical failure load for type A1 with the 'smooth' as-cast surface is 2% higher than the experimental failure load obtained. Hence, there seems to be a good agreement between the EC2 theoretical and experimental values for type A1. This confirms that the EC2 'smooth' as-cast surface can be used to provide conservative estimates of the interface shear strength of twinwalls.

B. Effect of Concrete Strength

Results show that there is negligible difference between the EC2 theoretical values obtained by using the actual angle of inclination $\alpha = 38^0$ and the EC2 limit of $\alpha = 45^0$. This suggests that although the actual angle of inclination $\alpha = 38^0$ lies outside the EC2 limitation of $45^0 \leq \alpha \leq 90^0$, the EC2 equation is still valid. Thus, the validity of the EC2 equation can be extended to take into account a smaller angle of inclination of $\alpha = 38^0$.

The EC2 theoretical predictions base the value of the tensile strength of concrete, f_{ctd} on the lower strength of concrete. However, as discussed previously, the experimental results show that the failure load increases with increasing strength of the concrete in the biscuits but is not affected by the strength of the concrete in the core. Hence, it would be more sensible to base f_{ctd} on the concrete used in the biscuits rather than the core.

C. Effect of Embedment Depth

The results indicate that the EC2 theoretical values obtained by using the actual angle of inclination $\alpha = 38^0$ and the EC2 limit of $\alpha = 45^0$ are almost equal. This suggests that although the actual angle of inclination $\alpha = 38^0$ lies outside the EC2 limitation of $45^0 \leq \alpha \leq 90^0$, the EC2 equation is still valid. Thus, the validity of the EC2 equation can be extended to take into account a smaller angle of inclination of $\alpha = 38^0$.

As discussed earlier, EC2 assumes that assumes that the steel shear connector is fully anchored on both sides of the interface. Thus, it is recommended that the critical

embedment depth is calculated in accordance with the requirements of Eurocode 4 prior to using Clause 6.2.5 of EC2 to ensure full anchorage of the lattice bars in twinwall applications.

D. Effect of Dowel Bar Diameter

The results also show that there is a maximum difference of 2% between the EC2 theoretical values obtained by using the actual angle of inclination $\alpha = 38^0$ and the EC2 limit of $\alpha = 45^0$ for types A1 and K1. This suggests that although the actual angle of inclination $\alpha = 38^0$ lies outside the EC2 limitation of $45^0 \leq \alpha \leq 90^0$, the EC2 equation is still valid for larger diameter dowels. Thus, the validity of the EC2 equation can be extended to take into account a smaller angle of inclination of $\alpha = 38^0$.

The theoretical and experimental failure loads are plotted against dowel bar diameter as shown in Figure 4.11. It can be seen that both the experimental and theoretical failure loads increase with increasing lattice bar diameters.

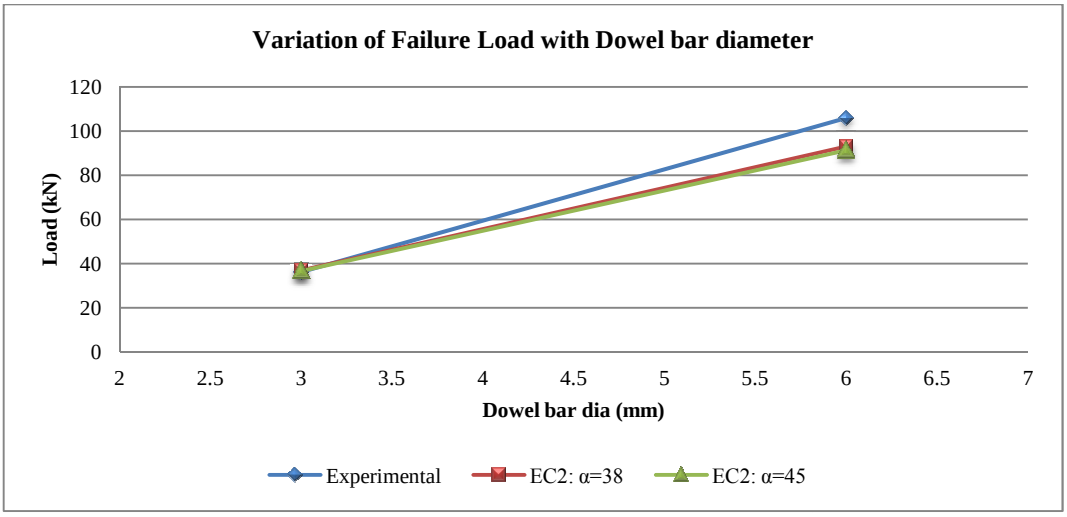

Figure 4.11- Effect of Dowel Bar Diameter on Failure Load

It is also noted that when the bar diameter is less than circa 3.5 mm, the experimental failure load is less than the theoretical load. However, beyond diameters of 3.5 mm, the experimental failure load exceeds that theoretical load. This confirms that EC2 provides conservative estimates of the interface shear strength in twinwalls when the dowel bar diameter is greater than 3.5 mm. In practice, the minimum dowel bar diameter used in twinwalls is 6 mm, thereby justifying the use of the EC2 recommendations for the design of twinwalls.

4.3.4 Deflection at Failure

4.3.4.1 Results

The deflections at the bottom of the core for all specimens are presented. The deflections correspond to the average values of two dial gauge readings recorded at each load increment as shown in Table 4.15.

Type	Parameter varied	Deflection at Failure (mm)					Deflection (Average, mm)
		1	2	3	4	5	
A1	Control	0.90	1.08	0.87	1.01	1.37	1.05
B1	Restraints: PTFE/PTFE	1.53	1.43	1.29	1.38	0.99	1.32
C1	Restraints: Fixed/Roller	0.62	0.89	0.75	0.58	0.61	0.69
D1	Restraints: Roller/Roller	1.23	1.20	1.15	1.18	1.17	1.19
E1	Roughness: Very smooth	1.02	1.01	1.38	1.29	1.59	1.26
F1	Roughness: Rough	1.01	1.15	1.12	1.00	1.04	1.06
G1	Concrete Strength: 50/10/50	0.86	1.11	0.89	0.92	0.93	0.94
H1	Concrete Strength: 10/50/10	0.94	1.11	1.02	0.98	1.01	1.01
I1	Embedment: 15mm	0.80	0.85	0.87	0.75	0.79	0.81
J1	Embedment: 25mm	0.93	1.09	0.91	1.02	1.09	1.01
K1	Dowel bar dia: 6 mm	1.36	1.73	2.30	1.49	2.02	1.78

Table 4.15 - Average deflection at failure: A1-K1

4.3.4.2 Discussion

A. Effect of Base Restraints

The average deflections at the bottom of the core for types A1, B1, C1 and D1 are 1.05 mm, 1.32 mm, 0.69 mm and 1.19 mm respectively. The bottom deflection for type B1 where the PTFE sheets are used is 27 % greater than type A1. Since the failure load for type B1 does not change in comparison with type A1, it seems that the PTFE sheet has an influence on the distribution of forces and the stiffness of the test specimens resulting in an increase in the bottom deflection.

In contrast, it has been discussed that the introduction of the roller supports types C1 and D1 leads to a decrease in the failure load. However, the bottom deflection for type C1 is 34 % smaller than those in type A; and the bottom deflection for type D1 is 13 % greater than type A1. The inconsistency in the bottom deflections confirms that the introduction of roller supports also alters the distribution of forces and stiffness of the test specimens.

B. Effect of Surface Roughness

It is observed that reducing the surface roughness from ‘smooth’ to ‘very smooth’ leads to an increase in the bottom deflection of approximately 17 %. This can be attributed to the decrease in the bond at the core-biscuit interfaces which reduces the stiffness of the test specimens resulting in larger bottom deflections. In contrast, increasing the surface roughness from ‘smooth’ to ‘rough’ has almost no effect on the bottom deflection (2 %

difference). Thus the 'rough' surface seems to have no effect on the stiffness of the test specimens.

C. Effect of Concrete Strength

Table 4.15 shows that the bottom deflection in type G1 (50/10/50) is 10% lower than that of type A1 (50/50/50). On the other hand, the bottom deflection in type H1 (10/50/10) is only 3% smaller than that of type A1. This shows that the bottom deflection changes when strengths of the concrete used in the core and the biscuits are different (G1: 50/10/50) but is not affected when the strengths of the concrete in the core and the biscuits are the same (A1: 50/50/50 and G1: 10/50/10). Hence the strengths of the concrete in the core and biscuits seem to have an effect on the stiffness of the specimens.

D. Effect of Embedment Depth

Results indicate that the bottom deflection decreases by 22% when the embedment depth is reduced from 20 mm in type A1 to 15 mm in type I1. This can be attributed to the lower failure load of type I1 which results in smaller deflections. In contrast, the difference between type J1 with a 25 mm embedment depth and type A1 with a 20 mm embedment depth is only 2%. This suggests that the distribution of forces in the test specimens is not altered when the embedment depth is increased beyond 20 mm, i.e. at full anchorage.

E. Effect of Dowel Bar Diameter

The deflections at failure observed show that increasing the diameter of the dowel bar from 3 mm to 6 mm leads to an increase in the bottom deflection of approximately 41 %. This increase can be due to the increase in the failure load in type K1 in comparison to type A1. The increase in bottom deflection in type K1 may also indicate a reduction in the stiffness of the test specimen.

4.3.5 First Crack Load

The first crack in all test specimens occurred at the core/biscuit interface. The crack either occurred across the core/biscuit 2 interface with a second crack occurring shortly afterwards at the core/biscuit 1 interface or it occurred simultaneously at both core/biscuit interfaces.

4.3.5.1 Results

The load at which the first crack occurred for each type is given in Table 4.16. The maximum and minimum values of the first crack load are also expressed as a percentage of the average failure load for types A1-K1.

Type	Parameter varied	Experimental First Crack Failure Load (kN)					First crack occurs at % FL	
		S1	S2	S3	S4	S5	Min	Max
A1	Control	32	30	34	34	34	75%	85%
B1	Restraints: PTFE/PTFE	36	32	32	32	34	76%	86%
C1	Restraints: Fixed/Roller	32	32	30	28	30	74%	84%
D1	Restraints: Roller/Roller	26	28	30	28	30	72%	83%
E1	Roughness: Very smooth	20	22	26	20	24	67%	87%
F1	Roughness: Rough	60	56	52	58	60	74%	88%
G1	Concrete Strength:	30	32	32	32	30	75%	80%
H1	Concrete Strength:	30	32	30	30	32	100%	100%
I1	Embedment: 15mm	34	34	32	34	32	100%	100%
J1	Embedment: 25mm	34	32	36	34	30	75%	86%
K1	Dowel bar dia: 6 mm	90	92	90	92	94	74%	78%

Table 4.16 - First crack load: A1-K1

4.3.5.2 Discussion

A. Effect of Base Restraints

The first crack occurs at a minimum of 75 %, 76 %, 74 % and 72 % of the failure load for types A1, B1, C1 and D1 respectively. The results indicate that the use of different base restraints does not affect the load at which the first crack forms. The first crack load could therefore be interpreted as the point at which the aggregate interlock forces are overcome causing the core/biscuit interface to slip relative to each other.

Additionally, the first crack load could be taken as the serviceability limit for design purposes under which cracking would not be expected in twinwalls. It can therefore be assumed that under serviceability loads of approximately 70% of the ultimate load,

cracking is not expected in the twinwalls. It can also be concluded that the variation of the base restraints does not seem to affect the load at which the first cracks forms at the core/biscuit interfaces.

B. Effect of Surface Roughness

The first crack occurs at a minimum of 75 %, 68 % and 74 % of the failure load for types A1, E1 and F1 respectively. The results show that using a 'very smooth' surface leads to a small decrease in the load at which the first crack occurs which may be attributed to the lower bond at the core/biscuit interface. Conversely, increasing the surface roughness from 'smooth' to 'rough' results in a significantly smaller change in the first crack load. It can be concluded that the variation of the surface roughness does not seem to affect the load at which the first cracks forms at the core/biscuit interfaces.

C. Effect of Concrete Strength

The first crack occurs at a minimum of 75 %, 75% and 100 % of the failure load for types A1, G1 and H1 respectively. The results show that when the strength of the core is reduced from 50 N/mm^2 in type A1 to 10 N/mm^2 in type G1, there is no change in the load at which the first crack forms. On the other hand, when the strength of the biscuits is reduced from 50 N/mm^2 in type A1 to 10 N/mm^2 in type H1, the first crack occurs at the failure load in type H1. This indicates that the strength of the concrete in the biscuits influences the distribution of the forces and the failure mechanism of the test specimens.

It can be concluded that the load at which first crack forms at the core/biscuit interface is influenced by the strength of the concrete in the biscuits but is not affected by the strength of the concrete in the core.

D. Effect of Embedment Depth

The first crack occurs at a minimum of 75 %, 100% and 75 % of the failure load for types A1, I1 and J1 respectively. The results show that when the embedment depth is reduced from 20 mm in type A1 to 15 mm in type I1, the first crack occurs at the failure load in type I1. This indicates that the distribution of forces and the failure mechanism of the specimens changes when the embedment depth is reduced from 20 mm to 15 mm. On the other hand, when the embedment depth is increased from 20 mm to 25 mm in type J1, there is no change in the load at which the first crack forms.

This confirms load at which first crack forms at the core/biscuit interface changes when the embedment depth is reduced from 20 mm to 15 mm but any increase in the embedment depth beyond 20 mm has no effect on the first crack load.

E. Effect of Dowel Bar Diameter

The first crack occurs at a minimum of 75 % and 76 % of the failure load for types A1 and K1 respectively. The results show that varying the diameter of the bars from 3 mm to 6 mm seems to have almost no effect on the load at which the first crack forms at the core/biscuit interfaces.

4.3.6 Load-Bottom Deflection Profile

4.3.6.1 Results

The strength of shear connectors depends on their ability to redistribute shear forces among themselves which is determined by their load/deflection characteristics. The load-bottom deflection profile obtained from push-out tests gives an indication of the stiffness and ductility of the shear connectors used. The load-bottom deflection curves for all specimens of type A1-K1 are plotted in Figures 4.12-4.22.

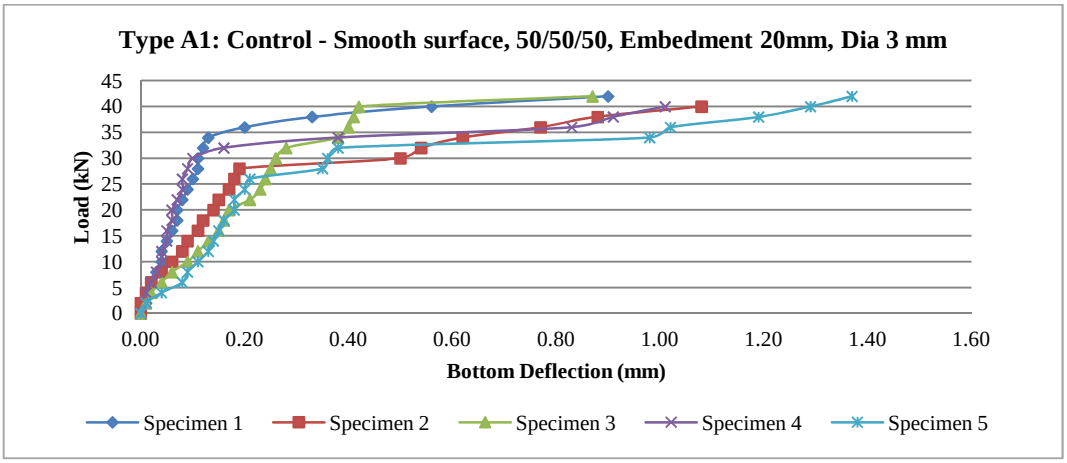

Figure 4.12 - Load v/s Bottom Deflection – A1

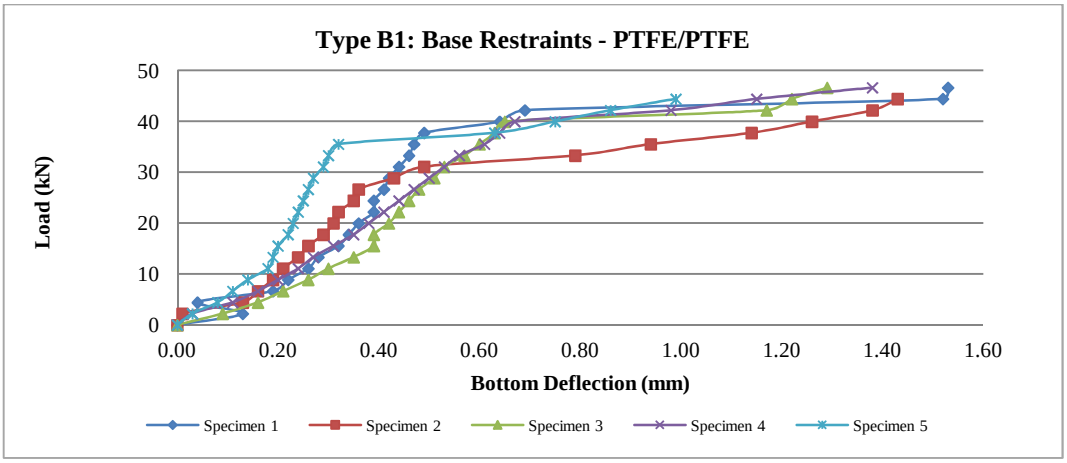

Figure 4.13 - Load v/s Bottom Deflection – B1

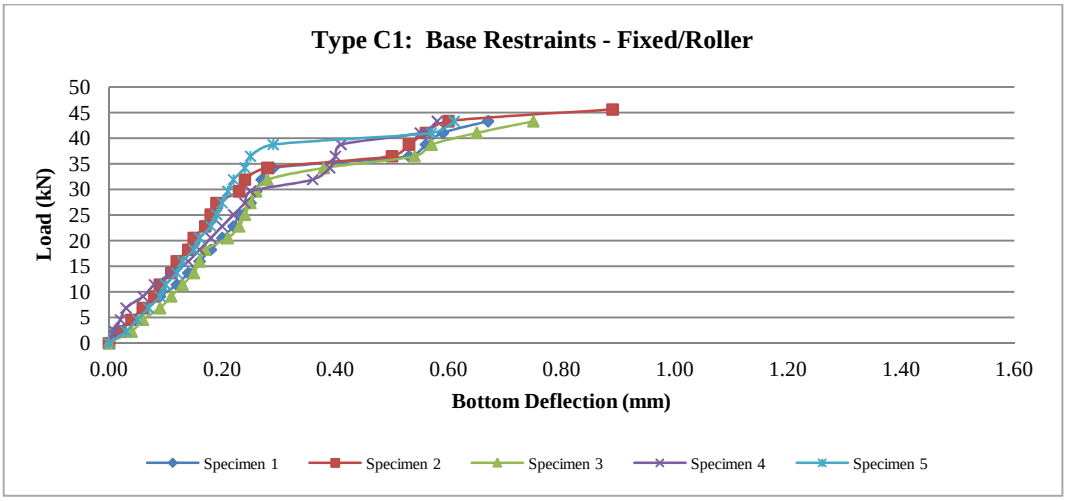

Figure 4.14 - Load v/s Bottom Deflection – C1

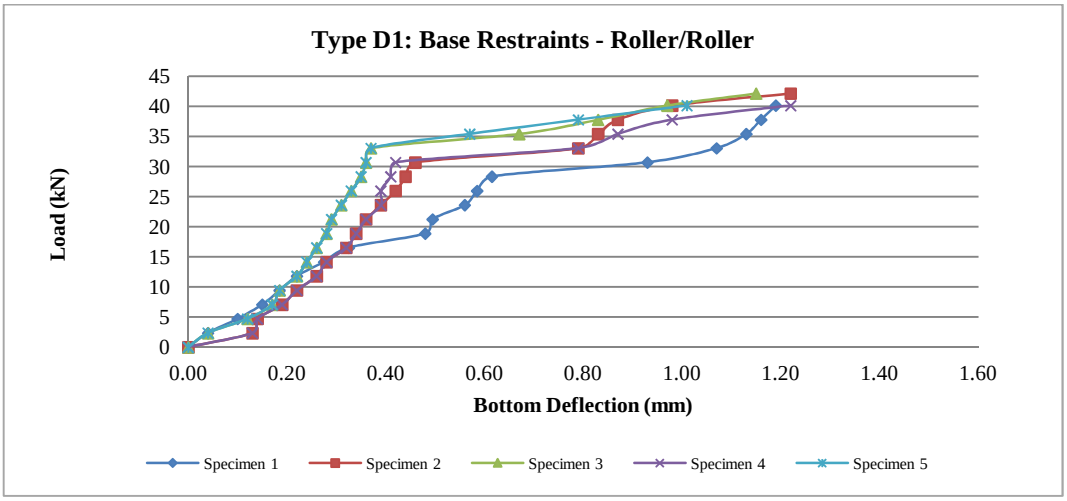

Figure 4.15 - Load v/s Bottom Deflection – D1

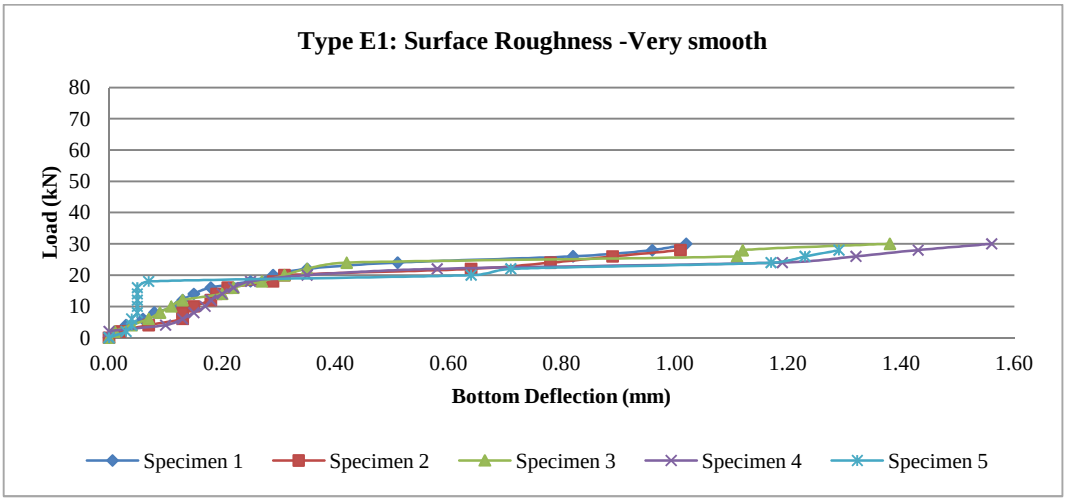

Figure 4.16 - Load v/s Bottom Deflection – E1

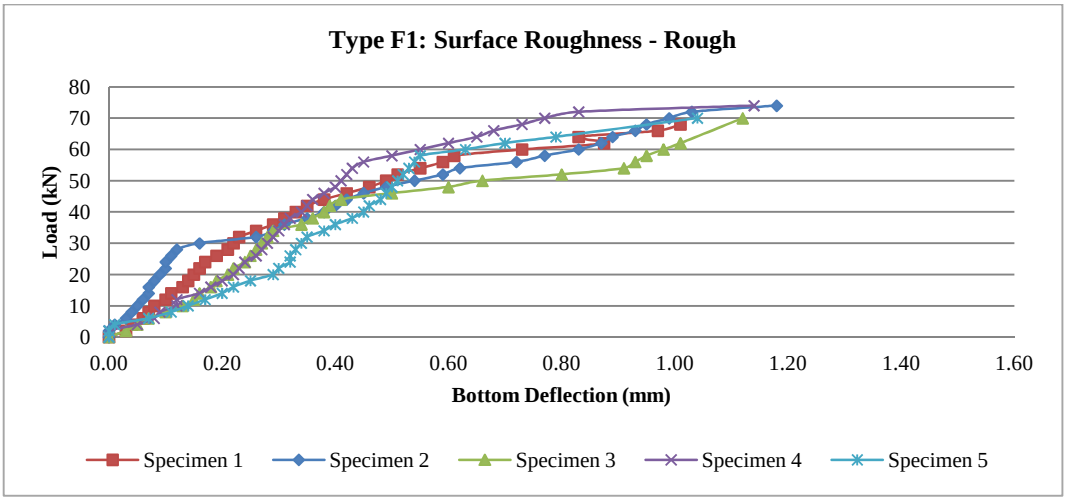

Figure 4.17 - Load v/s Bottom Deflection – F1

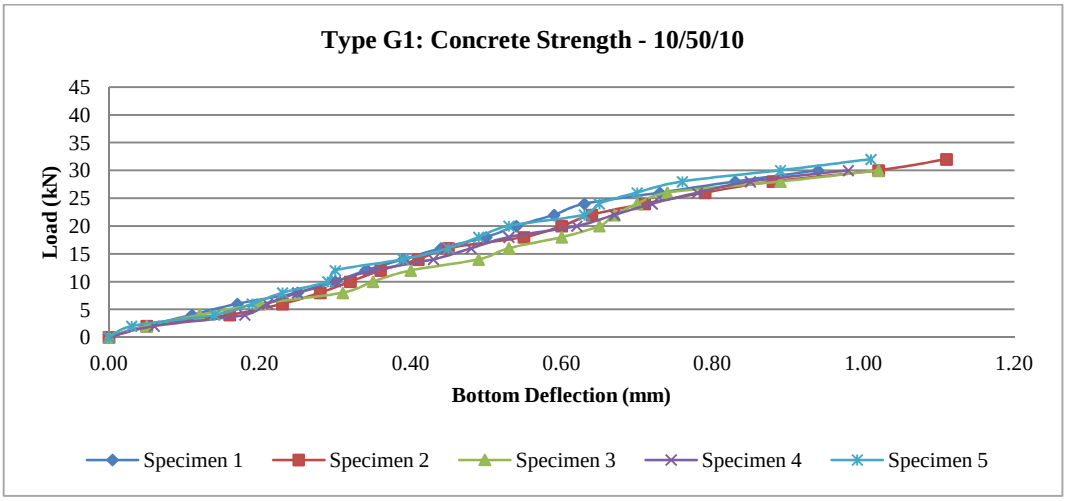

Figure 4.18 - Load v/s Bottom Deflection – G1

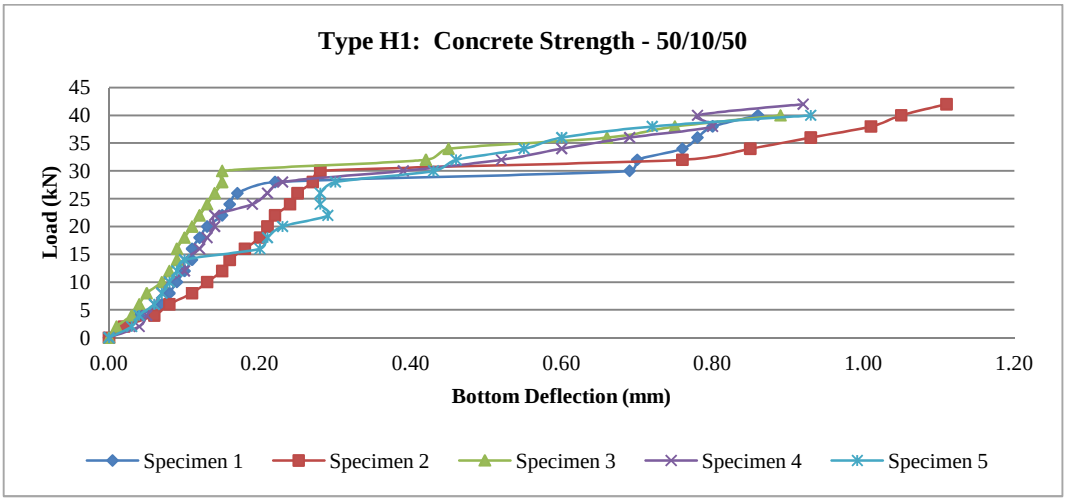

Figure 4.19 - Load v/s Bottom Deflection – H1

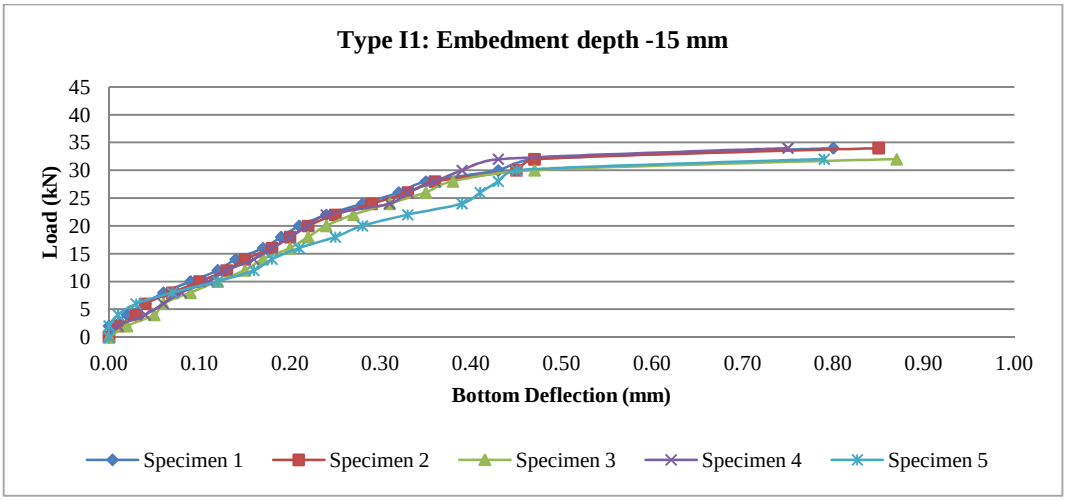

Figure 4.20 - Load v/s Bottom Deflection – I1

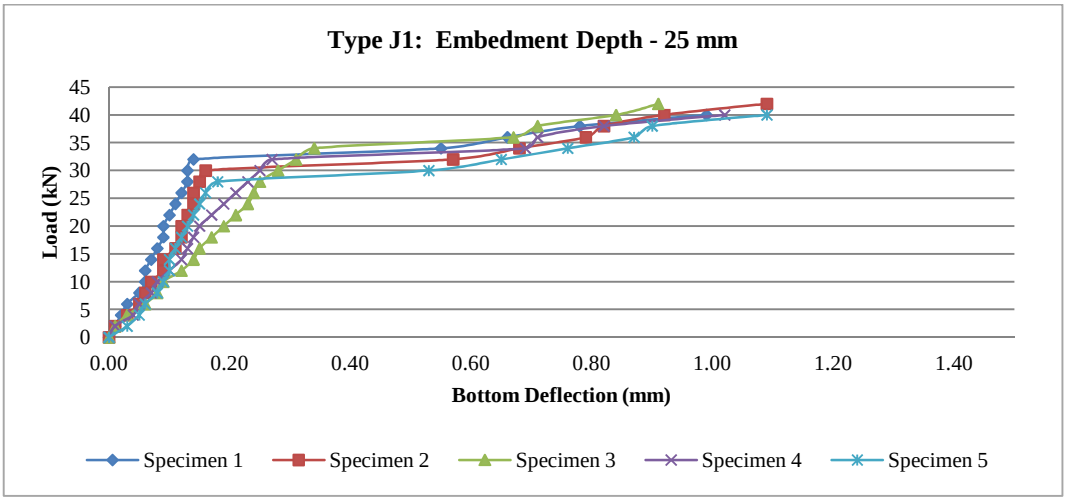

Figure 4.21 - Load v/s Bottom Deflection – J1

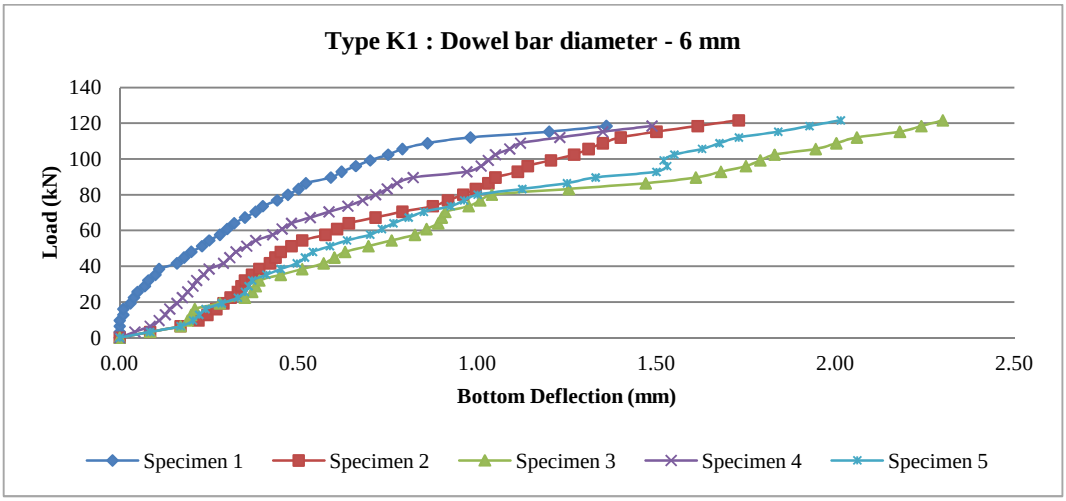

Figure 4.22 - Load v/s Bottom Deflection – K1

The load-bottom deflection profiles for types A1-K1 are also plotted relative to each other to obtain a direct comparison between the results. The average bottom deflection for the five specimens tested for each test type is plotted for each load increment as shown in Figures 4.23-4.27.

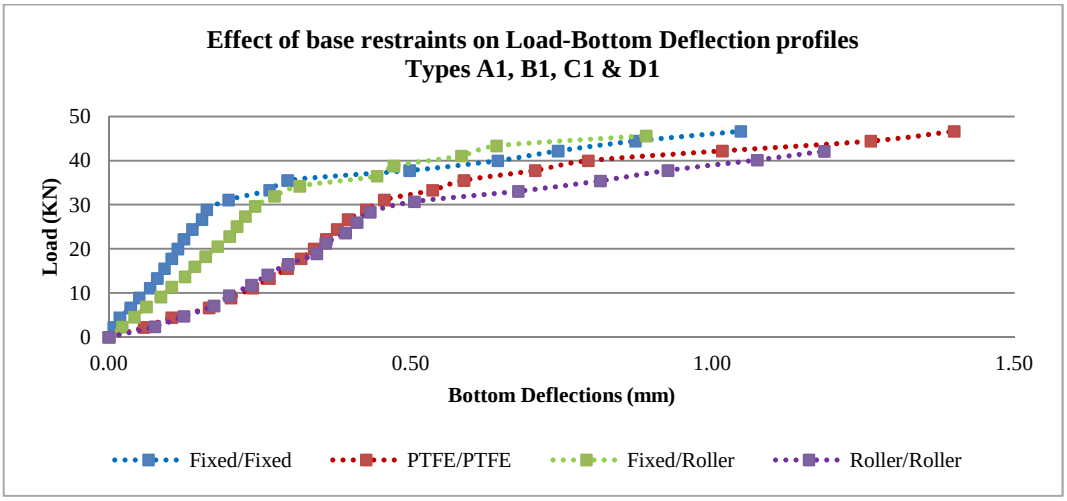

Figure 4.23 - Effect of Base Restraints on Load-Bottom Deflection profiles

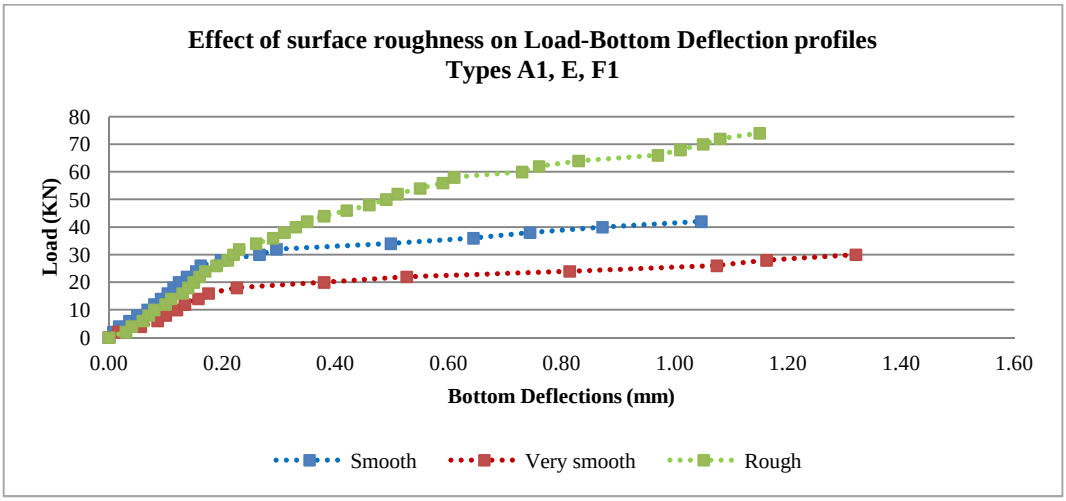

Figure 4.24 - Effect of Surface Roughness on Load-Bottom Deflection profiles

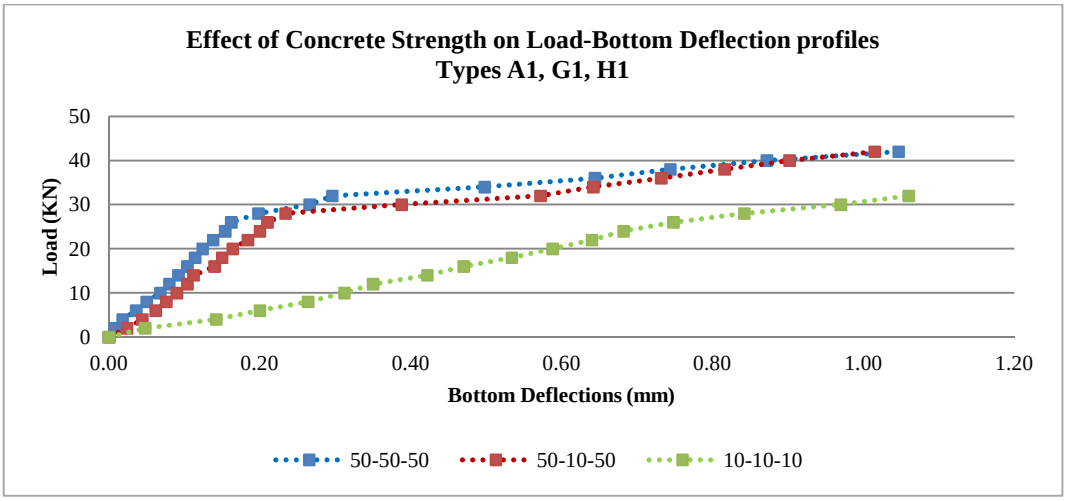

Figure 4.25 - Effect of Concrete Strength on Load-Bottom Deflection profiles

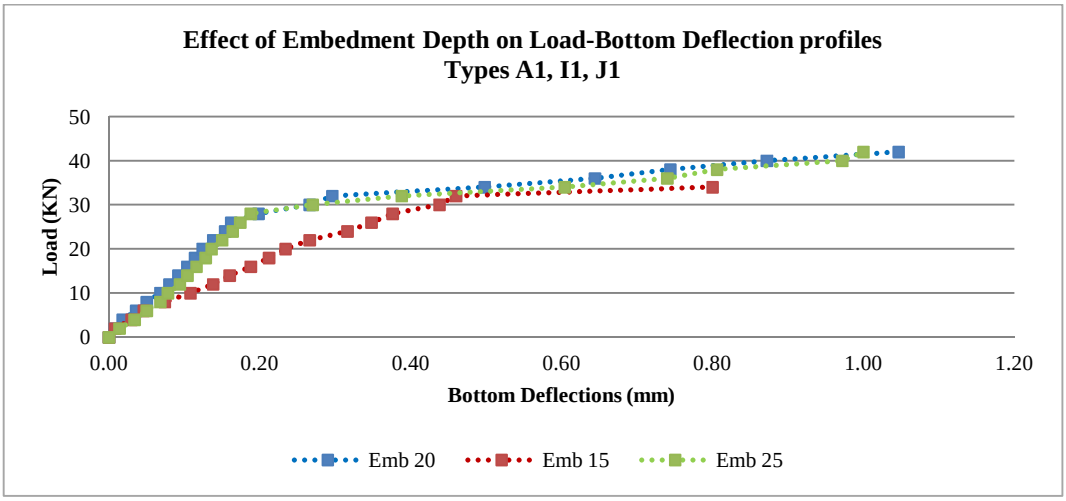

Figure 4.26- Effect of Embedment Depth on Load-Bottom Deflection profiles

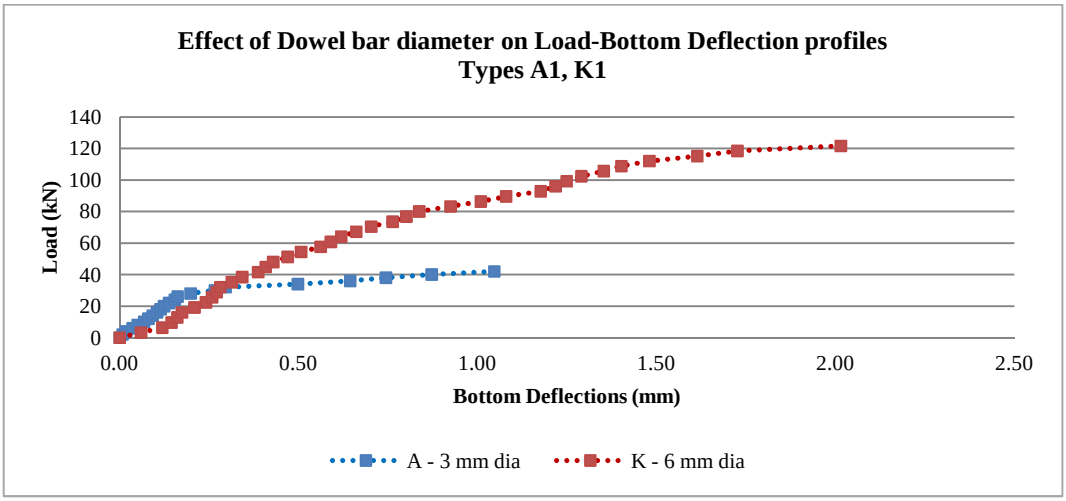

Figure 4.27- Effect of Dowel bar diameter on Load-Bottom Deflection profiles

4.3.6.2 Discussion

A. General Trend

The load-deflection profiles for most specimen types indicate that the test specimens deform in three stages:

1. Firstly, the specimens deform elastically before the first crack appears with the load-deflection profiles being approximately linear.

2. Cracking occurs at the core/biscuit interface which leads to a sharp increase in the bottom deflection. This is reflected by the horizontal shift observed in the load-deflection profiles at loads where the cracking occurs. When the load is applied, aggregate interlock takes place and the interfaces between the core and the biscuits slide against one another. As the load increases, slip occurs at the core/biscuit interface resulting in a crack being formed and an increase in bottom deflection is observed.

3. After cracking at the core/biscuit interface occurs, the specimens exhibit a non-linear load-deflection relationship until failure. At this stage, the aggregate interlock forces at the core/biscuit interface have been overcome and dowel action begins to occur in the lattice bars. Tensile forces are induced in the bars and the slip is resisted by bending of the lattice bars at the core/biscuit interface. This explains the non-linear behaviour in the load-deflection profiles.

It can also be observed that all specimens also undergo significant deformations prior to failure. It can be concluded that the lattice girder has good ductility and are effective in its use as a shear connector in the twinwall.

B. Effect of Base Restraints

The load-deflection plots for types A1, B1, C1 and D1 in Figure 4.23 confirm that varying the restraints at the base of the specimens influences the stiffness of the test specimens. The stiffness of the specimens increases when the PTFE sheets are used. On the other hand, as the number of roller supports increases, the stiffness and the failure load decreases. Hence, it can be concluded that the use of different restraints alters the distribution of forces in the twinwalls which may also have an effect on their failure mechanism.

C. Effect of Surface Roughness

From load-deflection plots for types A1, E1 and F1 in Figure 4.24, it is observed that the stiffness of the test specimens is influenced by the surface roughness. It can be seen that type E1 with the 'very smooth' surface is less stiff that type A1 and F1. This is due to the weaker bond at the core/biscuit interface which reduces it resistance to deformations. There is almost no difference in the stiffness of the specimens with the 'smooth' and 'rough' surfaces. It can be concluded that increasing the stiffness from 'smooth' to 'rough' has no influence on the stiffness of the test specimens.

D. Effect of Concrete Strength

Figure 4.25 shows that the load-deflection plots for type G1 (10/50/10) remain approximately linear with the first crack at the core/biscuit interface occurring at the failure load. This suggests that the strength of the core affects the distribution of forces in the test specimens and is indicative of brittle failure. Thus, the failure of the test specimens for type G1 may have primarily caused by the failure of the concrete rather than the steel.

The load-deflection plots for types A1, G1 and H1 in Figure 4.25 confirm the stiffness of the test specimens is mainly influenced by the strength of the concrete in the biscuit. It can be seen that types A1 and H1 where the concrete strength in the core is varied have almost the same stiffness. In contrast, the stiffness decreases with the decreasing strength of the concrete in the biscuits in type G1. But in all cases, the specimens did undergo significant deformations prior to failure indicating that lattice girder has good ductility and are effective in its use as a shear connector in the twinwall. It can be concluded that the stiffness of the test specimens is influenced by the strength of the concrete in the biscuits but is not affected by the strength of the concrete in the core.

E. Effect of Embedment Depth

Figure 4.26 shows that the load-deflection plots remain approximately linear up to the load prior to failure where the first crack at the core/biscuit interface occurs resulting in a significant increase in bottom deflection. This suggests that reduction in the embedment depth from 20 mm in type A1 to 15 mm in type I1 influences the

distribution of forces in the test specimens. The linear load-deflection behaviour is also indicative of brittle failure which suggests that the failure of the test specimens in type I1 may have primarily caused by the failure of the concrete rather than the steel. In all test types, the specimens did undergo significant deformations prior to failure indicating that lattice girder has good ductility and are effective in its use as a shear connector in the twinwall.

The load-deflection plots for types A1 and J1 in Figure 4.16 show the stiffness of the test specimens is almost the same. This confirms that increasing the embedment depth 20 mm in type A1 to 25 mm in type J1 does not influence the stiffness of the specimens. In contrast, the stiffness decreases when the embedment depth reduces from 20 mm in type A1 to 15 mm in type I1. It can be concluded that the stiffness of the specimens is only affected if the embedment depth is decreased from 20 mm but remains unchanged if the embedment depth is increased beyond 20 mm.

F. Effect of Dowel Bar Diameter

Figure 4.17 shows that the stiffness of type K1 is slightly less than that of type A1. This confirms that increasing the diameter of the bar from 3 mm to 6 mm does not have a significant influence on the stiffness of the test specimen in type K1.

4.3.7 Variation of Lateral Deflection

The lateral deflection of the test specimens was recorded by taking DEMEC measurements at each load increment and the change in length from the pre-set DEMEC gauge length of 100 mm was measured.

4.3.7.1 Results

A. Variation of lateral deflection with height

The variation of the lateral deflections with the height of the specimen (from the supports to the top) at different load increments is plotted for types A1-K1 in Figures 4.28-4.38. All the test specimens in each test type behave in almost the same manner and thus a typical height-lateral deflection profile is plotted for each case. The height of the specimen is plotted against the maximum lateral deformation at the failure in Figures 4.39-4.43.

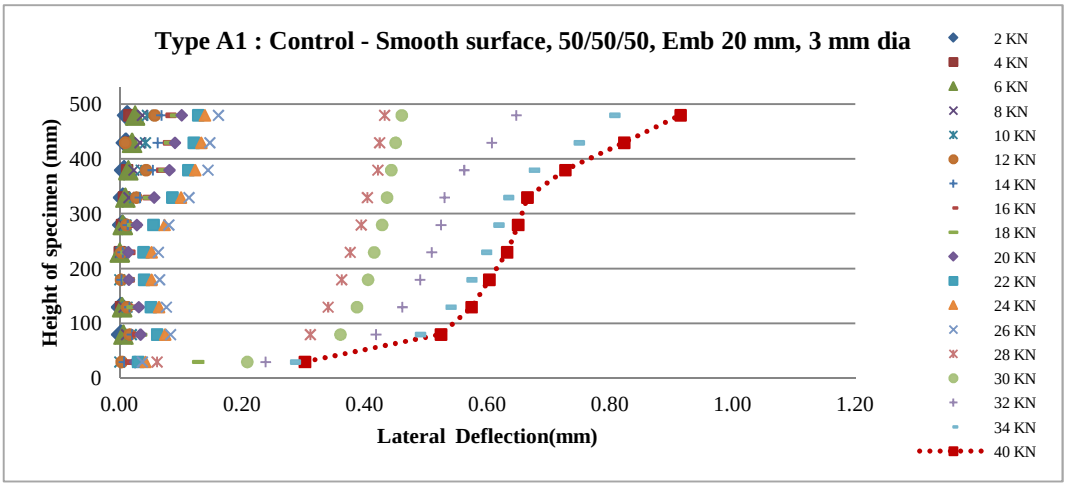

Figure 4.28 - Height v/s Lateral Deflection – A1

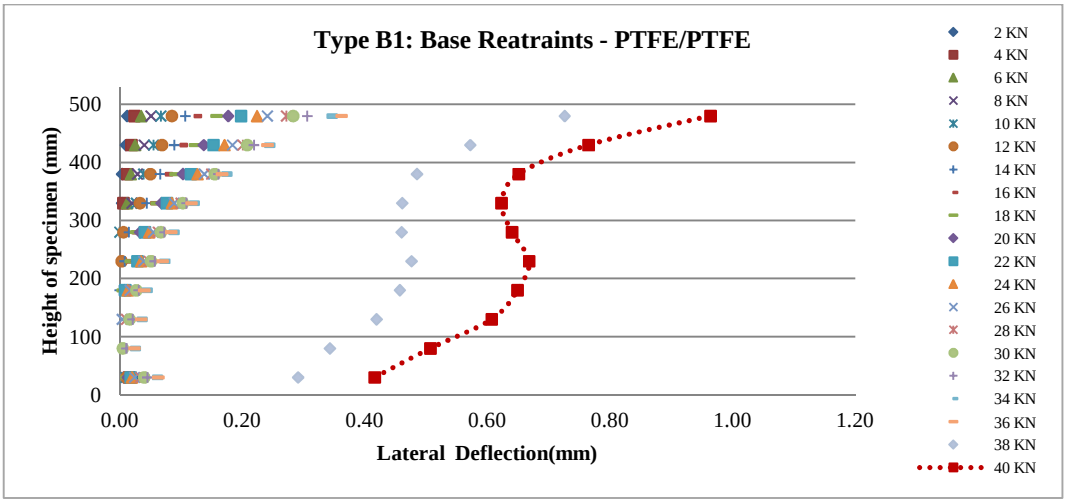

Figure 4.29 - Height v/s Lateral Deflection – B1

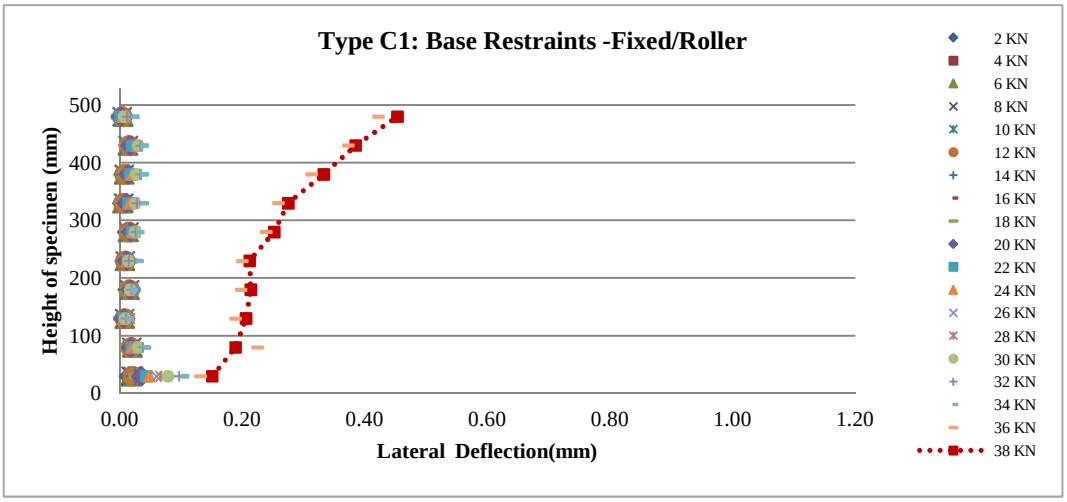

Figure 4.30 - Height v/s Lateral Deflection – C1

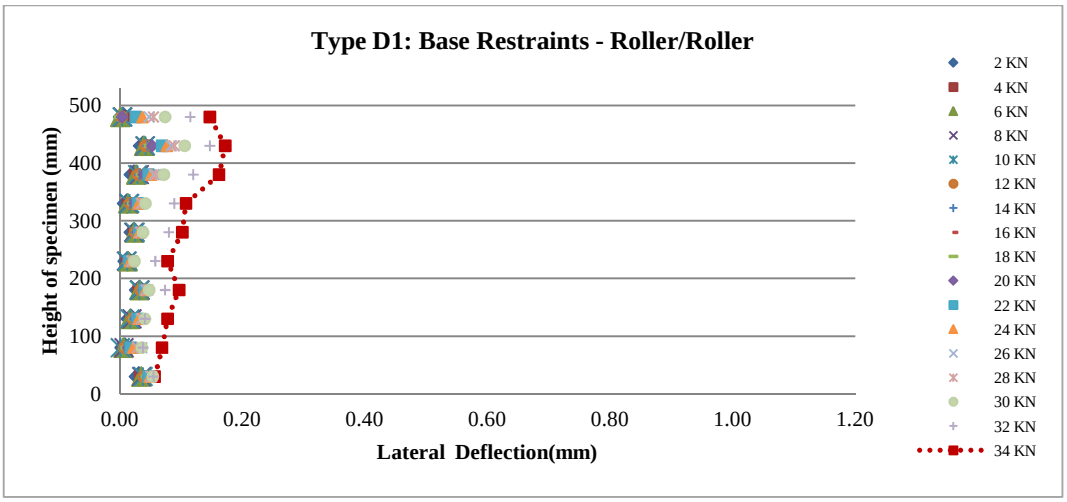

Figure 4.31 - Height v/s Lateral Deflection – D1

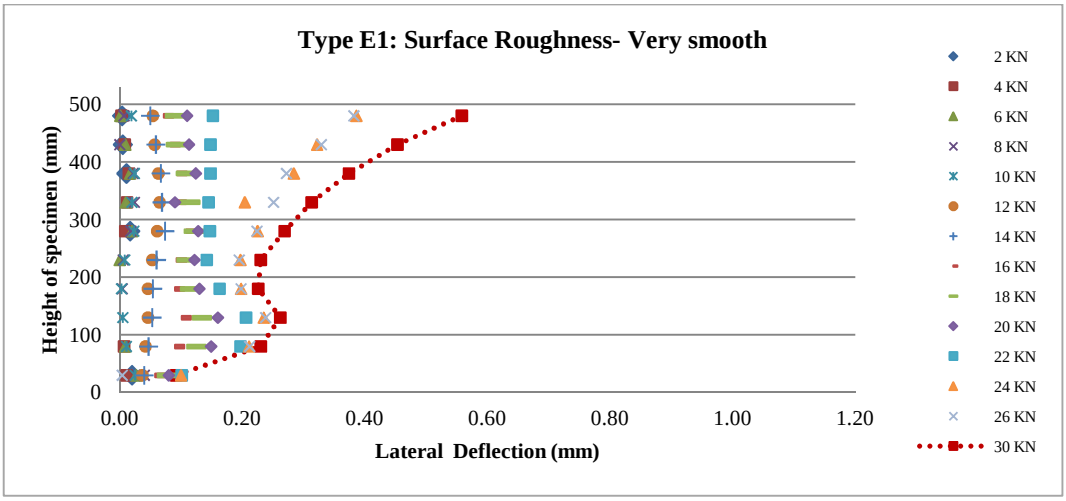

Figure 4.32 - Height v/s Lateral Deflection – E1

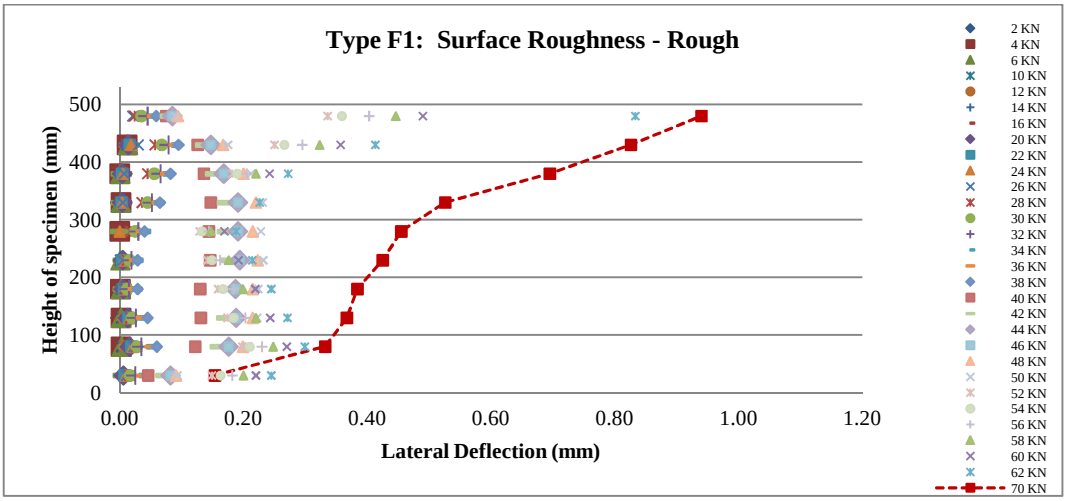

Figure 4.33 - Height v/s Lateral Deflection – F1

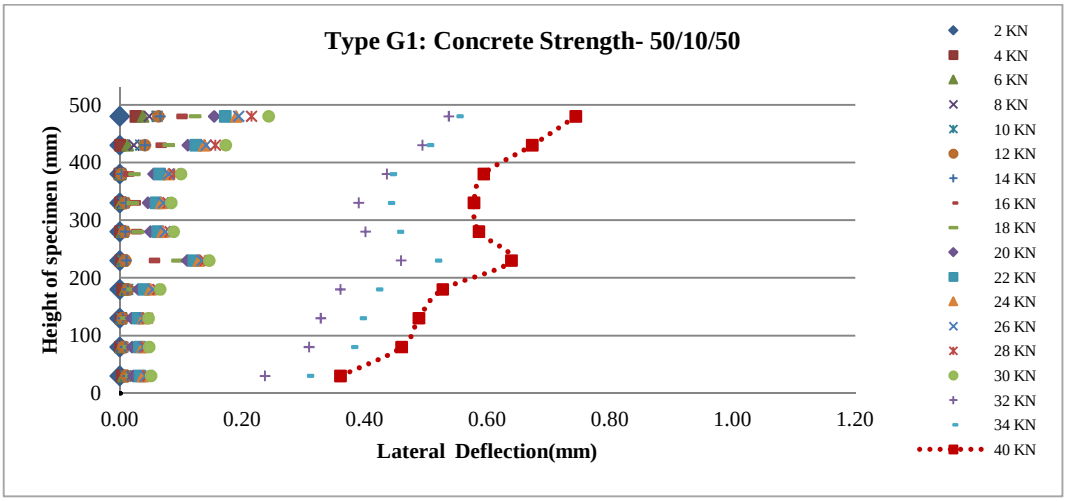

Figure 4.34 - Height v/s Lateral Deflection – G1

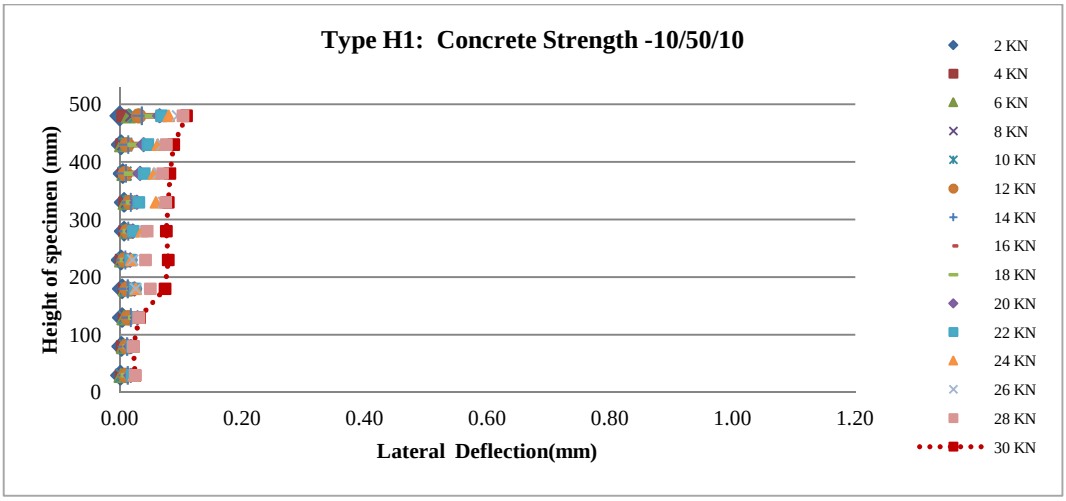

Figure 4.35 - Height v/s Lateral Deflection – H1

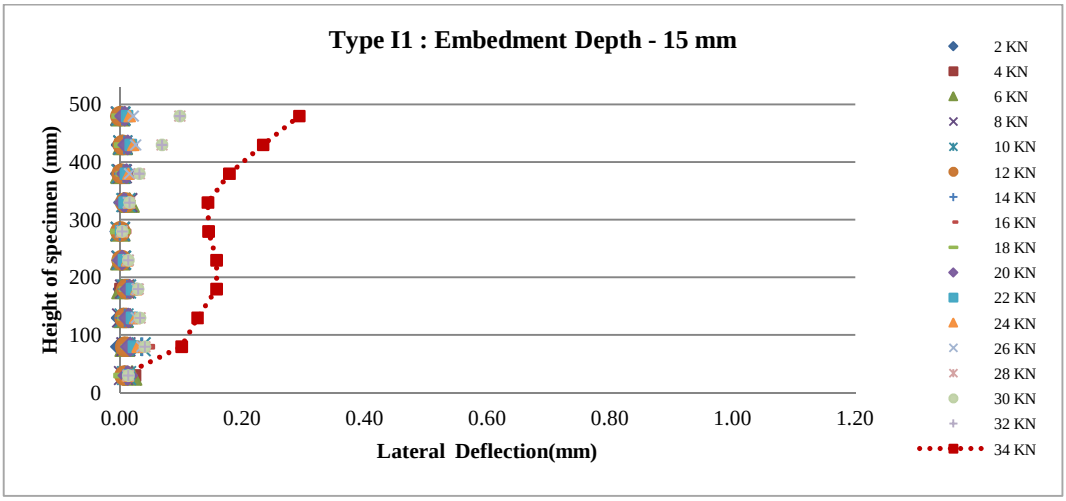

Figure 4.36 - Height v/s Lateral Deflection – I1

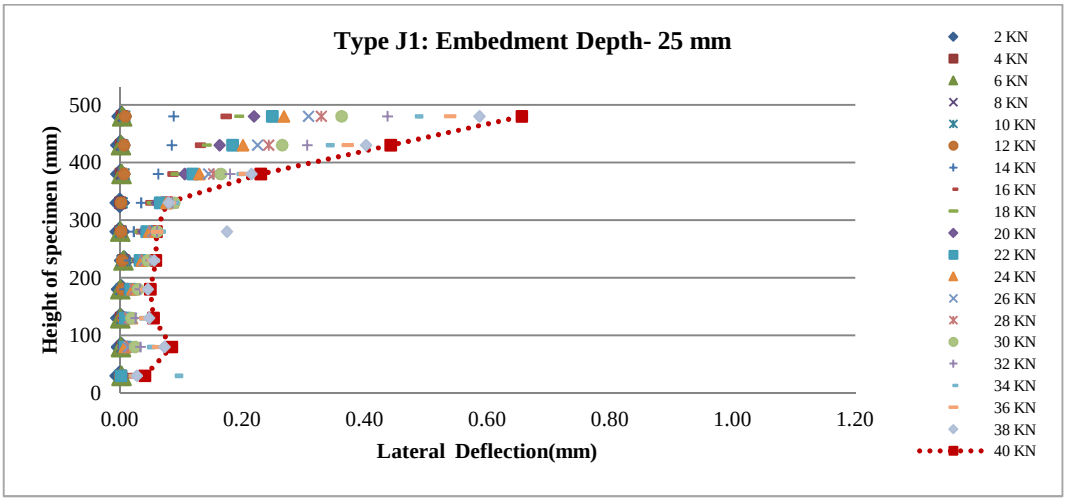

Figure 4.37 - Height v/s Lateral Deflection – J1

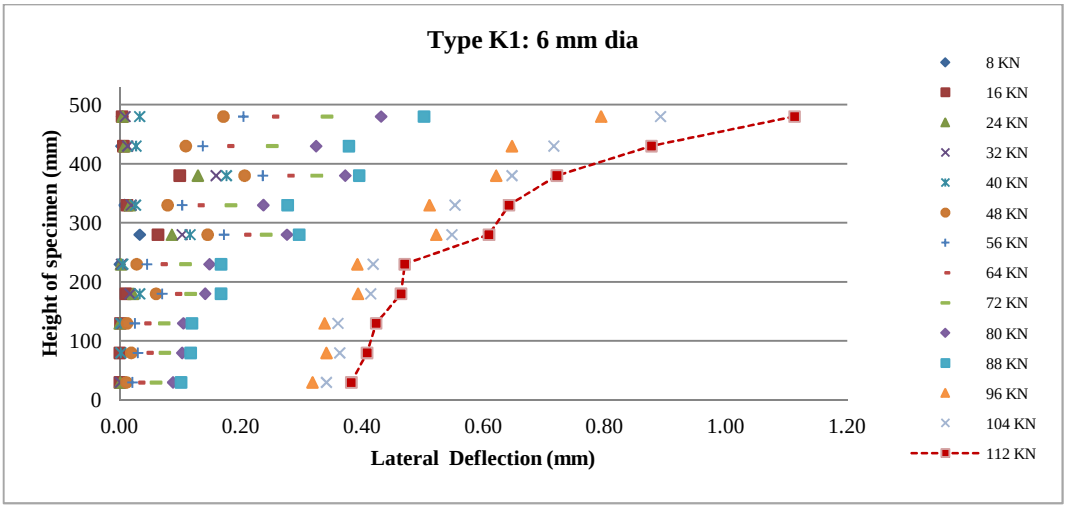

Figure 4.38 - Height v/s Lateral Deflection – K1

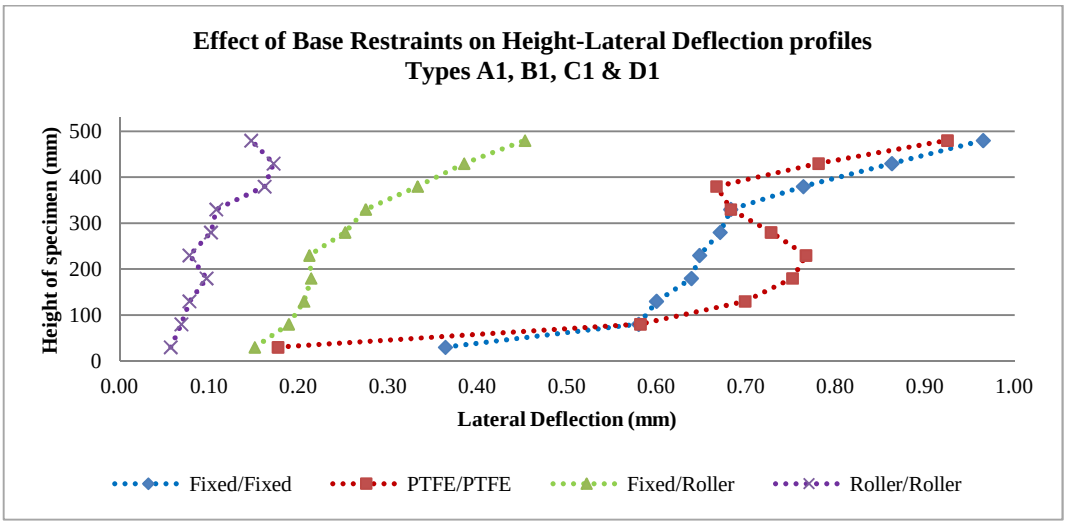

Figure 4.39 – Effect of Surface Roughness on Height-Lateral Deflection profiles – A1, B1, C1 & D1

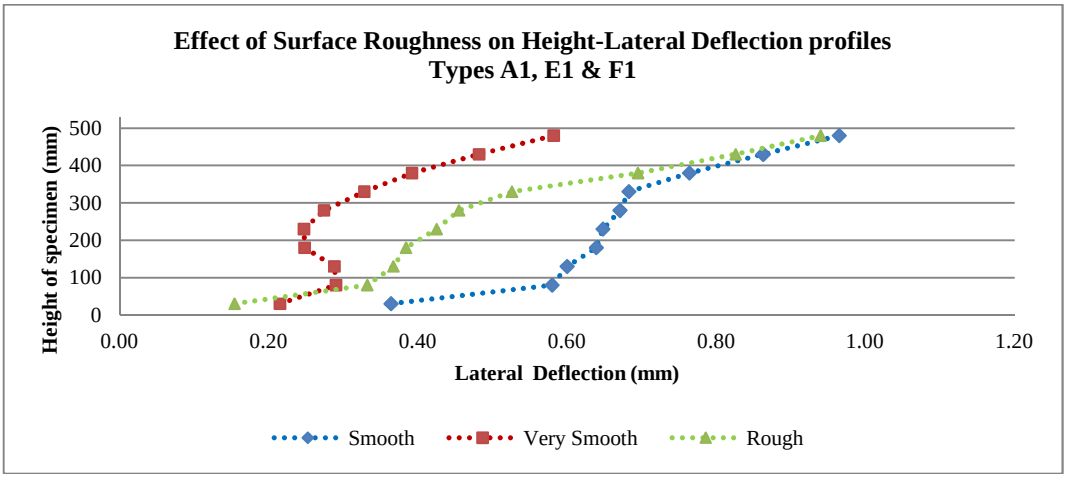

Figure 4.40 – Effect of Surface Roughness on Height-Lateral Deflection profiles – A1, E1 & F1

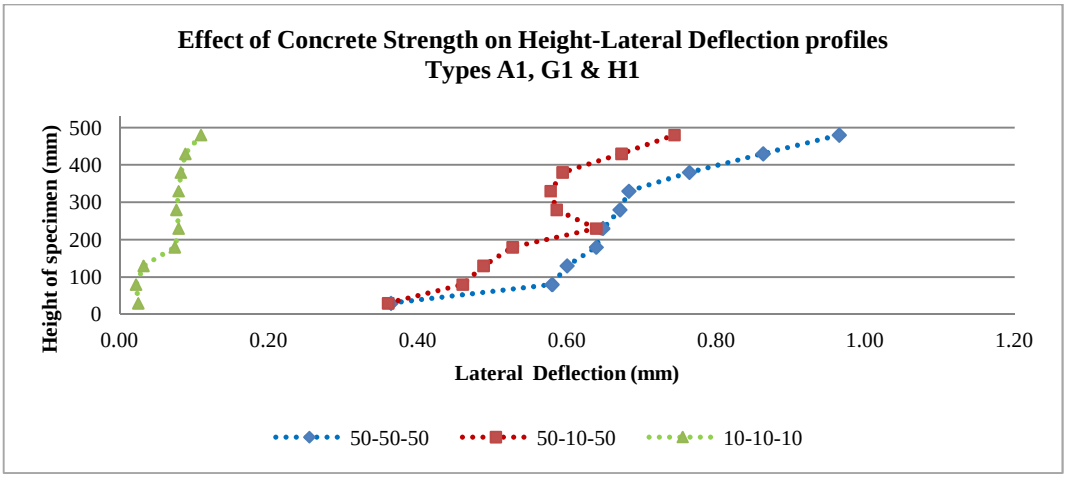

Figure 4.41 – Effect of Concrete Strength on Height-Lateral Deflection profiles – A1,G1 & H1

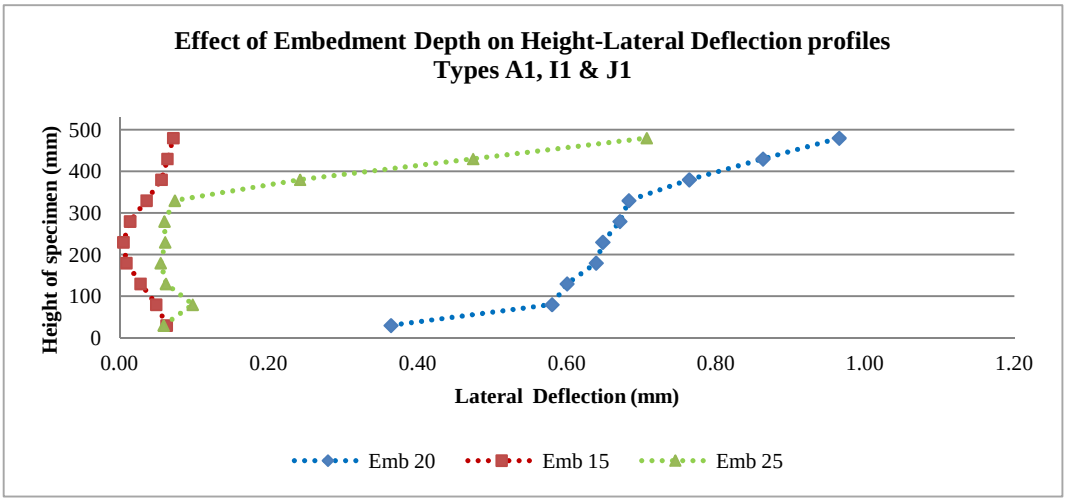

Figure 4.42 – Effect of Embedment Depth on Height-Lateral Deflection profiles – A1, I1 & J1

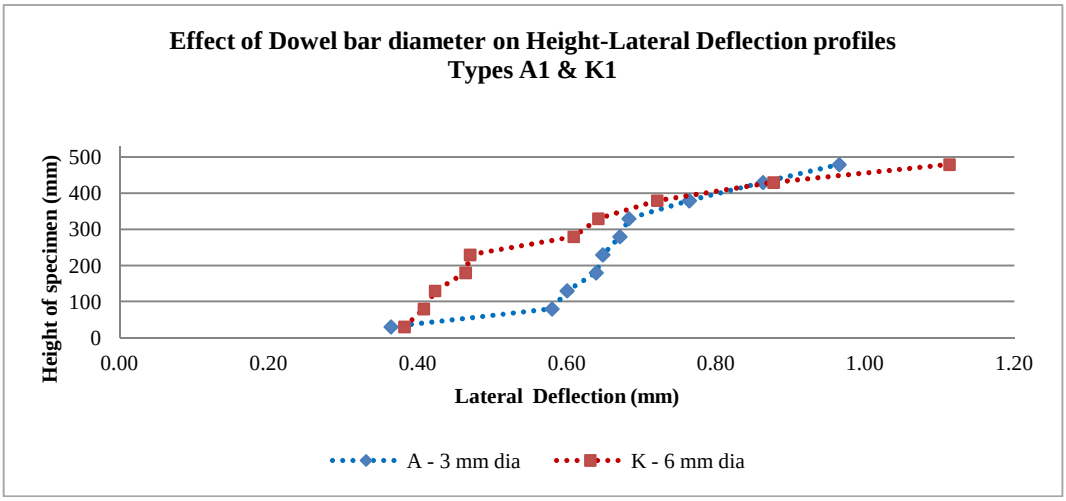

Figure 4.43 – Effect of Dowel bar diameter on Height-Lateral Deflection profiles

B. Variation of lateral deflection with load

The maximum lateral deflections occurring at failure in each specimen type is also plotted for each load increment in Figures 4.44 – 4.48.

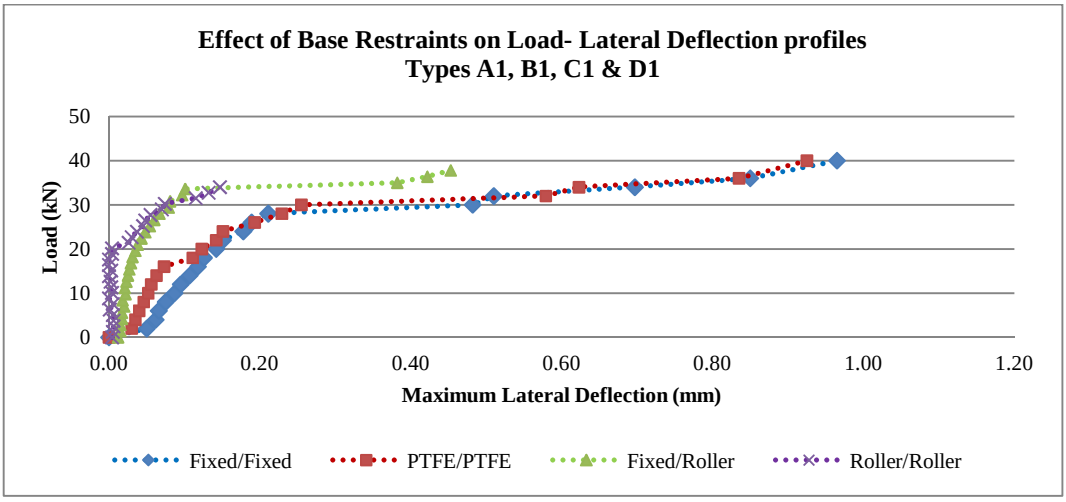

Figure 4.44 – Effect of Surface Roughness on Load-Lateral Deflection profiles – A1, B1, C1& D1

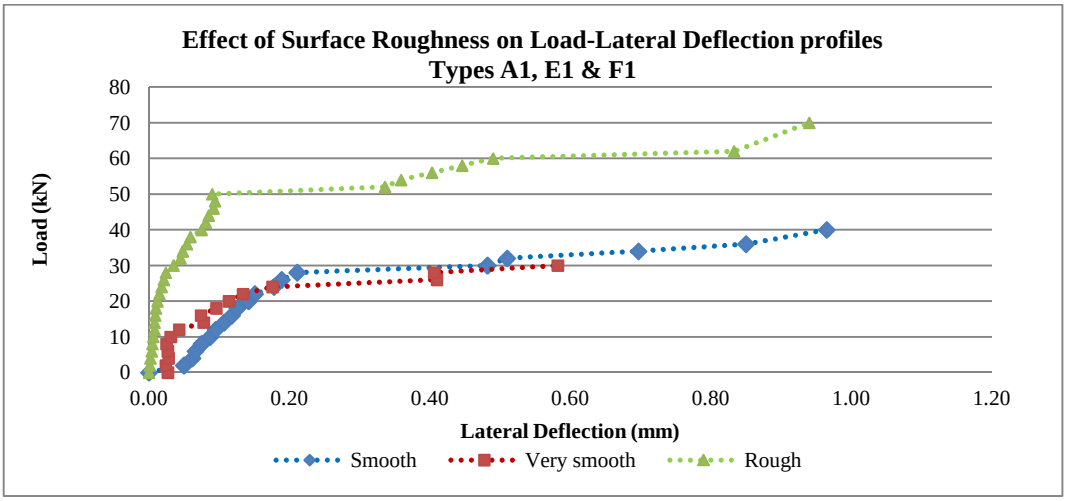

Figure 4.45 – Effect of Surface Roughness on Load-Lateral Deflection profiles – A1, E1 & F1

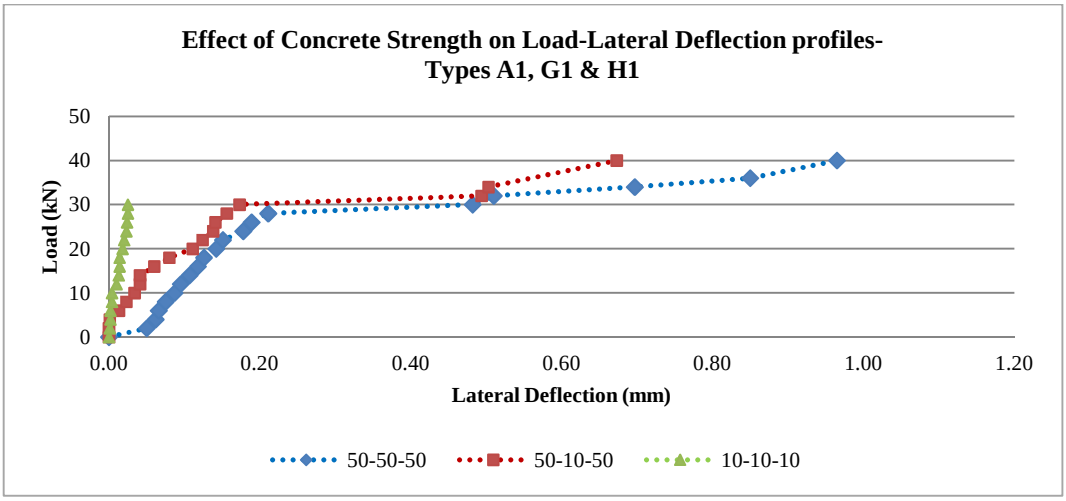

Figure 4.46 – Effect of Concrete Strength on Load-Lateral Deflection profiles – A1, G1 & H1

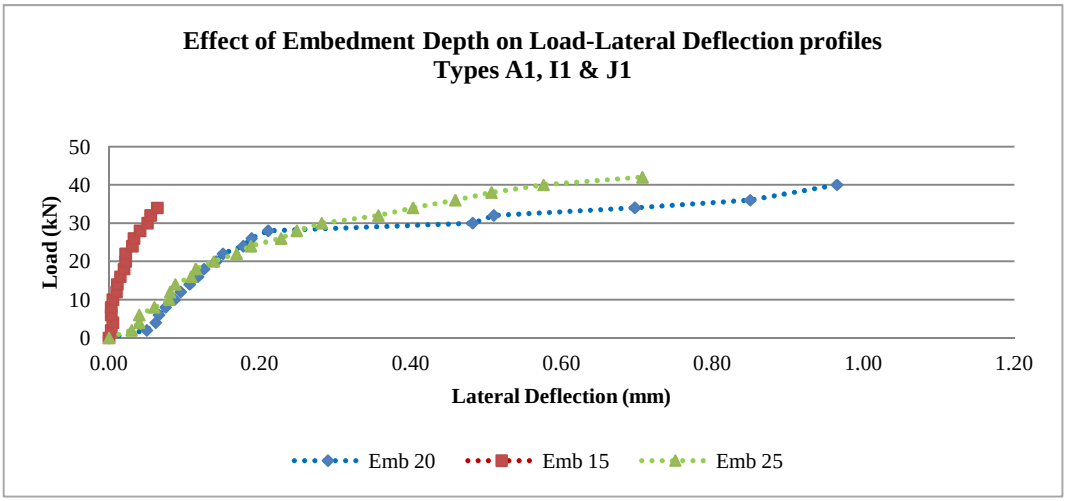

Figure 4.47 – Effect of Embedment Depth on Load-Lateral Deflection profiles – A1, I1 & J1

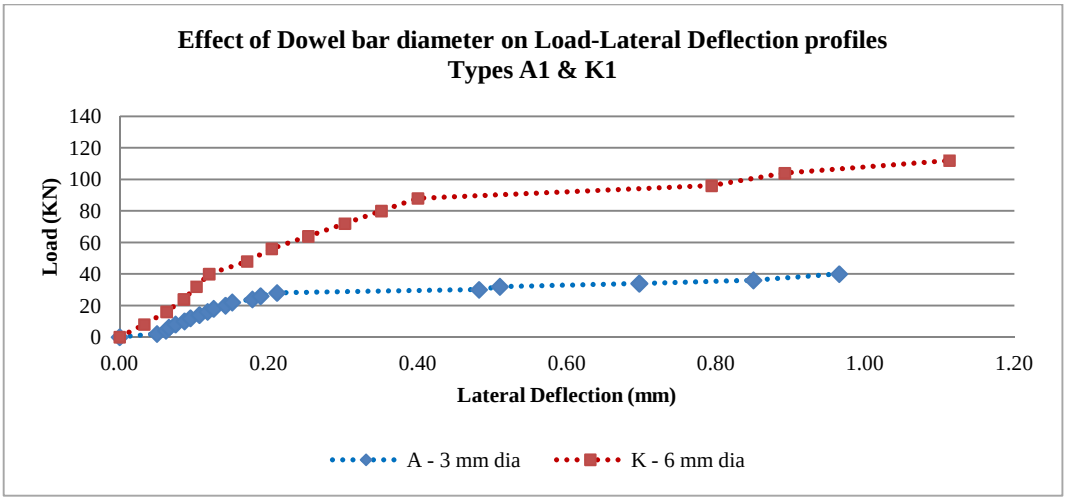

Figure 4.48 – Effect of Dowel bar diameter on Load-Lateral Deflection profiles – A1 & K1

4.3.7.2 Discussion

A. General Trends

The Height-Lateral deflection profiles indicate that the test specimens for most types exhibit similar trends. Prior to the formation of the first crack at the core/biscuit interface, the change in the lateral deflection is very small with the maximum lateral deflection occurring at the top of the specimens and the minimum lateral deflection occurs at the base. At the point when the first crack occurs at the core/biscuit interface, there is a noticeable increase in the lateral deflection which is reflected by the horizontal shift in the height-lateral plots. The lateral deflection continues to increase whilst maintaining maximum deflection at the top of the specimen and minimum at the base until failure.

In fact, at the early stages of loading, the slip at the core/biscuit interfaces is resisted by aggregate interlock which explains that small change in lateral deflection. When the first crack occurs, the sudden increase in deflection is due to the increase in the slip at the core/biscuit interface. At this point, the maximum change in lateral deflection seems to occur at mid-height suggesting that the lattice bars mid-height of the test specimens deform and yield first. This confirms that the forces in the lattice bars are not distributed evenly. As the load continues to increase, the increase in slip may be attributed to the deformation and yielding of the lattice bars by dowel action.

B. Effect of Base Restraints

Figure 4.39 shows that the lateral deflections for type A1 and B1 are greater than those for type C1 and D1. It can be concluded that the PTFE sheets in type B1 are not effective in altering the friction at the base which explains why its behaviour is similar to that of type A1 where fixed supports are used. The use one roller support in type C1 reduces the lateral deflection significantly and the use of two roller supports in type D1 results in a further decrease in the lateral deflection. This confirms that the introduction of the roller supports decreases the friction at the base and the corresponding horizontal forces induced in the shear connectors thereby reducing the lateral deflections observed. It can be concluded that the use of roller supports are an effective means of reducing friction at the base of push-out specimens.

In Figure 4.44, a similar trend to the load-bottom deflection profiles is observed. The relationship between the load and lateral deflection is linear up to the point of first cracking after which a non-linear behaviour is observed. However, unlike the load-bottom deflection profiles, the use of the roller supports increases the lateral stiffness of the test specimens. This is because the roller supports decrease the magnitude of the horizontal force induced in the shear connectors as a result of decreased friction at the base. Once again, the use of the PTFE sheets has almost no effect on the lateral stiffness of the specimens and exhibits a similar behaviour to type A1 (Fixed/Fixed) test specimens.

C. Effect of Surface Roughness

Figure 4.40 shows that the lateral deflection of type A1 is lower than that of type F1 and type E1. The lower deflection in type F1 specimens with the rough surface roughness can be attributed to the stronger bond at the core/insitu interface. Hence, the specimens are more resistant to lateral deflection in spite of the larger failure load observed. The lateral deflections in type E1 specimens with the very smooth surface roughness are the smallest. This is due to the significantly smaller failure loads observed in type E1 specimens in comparison with type A1 and F1.

In Figure 4.45, a similar trend to the load-bottom deflection profiles is observed. The relationship between the load and lateral deflection is linear up to the point of first cracking after which a non-linear behaviour is observed. The lateral stiffness of type A1 and E1 specimens are almost the same. This implies that decreasing the stiffness from ‘smooth’ to ’very smooth’ has no effect on the lateral stiffness of the test specimens. In contrast, when the surface roughness is increased from ‘smooth’ to ‘rough’; the lateral stiffness increases. This can be attributed to the stronger bond at the core/biscuit interface.

D. Effect of Concrete Strength

Figure 4.41 shows that the lateral deflection of type H1 (10/50/10) is lower than that of types A1 and G1. This can either be due to the lower failure load which would result in smaller deflections or to the reduction in dowel action due to the premature failure of the concrete.

In Figure 4.46, a similar trend to the load-bottom deflection profiles is observed. For types A1 and G1, the relationship between the load and lateral deflection is linear up to the point of first cracking after which a non-linear behaviour is observed. Types A1 and G1 specimens also have almost the same lateral stiffness. In contrast, the load-lateral deflection profile remains linear for type H1 specimens. This confirms that the lateral stiffness of the specimens is not influenced by the strength of the concrete in the core but is dependent on the strength of the concrete in the biscuits.

E. Effect of Embedment Depth

The behaviour of type A1 and J1 specimens is different from that of type I1. The height-lateral deflection plot of type I1 specimens with the 15 mm embedment depth shows that the sudden increase in lateral deflection, which corresponds to the formation at the first crack at the core/biscuit interface, occurs at failure. This confirms that the type I1 specimens failed as a result of sudden concrete failure rather than steel yielding.

Figure 4.42 shows that the lateral deflection of type I1 (Emb 15) is lower than that of types A1 and J1. This can either be due to the lower failure load which would result in smaller deflections or to the reduction in dowel action due to the premature failure of the concrete. The plot also shows that the lateral deflection taking place in type J1 (Emb 25) specimens is lower than that in type A1 (Emb 20) specimens. This shows that the 5 mm increase in the embedment depth has altered the distribution of forces in the test specimens. The additional depth of concrete around the lattice in the biscuit increases the resistance of the specimens to lateral deflection.

In Figure 4.47, a similar trend to the load-bottom deflection profiles is observed. For types A1 and J1, the relationship between the load and lateral deflection is linear up to the point of first cracking after which a non-linear behaviour is observed. Types A1 and J1 specimens also have almost the same lateral stiffness. In contrast, the load-lateral deflection profile remains linear for type I1 specimens. This confirms that the lateral stiffness of the specimens is not affected when the embedment depth is increased beyond 20 mm but reduces when the embedment depth is decreased below 20 mm.

F. Effect of Dowel Bar Diameter

Figure 4.43 shows that the lateral deflection of type K1 is less than that of type A1 at the bottom of the specimen. This suggests that the larger bar diameter in type K1 has a restraining effect on the lateral deflection of the test specimen in comparison with type A1.

In Figure 4.48, a similar trend to the load-bottom deflection profiles is observed. The relationship between the load and lateral deflection is linear up to the point of first cracking after which a non-linear behaviour is observed.

4.3.8 Failure Mechanism

The failure mechanism of the test specimens was observed with particular attention to the formation of cracks during the push-out tests.

4.3.8.1 General Trend

A. Results

The general behaviour of all test specimens was very similar. When the load was increased, the first crack either occurred along the interface between the core and Biscuit 2 which was closely followed by another crack along the core/Biscuit 1 interface; or simultaneously along both interfaces. The first and second cracks occurred between 72% and 86% of the failure load. As the load continued to increase, the interface cracks deepened and further smaller cracks began to develop on the surface of the test specimens. This was closely followed by 'bang' noises suggesting the fracture of the lattice bars and excessive lateral and bottom deflections until the load began to drop beyond its maximum. No cracks were observed on the side faces of the biscuits. Figure 4.49 shows a typical push-out test specimen for types A1-K1 after failure. The core was also removed after the tests to expose the lattice bars and to gain a better understanding of the failure mechanism of the test specimens as shown in Figure 4.50.

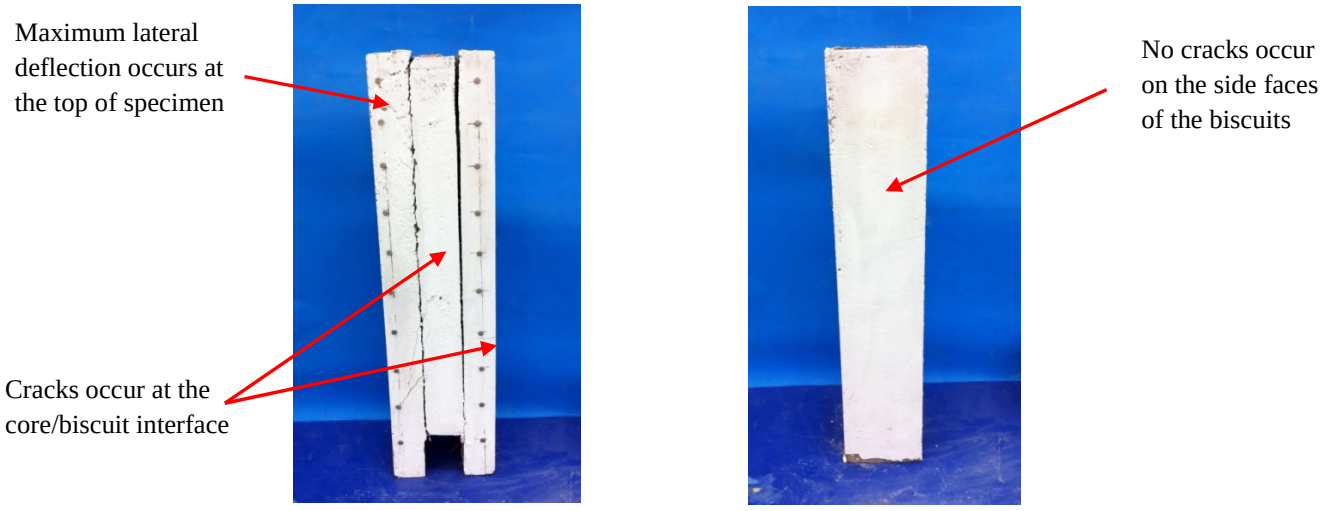

Figure 4.49 - General Behaviour of test specimens

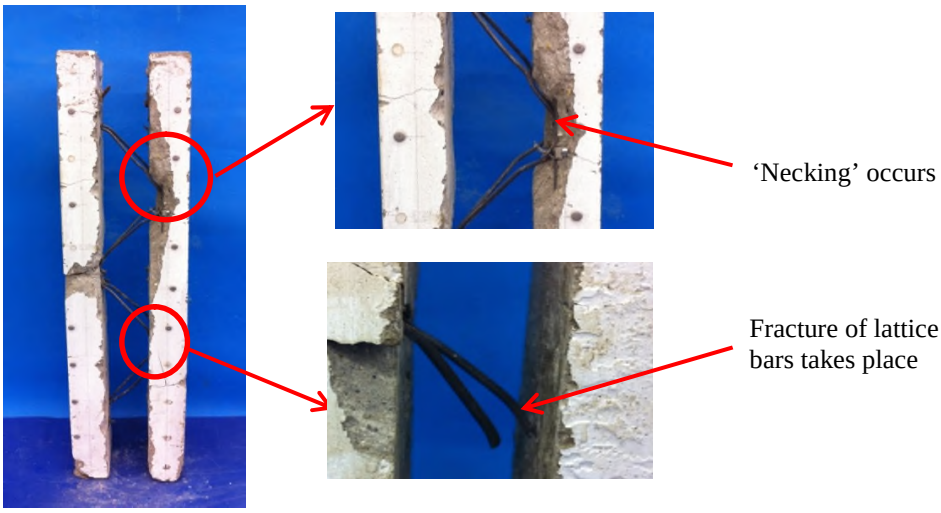

Figure 4.50 - Behaviour of specimens with core removed

B. Discussion

The general behaviour gives an indication of the failure mechanism of the test specimens. As explained previously, when the load is applied, longitudinal shear forces develop along he interfaces between the core and the biscuits which are resisted by the aggregate interlock mechanism. As the load is increased further, cracking occurred at the core/biscuit interface and dowel action was induced in the lattice bars which are subjected to tensile forces. This is confirmed by the necking and fracture observed in the diagonal bars. In addition, it can be concluded that failure of the test specimens is caused by steel yielding.

Another important observation was that no cracks were observed on the sides of the specimen. This confirms that the transverse reinforcement provided in the biscuits were adequate in preventing the formation of splitting cracks in the outer biscuits.

4.3.8.2 General behaviour of Types H1 & I1

A. Results

Types H1 (10/50/10) and I1 (Embedment 15 mm) exhibited a different behaviour from other specimen types. In these test specimens with the rough surface, a conical failure at the points where the nodes of the lattice were located was also observed as shown in Figure 4.51. This was closely followed by 'bang' noises suggesting the fracture of the lattice bars and excessive lateral and bottom deflections until the load began to drop beyond its maximum. No cracks were observed on the side faces of the biscuits in all types of tests.

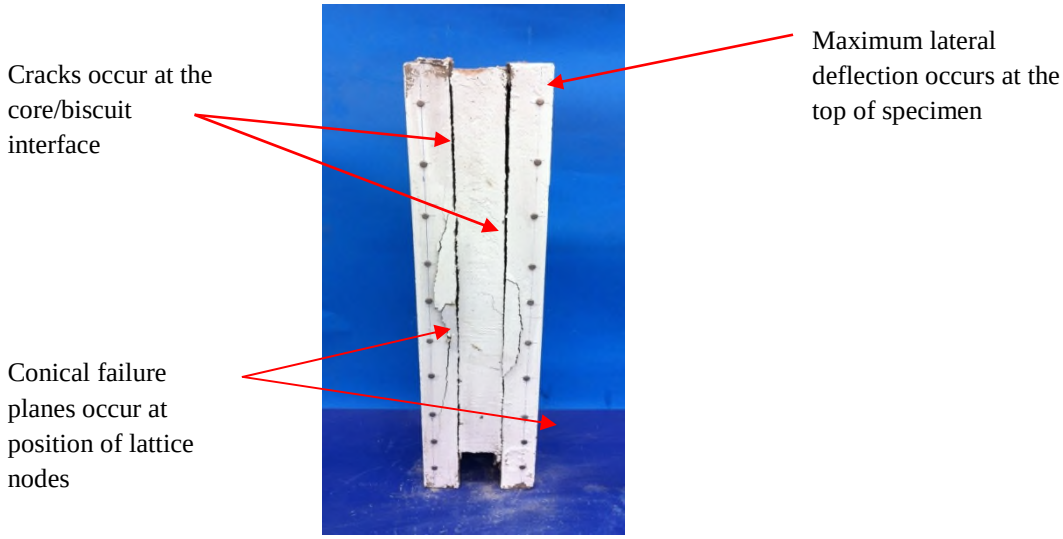

Figure 4.51 – General Behaviour of tests specimens: Types H1 and I1

B. Discussion

In Type H1 (10/50/10), the extensive cracks in the concrete core and biscuits indicate that failure of the test specimens is caused as a result of concrete crushing rather than

steel yielding. This is confirmed by close inspection of the test specimens which reveals significantly smaller deformations of the steel bars at the core/biscuit interface. It can be concluded that failure in type H1 specimens is caused by concrete crushing rather than steel yielding and that the strength of the concrete in the biscuit significantly influences the failure mechanism of the test specimens.

Similarly, in type I1 (Embedment 15 mm), extensive cracks in the concrete core and biscuits of the test specimens are caused as a result of concrete crushing rather than steel yielding. The conical failure planes are also an indication of embedment failure in the concrete. When the load is applied, tensile forces are induced in the lattice bars with high stress concentrations at the nodes. This causes tensile cracks to develop and extend further due to the reduced embedment depth and consequently forms a shear embedment failure cone. A close inspection of the test specimens also confirms that significantly smaller deformations of the steel bars occur. It can be concluded that failure in type I1 specimens is caused by concrete crushing due to embedment failure.

4.4 Overview of Push-out Tests

4.4.1 Set 1

The shear resistance obtained from the push-out tests of P1 and P2 are 255 kN and 39 kN respectively. Additionally, the average deflections at the bottom of the core for P1 and P2 are 3.19 mm and 1.05 mm respectively.

The cyclic unloading and loading increased the bottom deflection by 0.63% and 0.43% of the average bottom deflections in P1 and P2 respectively. This shows that the effect of the cyclic unloading/loading is not critical to the failure of the push-out test specimens.

The first crack occurs along the core/biscuit interface at a minimum of 74 % and 75 % of the failure load for P1 and P2 specimens respectively. It can be concluded that in twinwalls where lattice girders are used as shear connectors, cracking is not expected under serviceability loads of approximately 70%.

The load-bottom deflection profiles for P1 and P2 show that the specimens deflect in three main stages. Before the first crack is formed, a linear behavior is observed. The first crack then occurs at the core/biscuit interface beyond which the specimens deform in a non-linear manner until failure.

All specimens undergo significant deformations prior to failure which confirms that the lattices used in twinwalls are ductile and efficient as shear connectors. All specimens fail by yielding in the form of necking or fracture of the steel lattice bars at the core/biscuit interface of the test specimens.

Results confirm that the small scale specimens in P2 can be used instead of the large scale specimens in P1 for subsequent push-out tests to investigate the shear behaviour of twinwalls.

4.4.2 Set 2

4.4.2.1 Effect of Base Restraints

The shear resistance obtained from the push-out tests of types A1, B1, C1 and D1 are 39 kN, 39 kN, 36 kN and 34 kN respectively. The PTFE sheets have no effect on the failure load. Using a roller support at the base of one biscuit reduces the failure load by 5% and using roller supports at the base of both biscuits reduces the failure load by 12% in comparison with biscuits which are restrained by fixed supports.

The average deflections at the bottom of the core for types A1, B1, C1 and D1 are 1.05 mm, 1.32 mm, 0.69 mm and 1.19 mm. This shows that varying the restraints alters the stiffness of the test specimens. Additionally, all specimens undergo significant deformations prior to failure which confirms that the lattices used in twinwalls are ductile and efficient as shear connectors.

The first crack occurs along the core/biscuit interface at a minimum of 72 % - 75 % of the failure load. It can be concluded that the variation of the base restraints does not have a significant effect on the load at which the first cracks forms at the core/biscuit interfaces.

In the load-bottom deflection and load-lateral deflection profiles, the specimens deflect in three main stages. Before the first crack is formed, a linear behaviour is observed. The first crack then occurs at the core/biscuit interface beyond which the specimens deform in a non-linear manner until failure.

The lateral deflections show that the roller supports are effective in reducing friction at the base of the biscuits. All specimens fail by yielding in the form of necking or fracture of the steel lattice bars at the core/biscuit interface of the test specimens.

4.4.2.2 Effect of Surface Roughness

The experimental failure obtained from the push-out tests of types A1, E1 and F1 are 41 kN, 29 kN and 71 kN respectively. If the friction at the base of the specimens is taken into account, the failure loads for types A1, E1 and F1 are 36 kN, 26 kN and 63 kN respectively. $P_{very\ smooth} \approx 1.4\ P_{smooth} \approx 1.7\ P_{rough}$. Thus, increasing the surface roughness leads to an increase in the shear strength of the test specimens. The experimental and theoretical (EC2) failure loads increases as the surface roughness increases.

Result show that the EC2 theoretical values obtained by using the actual angle of inclination $\alpha = 38^0$ and the EC2 limit of $\alpha = 45^0$ are almost equal. Thus, the validity of the EC2 equation ($45^0 \leq \alpha \leq 90^0$) can be extended to take into account a smaller angle of inclination of $\alpha = 38^0$. The EC2 'smooth' surface roughness can be used to provide estimates of the interface shear resistance of twinwalls.

The average bottom deflections at failure of type A1, E1 and F1 specimens are 1.05 mm, 1.26 mm and 1.06 mm respectively. Reducing the surface roughness from 'smooth' to 'very smooth' leads to an increase in the bottom deflection of approximately 17 % but increasing the surface roughness to 'rough' seems to have no effect on the stiffness of the test specimens. All specimens undergo significant

deformations prior to failure which confirms that the lattices used in twinwalls are ductile and efficient as shear connectors.

The first crack occurs at a minimum of 75 %, 68 % and 74 % of the failure load for types A1, E1 and F1 respectively. Reducing the surface roughness from ‘smooth’ to ‘very smooth’ leads to a 7% decrease in the first crack load but increasing the surface roughness to ‘rough’ seems to have almost no effect on the stiffness of the test specimens.

In the load-bottom deflection and load-lateral deflection profiles, the specimens deflect in three main stages. Before the first crack is formed, a linear behaviour is observed. The first crack then occurs at the core/biscuit interface beyond which the specimens then deform in a non-linear manner until failure.

Results show that surface roughness has an influence on the lateral deflections of the test specimens. Type E1 specimens with the ‘very smooth’ surface undergo the least lateral deflections whereas the lateral stiffness of type F1 specimens with the ‘rough’ surface is the greatest. All specimens fail by yielding in the form of necking or fracture of the steel lattice bars at the core/biscuit interface.

4.4.2.3 Effect of Concrete Strength

The experimental failure obtained from the push-out tests of types A1 (50/50/50), G1 (50/10/50) and H1 (10/50/10) are 41 kN, 41 kN and 31 kN respectively. If the friction at the base of the specimens is taken into account, the failure loads for types A1, G1 and

H1 are 36 kN, 36 kN and 27 kN respectively. The failure load increases with increasing strength of concrete in the biscuits but is unaffected by the strength of concrete used in the core.

Results confirm that the value of the tensile strength of concrete (f_{ctd}) in Cl. 6.2.5 of EC2 should be based on the concrete used in the biscuits rather than the core. It is also confirmed that the validity of the EC2 equation ($45^0 \leq \alpha \leq 90^0$) can be extended to take into account a smaller angle of inclination of $\alpha = 38^0$.

The average bottom deflections at failure of type A1, G1 and H1 specimens are 1.05 mm, 0.94mm and 1.01 mm respectively. The first crack occurs at a minimum of 75 %, 75% and 100 % of the failure load for types A1, G1 and H1 respectively. The results show that the load at which the first crack occurs is influenced by the strength of concrete in the biscuits but not affected by the strength of the concrete in the core.

The load-bottom deflection plots for types A1 and G1 specimens are linear before the first crack appears after which the specimens exhibit non-linear behaviour. In Type H1 specimens, the load-bottom deflection curves remain almost linear. It can be concluded that the stiffness of the test specimens is influenced by the strength of the concrete in the biscuits but is not affected by the strength of the concrete in the core.

Results show that the lateral stiffness of the specimens is not influenced by the strength of the concrete in the core but is dependent on the strength of the concrete in the biscuits. Types A1 and G1 specimens fail by yielding in the form of necking or fracture of the steel lattice bars at the core/biscuit interface. Type H1 specimens fail by concrete

crushing rather than steel yielding. The failure mechanism is therefore not affected by the strength of the concrete in the core but is significantly influenced by strength of the concrete in the biscuits.

4.4.2.4 Effect of Embedment Depth

The experimental failure obtained from the push-out tests of types A1 (Emb 20), I1 (Emb 15) and J1 (Emb 25) are 41 kN, 36 kN and 41 kN respectively. If the friction at the base of the specimens is taken into account, the failure loads for types A1, I1 and J1 are 36 kN, 29 kN and 36 kN respectively. The failure load increases by 21% when the embedment depth is increased from 15 mm to 20 mm. However, when the embedment depth is increased from 20 mm to 25 mm, there is no change in the failure load. This suggests that the lattice is fully anchored at an embedment depth of 20 mm which is greater than the EC2 critical embedment value of 17.5 mm.

The average bottom deflections at failure of type A1, I1 and J1specimens are 1.05 mm, 0.81 mm and 1.01 mm respectively. The first crack occurs at a minimum of 75 %, 100% and 75 % of the failure load for types A1, I1 and J1 respectively. The results show that the distribution of forces in the specimens is affected when the embedment depth is reduced from 20 mm to 15 mm but any increase in the embedment depth beyond 20 mm has no effect on the first crack load.

The load-bottom deflection plots for types A1 and J1 specimens are linear before the first crack appears after which the specimens exhibit non-linear behaviour. In Type I1 specimens, the load-bottom deflection curves remain almost linear. It can be concluded

that the stiffness of the specimens is only affected if the embedment depth is decreased from 20 mm but remains unchanged if the embedment depth is increased beyond 20 mm.

Results show that that the lateral stiffness of the specimens is not affected when the embedment depth is increased beyond 20 mm but reduces when the embedment depth is decreased below 20 mm.

Types A1 and J1 specimens fail by yielding in the form of necking or fracture of the steel lattice bars at the core/biscuit interface. Type I1 specimens fail by concrete embedment failure. The failure mechanism is therefore only affected when the embedment depth is reduced below 20 mm.

4.4.2.5 Effect of Dowel Bar Diameter

The experimental failure obtained from the push-out tests of types A1 (3 mm dia) and K1 (6 mm dia) are 41 kN and 120 kN respectively. If the friction at the base of the specimens is taken into account, the failure loads for types A1 and K1 are 36 kN and 106 kN respectively.

Increasing the diameter of the lattice bar from 3 mm to 6 mm triples the failure load of the test specimens in type K1, i.e. $P_{3mm} \approx 3\ P_{6mm}$. The experimental values are also higher than the EC2 theoretical values. Hence, EC2 provides conservative estimate of the interface shear strength in twinwalls.

The average deflections at the bottom of the core for types A1 and K1 are 1.05 mm, and 1.78 mm. All specimens undergo significant deformations prior to failure which confirms that the lattices used in twinwalls are ductile and efficient as shear connectors. The first crack occurs along the core/biscuit interface at between 75 % - 76 % of the failure load. It can be concluded that the variation of the lattice bar diameter has no significant effect on the load at which the first cracks forms at the core/biscuit interfaces.

In the load-bottom deflection and load-lateral deflection profiles, the specimens deflect in three main stages. Before the first crack is formed, a linear behaviour is observed. The first crack occurs at the core/biscuit interface. The specimens then deform in a non-linear manner until failure. All specimens fail by yielding in the form of necking or fracture of the steel lattice bars at the core/biscuit interface.

Chapter 5

Phase II: Experimental Procedure

Flexural Tests

5.1 Introduction

As discussed, in Chapter 2, the structural behaviour of the twinwalls is very complex. In water tank applications, twinwalls behave as cantilevers which are subject to combined bending and shear. The shear behaviour of twinwalls was investigated using push-out tests as described in Chapters 3 and 4. However, the flexural behaviour of twinwalls is still not well understood.

A series of experimental tests were therefore carried out to provide a better understanding of the flexural behaviour of twinwalls. Two key aspects were investigated:

1) Role of lattice girder in twinwalls
2) Role of concrete biscuits in twinwalls

5.2 Flexural Tests

5.2.1 Details of Test Specimens

Details of the test specimens are summarised in Table 5.1.

Type.	Depth of Biscuits	Depth of Core	Depth of Lattice	Diameter of lattice bars
A2	30	No core	No lattice	No bars
B2	30	No core	60	Top – 5 mm Diagonal – 3 mm Bottom - 3 mm
C2	40	No core	80	"
D2	30	30	60	"
E2	30 (Solid Section)	30 (Solid Section)	60	"

Table 5.1 – Test Details: A2-E2

As mentioned above, two main aspects were investigated:

1) Role of lattice girder in twinwalls in terms of the following:
   - *Effect of using lattice girder in twinwalls*

     The results from type A2 specimens (*with no lattice girders*) were compared with those from type B2 specimens (*with lattice girders*) were compared.
   - *Effect of varying the depth of lattice girder*

     The results from type B2 (*60 mm deep lattice*) were compared with those from type C2 (*80 mm deep lattice*) to investigate the effect of varying the lattice depth on the flexural behaviour of twinwalls.

2) Role of concrete biscuits and core in terms of the following:
   - The results from type A2 (*with no concrete core*) were compared with type D2 (*biscuits cast in three stages*) and type E2 (*biscuits cast in one stage*).

Details of the test specimens used for the flexural tests are shown in Figure 5.1. All specimens were 1200 mm long and 200 mm wide and the two biscuits (top and bottom) were reinforced with 4 mm diameter steel bars placed mid-depth at 75 and 40 mm centres in the longitudinal direction in the top and bottom biscuits respectively and 100 mm centres in the transverse direction in both biscuits. The lattice girders were at 100 mm centres.

Tensile tests were carried out on the reinforcement and lattice diagonal bars to determine the yield strength of the steel. Five bars were tested in each case and the average stresses and strains were calculated. The yield stress was taken as the proof stress occurring at 0.2% strain. The yield stress for the lattice and reinforcement bars were 280 N/mm^2 and 305 N/mm^2 respectively.

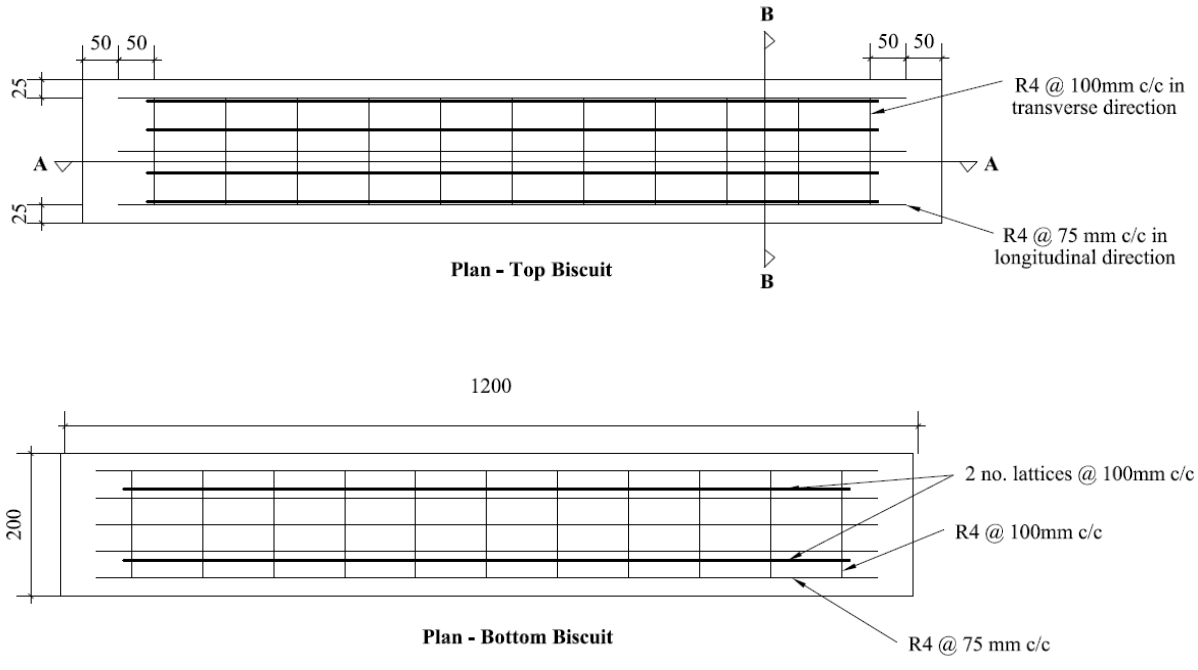

TYPE A2

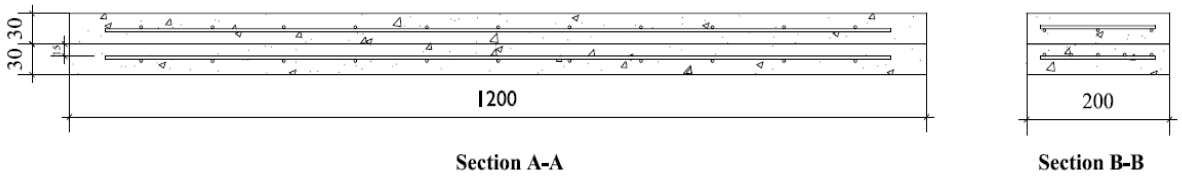

Section A-A **Section B-B**

TYPES B2 & C2

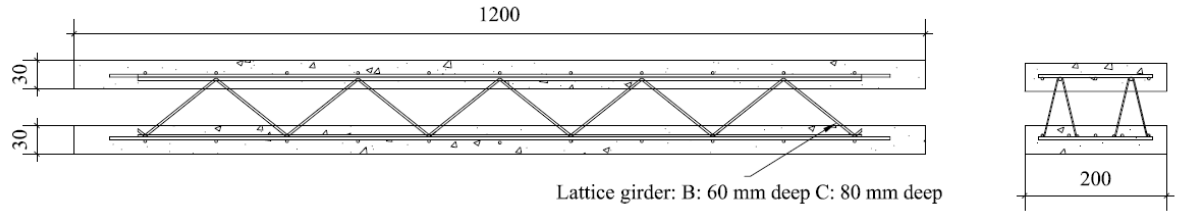

Depth of top and bottom biscuits:
B & C : 30 mm

Section A-A **Section B-B**

TYPE D2

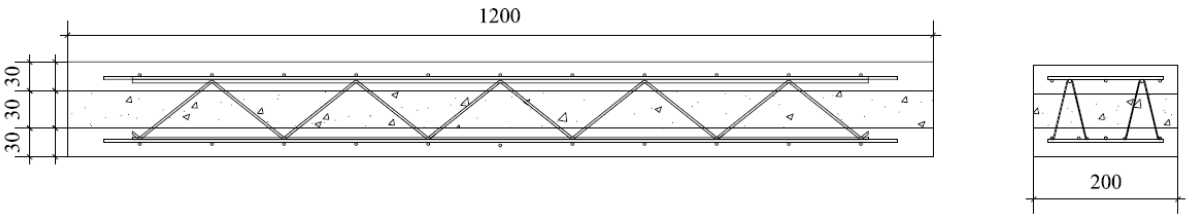

Section A-A **Section B-B**

TYPE E2

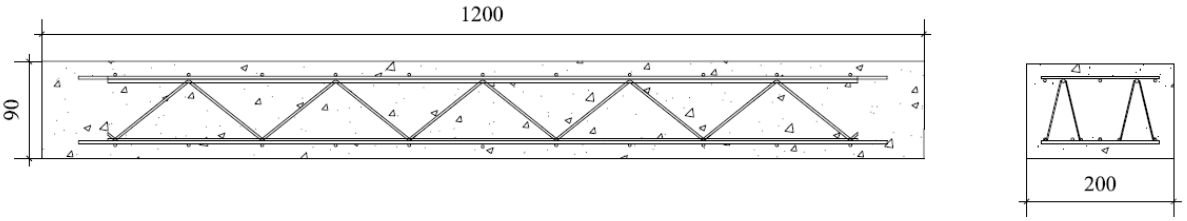

Section A-A **Section B-B**

Figure 5.1 - Details of test specimens

5.2.2 Casting Procedure

The casting procedure for Type A2 specimens occurred in two stages. The bottom half of the reinforcement was placed in in a clean timber mould and supported on spacers. Sufficient concrete was poured and compacted by vibration form the top biscuit. After curing for 24 hours, the specimens were inverted and the reinforcement was supported on spacers to achieve the correct embedment. The assembly was positioned in a second timber mould and concreted to form the bottom biscuit. The casting procedure for Types B2 and C2 was similar to the above procedure. However, the lattices were attached to the reinforcing bars in the biscuits using steel ties prior to casting the top biscuit. After the final concrete pouring, the test specimens were air conditioned for a further seven days. The casting procedure to Type D2 specimens occurred in three main stages as shown in Figure 5.2.

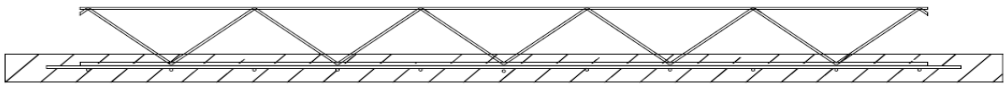

DAY 1: Steel reinforcement and lattices placed in formwork and concrete poured to form top biscuit. Types B2-E2

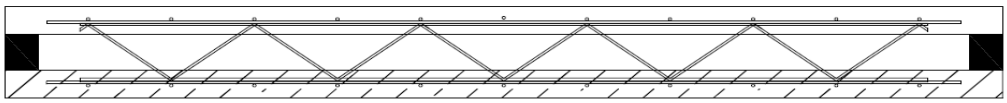

DAY 2: Top biscuit rotated by 180° and supported over another timber formwork. Concrete poured in formwork to form bottom biscuit: Types B2-E2

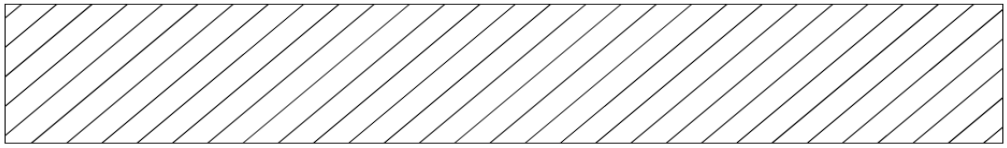

DAY 3: Specimen rotated 90° and supported over another timber formwork. Concrete poured in formwork to form core in Type D2 specimen.

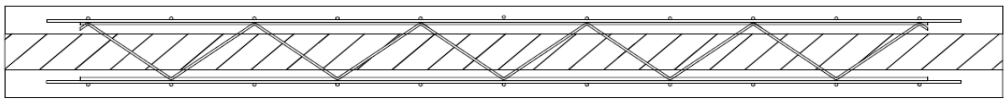

DAY 3: View of core in Type D2

Figure 5.2 – Casting Procedure: A2-E2

The bottom half of the reinforcement and lattice cage were placed in a clean timber mould and supported on spacers. Sufficient concrete was poured and compacted by vibration to form the top biscuit. After curing for 24 hours, the specimens were inverted and the upper half of the cage was supported on spacers to achieve the correct embedment. The assembly was positioned in a second timber mould and concreted to form the bottom biscuit.

After curing the concrete in the bottom biscuit for 24 hours, the two sets of moulds were removed. The specimen was rotated by 90 degrees and shuttering was attached to the outside face. The core was then cast and the shuttering was removed after 24 hours. For Type E2 specimens, the concrete was poured in one go. All test specimens were air conditioned for seven days.

Three cubes were also cast from each batch of concrete and cured and conditioned in the same way as the test specimens. The target 28-day strength of the concrete used for both biscuits and the core was 50 N/mm^2 and details of the concrete mix are provided in Table 5.2. The concrete was designed assuming water/cement ratios of 0.50 and 0.90.

Materials	**Batch Weights (kg/litre of**
Cement	0.770
Fine Aggregate	1.110
Water	0.385

Table 5.2 – Batch weights of concrete: A2-E2

After a total of six days after the final concrete pour, the specimens were tested. The specimens were painted white to help monitor crack development during testing.

5.2.3 Test Set-up

Figures 5.3 & 5.4 show the test set-up for type A2-E2 specimens. DEMEC studs were positioned at 100 mm centres on various points of the top and bottom biscuits and the core where applicable to provide an indication of the lateral deflections and strains in the concrete during testing. Strain gauges were also installed on the lattice bars in types B2 and C2 specimens.

Four point bending tests were carried out to simulate the application of a uniformly distributed load over the top biscuit of the specimens. The specimens were placed in the testing frame and load was applied until failure. Failure was taken as the maximum load reached by the test specimens.

At each load increment, the deflections at the top and bottom of the specimens was measured using dial gauges, the strain in the steel (types B2 and C2) and the strains in the concrete (using DEMEC readings) were measured. The general behaviour of the specimens was also observed with particular attention to crack formation and propagation.

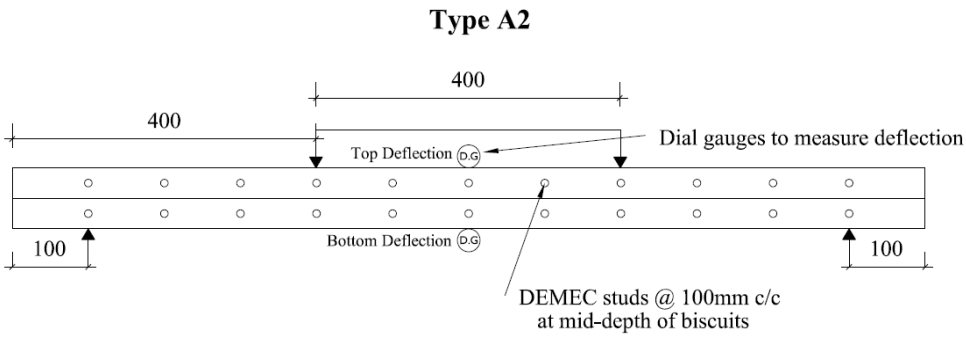

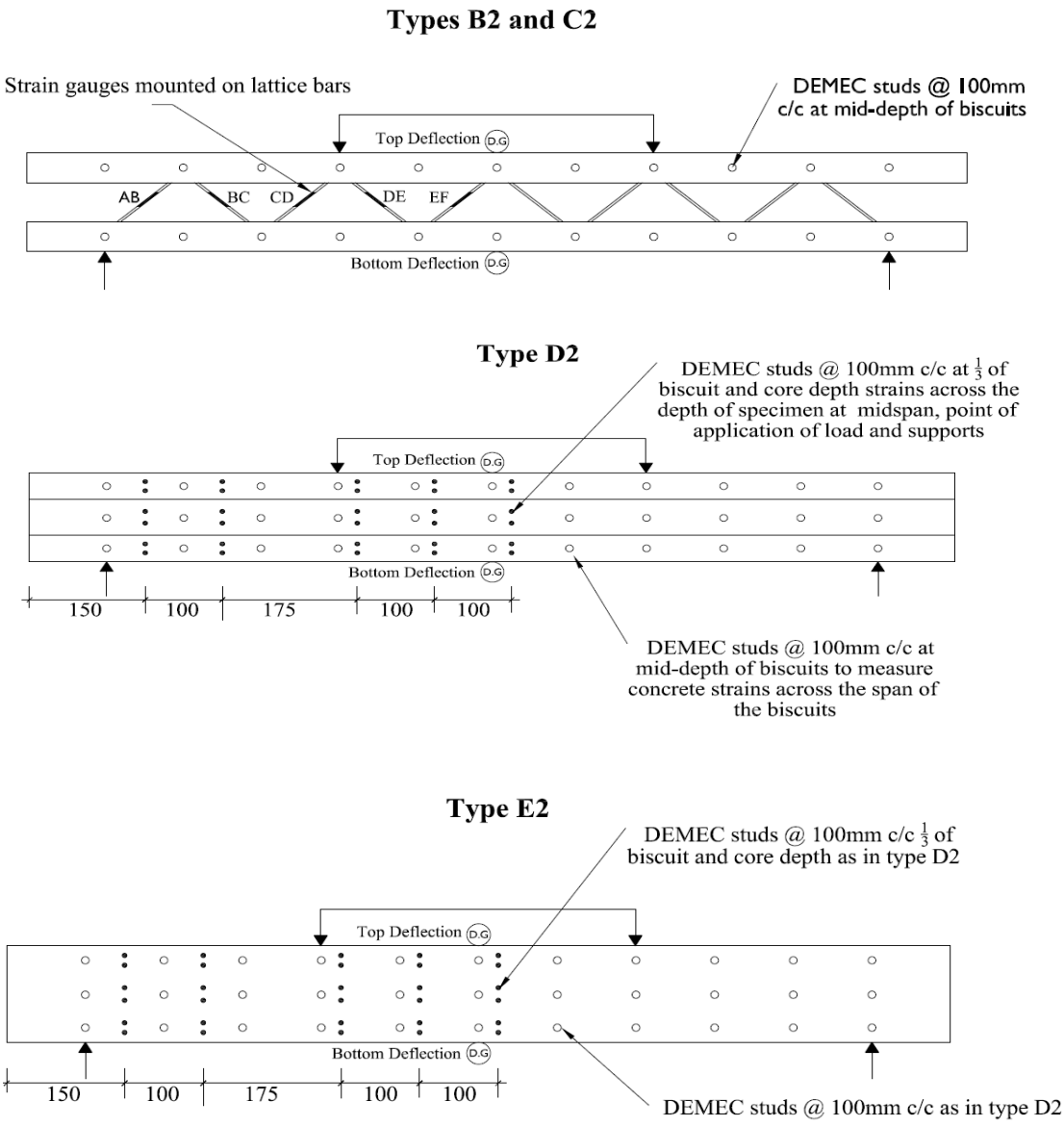

Figure 5.3 – Flexural Test set-up: Types A2-E2

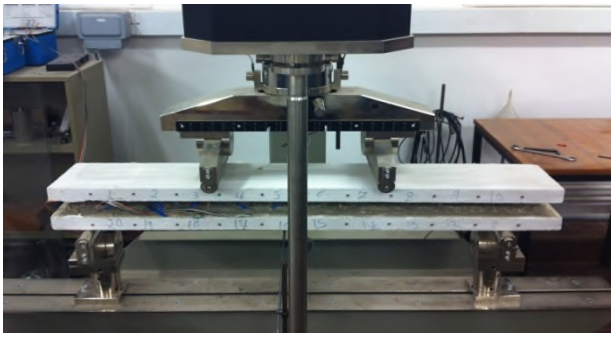

Test set-up: Types B2 and C2

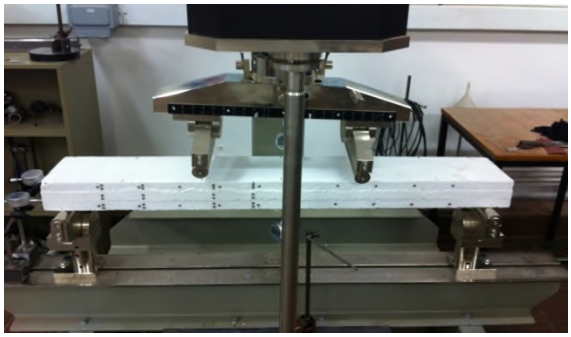

Test set-up: Type D2

Figure 5.4 – Actual Test set-up: Types B2, C2 & D2

5.3 Comparison with Theoretical Approach

5.3.1 Failure Mechanism

The experimental results were compared to the results from the theoretical analysis which is based on the application of fundamental engineering principles. When the twinwall panel is subjected to four-point bending, failure can occur as a result of several structural actions:

5.3.1.1 Flexural Failure

Flexural failure occurs when the bending capacity of the twinwall panel is exceeded and can be caused by either:

- Steel failure leading to yielding of the steel reinforcement in the bottom biscuit if the section is under-reinforced or;
- Concrete failure giving rise to crushing of the concrete if the section is over-reinforced.

In the experimental tests carried out, flexural failure can occur in types A2-E2.

5.3.1.2 Shear Failure

Shear failure occurs when the shear capacity of the test specimen is exceeded, resulting in two failure mechanisms, (a) diagonal tension failure and (b) diagonal compression failure, as shown in Figure 5.5 below:

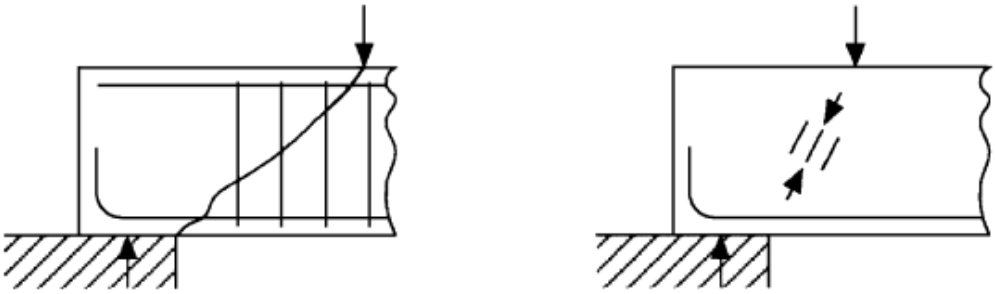

a) Diagonal tension failure

b) Diagonal compression failure

Figure 5.5 - Shear failure mechanisms (Source: Arya, 2004)

As seen in Figure 5.5(a), diagonal tension failure result in the formation of a diagonal crack between the edge of the support and the load point. In practice, such failure is usually avoided by provided shear connectors. In the case of the twinwall panel, the lattice girder acts as shear connectors which resists the shear forces applied by developing tensile forces in the diagonal lattice bars. Hence, if diagonal shear tension failure occurs in the twinwall specimens, high tensile forces will be induced in the diagonal bars leading to steel yielding of the lattice bars.

Diagonal compression failure, shown in Figure 5.5(b) leads to crushing of the concrete near the supports. In BS 8110, this failure is avoided by limiting the maximum shear stress to 5 N/mm^2 or $0.8\sqrt{f_{cu}}$, whichever the lesser. In EC2, the maximum shear capacity of the concrete is not a fixed value (unlike BS 8110) but depends on the applied shear. In the experimental tests carried out, flexural failure can occur in types B2-E2.

5.3.1.3 Interface Shear Failure

Interface shear failure is also expected to occur in type D2 where the void between the top and bottom biscuits is filled with a concrete core. As the load is applied, interface

shear forced develop at the interface between the core and biscuits causing the interfaces to slip relative to each other. Further shear distortion at the interface is resisted by three main mechanism (1) aggregate interlock, (2) friction and (3) dowel action. Hence, if interface shear failure occurs, slip will be observed at the core/biscuit interfaces followed by yielding of the diagonal lattice bars due to an increase in dowel action.

Based on the above failure mechanisms, the bending, shear and interface shear failure loads can be determined for types A2-E2 specimens and results were compared with experimental data.

5.3.2 Degree of Composite Action

The experimental results from the flexural tests were compared with theoretical predictions to determine the degree of composite action of the twinwalls. This is described below.

5.3.2.1 Load-deflection profiles

The theoretical failure loads and deflections were first determined for fully composite and non-composite limits and plotted on the experimental load-deflection profiles for the test specimens. This provided an initial indication of the degree of composite action of the test specimens.

5.3.2.2 Degree of composite action at elastic stage

From the experimental load-stress profiles, the linear stage is first identified, i.e. the stage where the load is directly proportional to the top and bottom stresses. The stress corresponds to that in the top and bottom concrete biscuits. The effective moment of inertia, I_c is then calculated using the following formula:

$$I_c = \frac{Mh}{\sigma_b - \sigma_t}$$

Equation 5.1 – I_c at elastic stage

In Equation 5.1, σ_b and σ_t are the stresses at the bottom and the top face of the concrete biscuits of the specimens respectively. M refers to the bending moment and h is the depth of the twinwall specimens.

The ratio of the effective moment of inertia, I_c to the gross moment of inertia, I_g provides an indication of the degree of composite action at the elastic stage. The gross moment of inertia, I_g is calculated assuming that fully composite action occurs in the test specimens and is taken as the uncracked fully composite moment of inertia, I_u summarised in Table 5.3.

$$\textit{Degree of composite action at elastic stage} = I_c/I_g$$

Equation 5.2 – Degree of composite action at elastic stage

5.3.2.3 Degree of composite action at ultimate stage

The degree of composite action at ultimate stage can be obtained by comparing the experimental failure loads with that of a fully monolithic member. In this case, type E2 has been cast as a solid section and can therefore be used as the fully composite upper bound value.

The degree of composite action was therefore calculated as the ratio of the experimental failure load to that obtained for E2 specimens.

$$Degree\ of\ composite\ action\ at\ ultimate\ stage = \frac{Experimental\ Failure\ Load}{Failure\ Load\ for\ Type\ E2}$$

Equation 5.3 – Degree of composite action at ultimate stage

5.3.3 Determination of Theoretical Deflections

The deflections of types A2-E2 specimens can be theoretically determined from the test arrangement shown below. The values of a and L are constant at 300 mm and 1000 mm respectively and P is the applied load.

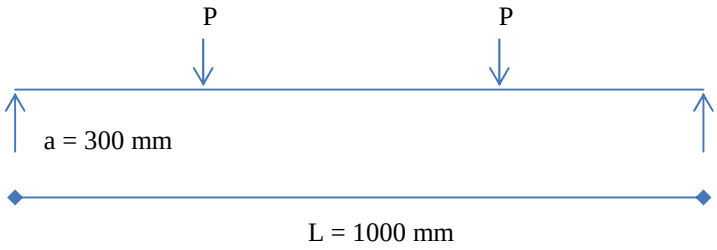

From above, the maximum deflection can be calculated as:

$$\partial_{max} = \frac{Pa^2 (3L-4a)}{6EI}$$

Equation 5.4 - Determination of maximum deflection

The modulus of elasticity, E can either be based on that of the steel or the concrete. However, according to Oehlers and Bradford (1995), the flexural rigidity (EI) of a fully composite beam should be based on the modulus of elasticity of concrete (E_c = 30 GPa) and the second moment of area of a transformed section (I_t) which takes into account the contribution from concrete and steel. The second moments of area of the transformed section (I_t) can be determined for two cases: (1) uncracked and (2) cracked section.

In both cases, the areas of the steel are transformed into an equivalent area of concrete by using the modular ratio, m as follows:

$$\text{Modular ratio, } m = E_s/E_c$$

,where, E_s is the elastic modulus of the steel taken as 200 GPa and E_c is the elastic modulus of the concrete taken as 30 GPa. Hence, the modular ratio, m = 200/30 = 6.67.

a) Uncracked Section

The second moment of area of a transformed uncracked section can be determined from the following:

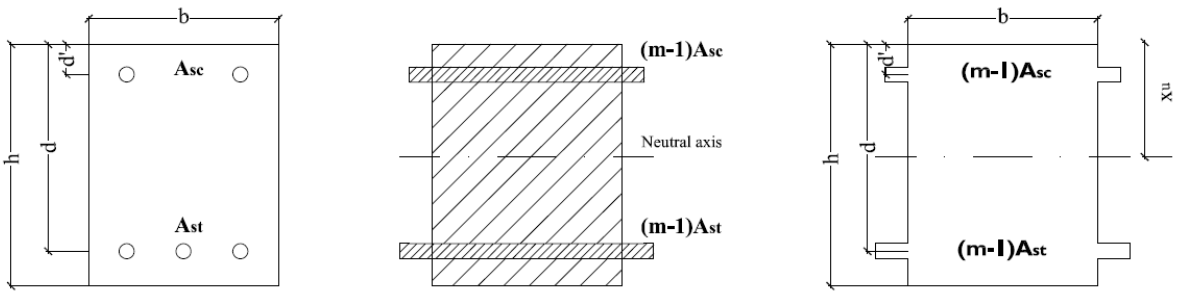

Figure 5.6 - Transformed area – Uncracked Section

Taking moments about the upper edge gives:

$$x_u = \frac{\sum(Ax)}{\sum(A)}$$

$\sum (Ax) = bh\,(h/2) + (m\text{-}1)A_{sc}d' + (m\text{-}1)A_{st}d$

$\sum (A) = bh + (m\text{-}1)A_{sc} + (m\text{-}1)A_{st}$

Hence, depth of neutral axis, $x_u = \frac{bh\,(h/2) + (m\text{-}1)A_{sc}d' + (m\text{-}1)A_{st}d}{bh + (m\text{-}1)A_{sc} + (m\text{-}1)A_{st}}$

The second moment of area, I_u can be determined from: $I_u = I_{u,\,concrete} + I_{u,asc} + I_{u,ast}$

$$I_{u,\,concrete} = \frac{bh^3}{2} + bh\left(x_u - \frac{h}{2}\right)^2$$

$$I_{u,\,asc} = (m\text{-}1)\,A_{sc}\left(x_u - d'\right)^2$$

$$I_{u,\,ast} = (m\text{-}1)\,A_{st}\left(d - x_u\right)^2$$

Thus, the second moment of area for an uncracked section is given by:

$$I_u = \frac{bh^3}{2} + bh\left(x_u - \frac{h}{2}\right)^2 + (m\text{-}1)\,A_{sc}\left(x_u - d'\right)^2 + (m\text{-}1)\,A_{st}\left(d - x_u\right)^2$$

Equation 5.5 – Uncracked second moment of area, I_u

b) Cracked Section

The second moment of area of a transformed cracked section can be determined from the following:

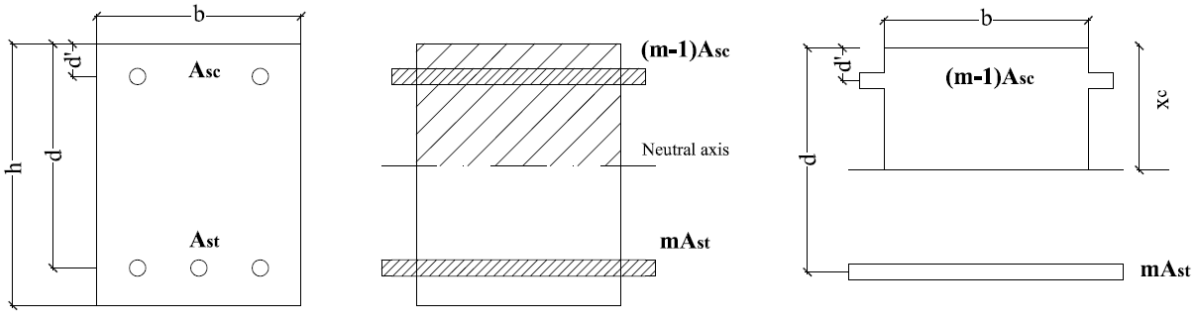

Figure 5.7 - Transformed area – Cracked Section

Taking moments about the upper edge gives:

$$x_c = \frac{\sum(Ax)}{\sum(A)}$$

$\sum (Ax) = bx\,(x/2) + (m\text{-}1)A_{sc}d' + (m\text{-}1)A_{st}d$

$\sum (A) = bx + (m\text{-}1)A_{sc} + (m\text{-}1)A_{st}$

Hence, depth of neutral axis, $x_u = \frac{bx\,(x/2) + (m\text{-}1)A_{sc}d' + (m\text{-}1)A_{st}d}{bx + (m\text{-}1)A_{sc} + (m\text{-}1)A_{st}}$

Rearranging the above equation gives:

$$\frac{b}{2}x^2 + [(m\text{-}1)A_{sc} + mA_{st}]x + [(m\text{-}1)A_{sc}d' + mA_{st}d] = 0$$

The above equation can be expressed in the form: $Ax^2 + Bx + C$ where,

$A = \frac{b}{2}$,

$B = (m-1)A_{sc} + mA_{st}$ and,

$C = (m-1)A_{sc}d' + mA_{st}d$

The value of x can be determined by the following:

$$x_c = \frac{-B+\sqrt{B^2 - 4AC}}{2A}$$

The second moment of area, I_c can be determined from: $I_c = I_{c,\ concrete} + I_{c,asc} + I_{c,ast}$

$$I_{u,\ concrete} = \frac{bx^3}{2} + bx\left(\frac{x}{2}\right)^2 = \frac{bx^3}{3}$$

$$I_{u,\ asc} = (m-1)\ A_{sc}(x_c - d')^2$$

$$I_{u,\ ast} = (m-1)\ A_{st}(d - x_c)^2$$

Thus, the second moment of area for a cracked section is given by:

$$I_c = \frac{bx^3}{3} + (m-1)\ A_{sc}(x_c - d')^2 + (m-1)\ A_{st}(d - x_c)^2$$

Equation 5.6 – Cracked second moment of area, I_c

c) Fully composite deflections

At the early stages of flexural loading, the test specimens for types A2-E2 can be considered to act in fully composite manner; in other words, they behave as a solid beam with a single neutral axis. Additionally, the test specimens are uncracked at this stage. Hence, Equation 5.5 can be used to determine the uncracked second moment of area, I_u can be determined. Results summarised in Table 5.3. The second moment of area can then be used to determine the deflections at various loads using Equation 5.4.

Type	Fully composite - Uncracked	
	x_c (mm)	I_u ($x10^6$) (mm^4)
A2	30.09	3.814
B2	45.13	13.007
C2	50.13	17.833
D2	45.13	13.007
E2	45.13	13.007

Table 5.3 – Fully composite, I_u: Types A2-E2

d) Non composite deflections

At failure, the test specimens for types A2-E2 can be considered to act in a non-composite manner; in other words, the concrete biscuits act independently of each other and have their own neutral axes. Additionally, the test specimens can be assumed to be cracked at failure. The top and bottom biscuits are treated as individual specimens with tension reinforcement taken as the area of steel provided by the reinforcement and lattice bars in each biscuit. Equation 5.6 can be used to determine the cracked second moment of area, I_c for each biscuit. The total value of I_c is taken as the sum of the second moments of area calculated for each biscuit. Results are summarised in Table 5.4. The second moment of area can then be used to determine the deflections at various loads using Equation 5.4.

Type	Non-composite – Cracked					$I_{c,\ non\text{-}composite}$ [$x\ 10^6$] (mm^4)
	Top Biscuit		Bottom Biscuit		Core	
	x_{c1} (mm)	I_{c1} [$x\ 10^6$]	x_{c2} (mm)	I_{c2} [$x\ 10^6$]	I_{c3} [$x\ 10^6$]	
A2	15	0.050	15	0.056	-	0.106
B2	15	0.050	15	0.056	-	0.106
C2	15	0.050	15	0.056	-	0.106
D2	15	0.050	15	0.056	0.450	0.556
E2	15	0.050	15	0.056	0.450	0.556

Table 5.4 – Non composite, I_c : Types A2-E2

The results from the flexural tests are presented and discussed in Chapter 6.

Chapter 6

Phase II: Results and Discussion

Flexural Tests

6.1 Introduction

This section presents the results from the flexural tests carried out on the twinwall specimens. As discussed in Chapter 5, three main aspects were investigated:

1. *Effect of using lattice girder in twinwalls*

The role of the shear connectors in the twinwalls is not clear. The results from type A2 with no lattice girder were compared with those from type B2 where lattice girders were used as shear connectors in order to provide a better understanding of the role of the lattice shear connector. Two specimens were tested for each type.

2. Effect of varying the depth of lattice girder

The effect of varying the depth of the lattice girder between the precast concrete biscuits was investigated. Flexural tests were carried out on type B2 (60 mm deep lattice) and type C2 (80 mm deep lattice).

3. Role of concrete biscuits and core

The role of the concrete biscuits and core in the twinwalls was investigated by comparing the results from type B2 *(with no concrete core)* with those from types D2 *(biscuits cast in three stages)* and E2 *(biscuits cast in one stage).*

The results from the experimental tests are presented and discussed in terms of the following:

1) *Compressive strength of concrete*: 7-day cube compressive strength of the concrete in the top biscuit, bottom biscuit and the core (where applicable).
2) *Failure Load*: Maximum load applied to the test specimens.
3) *Top and Bottom Deflection at failure*: Maximum midspan deflection at the top and bottom of the test specimens.
4) *Load-Vertical Deflection Profile*: Top and bottom deflections observed at midspan in test specimens plotted for each load increment.
5) *Load-Lateral Deflection Profile*: Readings from the DEMEC gauges at each load increment plotted for load increment.
6) *Variation of Lateral Deflection along Length of test specimen*: Readings from the DEMEC gauges at each load increment are plotted at different points along the length of the test specimens.

7) *Variation of Lateral Deflection along Depth of test specimen*: Readings from the DEMEC gauges at each load increment are plotted at different points across the depth of the test specimens.
8) *Variation of Strains in Lattice bars:* The strain gauge readings recorded in the diagonal lattice bars for types B2 and C2 are plotted against load applied. The stresses in the bars are also derived from the experimental strain values.
9) *Failure Mechanism*: General behaviour of the test specimens in terms of cracking and failure mechanism observed.

The experimental results are then compared with the theoretical predictions in terms of the following:

1) *Shear Failure*: The theoretical load at which the diagonal bars fail are derived from the truss analogy and compared with the experimental values for types B2 and C2.
2) *Interface Shear Failure*: The interface shear failure load predicted by Clause 6.2.5 in EC2 is compared with the experimental failure load for type D2.
3) *Degree of Composite Action at Elastic Stage*: The degree of composite action at the elastic stage is calculated from the experimental load- concrete stress profiles for all specimen types
4) *Degree of Composite Action at Ultimate Stage*: The experimental failure loads are compared with that of type E2 which is representative of a fully monolithic section.

6.2 Experimental Results

6.2.1 Compressive Strength

The specimens were tested on the seventh day from the day when the core was cast. Thus, a 7-day compressive strength of approximately 70 % of the target 28-day compressive strength was expected. The target 7-day strength was 35 N/mm^2 for the 50 N/mm^2 mix. The compressive strengths are based on the strengths of three concrete cubes cast on the day of each concrete pour.

6.2.1.1 Results

Compressive Strengths (N/mm^2)	A2: No lattice			
	Specimen 1		Specimen 2	
	Top	Bottom	Top	Bottom
Cube 1	37.68	39.44	35.45	35.6
Cube 2	38.08	38.84	36.01	37.05
Cube 3	38.48	39.96	35.9	36.5
Mean	38.08	39.41	35.79	36.38
Standard deviation	0.40	0.56	0.30	0.73

Table 6.1- Compressive strength – A2

Compressive Strengths (N/mm^2)	B2: 60 mm lattice			
	Specimen 1		Specimen 2	
	Top	Bottom	Top	Bottom
Cube 1	39.28	39.84	38.28	37.23
Cube 2	39.28	39.16	35.01	37
Cube 3	38.8	38.36	36.5	37.98
Mean	39.12	39.12	36.60	37.40
Standard deviation	0.28	0.74	1.64	0.51

Table 6.2- Compressive strength – B2

Compressive Strengths (N/mm^2)	C2: 80 mm lattice			
	Specimen 1		Specimen 2	
	Top	Bottom	Top	Bottom
Cube 1	41.24	44.11	33.76	33.84
Cube 2	41.61	44.34	36.48	35.96
Cube 3	41.35	45.29	37.28	36.28
Mean	41.40	44.58	35.84	35.36
Standard deviation	0.19	0.63	1.85	1.33

Table 6.3- Compressive strength – C2

Compressive Strengths (N/mm^2)	D2: Three stages					
	Specimen 1			Specimen 2		
	Top	Core	Bottom	Top	Core	Bottom
Cube 1	40.88	39.88	39.44	42.28	39.9	44.16
Cube 2	39.28	40.3	40.36	43.48	40.3	41.32
Cube 3	40.44	40.8	41.56	40.64	40.8	44.44
Mean	40.20	40.33	40.45	42.13	40.33	43.31
Standard Deviation	0.83	0.46	1.06	1.43	0.45	1.73

Table 6.4- Compressive strength – D2

Compressive Strengths (N/mm^2)	E2: Solid section	
	Specimen 1	Specimen 2
	Top/Core/Bottom	Top/Core/Bottom
Cube 1	39.28	39.01
Cube 2	40.48	36.8
Cube 3	38.98	37.6
Mean	39.58	37.80
Standard deviation	0.79	1.12

Table 6.5- Compressive strength – E2

Table 6.6 provides the average cube compressive strengths and the standard deviations (std dev) for each specimen type.

Type	Parameter varied	Cube compressive Strength (N/mm^2)					
		Top Biscuit		Bottom Biscuit		Core	
		Average	Std Dev	Average	Std Dev	Average	Std Dev
A2	No lattice	36.93	0.35	37.90	0.65	-	-
B2	60 mm lattice	37.86	0.96	38.26	0.63	-	-
C2	80 mm lattice	38.62	1.02	39.97	0.98	-	-
D2	Cast in 3 stages	41.17	1.13	41.88	1.39	40.33	0.46
E2	Solid section	38.69	0.96	38.69	0.96	38.69	0.96

Table 6.6- Compressive strength: A2-E2

6.2.1.2 Discussion

Results show that the average cube compressive strengths of the concrete for the core and the biscuits for all specimen types A2-E2 were greater than the target strength of 35N/mm^2. The standard deviation of the concrete for all specimen types ranged between 0.96 N/mm^2 to 1.39 N/mm^2 which accounted for 1.00% - 3.98% of the target cube compressive strength of 35N/mm^2. Hence, the cube compressive strengths for all test specimens were deemed as being satisfactory.

6.2.2 Failure Load

6.2.2.1 Results

The loads at which the test specimens failed (i.e. the maximum load attained by the specimens) are provided in Table 6.7. The average value of the failure load for each of the five test specimens tested for types A2-E2 are calculated.

Type	Parameter varied	Failure Load (kN)		Failure Load (Average, kN)
		Specimen 1	Specimen 2	
A2	No lattice	2.45	2.55	2.50
B2	60 mm lattice	5.60	5.40	5.50
C2	80 mm lattice	11.20	11.40	11.30
D2	Cast in 3 stages	12.30	12.20	12.25
E2	Solid section	12.50	12.70	12.60

Table 6.7- Experimental Failure Load: A2-E2

6.2.2.2 Discussion

A. Effect of using lattice girder in twinwalls

From Table 6.7, the average values of the failure loads for types A2 and B2 are 2.50 kN and 5.50 kN respectively. The results show that the introduction of lattice shear connectors in type B2 more than doubles (by approximately 2.2 times) the failure load of the test specimen in comparison with type A2 where only the concrete biscuits are used.

B. Effect of Varying Depth of Lattice Girder

Table 6.7 shows that the average values of the failure loads for types B2 and C2 are 5.50 kN and 11.30 kN respectively. Hence, increasing the lattice depth from 60 mm to 80 mm more than doubles (by approximately 2.05 times) the failure load of the test specimen. The increase in the failure load in type C2 can either be attributed to (1) an increase in the lever arm resulting in an increase in the bending capacity or to (2) an

increase in the shear capacity as a result of the transfer of forces taking place due to the lattice.

C. Role of Concrete Biscuits and Core in Twinwalls

The average experimental failure loads for types B2 and D2 are 5.50 kN and 12.25 kN respectively. Hence, the introduction of a concrete core between the top and bottom biscuit more than doubles (by approximately 2.2 times) the failure load of the test specimen.

The average experimental failure load for types D2 and E2 are 12.25 kN and 12.60 kN respectively. Thus, casting the test specimen in three sections (outer biscuit and core) increases the failure load by 3% in comparison with the test specimen cast as a single solid section. This confirms that the behaviour of type D2 (representative of a typical twinwall) is very similar to that of a monolithic section as used in type E2.

6.2.3 Top and Bottom deflection at Failure

The top deflection and bottom deflections at midspan of specimen types of types A2-E2 specimens at failure are given in Table 6.8. The top and bottom deflections correspond to dial gauge readings recorded at each load increment at midspan of the top and bottom biscuits of the test specimens respectively.

6.2.3.1 Results

Type	Parameter varied	Deflection at failure (mm)				Average deflection (mm)	
		Specimen 1		Specimen 2		Top	Bottom
		Top	Bottom	Top	Bottom		
A2	No lattice	12.52	12.55	15.81	20.79	14.17	16.67
B2	60 mm lattice	3.77	4.74	3.66	4.47	3.72	4.61
C2	80 mm lattice	3.19	3.44	3.38	3.74	3.29	3.59
D2	Cast in 3 stages	10.9	12.2	10.28	11.3	10.59	11.75
E2	Solid	4.95	5.03	5.2	5.33	5.08	5.18

Table 6.8- Average Top And Bottom Deflection at Failure: A2-E2

6.2.3.2 Discussion

A. Effect of using Lattice Girder in Twinwalls

The average top deflections for types A2 and B2 are 14.17 mm and 3.72 mm respectively; and the average bottom deflections for types A2 and B2 are 16.67 mm and 4.61 mm respectively. Thus, the average top and bottom deflections of type B2 are 74% and 72% less than those in type A2. This shows that the introduction of the lattice increases the stiffness of the test specimens significantly.

B. Effect of Varying Depth of Lattice Girder

Results show that there is a 24% and 9% difference between the top and bottom deflections at failure for type B2 and type C2 respectively. This indicates that in type B2, the smaller lattice depth of 60 mm between the top and bottom may have caused the

bottom biscuit to behave independently of the top biscuit at a certain point during the application of the load, i.e. plane sections do not remain plane. Hence, the increase in lattice depth from 60 mm in type B2 to 80 mm in type C2 affects the behaviour of the top and bottom biscuits.

Additionally, the average top deflections for types B2 and C2 are 3.72 mm and 3.29 mm respectively; and the average bottom deflections for types B2 and C2 are 4.61 mm and 3.59 mm respectively. Thus, the average top and bottom deflections of type C2 are 13% and 28% less than those in type B2. This shows that the increasing the depth of the lattice leads to a rise in the stiffness of the test specimens.

C. Role of Concrete Biscuits and Core in Twinwalls

From the results, there is a 24%, 11% and 2% difference between the average top and bottom deflections at failure for types B2, D2 and E2 respectively. This trend indicates that the presence of the concrete between the top and bottom biscuits causes both the top and bottom biscuits to deflect as one unit, i.e. plane sections remain plane.

Additionally, the average top deflections for types B2, D2 and E2 are 3.72 mm, 10.59 mm and 5.08 mm respectively; and the average bottom deflections for types B2, D2 and E2 are 4.61 mm, 11.75 and 5.18 mm respectively. Thus, the average top and bottom deflections of type B2 are 65% and 61% less than those in type D2. This can be attributed to the significantly lower failure load of type B2 specimens which results in much lower deflection. On the other hand, the average top and bottom deflections of type E2 are 52% and 56% less than those in type D2. This shows that casting the

biscuits and the core in distinct stages significantly affects the stiffness of the test specimens in comparison with type E2.

6.2.4 Load- Deflection Profiles

The load- top/bottom deflection profile gives an indication of the stiffness and degree of composite action of the test specimens.

As discussed in Chapter 5, the theoretical failure loads and deflections for the non-composite and fully composite limits are also plotted on the experimental load-deflection profiles to provide an indication of the degree of composite action taking place. The theoretical non-composite and fully composite values are obtained by using the I values from Table 5.3 & 5.4 to determine the deflection at each load increment by applying Equation 5.4 described previously in Chapter 5.

6.2.4.1 Results

Figures 6.1-6.6 show the variation of vertical deflection is plotted at each load increment for types A2-E2.

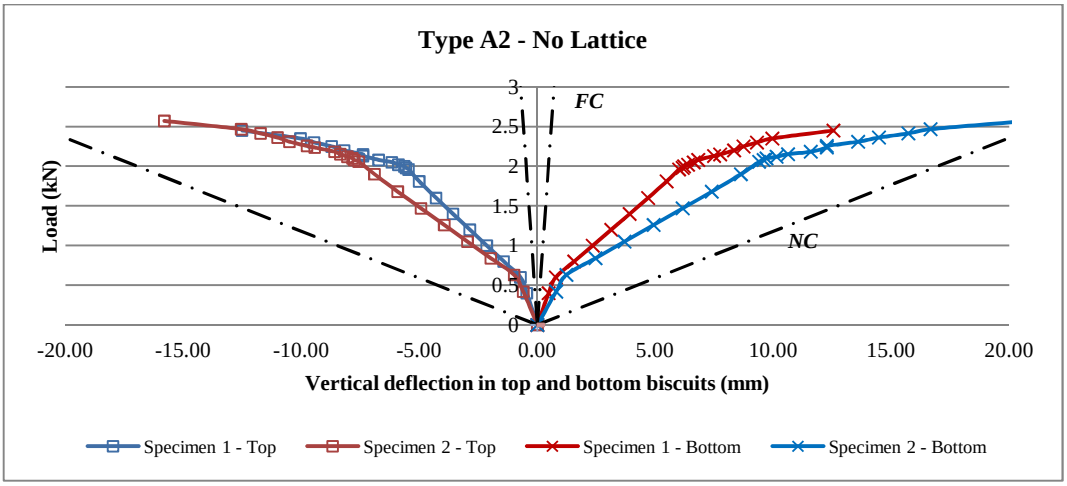

Figure 6.1 - Load v/s Vertical Deflection – A2

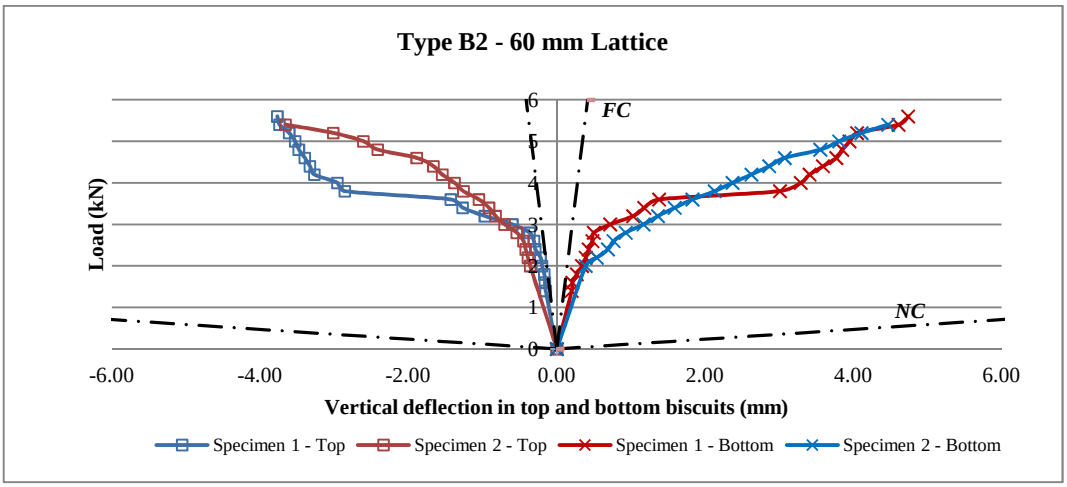

Figure 6.2 - Load v/s Vertical Deflection – B2

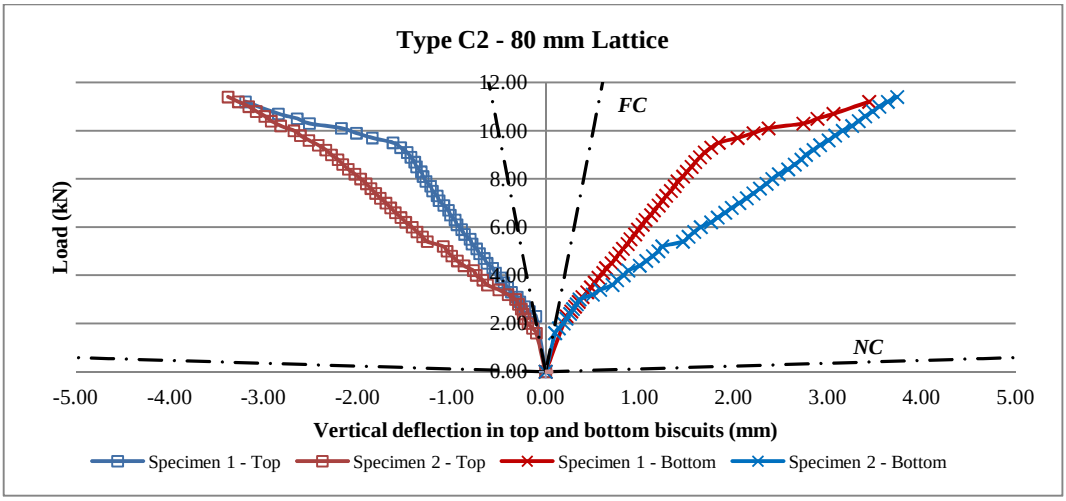

Figure 6.3 - Load v/s Vertical Deflection – C2

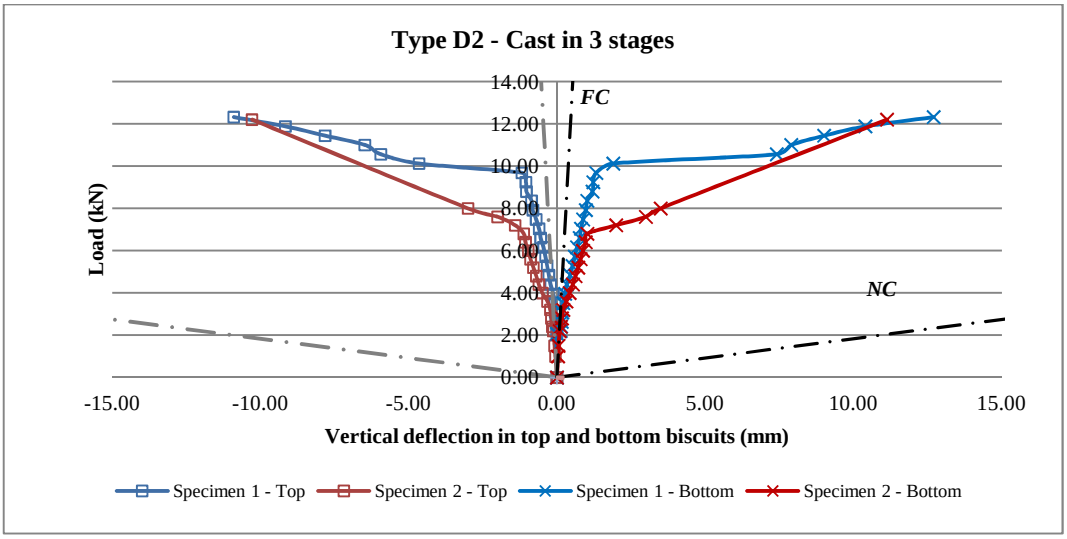

Figure 6.4 - Load v/s Vertical Deflection – D2

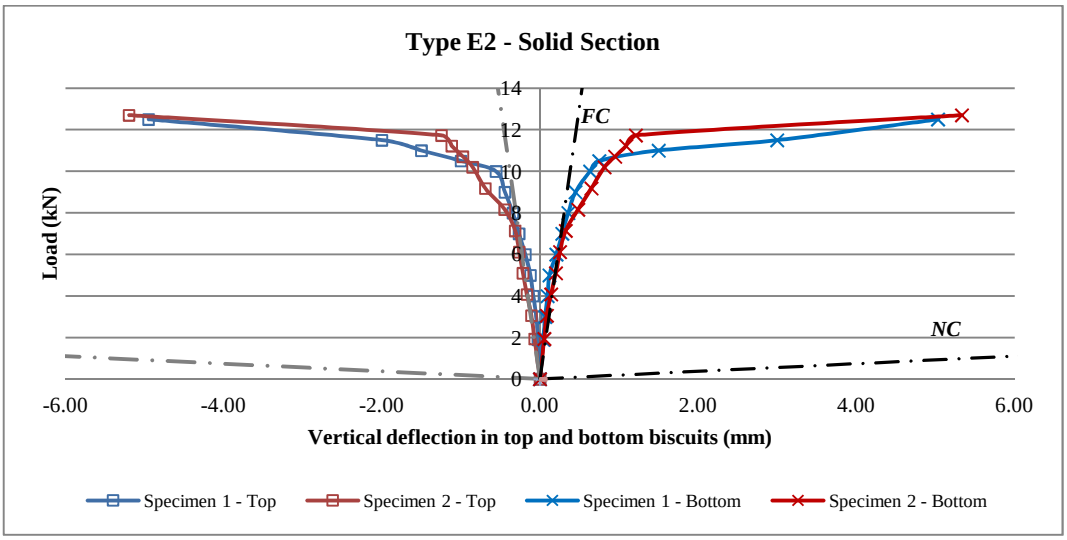

Figure 6.5 - Load v/s Vertical Deflection – E2

The load-vertical deflection profiles for types A2-E2 are also plotted relative to each other to obtain a direct comparison between the results. The average top and bottom deflections for the two specimens tested for each test type is plotted for each load increment as shown in Figures 6.6-6.8.

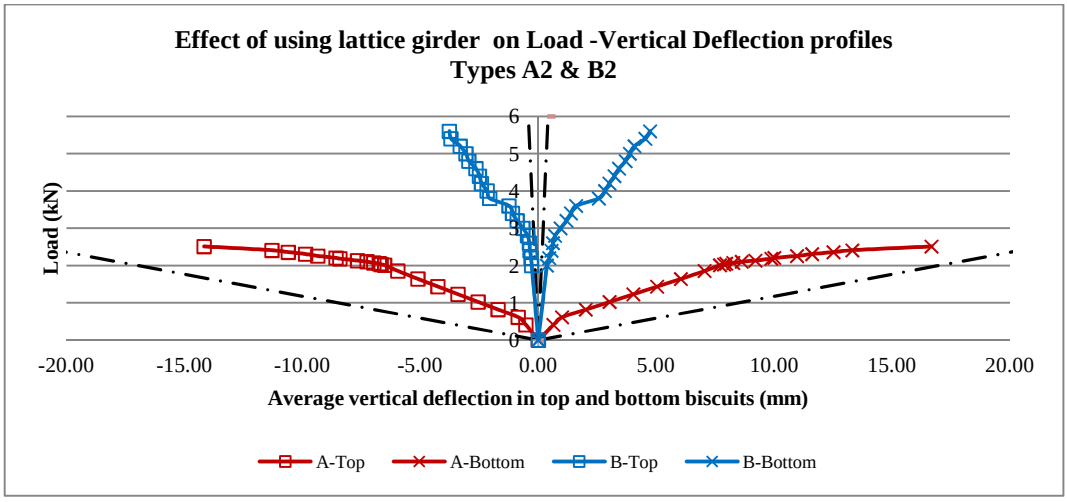

Figure 6.6 – Effect of using Lattice Girder on Load-Vertical Deflection profiles

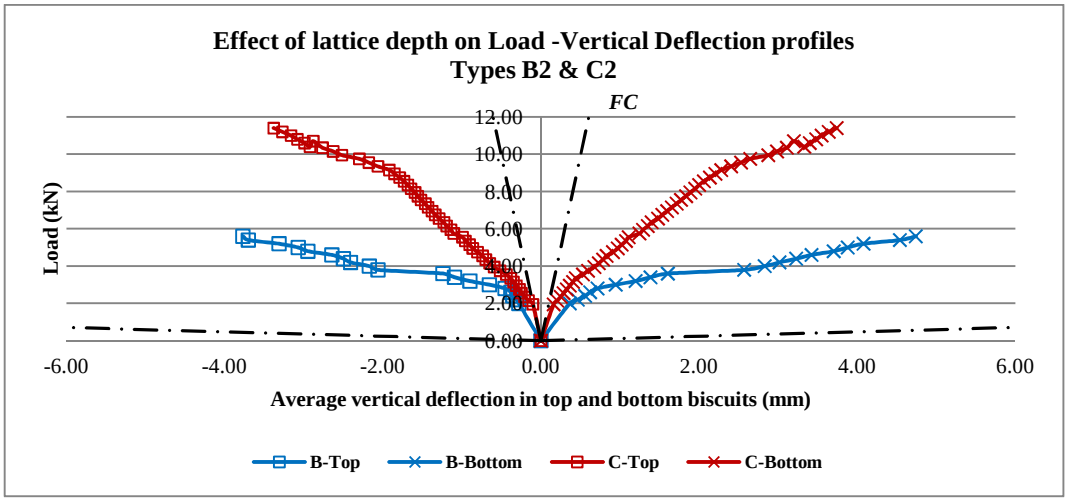

Figure 6.7 – Effect of Lattice Depth on Load-Vertical Deflection profiles

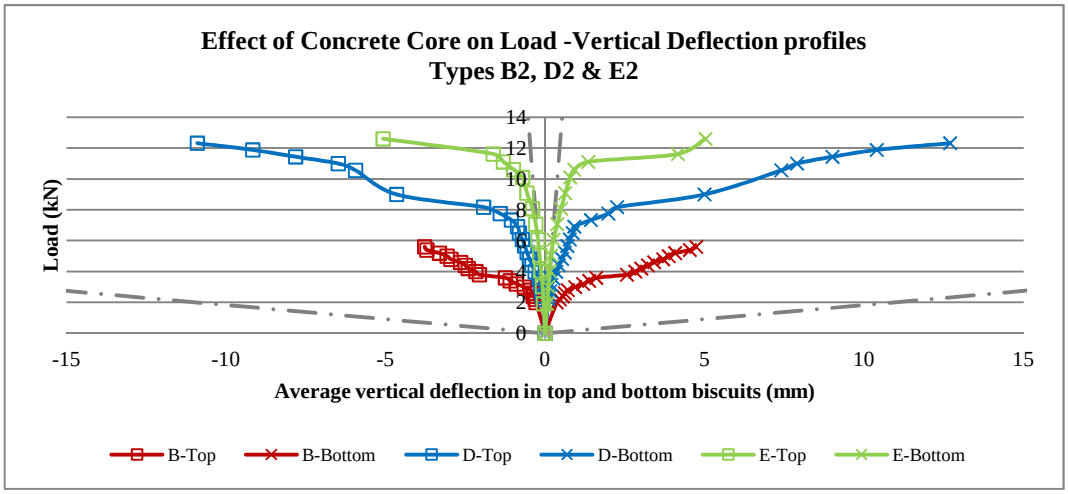

Figure 6.8 – Effect of Concrete Core on Load-Vertical Deflection profiles

A. General Trend

The load-vertical deflection profiles for most specimen types indicate that the test specimens deform in a similar fashion. It is observed that in early stages of loading, the top and bottom biscuits deform linearly thus exhibiting elastic behaviour. As the load is increased, the top and bottom biscuits exhibit non-linear behaviour confirming that the specimens have reached the plastic stage.

Results also show that during the elastic stage, the experimental load-deflection profiles lie close to the theoretical fully composite limit. As the load increases, the specimens behave non-linearly and shift towards the theoretical non-composite limit. Additionally, the load-deflection profiles for the test specimens lie between the theoretical fully composite and non-composite limits, thereby confirming that the specimens exhibit partially composite behaviour.

B. Effect of using Lattice Girder in Twinwalls

From Figure 6.6, it can be seen that load-deflection profiles remain elastic up to a load of 1.85 kN (74% of average failure load) and 3.60 kN (66% of average failure load) for type A2 and type B2 respectively. The shift from the elastic to the plastic stage can primarily be attributed to the formation of cracks in the top and bottom biscuits.

Results also show that the stiffness of type A2 is significantly less than that of type B2. This confirms that the introduction of the lattice girder in type B2 increases the stiffness of the test specimens.

C. Effect of Varying Depth of Lattice Girder

Figure 6.7 shows that average load-deflection profiles of the two specimens tested for types B2 and C2. The load-deflection profiles remain elastic up to a load of 2.75 kN (50% of average failure load) and 8.1 kN (72% of average failure load) for types B2 and C2 respectively. This shift from the elastic to the plastic stage can primarily be attributed to the formation of cracks in the top and bottom biscuits. Thus, an increase in the lattice depth of significantly alters the elastic-plastic behaviour of the test specimens.

It is also observed that the stiffness of type B2 is significantly less than that of type C2. This confirms that increasing the lattice depth from 60 mm to 80 mm increases the stiffness of the test specimens.

D. Role of Concrete Biscuits and Core in Twinwalls

The load-deflection plot for type B2 in Figure 6.2 shows that the experimental top and bottom deflections lie in the fully composite region up to a load of 2.75 kN (50% of failure load), beyond which the graph moves towards the non-composite extreme. Additionally, the top and bottom deflections in type B2 remain almost equal in the fully composite region, beyond which the bottom deflections are greater than the top deflections.

The load-deflection plot for type D2 in Figure 6.4 also shows that the experimental top and bottom deflections lie in the fully composite up to a load of 7.0 kN (57% of failure load), beyond which the graph moves towards the non-composite extreme.

A similar trend is also observed for type E2 in Figure 6.5 where the experimental top and bottom deflections lie in the fully composite region up to a load of 9.0 kN (71% of failure load), beyond which the graph moves towards the non-composite extreme. This shift from the elastic to the plastic stage can primarily be attributed to the formation of cracks in the top and bottom biscuits as well as the yielding of the steel lattice bars. Thus, an increase in the lattice depth of significantly alters the elastic-plastic behaviour of the test specimens.

These results confirm that types B2, D2 and E2 behave in a partially composite manner with type E2 behaving most compositely followed by type D2 and type B2. This indicates that the presence of a concrete core in type D2 and E2 increases the degree of composite action in comparison with type B2 where no core is used.

It must also be noted that although type E2 was cast as a single solid unit, the top and bottom deflections were not restricted to the fully composite region but moved towards the non-composite extreme. This is in conflict with theory which assumes that a section cast as one solid section should behave as a fully composite unit. This seems to suggest that the presence of the lattice girder may have altered the degree of composite action in type E2.

From Figure 6.8, it can be seen that the stiffness of type B2 is significantly less than that in types D2 and E2 where the stiffness is almost the same within the fully composite

region. Thus, it can be concluded that the presence of the concrete between the top and bottom biscuits in types D2 and E2 leads to an increase in the stiffness of the test specimens

6.2.5 Load vs. Lateral Deflection profiles

The lateral deflection in the top and bottom biscuits was recorded by taking DEMEC measurements at each load increment. The change in length from the pre-set DEMEC gauge length of 100 mm was measured.

The load-lateral deflection profiles for types A2-E2 are also plotted relative to each other to obtain a direct comparison between the results as shown in Figures 6.14-6.16.

6.2.5.1 Results

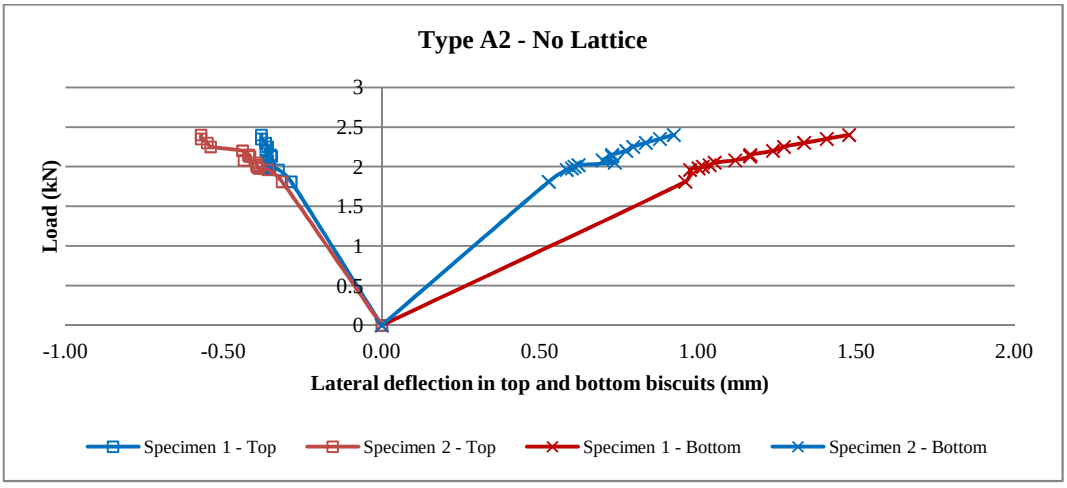

Figure 6.9 - Load v/s Lateral Deflection – A2

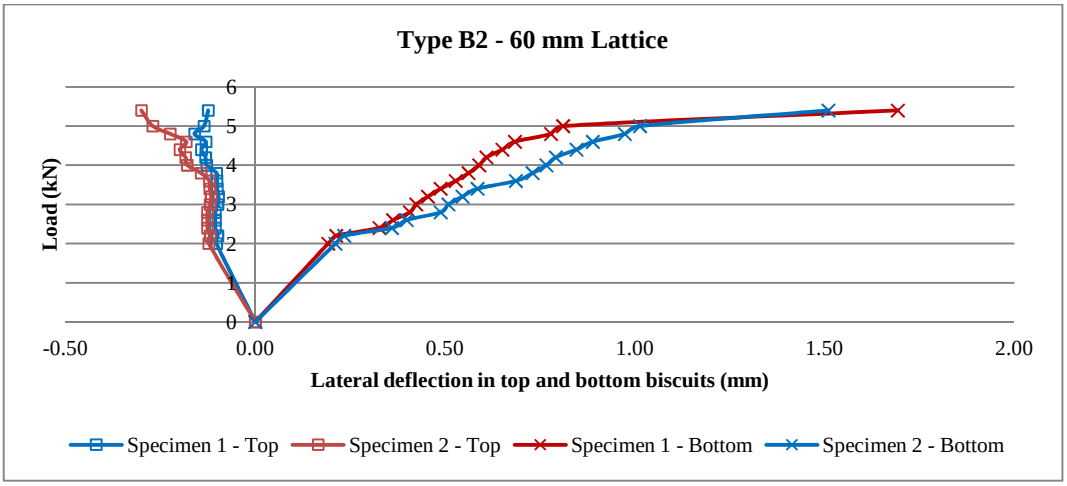

Figure 6.10 - Load v/s Lateral Deflection – B2

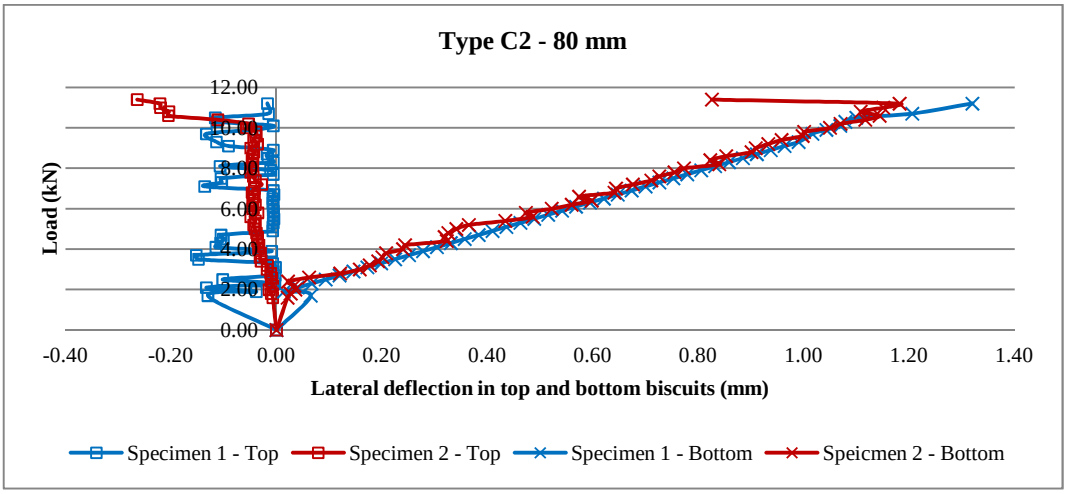

Figure 6.11 - Load v/s Lateral Deflection – C2

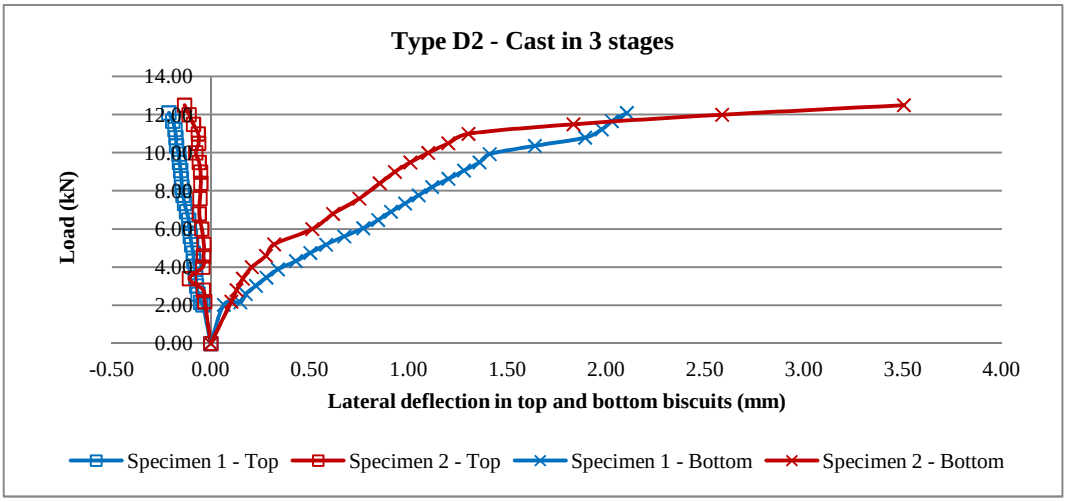

Figure 6.12 - Load v/s Lateral Deflection – D2

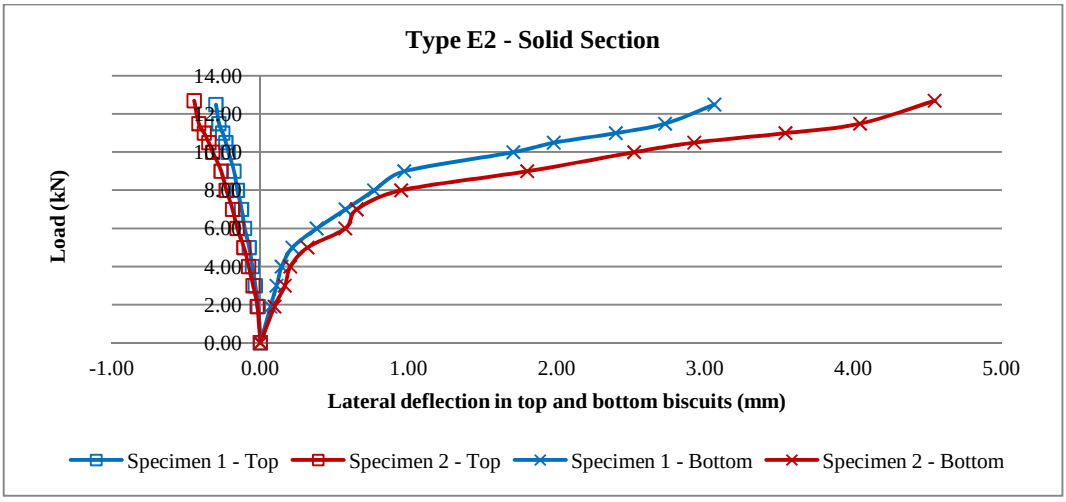

Figure 6.13 - Load v/s Lateral Deflection – E2

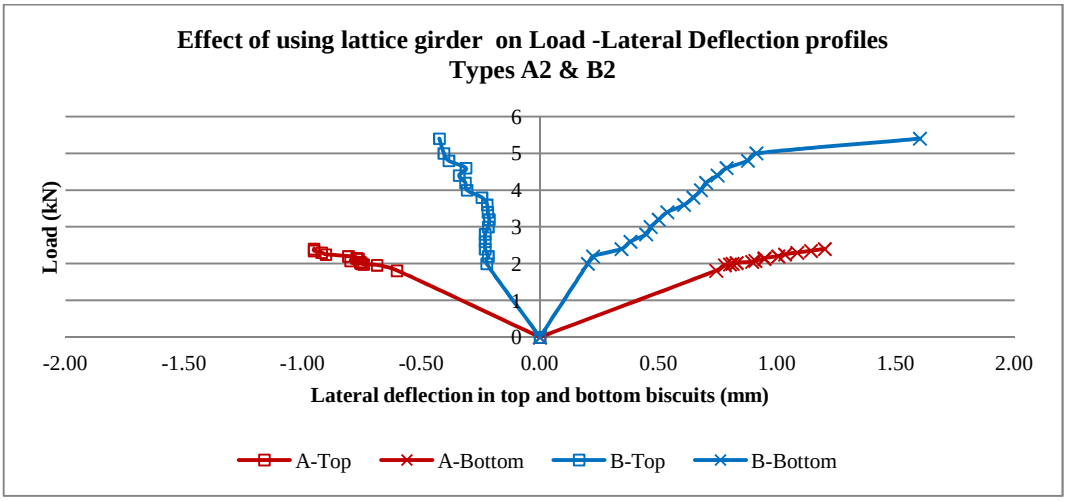

Figure 6.14 – Effect of using Lattice Girder on Load-Lateral Deflection profiles

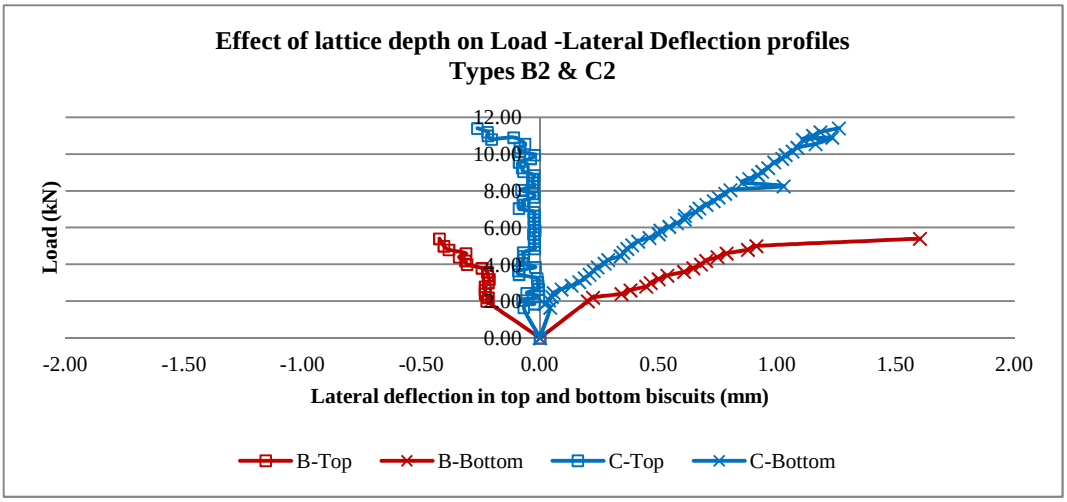

Figure 6.15 – Effect of Lattice depth on Load-Lateral Deflection profiles

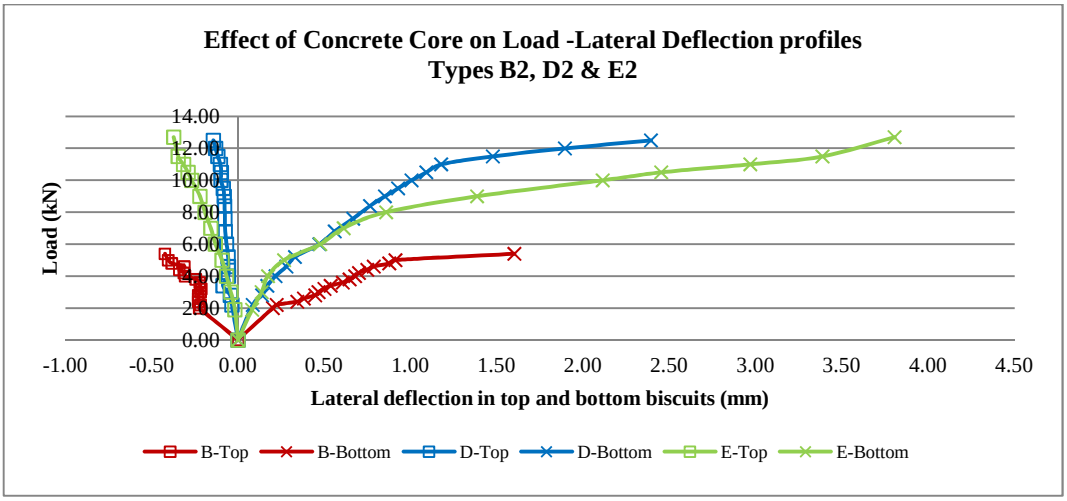

Figure 6.16 – Effect of Concrete Core on Load-Lateral Deflection profiles

6.2.5.2 Discussion

A. Effect of using Lattice Girder in Twinwalls

Results show that the bottom lateral deflections in both types A2 and type B2 specimens are greater that the top lateral deflections. This is expected because when the load is applied, the bottom biscuit is in tension while the top biscuit is in compression leading to greater lateral deformations to occur in the bottom biscuit. In additional, the bottom biscuits develop flexural cracks which contribute to an increase in the bottom lateral deflections in comparison with the top lateral deflection.

From Figure 6.14, is observed that the lateral stiffness of type A2 specimen is much lower than that of type B2. This can be attributed to the lattice girders in type B2 which are embedded in the faces of the top and bottom biscuits and restrict the biscuits from deforming laterally. This also suggests that the distribution of forces in type B2

specimen has been altered as a result of the lattice girder and that the forces applied are also being resisted by the lattice bars.

B. Effect of Varying Depth of Lattice Girder

From Figures 6.10-6.11, it can be seen that the bottom lateral deflections in both types B2 and C2 specimens are greater that the top lateral deflections. This is expected because when the load is applied, the bottom biscuit is in tension while the top biscuit is in compression leading to greater lateral deformations to occur in the bottom biscuit. In additional, the bottom biscuits developed flexural cracks which contribute to an increase in the bottom lateral deflections in comparison with the top lateral deflection.

The results seem to suggest that the bottom biscuits for both types B2 and C2 behave almost independently of the top biscuits in resisting the load applied. In fact, during the tests for types B2 and C2, it was observed that significant flexural cracking occurred in the bottom biscuit while almost no flexural cracks occurred in the top biscuit thereby explaining the difference between the top and bottom biscuit lateral deflections.
It must also be noted that the top biscuit in type C2 almost does not deflect laterally. This suggests that the deeper lattice in type C2 alters the distribution of the compressive and tensile forces in the top and bottom biscuits.

From Figure 6.15, it can be seen that the lateral stiffness of type B2 specimen is slightly lower than that of type C2. This confirms that increasing the depth of the lattice alters that distribution of forces in the test specimens and causes a rise in the lateral stiffness.

C. Role of Concrete Biscuits and Core in Twinwalls

Figures 6.10,6.12 & 6.13 show that the bottom lateral deflections in types B2, D2 and E2 specimens are greater that the top lateral deflections. This is expected because when the load is applied, the bottom biscuit is in tension while the top biscuit is in compression leading to greater lateral deformations to occur in the bottom biscuit. In additional, the bottom biscuits developed flexural cracks which contribute to an increase in the bottom lateral deflections in comparison with the top lateral deflection.

The results suggest that the bottom sections for both types B2, D2 and E2 behave almost independently of the top sections in resisting the load applied. In fact, significant flexural cracking occurred in the bottom biscuit while almost no flexural cracks occurred in the top biscuit thereby explaining the difference between the top and bottom biscuit lateral deflections.

From Figure 6.16, it can be seen that the lateral stiffness of types D2 and E2 are almost similar. This shows that the behaviour of type D2 (where the concrete is cast in three separate stages) is similar to that of type E2 which is representative of a solid section.

Results also show that the lateral stiffness of B2 is less than that of types D2 and E2. This suggests that the addition of the concrete core results in an increase in the lateral stiffness of the test specimens.

6.2.6 Variation of Lateral Deflection along Length of test specimen

6.2.6.1 Results

The variations of the lateral deflections for a typical test specimen for types A2-E2 along the length of the top and bottom biscuits are plotted in Figures 6.17-6.21.

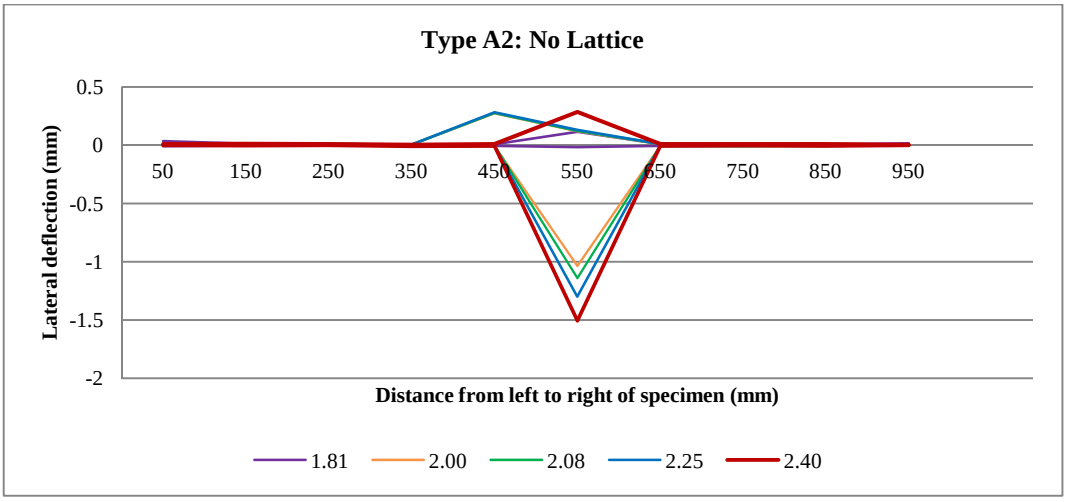

Figure 6.17 - Variation of lateral deflection along length of specimen: A2

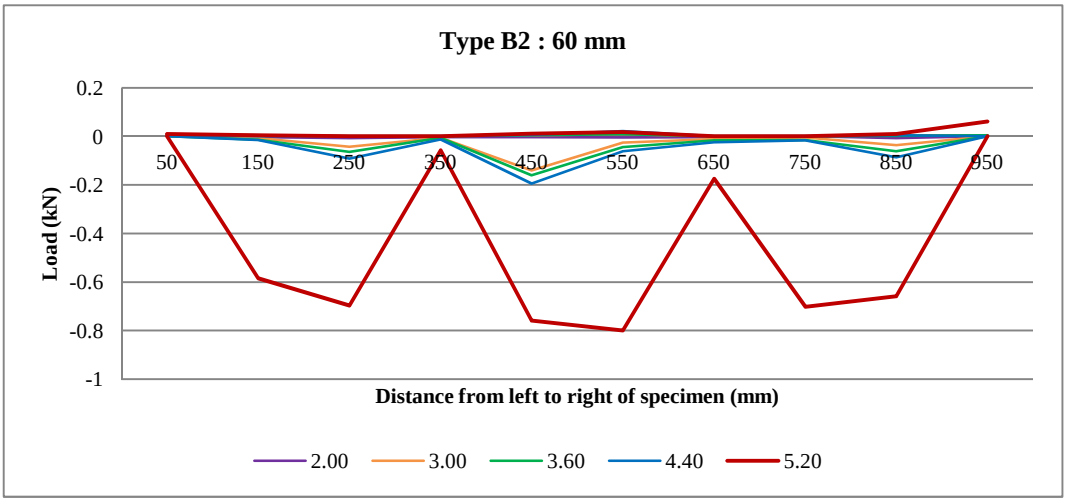

Figure 6.18 - Variation of lateral deflection along length of specimen: B2

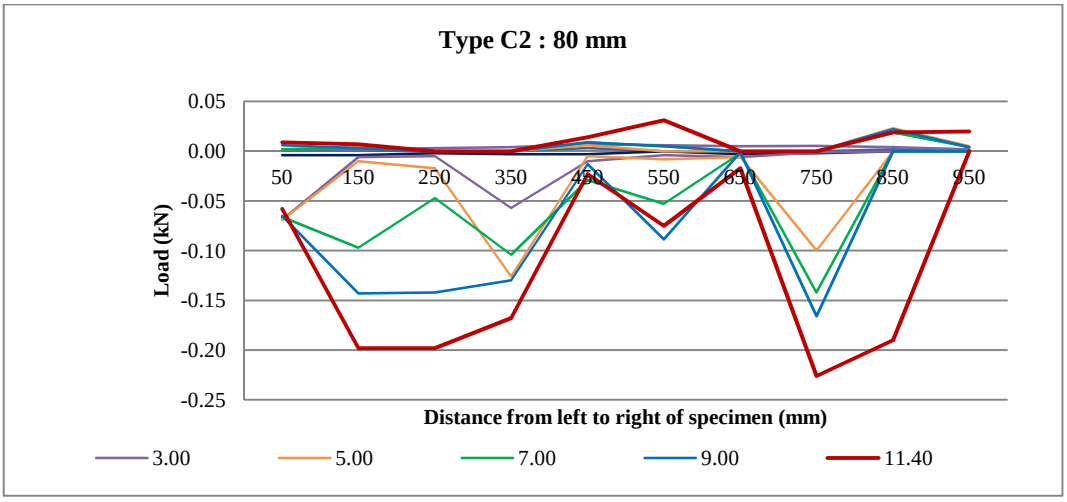

Figure 6.19 - Variation of lateral deflection along length of specimen: C2

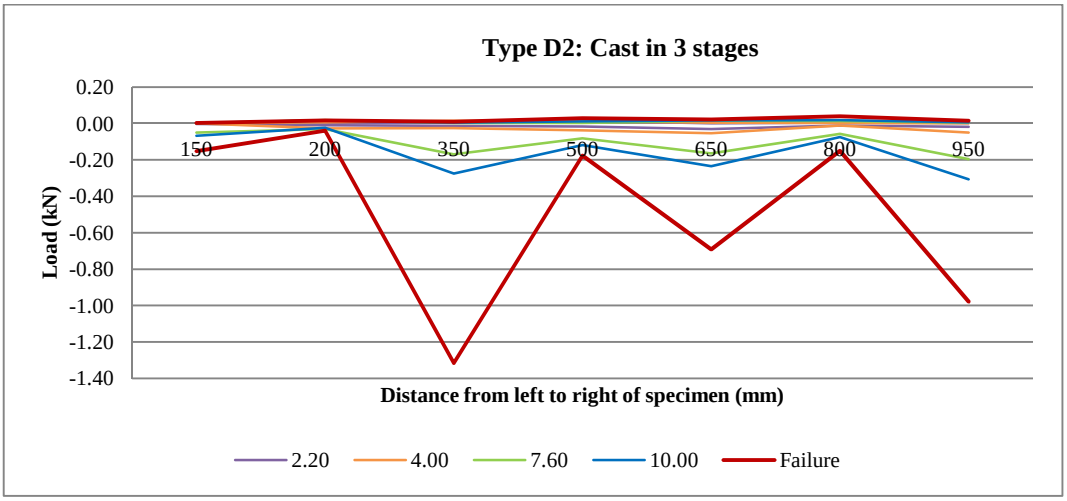

Figure 6.20 - Variation of lateral deflection along length of specimen: D2

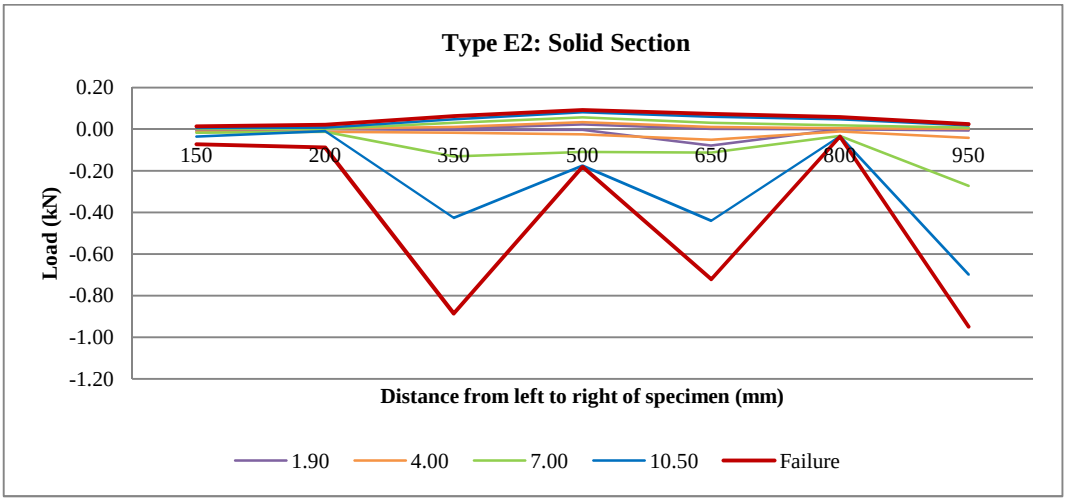

Figure 6.21 - Variation of lateral deflection along length of specimen: E2

The variation of the lateral deflection along the length of the specimens for types A2-E2 are also plotted relative to each other to obtain a direct comparison between the results as shown in Figures 6.22-6.24.

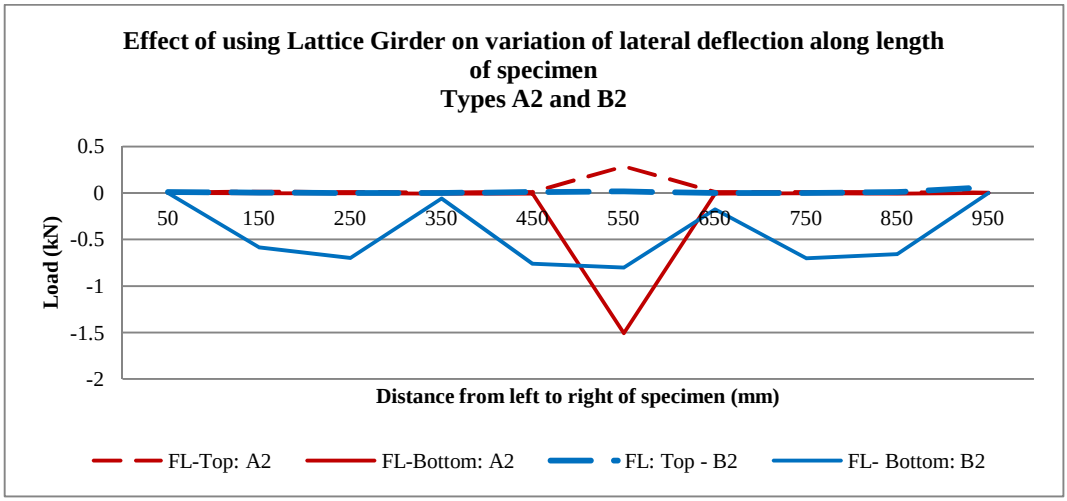

Figure 6.22 – Effect of using Lattice Girder on variation of lateral deflection along length of specimen

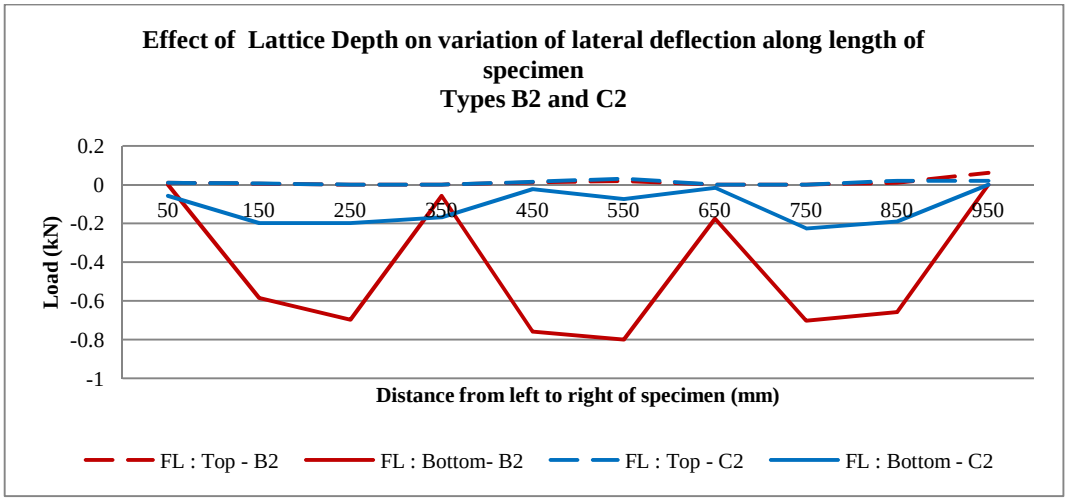

Figure 6.23 – Effect of Lattice Depth on variation of lateral deflection along length of specimen

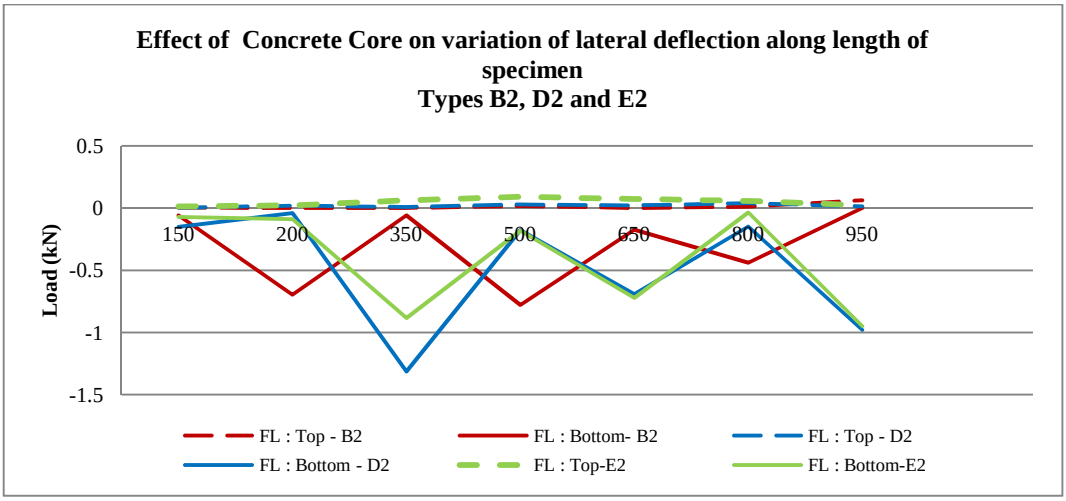

Figure 6.24 – Effect of Concrete Core on variation of lateral deflection along length of specimen

6.2.6.2 Discussion

A. Effect of using lattice girder in twinwalls

Figures 6.17-6.18 show the variation of the lateral deflections at failure across the span of type A2 and type B2 specimens. From Figures 6.17 and 6.22, it can be seen that the maximum lateral deflections in the top and bottom biscuits occur at midspan for type A2. This is because the maximum bending moments occur at midspan resulting in maximum lateral deflection to occur in this region. Once again, the top deflection is less than the bottom deflection as explained earlier.

From Figure 6.18 and 6.22, it can be seen that the lateral deflection in the top biscuit is almost constant and significantly less than that in the bottom biscuit in type B2. In the bottom biscuit, the lateral deflections peak at midspan and in the regions between the point of application of the load and the locations of the support. This region in fact corresponded with the location of cracks across the width of the test specimens in the

bottom biscuit in type B2. The contrast between the lateral deflections of types A2 and B2 clearly show that the introduction of the lattice girder in type B2 has a direct influence on the distribution of forces in the test specimen.

B. Effect of varying Depth of Lattice Girder

Figures 6.18-6.19 show the variation of the lateral deflections at failure across the span of types B2 and type C2 specimens. It can be seen that the lateral deflection in the top biscuit is almost constant and significantly less than that in the bottom biscuit in types B2-C2. For type B2, in the bottom biscuit, the lateral deflections peak at midspan and in the regions between the point of application of the load and the locations of the support. For type C2, peaks in the lateral deflections are observed at the points of load application. This suggests that distribution of the forces in types C2 and B2 are different. Additionally, the lateral deflection at failure for type C2 is much less than that in type C2. This confirms that the increasing the depth of the lattice girder has an influence on the distribution of forces in the biscuits as well as on the stiffness of the test specimens.

C. Role of Concrete Biscuits and Core in Twinwalls

From Figures 6.18, 6.20 and 6.21, it can be seen that the lateral deflection in the top biscuit is almost constant and significantly less than that in the bottom biscuit in all specimen types. For type B2, in the bottom biscuit, the lateral deflections peak at midspan and in the regions between the point of application of the load and the locations of the support. For types D2 and E2, peaks in the lateral deflections are

observed in the region of the point of application of the load. Hence, the presence of the concrete core in types D2 and E2 seems to have an effect on the distribution of the forces in the bottom biscuits.

6.2.7 Variation of Lateral Deflection along Depth of test specimens

The lateral deflections at midspan along the depth of the test specimens for all specimen types are plotted at different load increments. The variation of lateral deflection with depth is plotted for one test specimen for each type.

6.2.7.1 Results

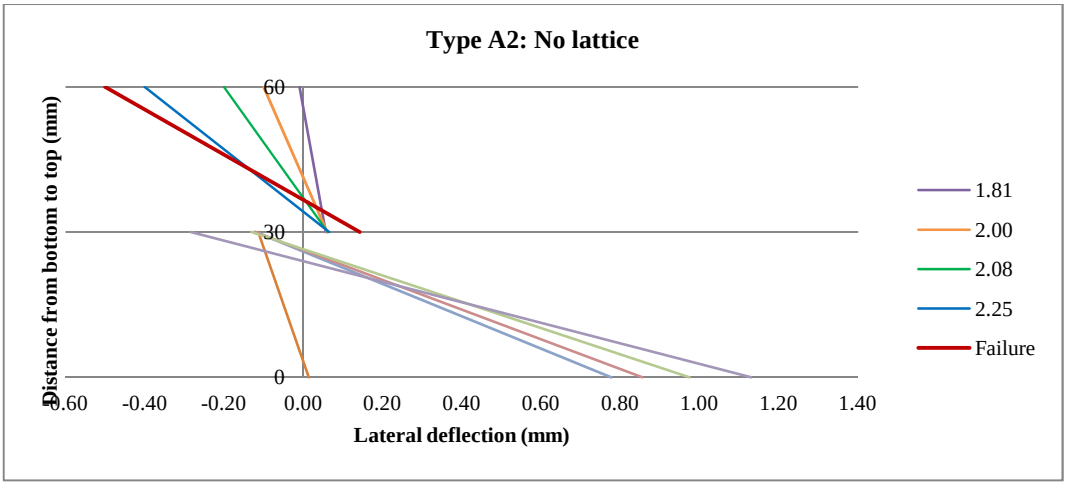

Figure 6.25 - Variation of lateral deflection with depth of specimen: A2

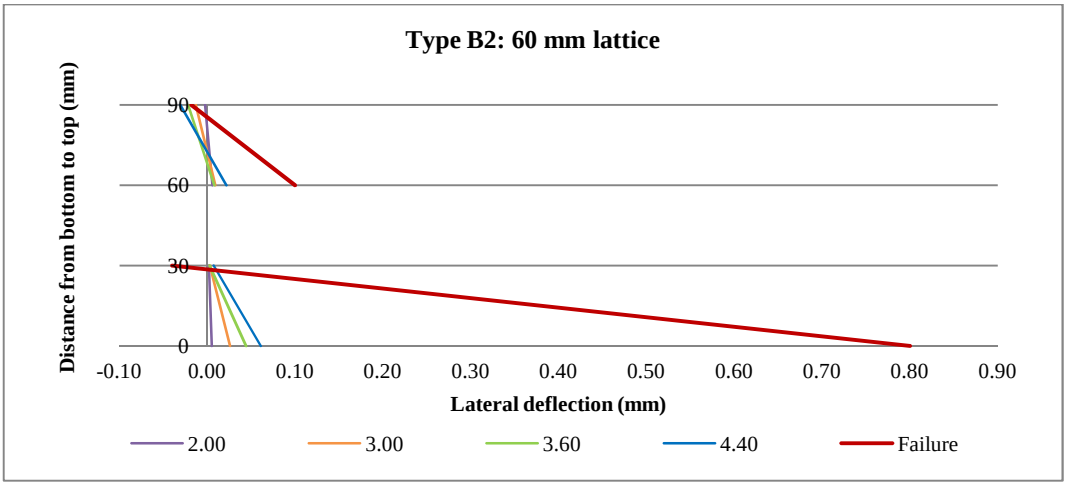

Figure 6.26 - Variation of lateral deflection with depth of specimen: B2

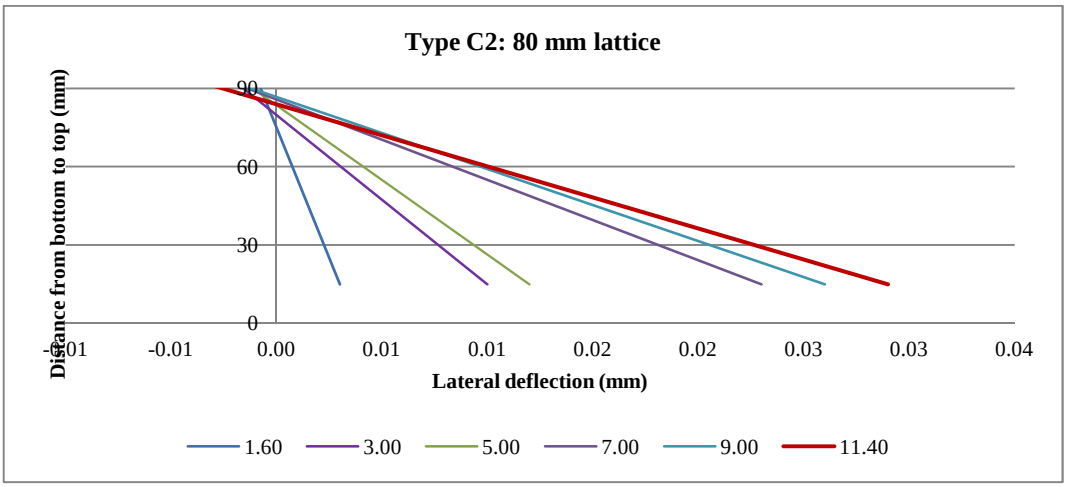

Figure 6.27 - Variation of lateral deflection with depth of specimen: C2

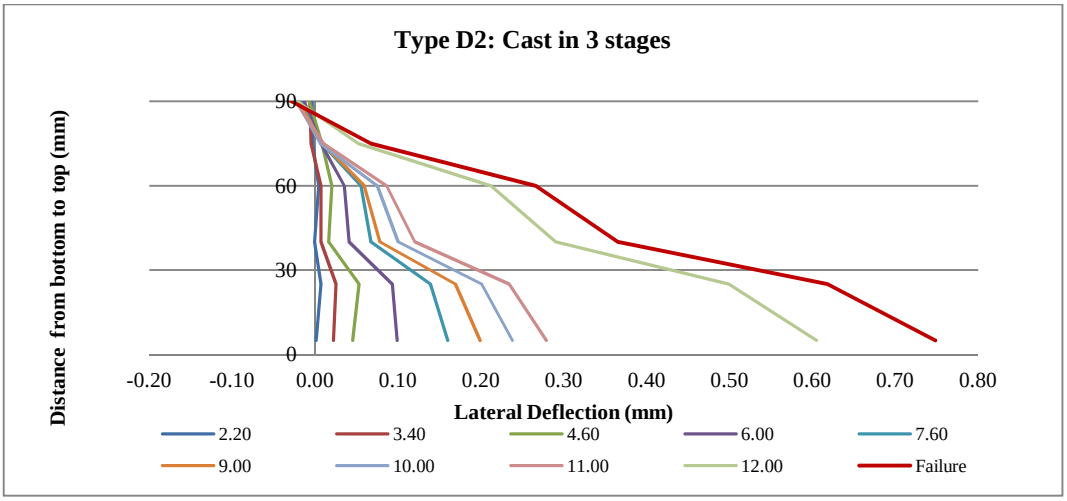

Figure 6.28 - Variation of lateral deflection with depth of specimen: D2

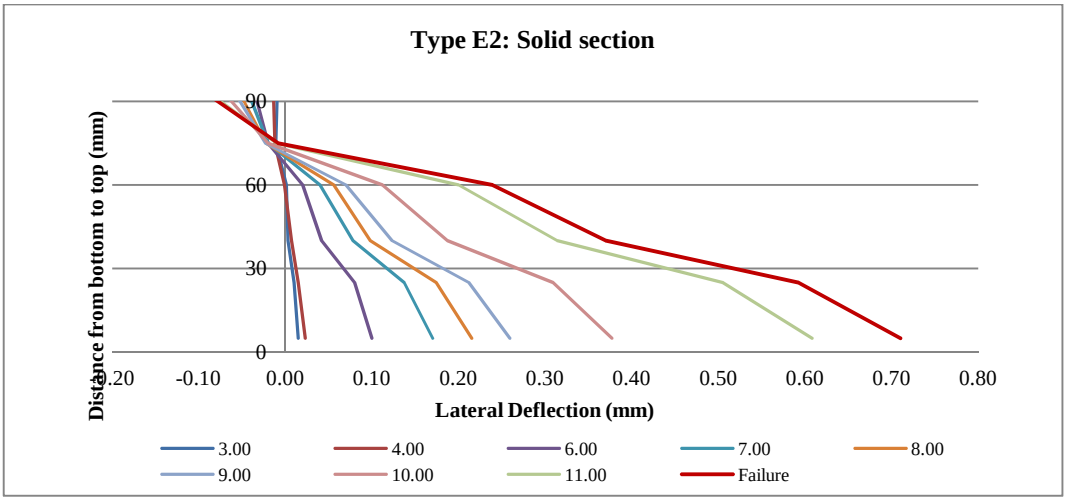

Figure 6.29 - Variation of lateral deflection with depth of specimen: E2

A. Effect of using Lattice Girder in Twinwalls

Figures 6.25-6.26 show the variation of lateral deflection with the depth of the test specimen for both types A2 and B2. The lateral deflection is indicative of the strains occurring in the concrete under the loads applied. The compressive lateral deflections (strains) are less than the tensile lateral deflections for both types A2 and B2. This is due to the formation of flexural cracks in the bottom biscuits under loading.

It can be noted that discontinuities in lateral deflection are relatively small during the early stages of loading. As the specimens approach the failure load, the discontinuities become larger.

The discontinuities in lateral deflection and hence concrete strains in type A2 are significantly different of those in type B2. The top and bottom biscuits in type A2 seem to have separate neutral axes in the top and bottom biscuits throughout most of the later stages of loading. This indicates that the top and bottom biscuits in type A2 behave

almost independently from each other close to failure and exhibit more non-composite behaviour.

In type B2, the neutral axes of the top and bottom biscuits lie in mid-depth region at early stages of loading. At failure, the top and bottom biscuits have their own neutral axes. This indicates that type B2 specimens initially behave in a partially composite manner initially but behave almost non-compositely at failure. This confirms that the lattice girder in type B2 not only increases the stiffness of the specimens but also causes the test specimens to behave in a partially composite manner.

B. Effect of varying Depth of Lattice Girder

Figures 6.26-6.27 show the variation of lateral deflection with the depth of the test specimen for both types B2 and C2 is very similar. Continuous lateral deflection profiles are observed throughout the depth of the specimens. The neutral axes at failure or types B2 and C2 are approximately 17 mm and 22 mm (from the top to the bottom) respectively.

The deeper neutral axis in C2 can be attributed to the deeper test specimens due to the extra 20 cm added to the depth of the specimen from 80 mm lattice girder used. However, at the neutral axes are well into the top biscuit for both types B2 and C2. This explains why the compressive lateral deflections in the top biscuit were found to be much less than the tensile lateral deflections in the bottom biscuit. The results also suggest that in spite of using the lattice girder in type B2 and C2, the test specimens behave like single units.

It is also observed that the neutral axis begins to rise close to the failure load. This is due to the formation of large cracks in the tension side of the concrete near the section of maximum bending moment, i.e. at midspan.

C. Role of Concrete Biscuits and Core in Twinwalls

Figures 6.26, 6.28 and 6.29 show the variation of the lateral deflection with the depth of types B2, D2 and F2 respectively. The lateral deflection is indicative of the strains occurring in the concrete under the loads applied. The compressive lateral deflections (strains) are significantly less than the tensile lateral deflections. This is due to the formation of flexural cracks in the bottom biscuits under loading. It can be noted that for types B2, D2 and E2, discontinuities in lateral deflection are relatively small during the early stages of loading. As the specimens approach the failure load, the discontinuities become larger.

The discontinuities in lateral deflection and hence concrete strains in type B2 are significantly different of those in type D2 and E2. The variation of lateral deflections indicate that the neutral axes of the top and bottom biscuits in type B2 lies in mid-depth region at early stages of loading. At failure, the top and bottom biscuits have their own neutral axes. This indicates that type B2 specimens initially behave in a partially composite manner initially but behave almost non-compositely at failure.

In contrast, the neutral axes for types D2 and E2 lie well into the top biscuit up until the failure of the test specimens. This suggests that the concrete core has a stiffening effect

on the test specimens thereby leading to an increase in the degree of composite action taking place.

6.2.8 Variation of Strains in Lattice bars

The strains in the lattice bars in types B2 and C2 were measured using strain gauges at various locations. The strains were recorded at each load increment until failure. The stresses at failure are also calculated for each of the diagonal bar by multiplying the strain with the Elastic Modulus of steel (200, 000 N/mm^2).

6.2.8.1 Results

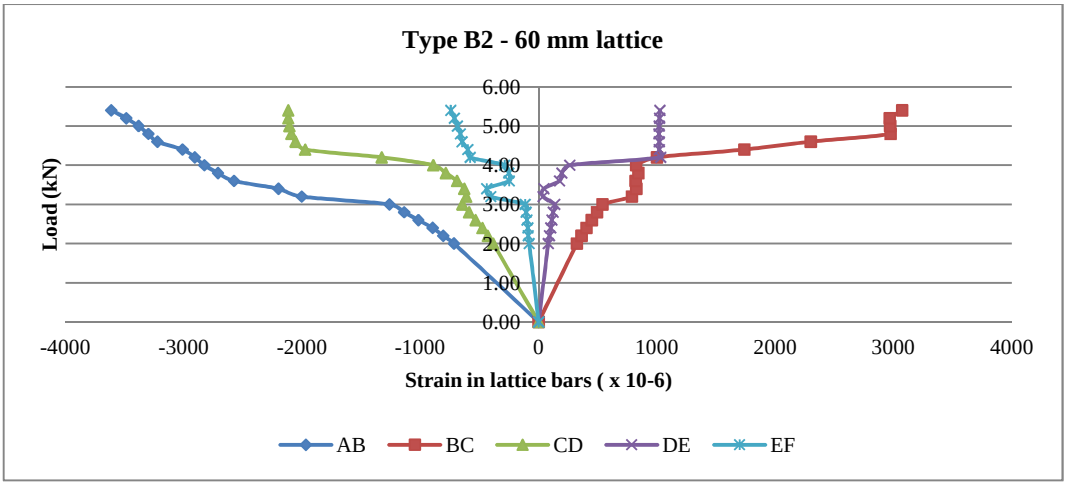

Figure 6.30 - Load v/s Strain in lattice bars: B2

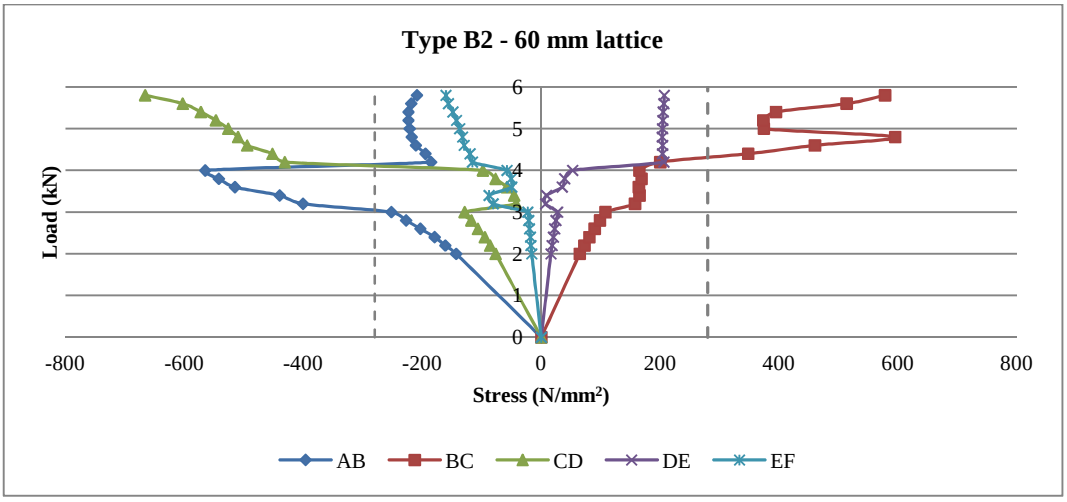

Figure 6.31 - Load v/s Stress in lattice bars: B2

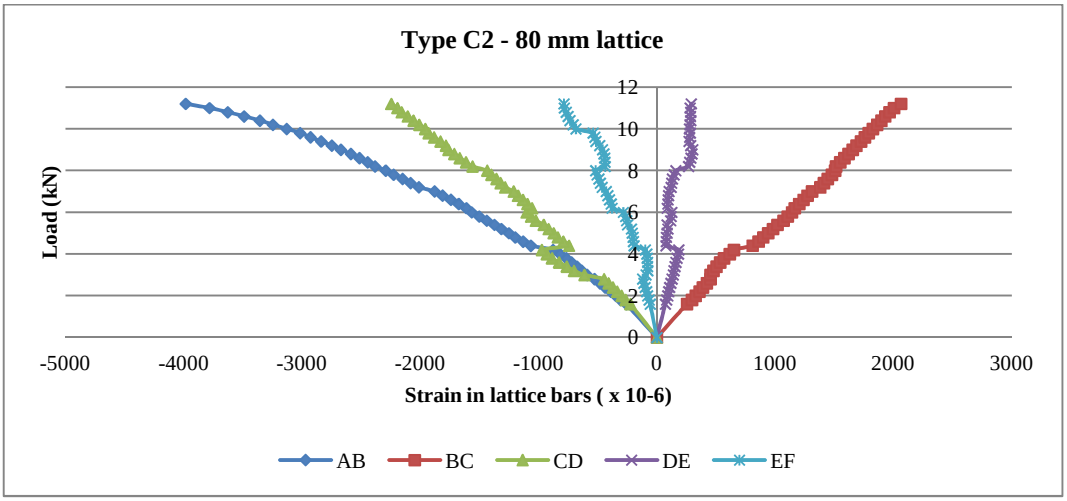

Figure 6.32 - Load v/s Strain in lattice bars: C2

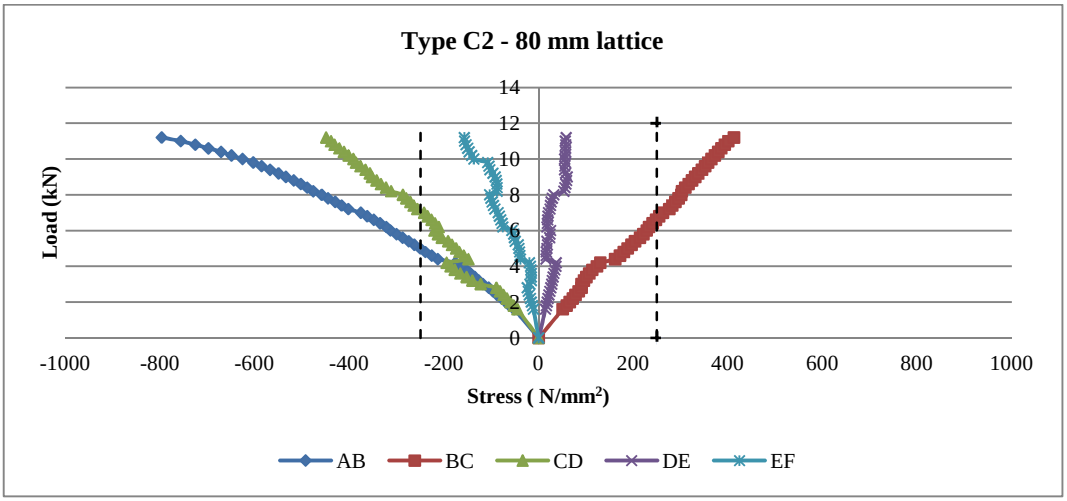

Figure 6.33 - Load v/s Stress in lattice bars: C2

6.2.8.2 Discussion

Results indicate that the lattice bars are subject to compression and tension for both types B2 and C2. This confirms the lattice bars transfer forces from the top to the bottom biscuits thereby exhibiting composite behaviour. It can also be seen that as the load increases, the lattice bar AB fails first followed by bars BC and CD. These indeed correspond to points where the shear forces are maximum.

For type B2, Bar AB fails at 3.6 kN (62 % of the ultimate failure load) while bars BC and CD fail simultaneously at 4.8 kN (83 % of failure load). For types C2, Bar AB fails at 5.0 kN (44 % of the ultimate failure load) while bars BC and CD fail simultaneously at 7.0 kN (62 % of failure load). Thus, the strains in the bars suggest that the increase in the lattice depth to 80 mm in type C2 induces more tensile and compressive forces in the lattice bars which contributed to the overall increase in composite behaviour.

Bars DE and EF do not yield at failure and are subject to significantly less strains and stresses in comparison with bars AB, BC and CD. This is because at these points the shear forces are minimum. Hence, these results differ from theory which suggests that the shear forces in bars DE and EF should be equal to zero.

Results still show that failure in type B2 and C2 occurs as a result of steel yielding of the lattice bars which is indicative of shear failure. Hence, it can be concluded that the lattice girder primarily behaves as a shear connector in types B2 and C2 specimens irrespective of the depth of the lattice girder.

6.2.9 Failure Mechanism

6.2.9.1 Results

The crack patterns observed in types A2-E2 are provided below.

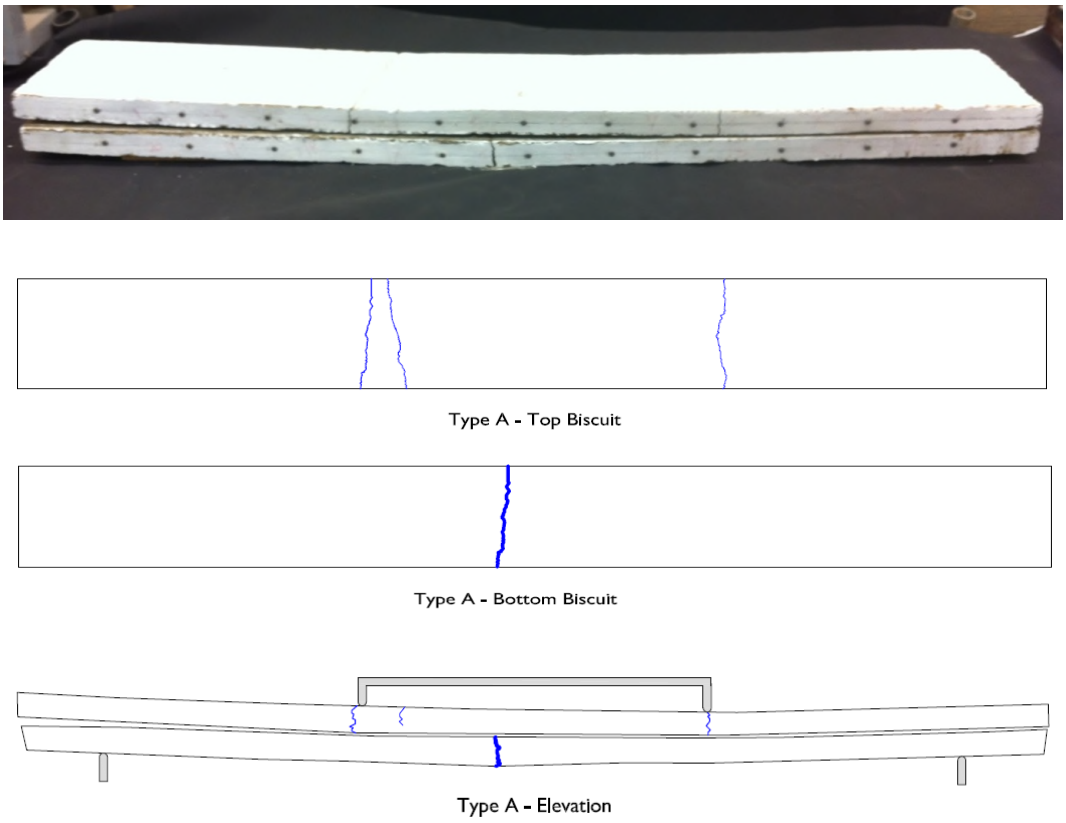

Figure 6.34 – Crack patterns: Type A2

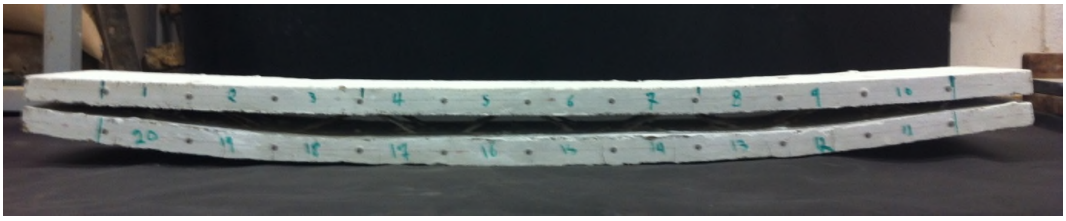

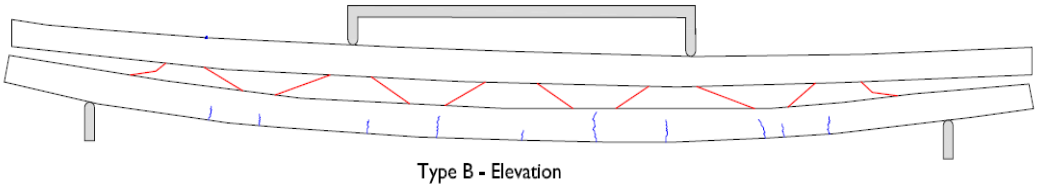

Type B - Elevation

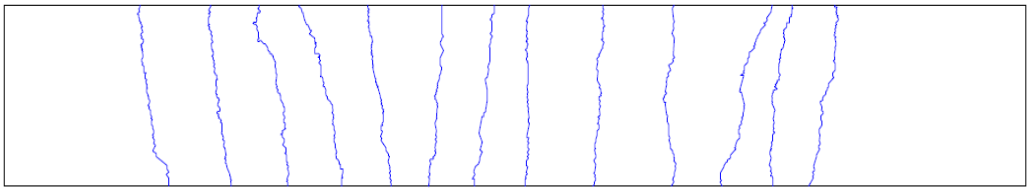

Type B - Bottom Biscuit

Figure 6.35 – Crack patterns: Type B2

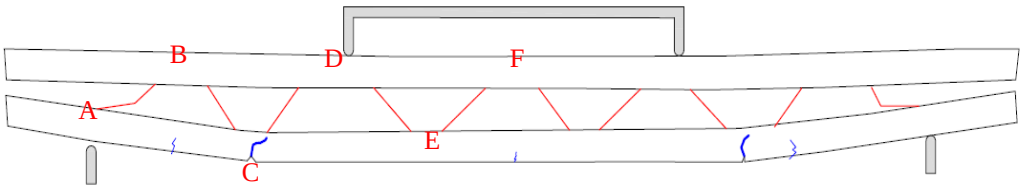

Type C - Elevation

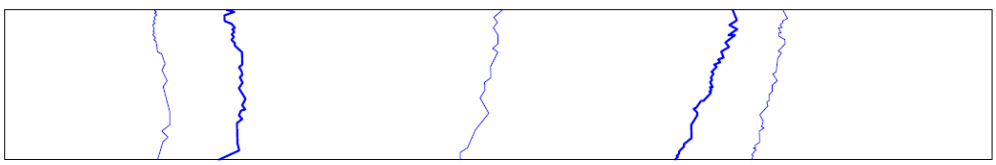

Type C - Bottom Biscuit

Figure 6.36 – Crack patterns: Type C2

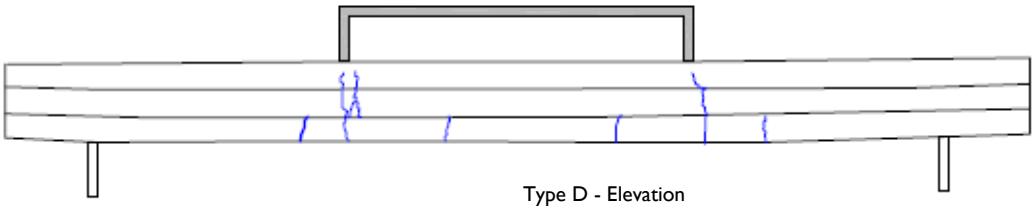

Type D - Elevation

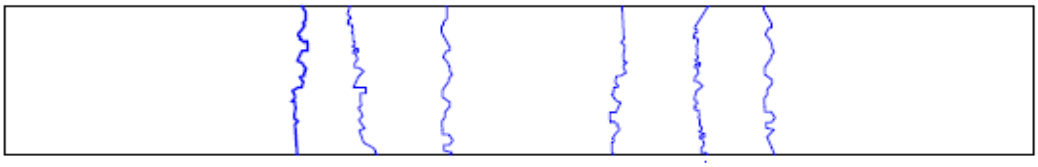

Type D – Bottom Biscuit

Figure 6.37 – Crack patterns: Type D2

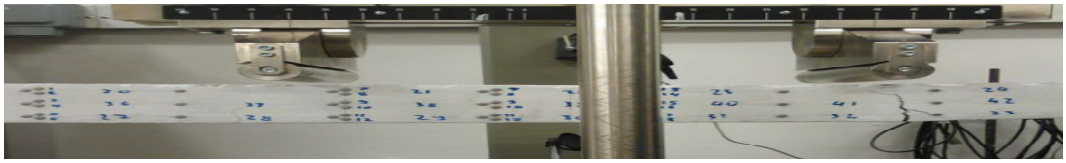

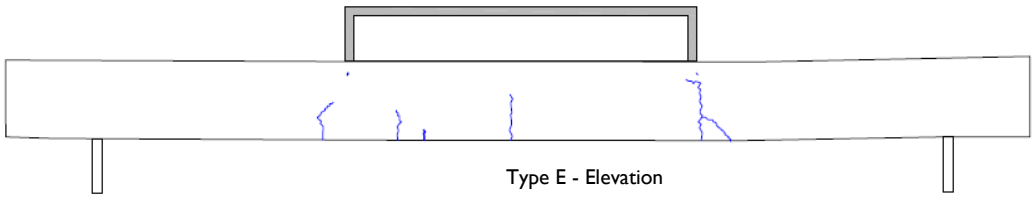

Type E - Elevation

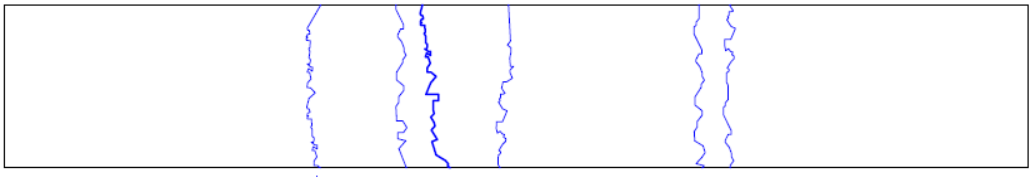

Type E – Bottom Biscuit

Figure 6.38 – Crack patterns: Type E2

6.2.9.2 Discussion

A. Effect of using Lattice Girder in Twinwalls

From Figure 6.29, it can be seen that for type A2, a deep flexural crack occurs at midspan of the bottom biscuit at failure and minor cracks appear under the load points in the top biscuit. As the load was applied, flexural cracks developed at midspan in the bottom biscuit with the first crack occurring at 48% of the ultimate failure load. The crack deepened and further cracks developed in the bottom biscuit as the load increased. Cracks occurred underneath the points of application of the load at approximately 96% of failure load. It was also observed that the interfaces between the top and bottom biscuits slipped relative to each other as the load was applied. Failure occurred due to the sudden brittle failure of the concrete biscuits. Further investigation revealed that no yielding of the reinforcement bars occurred, confirming that failure was caused due to concrete crushing.

Figure 6.30 shows the crack patterns for type B2 at failure. It is observed that unlike type A2, the bottom biscuit deflects more than the top biscuit with classic flexural cracks occurring in the bottom biscuit. Flexural cracks occurred at midspan in the bottom biscuit with the first crack occurring at 44% of the ultimate failure load. The crack deepened and further cracks developed in the bottom biscuit as the load increased. Buckling of lattice bar at the supports (Bar AB) was observed at 62 % of the failure load. Bars BC and CD also deformed and buckled at 83% of the failure load. Cracks occurred underneath the points of application of the load at approximately 85% of failure load. Further investigation revealed that the reinforcement bars in the concrete

biscuits did not yield which confirms that failure primarily occurred as a result of the yielding of the lattice bars, i.e. failure of shear connectors. Thus, it can be concluded the using the lattice girders influences the failure mechanism of the test specimens.

B. Effect of varying Depth of Lattice Girder

As discussed previously, failure in type B2 specimen occurred due to bending of the bottom biscuit and shear failure of the lattice girder.

Figure 6.31 shows the crack patterns for type C2 at failure. When the load was applied to the test specimen, minor flexural cracks began to form in region C of the bottom biscuit. As the load was increased further, other minor flexural cracks occurred in the bottom biscuit and the cracks in region C deepened. Prior to failure, the lattice bars closest to the support (AB) began to buckle and further deepening of the cracks in region C occurred until failure. No cracking was observed in the top biscuit. This suggests that high concentration of stresses occurred in the region between the point of application of the load and the supports at early stages. As the load increased these stresses were transferred to the adjacent bars AB, BC and CD as well as the flexural crack. Hence, failure occurred due to a combination of bending and shear failure of the bar AB.

The behaviours of types B2 and C2 indicates that using a shallower lattice in type B2 seems to distribute the forces in the biscuits more evenly thereby resulting in more uniformly distributed flexural cracks in the bottom biscuit. In type C2 where the depth of the lattice was increased from 60 mm to 80 mm, stress concentrations occurred at

locations which corresponded to the nodes of the lattice. However, for both types, failure seemed to occur as a result of combined bending and shear.

Hence, it can be concluded that varying the depth of the lattice girder influences the distribution of the forces in the test specimens but does not seem to affect the overall failure mechanism.

C. Role of Concrete Biscuits and Core in Twinwalls

As already discussed, in type B2, failure occurred due to bending of the bottom biscuit and shear failure of the lattice girder.

Figure 6.32 shows the crack patterns for type D2 at failure. When the load was applied to the test specimen, the minor flexural cracks began to form in the bottom biscuit. Surface cracks began to appear on the underside of the bottom biscuit at a load of approximately 4.6 kN (37% of failure load) and deepened with each load increment. As the load was applied, cracks also began to form at the top biscuit/core and bottom biscuit/core interfaces at a load of approximately 7.8 kN (64% of failure load). Cracking was also observed on the face of the test specimens. Failure occurred as a result of the yielding of the tension steel of the test specimen.

The above behaviour is analogous of the behaviour of solid concrete beams under flexure. The presence of the flexural cracks in the bottom biscuits suggests that the forces were effectively being transmitted from the top biscuit to the core and ultimately to the bottom biscuit. The formation of the crack at the biscuit/core interfaces is due to

the overcoming of the aggregate interlock forces between the two concrete layers. In fact, after the experiment was carried out, the core and biscuits were stripped from the lattice bars. Close inspection of the bars confirmed that some of the lattice legs had yielded. This suggests that the lattice legs transfer the forces from the top biscuits to the bottom biscuits and therefore act as shear connectors. Hence, failure in type D2 occurred due to a combination of bending, shear and interface shear failure of the test specimen.

The failure in type E2 was very similar to that of type D2 except that no interface shear failure occurred since the test specimens were cast in one stage as a solid section. The first flexural cracks appeared in the bottom biscuit at a load of approximately 5.2 kN (41% of failure load). Hence, it can be concluded that casting the specimens in three stages (type D2) does not seem to affect the failure mechanism.

6.3 Comparison with Theoretical Predictions

6.3.1 Shear Failure

6.3.1.1 Results

As discussed in Chapter 5, the lattice steel girder in the test specimens act as shear connectors and develop tensile forces in their diagonal bars to resist the shear applied. The axial forces in the members of the truss can therefore be calculated. Note that tension is taken as positive.

For type B2, the depth of the truss is 60 mm, the angle of inclination Ø = tan-1 (60/100) = 31^0. For type C2, the depth of the truss is is 80 mm, the angle of inclination Ø = tan-1 (80/100) = 39^0.

The axial forces in one typical truss in types B2 and C2 are shown in Figures 6.39 and 6.40.

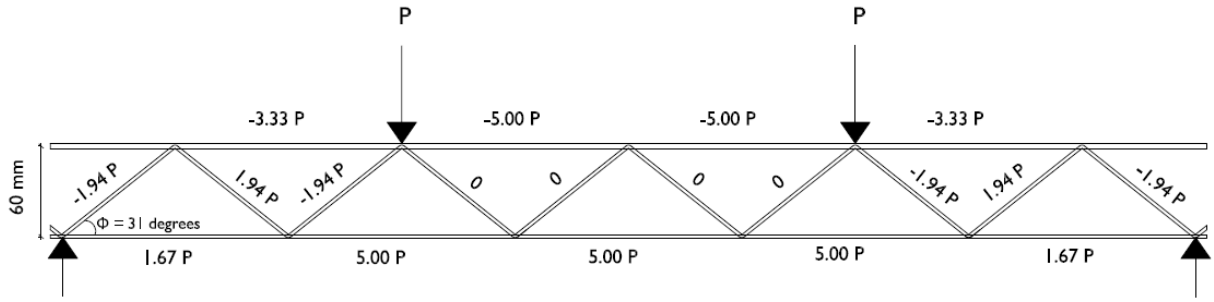

Figure 6.39 - Forces in 60 mm deep truss - Type B2

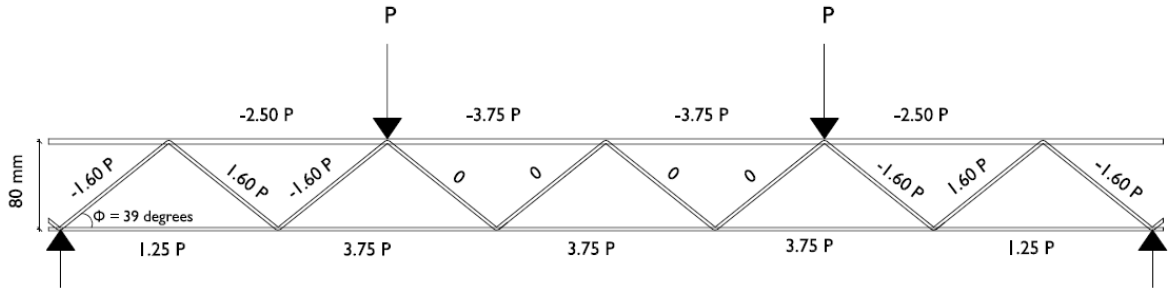

Figure 6.40 - Forces in 80 mm deep truss - Type C2

For type B2, the load at which the first diagonal bar yields is given by:

- The diagonal bar diameter of 3 mm, $A_s = \prod$ x 3^2 / 4 = 7.069 mm^2
- The yield strength f_y from stress-strain curve = 280 N/mm^2
- $F_{(diagonal)} = P_{(diagonal)}$ /sinØ = A_s f_y = (7.069 x 280) = 1.98 kN; hence, $P_{(diagonal)} = F_{(diagonal)}$ sinØ = 1.979 x sin 31^0 = 1.02 kN

- Each lattice girder comprises 2 identical trusses: $F_{(lattice)} = 2\ F_{(diagonal)} = 2 \times 1.02 = 2.04$ kN.
- Each test specimen consists of 2 lattice girders: $P = F_{(specimen)} = 2\ F_{(lattice)} = 2 \times 2.04 = 4.08$ kN
- The total failure load at which the first diagonal bar yields = $2P = 2 \times 4.08 = 8.16$ kN

Thus, the shear failure load at which the first lattice bars yield in type B2 is 8.16 kN. Similarly, the load at which the first diagonal lattice in type C2 yields can be calculated as 8.90 kN.

6.3.1.2 Discussion

For type B2, the average experimental failure load of 5.50 kN is 33% less than the predicted shear failure load of 8.16 kN. For type C2, the experimental load of 11.30 kN is 27% greater than the predicted shear failure load of 8.90 kN. This suggests that failure in types B2 and C2 may have primarily been caused by a bending failure rather than tensile shear failure of the diagonal steel lattices or by a combination of both bending and shear failure. Hence, varying the depth of the lattice does not seem to have an influence on the mode of failure of the test specimen.

The lower experimental shear failure load also indicates that the load applied may not have been distributed uniformly in the diagonal bars as suggested by the truss analogy. This has been confirmed by the experimental determination of the strains in the lattice bars discussed previously.

6.3.2 Interface Shear Failure

The interface shear failure can occur at the interface between the outer top and bottom biscuits and the core in type D2. The interface shear strength at this interface is provided by three main mechanisms (1) aggregate interlock, (2) friction and (3) dowel action.

6.3.2.1 Results

The interface shear strength at the biscuit/core interface can be calculated by using Section 6.2.5 of EC2 as follows:

- $v_{Ei} < v_{Rdi}$ where,
  - v_{Ei} is the design value of the shear stress in the interface given by: $v_{Ei} = \beta V_{Ed} / z b_i$ where,
  - β: ratio of longitudinal force in new concrete and the total longitudinal force, $\beta = 1$
  - Lever arm, $z = d - 0.45 x$
  - Taking the section as being fully composite, from Table 3.15: $x = 9.59$ mm
  - Hence, $z = 85 - (0.45 \times 9.59) = 80.69$ mm
  - b_i: Width of section = 200 mm
  - $v_{Ei} = \beta V_{Ed} / z b_i = V_{Ed} / (81.03 \times 200) = 6.20 \times 10^{-5} V_{Ed}$
- v_{Rdi} is the design shear resistance at the interface given by:
  - $v_{Rdi} = c f_{ctd} + \mu \sigma_n + \rho f_{yd} (\mu \sin \alpha + \cos \alpha) \leq 0.5 \nu f_{cd}$ where,
  - c and μ : depend on roughness of the interface. From 6.2.5 (2), assuming a smooth interface, $c = 0.20$ and $\mu = 0.60$

- f_{ctd}: Design tensile strength obtained from 3.1.6 (2)
  - $f_{ctd} = \alpha_{ct} f_{ctk,0.05} / \gamma_c$ where, $\alpha_{ct} = 1$; for type D2, $f_{ck} = 41.12$ N/mm^2 based on the average strength of the concrete biscuits and core and from EC2, Table 3.1, $f_{ctk,0.05} = 2.50$ N/mm^2 for $f_{ck} = 41.12$ N/mm^2
  - γ_c is taken as 1.0 since the factors of safety are ignored.
  - Hence, $f_{ctd} = 1 \times 2.50 / 1.0 = 2.50$ N/mm^2
- σ_n: Stress per unit area caused by minimum external normal force across interface. In this case, there is no normal force at the interface, ie. $\sigma_n = 0$
- $\rho = A_s/A_i$ where,
  - A_s: Area of reinforcement (including shear reinforcement) crossing the interface. In this case, 40 no. 3 mm diameter lattices cross the interface:

    $A_s = 40 \times \pi \times 3^2/4 = 282.74$ mm^2
  - A_i: Area of joint, which in this case = (200 x 1000) mm^2
  - Hence, $\rho = A_s/A_i = 282.74 / (200 \times 1000)$
- α: Angle defined in EC2: Figure 6.9
  - For a 60 mm deep truss, angle $\alpha = 31^0$
  - EC2 suggests that $45^0 \leq \alpha \leq 90^0$, hence angle α is taken as 45^0
- f_{yd} from previous tensile tests = 280 N/mm^2
- $v_{Rdi} = c f_{ctd} + \mu \sigma_n + \rho f_{yd} (\mu \sin \alpha + \cos \alpha)$

  $= (0.2 \times 2.50) + 0 + \{(282.74 / (200 \times 1000)) \times (0.6 \sin 45 + \cos 45)$

  $v_{Rdi} = 0.500 + 0 + (0.396 \times 1.131) = 0.955$ N/mm^2

- v: Reduction factor obtained from 6.2.2 (6)
  - $v = 0.6 (1-f_{ck}/250) = 0.6 (1-41.12/250) = 0.501$

- $v_{Rdi} = 0.955 \leq 0.5\ v\ f_{cd} = 0.5 \times 0.501 \times (41.12) = 10.307\ N/mm^2$ ... ok
- Thus, $v_{Rdi} = = 0.955\ N/mm^2$

- Now equating v_{Edi} and v_{Rdi} to find V_{Ed} :
  - $v_{Ei} = 6.197 \times 10^{-5}\ V_{Ed} = 0.955$
  - Load to cause interface shear failure, $V_{Ed} = 0.955 / (6.197 \times 10^{-5}) = 15.30$ kN

Thus, from the above calculation the load required to cause failure at the interface between the top biscuit/bottom biscuit and the core is 15.30 kN.

6.3.2.2 Discussion

For type D2, the experimental failure load is 12.25 kN. The theoretical failure load required to cause interface shear failure at the biscuit/core interface was calculated as 15.30 kN which is 25% greater than the experimental load.

As discussed, interface shear failure comprises of three types of failure mechanisms (1) aggregate interlock, (2) friction and (3) dowel action. From the above interface shear calculations where $v_{Rdi} = c\ f_{ctd} + \mu\ \sigma_n + \rho\ f_{yd}\ (\mu \sin \alpha + \cos \alpha) = 0.955\ N/mm^2$, the aggregate interlock stress, $c\ f_{ctd} = 0.500\ N/mm^2 = 53\%\ v_{Rdi}$. Hence, the load required to cause aggregate interlock failure = 53% x V_{Ed} = 8.07 kN.

The above result shows that aggregate interlock failure did occur in type D2 specimen. This was in fact confirmed by the appearance of a crack or separation at the interfaces between the outer top and bottom biscuits and the core.

The dowel action part of the theoretical interface shear calculation [$\rho f_{yd} (\mu \sin \alpha + \cos \alpha)$] assumes that all the bars crossing the biscuit/core interface yield. The lower experimental failure load of 12.25 kN in comparison with the theoretical value of 15.30 kN therefore seems to suggest that not all bars crossing the core/biscuit interface yielded at failure.

6.3.3 Degree of Composite Action at Elastic Stage

6.3.3.1 Results

The degree of composite action at the elastic stage can be calculated from the experimental load-stress profiles. The stress in the concrete biscuits is derived from the DEMEC readings as follows:

$$Stress = Strain \; x \; E_{concrete}$$

where,

- Strain in concrete = Lateral deflection in concrete at midspan x Calibration Factor of DEMEC gauge. The lateral deflections are obtained experimentally by the DEMEC readings and the calibration factor of DEMEC gauge is 0.0001 as per manufacturer guidelines.
- $E_{concrete}$ is taken as 30,000 N/mm^2.

The load-stress in concrete profiles for types A2-E2 are compared relative to each other below.

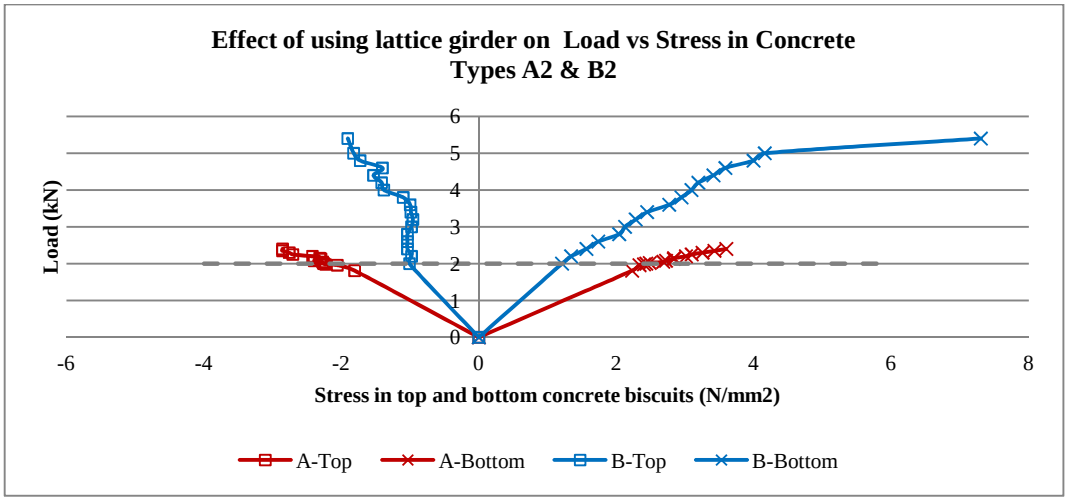

Figure 6.41 – Load- Concrete Stress profiles: Types A2 & B2

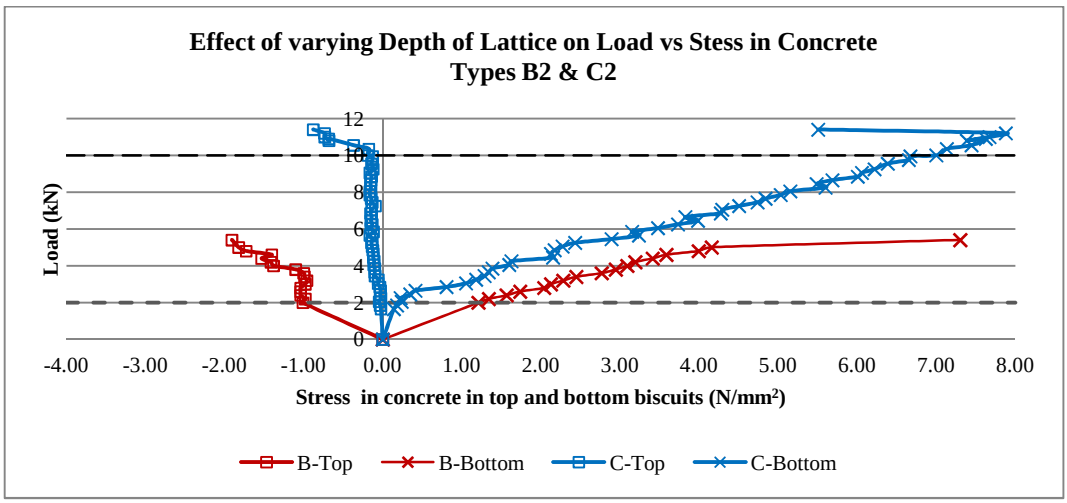

Figure 6.42 – Load- Concrete Stress profiles: Types B2 & C2

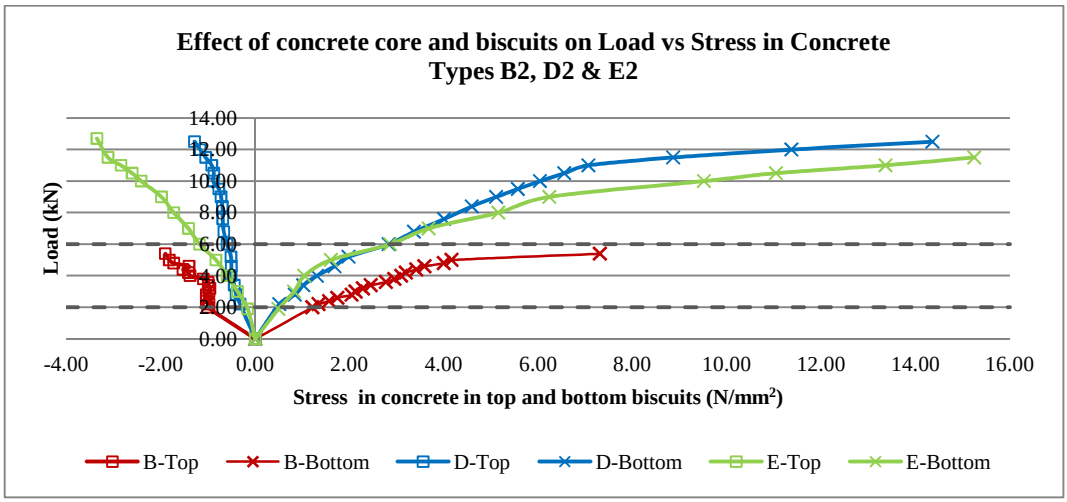

Figure 6.43 – Load- Concrete Stress profiles: Types B2, D2 & E2

From the load-stress profile, a load within the linear stage (i.e. when the load is directly proportional to the stresses in the top and bottom deflection) is taken. Based on this load, the effective moment of inertia, Ic is then calculated using the following formula:

$$I_c = \frac{Mh}{\sigma_b - \sigma_t}$$

- σ_b and σ_t are the stresses at the bottom and the top faces of the concrete biscuits of the specimens respectively obtained from the Load-Stress in concrete profiles for each specimen type.
- M is the bending moment calculated as Load/2 due to two load points x Lever arm.
- h is the depth of the twinwall specimens.

The ratio of the effective moment of inertia, I_c to the gross moment of inertia, I_g provides an indication of the degree of composite action at the elastic stage. The gross moment of inertia, I_g is calculated assuming that fully composite action occurs in the test specimens.

Based on the values of the load, σ_b and σ_t obtained for each specimen type, the corresponding degree of composite action at the elastic stage is summarised in Table 6.9 below.

Type	Parameter varied	Load (kN)	Moment (kNm)	h (mm)	σ_t (N/mm^2)	σ_b (N/mm^2)	I_e (10^6)	I_g (10^6)	I_e/I_g
A2	No lattice	2	0.6	60	-2.5	2.4	3.67	3.81	96.33%
B2	60 mm lattice	2	0.3	90	-1	1.2	12.27	13.01	94.31%
C2	80 mm lattice	10	1.5	110	-0.02	7	23.5	23.71	99.11%
D2	Cast in 3 stages	6	0.9	90	-0.8	3	21.32	13.01	163.87%
E2	Solid	6	0.9	90	-1.2	3	19.29	13.01	148.27%

Table 6.9 –Degree of composite action at elastic stage: A2-E2

6.3.3.2 Discussion

A. Effect of using Lattice Girder in Twinwalls

Results from Table 6.9 indicate that during the elastic stage, the degree of composite action between the top and bottom concrete biscuits is very high. Type A2 behaves more compositely than type B2. This may due to the presence of the lattice girder in type B2. However, it should be noted that the degree of composite action occurring in type B2 specimens is a 94.36% thereby confirming that the lattice girder effectively transfers the force applied from the top biscuit to the bottom biscuit. Hence, the lattice girders behave as shear connectors in twinwalls.

B. Effect of varying Depth of Lattice Girder

Results show that during the elastic stage, the degree of composite action between the top and bottom concrete biscuits is very high. Type C2 behaves more compositely than type B2. This may due to the deeper lattice used in type C2. It should also be noted that the degree of composite action occurring in types B2 and C2 specimens are 94.36% and 99.15%. This confirms that thereby confirming that the lattice girder effectively transfers the force applied from the top biscuit to the bottom biscuit thereby acting as shear connectors in twinwalls. Results also suggest that increasing the depth of the lattice leads to an increase in the degree of composite action during the elastic stage.

C. Role of Concrete Biscuits and Core in Twinwalls

It is observed that during the elastic stage, the degree of composite action between the top and bottom concrete biscuits is very high in type B2. It must also be noted that the I_e/I_g ratio does not seem to be valid for types D2 and E2 since the degree of composite action exceeds 100%. This may be due to the differences between the actual stresses developed in the concrete biscuits during the experiment in comparison to the theoretical predictions. However, the degree of composite action for types D2 and E2 still remain higher than that of B2. This confirms that the presence of the concrete core leads to an increase in the degree of composite action during the elastic stage

6.3.4 Degree of Composite Action at Ultimate Stage

6.3.4.1 Results

The experimental failure load obtained for type E2 is representative of a fully composite, monolithic member.

Hence, the experimental failure loads for types A2-D2 can be expressed as a ratio of the E2 experimental load to provide an indication of the degree of composite action at ultimate stage as summarised in Table 6.10.

Type	Parameter varied	Experimental Failure Load (kN)	Experimental/E2 Failure load (kN)
A2	No lattice	2.50	19.84%
B2	60 mm lattice	5.50	43.65%
C2	80 mm lattice	11.30	89.68%
D2	Cast in 3 stages	12.25	97.22%
E2	Solid	12.60	100.00%

Table 6.10 –Degree of composite action at ultimate stage: A2-E2

6.3.4.2 Results

A. Effect of using Lattice Girder in Twinwalls

Result show that when the specimens move from the elastic to the plastic stage, the degree of composite action between the top and bottom biscuits reduces significantly. For types A2 and B2, the degree of composite action reduces by 76% and 51% respectively. In type A2, the loss in compositeness can be attributed to the formation of deep cracks in the top and bottom biscuits. In type B2, the formations of flexural cracks in the concrete biscuits as well as the yielding of the lattice bars contribute to the loss in compositeness of the test specimens.

The degree of composite action at ultimate stage in type B2 is also approximately 24% greater than that in type A2. This confirms that the presence of the lattice girder in type B2 contributes towards the degree of composite action in the test specimens.

B. Effect of varying Depth of Lattice Girder

It is observed that as the specimens move from the elastic to the plastic stage, the degree of composite action between the top and a bottom biscuit reduces significantly. For types B2 and C2, the degree of composite action reduces by 51% and 9% respectively. This is due to the formation of flexural cracks in the concrete biscuits as well as the yielding of the lattice bars thereby contributing to the loss in compositeness of the test specimens.

The degree of composite action in type C2 is also approximately 46% greater than that in type B2. This confirms that increasing the lattice depth from 60 mm to 80 mm leads to a rise in the degree of composite action taking place at the ultimate stage.

C. Role of Concrete Biscuits and Core in Twinwalls

Results show that the experimental failure loads for types B2, D2 and E2 lie between the non-composite and fully composite failure loads. This shows that the test specimens behave in a partially composite manner.

The degree of composite action at ultimate stage in types B2, D2 and E2 are 44%, 97 % and 100 % respectively. This confirms that using the concrete core in types D2 and E2 significantly increases the degree of composite action. Additionally, there is only a 3% difference between the degree of composite action in type D2 and type E2. Hence, casting the specimen in three separate sections (type D2) or as one solid unit (type E2) does not seem to influence the degree of composite action observed. It can be concluded

that the degree of composite action increases when the concrete core is used but is not affected by the casting procedure of the test specimens.

6.4 Overview of Flexural Tests

6.4.1 Effect of using lattice girder in twinwalls

The influence of using lattice girders on the flexural behaviour of twinwall panels was determined. The failure load in type B2 is approximately 2.2 times that in type A2. This suggests that using the lattice girder in type B2 has a significant influence on the failure load of the test specimens.

The top and bottom deflections in type A2 are respectively 74% and 72 % greater than those in type B2. This confirms that the use of the lattice girder significantly increases the stiffness of the test specimen in type B2.

The load-deflection profile for type A2 and B2 confirm that the test specimen exhibit partially composite manner behaviour.

The lateral stiffness of type A2 specimen is much lower than that of type B2. This can be attributed to the lattice girders in type B2 which are embedded in the faces of the top and bottom biscuits and restrict the biscuits from deforming laterally.

The strains in the lattice bars show that failure in type B2 occurs due to steel yielding of the bar closest to the support, which is indicative of shear failure. Sudden brittle failure with a deep crack in the bottom biscuit occurs in type A2. This suggests that failure in type A2 primarily occurs as a result of premature failure of the concrete in the bottom biscuit. In type B2, classic flexural cracks occurs in the bottom biscuit followed by yielding of the lattice bar closest to the support. This suggests that failure in type B2 specimen occurs due to bending and shear failure. It can be concluded the using the lattice girders influences the failure mechanism of the test specimens.

The theoretical degree of composite action at elastic stage is 96% in type A2 and 94% in type B2. The theoretical degree of composite action at ultimate stage is 20% for type A2 and 44% for type B2. This confirms that during the elastic stage, the specimens behave as fully composite units and as the specimens move from the elastic to the plastic stage, the degree of composite action between the top and bottom biscuits reduces significantly. The degree of composite action in type B2 is also approximately 7% greater than that in type A2. This confirms that the presence of the lattice girder in type B2 contributes towards the degree of composite action in the test specimens.

6.4.2 Effect of Varying Depth of Lattice Girder

Tests were carried out to determine the influence of using lattice girders on the flexural behaviour of twinwall panels. It was observed that the failure load in type C2 is approximately twice that in type B2. This suggests that increasing the lattice depth from 60 mm to 80 mm significantly increases the failure load of the test specimens.

The top and bottom deflections in type B2 are respectively 13% and 28 % greater than those in type C2. This confirms that increasing the lattice depth from 60 mm to 80 mm significantly increases the stiffness of the test specimens.

The load-deflection profiles for types B2 and C2 show that the test specimen behaves in a partially composite manner. However, type C2 behaves more compositely than type B2. This further confirms that increasing the lattice depth from 60 mm to 80 mm increases the degree of composite action observed.

For types B2 and C2, the lateral deflection in the concrete in the bottom biscuits increases with increasing load but the strains in the top biscuit do not change significantly. The strains in the lattice bars show that failure in types B2 and C2 occurs due to steel yielding of the bar closest to the support, which is indicative of shear failure.

In type B2, classic flexural cracks occurs in the bottom biscuit followed by yielding of the lattice bar closest to the support. In type C2, flexural cracks occur at concentrated regions the bottom biscuit followed by yielding of the lattice bar closest to the support. This suggests that failure in types B2 and C2 specimen occurs due to bending and shear failure. Hence, it can be concluded that varying the depth of the lattice girder influences the distribution of the forces in the test specimens but does not seem to affect the overall failure mechanism.

The theoretical degree of composite action at elastic stage is 94% in type B2 and 99% in type C2. The theoretical degree of composite action at ultimate stage is 44% for type

B2 and 89% for type C2. This confirms that during the elastic stage, the specimens behave as fully composite units and as the specimens move from the elastic to the plastic stage, the degree of composite action between the top and bottom biscuits reduces significantly. The degree of composite action in type C2 is also approximately 46% greater than that in type B2. This confirms that increasing the depth of the lattice girder in type C2 results in a rise in the degree of composite action in the test specimens.

6.4.3 Role of Concrete Biscuits and Core in Twinwalls

The introduction of a concrete core between the top and bottom biscuit (type D2) more than doubles (by approximately 2.2 times) the failure load of the test specimen (in comparison with type B2). This confirms that the concrete core leads to a rise in the stiffness and the failure load.

Casting the test specimen in three stages (type D2) increases the failure load by 3% in comparison with the test specimen cast as a single solid section (type E2). This confirms that the behaviour of type D2 (representative of a typical twinwall) is very similar to that of a solid beam section.

The average top and bottom deflections of type B2 are 65% and 61% less than those in type D2. This can be attributed to the significantly lower failure load of type B2 specimens which results in much lower deflection. The average top and bottom deflections of type E2 are 52% and 56% less than those in type D2. This shows that

casting the biscuits and the core in distinct stages significantly affects the stiffness of the test specimens in comparison with type E2.

The load-deflection confirm that types B2, D2 and E2 behave in a partially composite manner with type E2 behaving most compositely followed by type D2 and type B2. This indicates that the presence of a concrete core in type D2 and E2 increases the degree of composite action in comparison with type B2 where no core is used. Results also show that the lateral stiffness of B2 is less than that of types D2 and E2.

In type B2, classic flexural cracks occurs in the bottom biscuit followed by yielding of the lattice bar closest to the support. In type D2, flexural cracks occur in the bottom biscuit as well as at the interfaces between the biscuits and core. This suggests that failure in due to a combination of bending, shear and interface shear failure in type D2. The failure in type E2 was very similar to that of type D2 except that no interface shear failure occurred since the test specimens were cast in one stage as a solid section.

The theoretical degree of composite action at elastic stage is 94% in type B2, 164% in type D2 and 148% in type E2. The theoretical degree of composite action at ultimate stage is 44% for type B2, 97% for type D2 and 100% in type E2. This confirms that during the elastic stage, the specimens behave as fully composite units and as the specimens move from the elastic to the plastic stage, the degree of composite action between the top and bottom biscuits reduces significantly. It can be concluded that the degree of composite action increases when the concrete core is used but is not affected by the casting procedure of the test specimens.

Chapter 7

Finite Element Modelling

7.1 Introduction

Finite Element (FE) modelling has now become an essential tool to solve a wide range of engineering problems numerically. The FE software ABAQUS 6.10 developed by Dassault Systems Simulia Corporation (2010) has been used to develop a three-dimensional (3-D) FE model in order to simulate the behaviour of twinwall test specimens. ABAQUS 6.10 offers linear and non-linear analysis capability for static, dynamic, heat transfer, soil consolidation and other problems. As well as efficiently representing the complex non-linear behaviour of concrete, ABAQUS can also depict the performance of the steel reinforcement and lattice bars independently of the concrete.

Two sets of FE analyses are carried out: (1) Validation Tests and (2) Parametric Tests. In the validation tests, the FE model is first validated against the experimental results for types A2-E2 test specimens presented in Chapters 5-6.

In the parametric test, FE analysis is carried out to investigate the effects of the following parameters on the behaviour of typical twinwalls:

1) Diameter of the dowel bar (i.e. diagonal bar of lattice girder)
2) Type of connector used, i.e. Single truss v/s. Double truss
3) Overall thickness of the twinwall (varied in terms of the height of the lattice girder)

The FE results are presented and discussed in terms of the (1) failure load, (2) maximum deflection at midspan, (3) load-midspan deflection profiles and (4) strains across depth of twinwall at midspan.

7.2 FE Modelling

7.2.1 Development of the FE Model

ABAQUS 6.10 adopts a step by step method in order to develop the FE model. The geometry of the model (parts, sections and profiles), material properties, boundary conditions, load and constraints are required to define the FE test specimen.

7.2.1.1 Details of Specimens

As discussed above, two sets of FE analyses were carried out: (1) Validation Tests and (2) Parametric Tests. The aim of the validation tests was to determine the accuracy of the FE model in predicting the behaviour of twinwalls specimens. The FE model was validated by comparing the experimental results obtained for types A2-E2 (discussed in

Chapters 5 and 6) with corresponding numerically simulated FE models, referred to as types A3-E3. To reiterate, details of test specimens A2-E2 are provided in Table 7.1.

Type.	Depth of Biscuits	Depth of Core	Depth of Lattice	Diameter of lattice bars
A2/3	30	No core	No lattice	No bars
B2/3	30	No core	60	Top – 5 mm Diagonal – 3 mm Bottom - 3 mm
C2/3	40	No core	80	"
D2/3	30	30	60	"
E2/3	30 (Solid Section)	30 (Solid Section)	60	"

Table 7.1 – Details of Validation Specimens

Following the validation of the FE model, numerical analysis was carried out on actual sized twinwall specimens. Details of the geometry of a typical twinwall specimens used for the parametric tests are given in Figure 7.1.

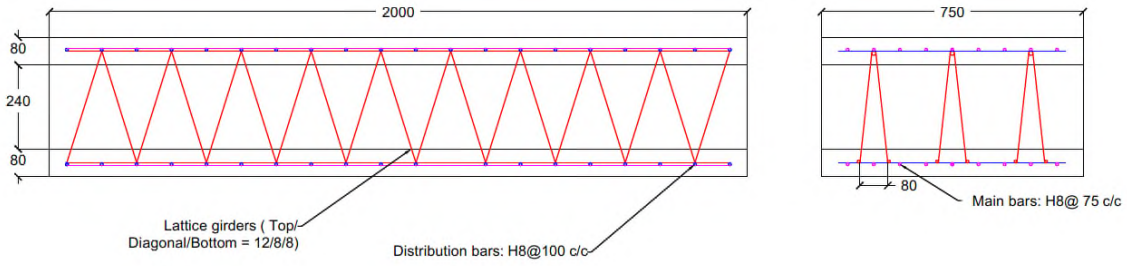

Figure 7.1- Details of Typical Parametric Specimens

The parametric study was used to determine the effects of the following parameters on the flexural behaviour of twinwalls:

1) *Dowel Bar Diameter* (i.e. diagonal bar of lattice girder)

The diameters of the dowel bar were varied to 4mm, 6mm, 8mm, 10mm, 12mm, 16mm and 20mm.

2) *Type of Connector* : Single truss v/s. Double truss

The effect of using two configurations of trusses was analysed. The double truss was representative of the 3-dimensional truss used in typical twinwalls, i.e. with one top chord, two bottom chords and four diagonal lattice chords at each top node. The single truss was a two-dimensional version of the double chord with one top chord, one bottom chord and two diagonal lattice chords at each top node.

The total area of the top bars in the single truss was modelled as being equivalent to the area of the double truss chord, i.e. the diameters of the top chord in the single and double truss were modelled as being 7.1 mm (Area = 39.5 mm^2) and 10 mm (Area = 79 mm^2) respectively. The diameters of the bottom chords in both the single and double trusses were 8 mm. Thus, two single trusses were used in lieu of one double truss.

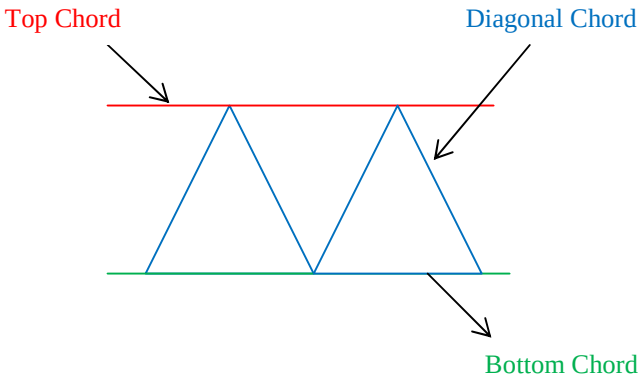

Single Truss

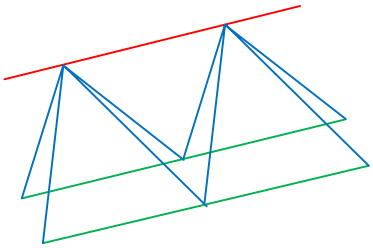

Double Truss

The diameters of the diagonal chords, in other words, the dowel bars, were varied to 4mm, 6mm, 8mm, 10mm, 12mm, 16mm and 20mm in the single truss and the results were compared with those obtained in (1) above.

3) Thickness of Twinwall

The overall thickness of the twinwall was varied in terms of the height of the lattice girder only. The thickness of the top and bottom biscuits was maintained at 80 mm. The lattice heights were varied to 320mm, 280mm, 240mm, 200mm and 160mm resulting in overall twinwall thicknesses of 400mm, 360mm, 320mm, 280mm and 240mm respectively. The thicknesses used in the FE analysis are representative of typical thicknesses of twinwalls used in industry. Details of the test specimens are provided in Table 7.2 below.

Parameters varied	**Type**	**Girder Height (mm)**	**Thickness (mm)**			**Overall Thickness (mm)**	**Dowel Bar Diameter (mm)**	**Single Truss**	**Double Truss**
			Biscuit 1	**Core**	**Biscuit 2**				
Dowel Bar Diameter	FA-1	320	80	240	80	400	4		x
	FA-2	"	"	"	"	"	6		x
	FA-3	"	"	"	"	"	8		x
	FA-4	"	"	"	"	"	10		x
	FA-5	"	"	"	"	"	12		x
	FA-6	"	"	"	"	"	16		x
	FA-7	"	"	"	"	"	20		x
Type of shear connector	FB-1	"	"	"	"	"	4	x	
	FB-2	"	"	"	"	"	6	x	
	FB-3	"	"	"	"	"	8	x	
	FB-4	"	"	"	"	"	10	x	
	FB-5	"	"	"	"	"	12	x	
	FB-6	"	"	"	"	"	16	x	
	FB-7	"	"	"	"	"	20	x	
Thickness	FC-1	320	80	240	80	400	8		x
	FC-2	280	80	200	80	360	8		x
	FC-3	240	80	160	80	320	8		x
	FC-4	200	80	120	80	280	8		x
	FC-5	160	80	80	80	240	8		x

Table 7.2 - Details of FE Test Specimens

7.2.1.2 Definition of the Geometry

The FE test specimens comprise the top and bottom biscuits, the core (where applicable), the steel reinforcement bars in the top and bottom biscuits as well as the lattice girders In order to construct the geometry of the model, the individual parts were defined.

The concrete biscuits were modelled as three-dimensional deformable solid parts. This feature is mostly used for relatively thin members under flexure, where strain variation across the depth of the biscuits must be linear. The steel members (i.e. the reinforcement and the lattice) were modelled as three dimensional deformable wires. The various components of the model were then assigned the correct section properties accordingly.

7.2.1.3 Mesh Refinement

Meshing of the elements is an integral part of FE analysis. Meshing divides the sections into smaller elements which are then analysed to produce a global solution. Hence, the correct mesh size needs to be adopted in order to ascertain the accuracy of the FE solution obtained.

Since the specimens used for the validation of the FE results and those used for the parametric study were different, two separate mesh refinement analysis were undertaken. For the validation model, type D2 (twinwall test specimen discussed in Chapters 5-6) was used and the mesh sizes were varied to 60mm, 50mm, 40mm, 30mm,

25mm, 20mm and 10mm. For the parametric study, the mesh sizes were first varied to 100mm, 80mm, 70mm, 60mm, 50mm, 40mm and 30mm for type FA-1 specimen.

A small load was then applied to the different FE specimens with varied mesh sizes and a load-midspan deflection profile for all the specimens was then plotted as shown in Figures 7.2-7.3.

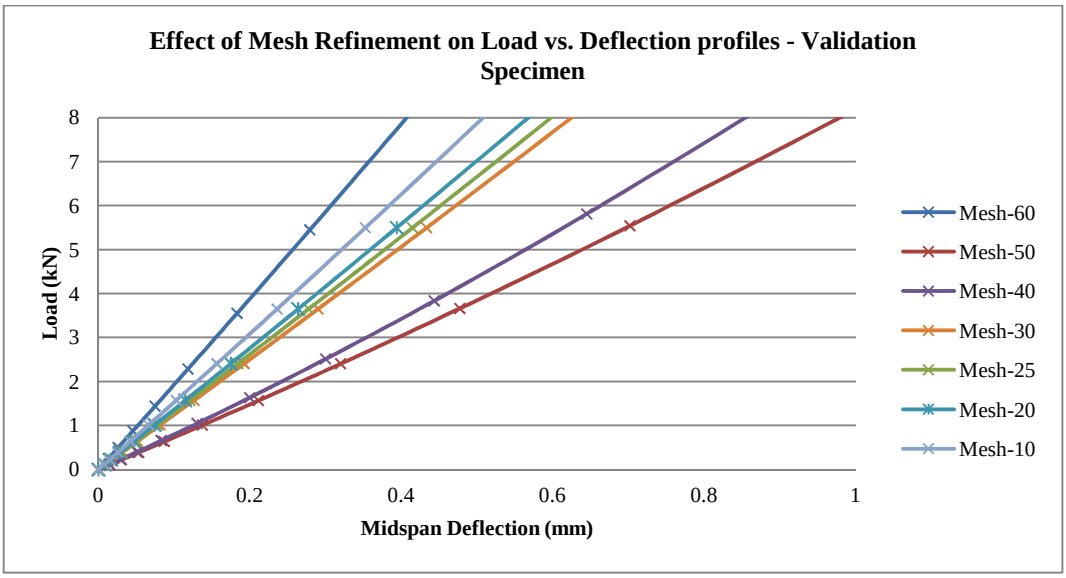

Figure 7.2- Effect of Mesh Refinement on Load-Deflection profiles: Validation specimens

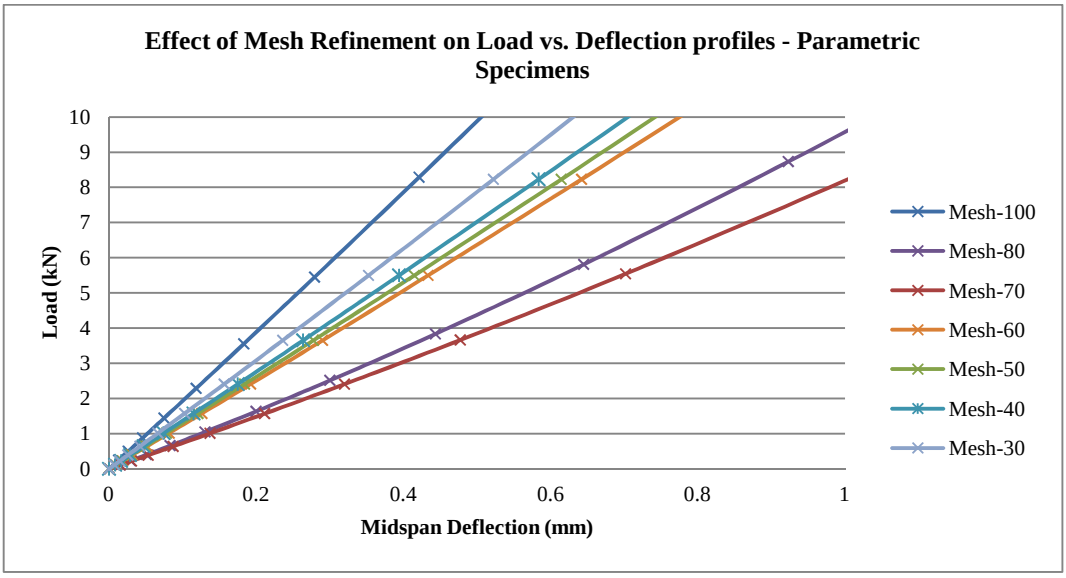

Figure 7.3- Effect of Mesh Refinement on Load-Deflection profiles: Parametric specimens.

From Figure 7.2, it is observed that the load-deflection profiles begin to converge at mesh sizes between 20mm and 30mm. Similarly, for the parametric specimens, the load-deflection profiles converge at mesh sizes between 30mm and 70mm. The results significantly deviate from this trend at larger mesh sizes.

Thus, mesh sizes of 25 mm and 50 mm were deemed to be suitable for the FE analysis of the validation and parametric specimens respectively.

7.2.1.4 Material Properties

A. Concrete Modelling

The two main approaches offered by ABAQUS for predicting concrete behaviour are the Concrete Damage Plasticity (CDP) model and the smeared crack model. The CDP model is used to simulate the behaviour of twinwall test specimens since it has higher potential for convergence as compared to the smeared crack model (Obaidat et al., 2010). This model uses concepts of isotropic damaged elasticity in combination with isotropic tensile and compressive plasticity to represent the inelastic behaviour of concrete. The CDP model is used for parametric study for the twinwall test specimens since it has higher potential for convergence as compared to the smeared crack model.

The two main modes of failure in the CDP model are tensile cracking and compressive crushing. Under uni-axial tension the stress–strain response follows a linear elastic relationship until the failure stress, σ_{to} is reached. The failure stress corresponds to the

onset of micro-cracking in the concrete material. Beyond the failure stress the formation of micro-cracks is represented with a softening stress–strain response.

Figure 7.4 shows a modified tension stiffening model developed by Wahalathantri et al (2011). This has been used in the FE idealisation of the twinwall panels as shown in Figure 7.5. The tensile stress was derived from Table 3.1 of EC2 and is determined as 3.2 N/mm^2.

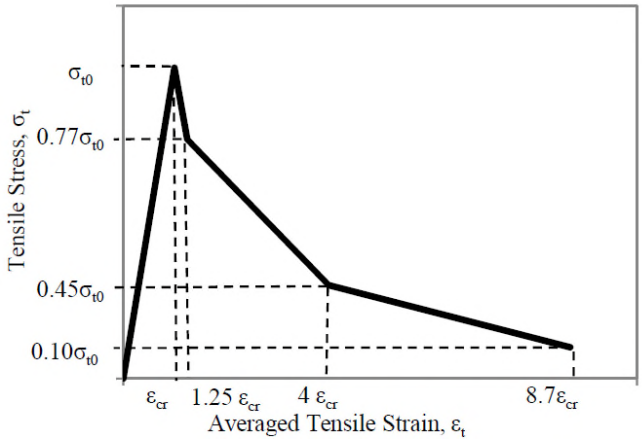

Figure 7.4- Modified tension stiffening model (Wahalathantri et al, 2011)

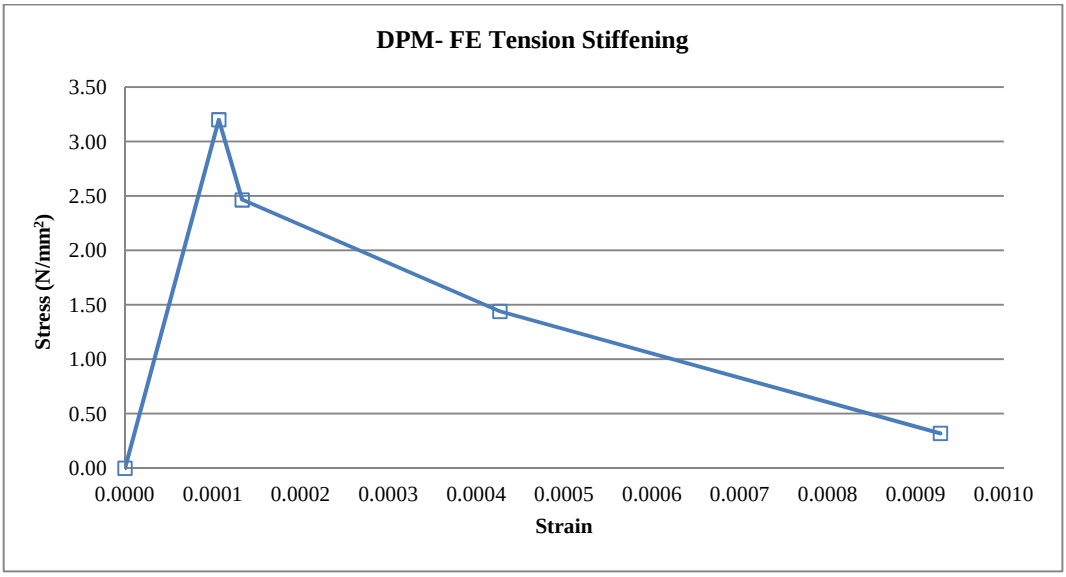

Figure 7.5 - FE Tension stiffening model

Under uniaxial compression the response is linear until the value of initial yield, σ_{co}. In the plastic regime the response is typically characterised by stress hardening followed by strain softening beyond the ultimate stress, σ_{cu} (Abaqus User Manual, 2010). The response of the concrete model under compression is shown in Figure 7.6.

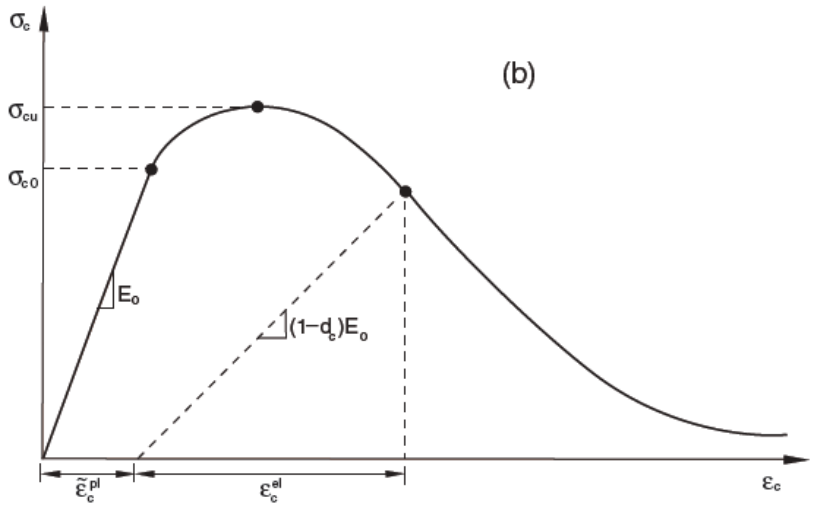

Figure 7.6 - Response of concrete to uniaxial loading in compression (Abaqus User Manual, 2011, Figure 22.6.3–1)

The curve defining the stress-strain behaviour of concrete in uniaxial compression was determined in accordance with Equation 3.14 of Eurocode 2 shown below:

$$\frac{\boldsymbol{\sigma_c}}{\boldsymbol{f_{cm}}} = \frac{\boldsymbol{k\eta - \eta^2}}{\boldsymbol{1 + (k - 2)\eta}}$$

where,

- σ_c = compressive stress in the concrete;
- f_{cm} = mean compressive strength at 28 days according to Table 3.1 (EC2)
- $\eta = \varepsilon_c/\varepsilon_{c1}$ where,

ε_c is the compressive strain in the concrete and ε_{c1} is the strain in the concrete at the peak stress f_c, usually considered to be 0.002

- $k = 1.05\ E_{cm}\ \frac{\varepsilon_{c1}}{f_{cm}}$ where,

  According to Eurocode 2, the ultimate strain (ε_{c1}) for concrete compressive strength of 12-50 N/mm^2 can be taken as 0.0035.

The compressive stress-strain profile used for the FE model is shown in Figure 7.7.

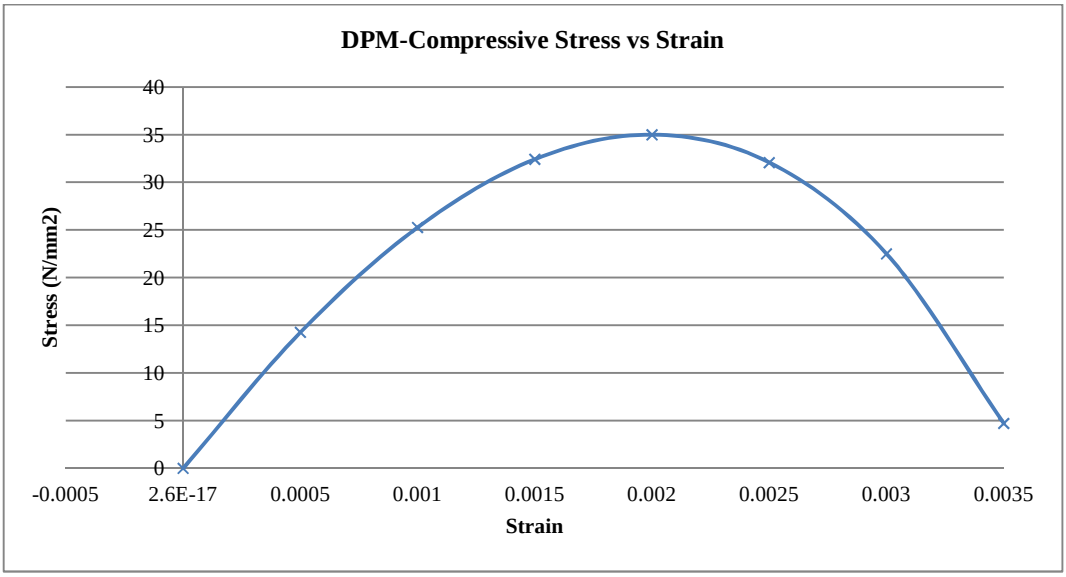

Figure 7.7- DPM Compressive Stress-Strain profile

The plastic damage model requires the values of elastic modulus, Poisson's ratio, the plastic damage parameters and descriptions of compressive strength and tensile behaviour. The dilation angle was assumed to be 38^o and the Poisson's ratio for concrete taken as 0.20 as per the recommendations of the CEB-FIP- Model Code 1990. The CDP model also requires other material parameters including the flow potential eccentricity, the ratio of the initial equibiaxial to the initial uniaxial stress, the ratio of the second stress invariant on tensile meridian and the viscosity parameter. These material properties are set to default values provided by Abaqus. Table 7.3 summarises

the values of other plastic damage parameters recommended by the Abaqus 6.10 user manual.

CDP Parameters	Values
Flow potential eccentricity (m)	0.1
Initial equibiaxial/initial uniaxial (σ_{c0} /σ_{b0})	1.16
Ratio of second stress invariant on tensile meridian (kc)	0.67
Viscosity Parameter (μ)	0

Table 7.3- CDP Material Parameters

The fracture energy is another important factor in the CDP model. Since the value of the fracture energy, G_F, was not determined experimentally, this value was determined using the CEB-FIP Model Code 1990. The fracture energy is primarily dependent on the compressive strength and the maximum size of the aggregate used in the concrete as follows:

$$G_F = (0.0469\, d_a^2 - 0.5\, d_a + 26) \times (f_c/10)^{0.7}$$

where,

- d_a is the maximum aggregate size = 4 mm
- f_c is compressive strength of concrete = 35 N/mm^2

B. Steel Modelling

The steel reinforcement responds as a linear material up to the initial yield stress. The steel for the finite element models is assumed to be an elastic-perfectly plastic material in both tension and compression. The elastic modulus, E_s was taken as 200 000 N/mm^2; the yield stress, f_y of the steel was taken as the experimentally determined value of 280 N/mm^2 for the validation tests; the yield stress, f_y of the steel was taken as the typical

design value of 500 N/mm^2 for the parametric FE tests and the Poisson's ratio was assumed to be 0.30.

7.2.1.5 Constraints and Interactions

The steel reinforcement and lattice girders were assumed to be fully embedded in the concrete biscuits. At the core and biscuit interaction, the friction between the biscuit faces was modelled as 0.6 which corresponds to the recommended in Clause 6.3.5 of EC2 for a smooth (as-cast) surface**.**

7.2.1.6 Loading and Boundary Conditions

Four point bending tests were simulated in the FE model. For the validation of the FE model, the point of application of the load corresponded with that of the experimental flexural tests discussed in Chapters 5 and 6. For the FE specimens summarised in Table 7.1, the load application was taken as being 750 mm from the edge of the slab

The supports, i.e. boundary conditions were assumed to be pinned. For validation tests, the supports corresponded with that of the experimental flexural tests discussed in Chapters 5 and 6. For the parametric tests, the supports were applied to the outer edge of the bottom biscuits of the specimens.

7.2.1.7 Observations

The results obtained from the FE model were discussed in terms of five main parameters:

1. *Failure Load:* The failure load was taken as the maximum load recorded from the FE analysis.

2. *Midspan Deflection:* The midspan deflections of the test specimens in bottom biscuits at failure were measured. Nodes corresponding to the midspan of the biscuits were chosen and the average value of the deflections recorded was calculated.

3. *Load-Deflection Profiles:* The load recorded was plotted against the average midspan deflection recorded in the bottom biscuit.

4. *Variation of Concrete Strain across Depth (Parametric Tests only):* The variation of the strain in the concrete across the depth of the FE specimens was observed. Nodes corresponding to various locations across the depth of the specimens at midspan were chosen and the strains in the concrete at these locations were recorded. The depth of the specimen was plotted against the strains observed at failure.

5. *General Behaviour:* The general behaviour of the specimens under the loading was observed in terms of the maximum bottom deflection at midspan and the stresses in the steel reinforcement and lattice bars.

7.3 Validation Tests Results

The results for the validation specimens are discussed in terms of the (1) load and midspan deflection at failure, (2) load-deflection profile, (3) general behaviour of specimens.

7.3.1 Load and Midspan Deflection at Failure

The experimental vertical deflections in bottom biscuit at midspan were compared with those obtained from the FE analysis. It was ensured that the measurements of the vertical and lateral deflections in the FE model corresponded with the same locations adopted in the experiment.

7.3.1.1 Results

A comparison of the load and deflection at failure from the experimental tests and FE analyses are presented and discussed below.

Type	Failure Load (kN)		% Difference
	Exp	FE	
A2/3	2.45	2.72	10.09%
B2/3	5.40	5.86	7.83%
C2/3	11.40	12.15	6.21%
D2/3	11.20	11.86	5.57%
E2/3	12.60	13.57	7.14%

Table 7.4 – Failure Load: Types A3-E3

Type	Deflection at Failure (mm)		% Difference
	Exp	FE	
A2/3	14.52	11.16	-30.16%
B2/3	4.63	3.53	-31.14%
C2/3	4.43	3.86	-14.77%
D2/3	12.70	10.96	-15.88%
E2/3	5.07	5.03	-0.68%

Table 7.5 – Deflection at Failure: Types A3-E3

7.3.1.2 Discussion

Results from Table 7.4 shows that the FE failure loads are higher than the experimental failure loads for all specimen types with a maximum difference of 10.09% (in A2/3) between the experimental and FE specimens. On the other hand, the midspan deflections at failure for all specimen types are lower than those obtained experimentally. This indicates that the FE test specimens are stiffer than the experimental specimens.

7.3.2 Load- Deflection Profile

The experimental midspan deflections in the bottom biscuit were compared with those obtained from the FE analysis at each load increment.

7.3.2.1 Results

Figure 7.8 shows that variation of the vertical deflections in the bottom biscuit at midspan for types A2-E2 (Experiment) and A3-E3 (FE) at various loads.

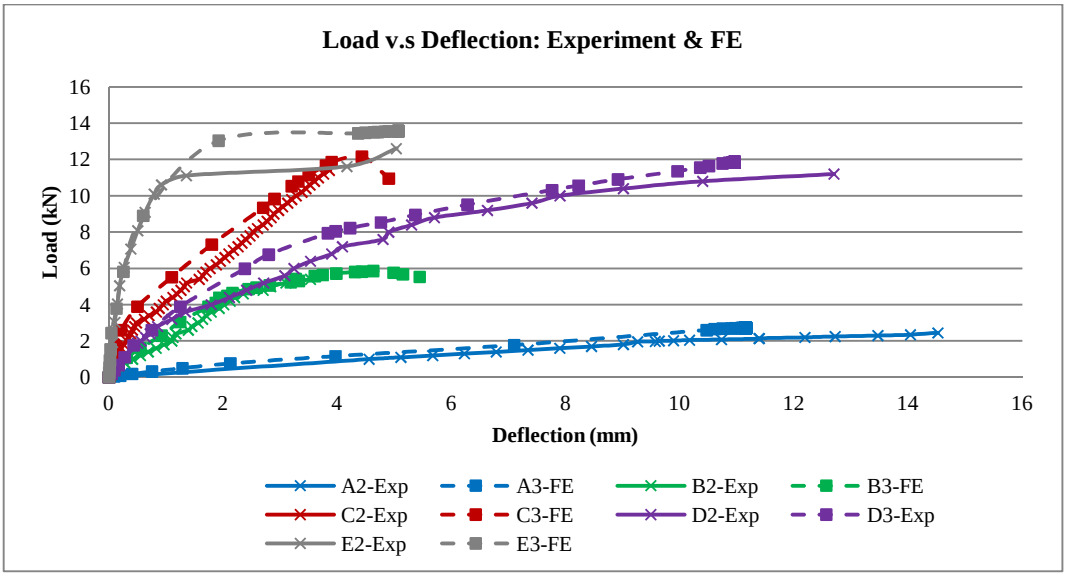

Figure 7.8 - Load-Deflection profile: Experiment & FE

7.3.2.2 Discussion

From Figure 7.8, it can be seen that the load-deflection profiles for the experimental and the FE specimens follow a similar trend. Results also show that in all cases, the FE specimens are stiffer than the experimental specimens. This is because that FE model assumes perfect bond between all the components and therefore does not allow for the imperfections that may occur due to the casting and testing of the test specimens during the experiment.

Thus, the load-deflection profiles confirm that the FE model provides an effective tool to accurately predict the behaviour of the twinwall specimen under four point bending tests.

7.3.3 Behaviour at Failure

The behaviour of the FE specimen at failure is presented in respect of the vertical deflection and stress in steel lattice bars for types A3-E3 specimens.

7.3.3.1 Results

The regions highlighted in red represent the areas of maximum deflection (vertical deflection at failure) and yielding og the steel (stresses in lattice bars).

Type	Vertical Deflection at Failure	Stresses in Lattice Bars
A3	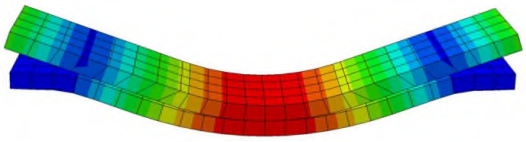	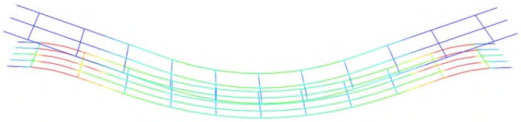
B3		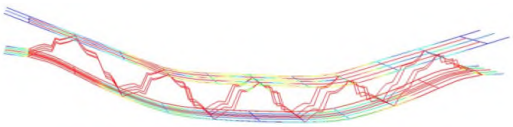
C3	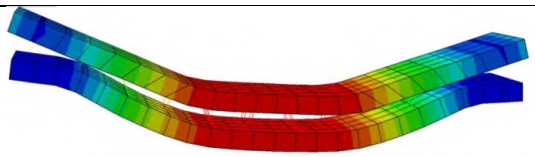	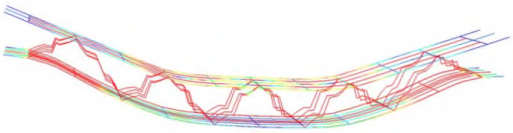
D3	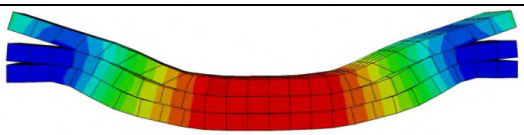	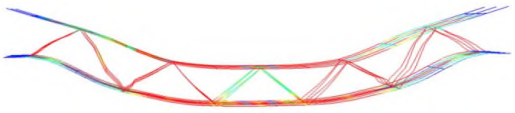
E3		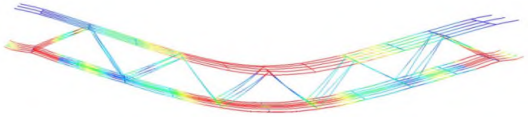

Table 7.6 – General Behaviour: Types A3-E3

7.3.3.2 Discussion

From Table 7.6, it is observed that the deformed shapes for all specimens are similar with maximum deflection (highlighted in red) occurring midspan. This is a typical behaviour of specimens subject to four point bending tests. A similar behaviour was also observed during the experimental tests discussed in Chapter 6.

The stresses observed in the lattice bars also provide valuable information on the mode of failure of the specimens. In type A3, the top and bottom steel have not yielded (in red). Hence, the mode of failure of type A3 is due to concrete failure. This was observed during the experimental tests for type A2 where the specimen failure due to sudden cracking at midspan.

For types B3-D3, most of the biscuit reinforcement as well as the lattice diagonal (dowel) bars yield. This indicates that the lattice bars have a significant role in transferring the forces from the top to the bottom biscuit in twinwalls. This also confirms the experimental observations where failure occurred due to a combination of bending and yielding of the diagonal dowel bars.

In type E3, the top and bottom biscuit reinforcement yield while the diagonal bars do not reach the yield stress. This is an important observation since it provides additional information on the behaviour of the test specimen which could not be captured during the experimental tests due to limitations and constraints of the testing environment. Hence, as well as closely replicating the behaviour of the twinwall specimens, the FE

model developed is a useful tool in providing additional information on the behaviour of twinwalls under various loading conditions.

It can therefore be concluded that the FE model developed is suitable to emulate the behaviour of twinwall test specimens.

7.4 Parametric Tests Results

7.4.1 Effect of Dowel Bar Diameter

As mentioned previously, the diameters of the dowel bar were varied to 4mm, 6mm, 8mm, 10mm, 12mm, 16mm and 20mm. Results are discussed in terms of the load and midspan deflection at failure, load-deflection profile and variation of concrete strain at midspan.

7.4.1.1 Load and Deflection at Failure

A. Results

The load and deflection recorded at failure for types FA-1 to FA-7 are summarised in Table 7.7. The variation of the load and deflection at failure with the dowel bar diameters is also presented in Figures 7.9-7.10.

Type	Dowel Bar Diameter (mm)	Failure Load (kN)	Failure Deflection (mm)
FA-1	4	192.44	8.07
FA-2	6	198.90	6.13
FA-3	8	207.63	5.17
FA-4	10	208.72	4.77
FA-5	12	210.31	4.51
FA-6	16	211.02	4.19
FA-7	20	211.15	4.40

Table 7.7 – Load and Deflection at Failure: Dowel Bar Diameter

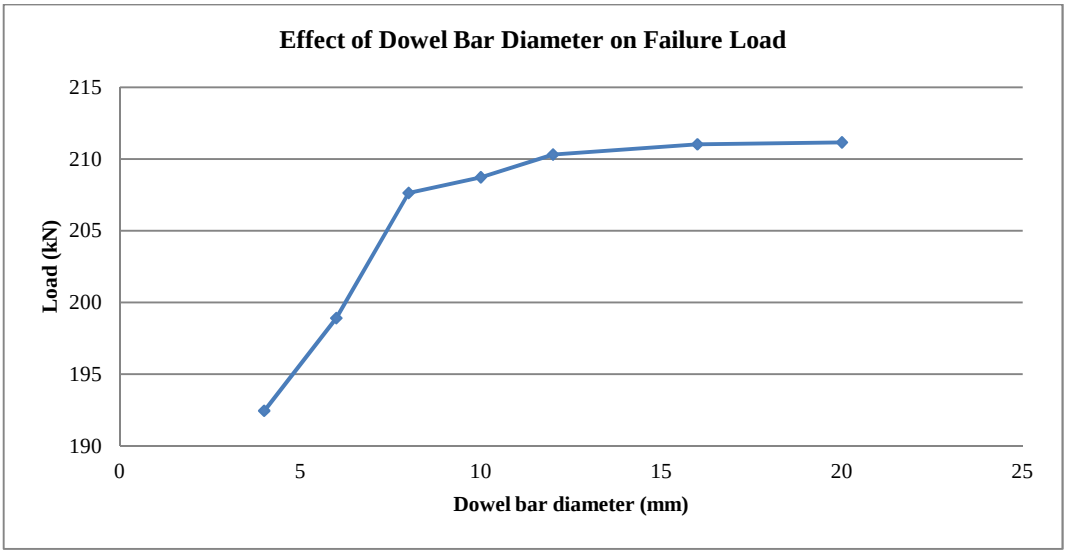

Figure 7.9 - Effect of Dowel Bar Diameter on Failure Load

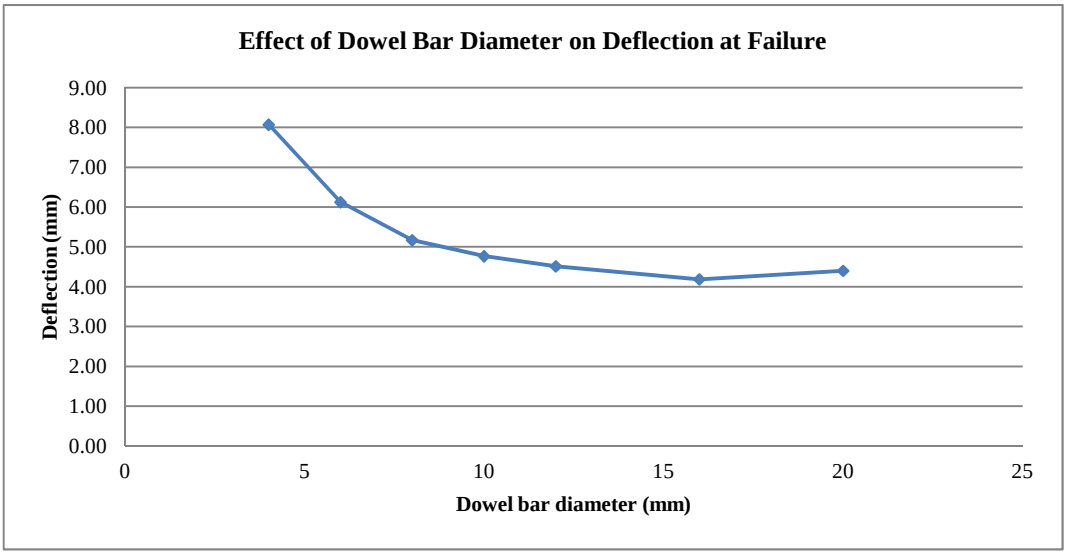

Figure 7.10 - Effect of Dowel Bar Diameter on Deflection at Failure

B. Discussion

From Table 7.7, it can be observed that as the dowel bar diameter increases, the failure load also increases. Figure 7.9 shows that this increase is non-linear. It can be seen that the failure load increases significantly in the 4mm – 8mm diameter region. In the 8mm-12mm region, the increase in failure load begins to decline and beyond the 12 mm diameter, there is a small change in the failure load.

It can therefore be concluded that increasing the diameter of the dowel bar beyond 12mm does not lead to significant increases in overall strength of the twinwall specimens. Hence, the dowel bar diameter in twinwalls should be limited to a maximum of 12 mm for optimum structural performance and efficiency.

Table 7.7 also shows that as the dowel bar diameter increases, the deflection at failure decreases. This is expected since an increase in the bar diameter leads to a rise in the overall stiffness of the test specimens which reduces the deflection. From Figure 7.10, it is observed that the deflection reduces non-linearly as the bar diameter increases. It is also noted that at dowel bar diameters beyond 16 mm, there is almost no change in the deflection at midspan. This indicates that when greater bar diameters are used, the concrete fails by cracking prior to the steel. Hence, to ensure that twinwalls are designed as being under-reinforced for a more economical design, the diameter of the dowel bars must be limited to a maximum of 12 mm.

7.4.1.2 Load-Deflection Profile

A. Results

The deflection at midspan of the bottom biscuit at failure for types FA-1 to FA-7 are plotted for each load increment as shown in Figures 7.11.

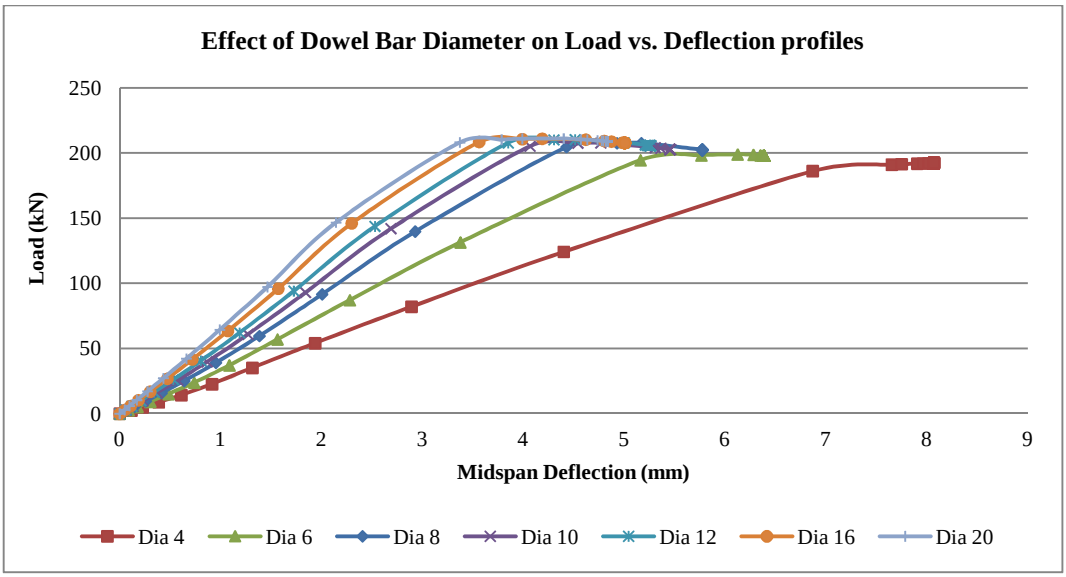

Figure 7.11 - Effect of Dowel Bar diameter on Load-Deflection profile

B. Discussion

From Figure 7.11, it can be seen that at smaller dowel bar diameters from 4mm and 6mm, the load-deflection profile is almost linear until failure. However, as the bar diameter increases, the load-deflection profiles seem to occur in three main stages. Initially, the deformations remain elastic up to around 50-55% of the total failure load. Beyond this stage, the specimens exhibit slightly non-linear behaviour. A few 'kinks'

are also observed in the load-deflection profiles which are representative of the formation of cracks in the bottom biscuits resulting in sudden increases in deformations.

The load-deflection profiles also show that when the bar diameter increases, the stiffness of the specimens increases. The increase in stiffness is more pronounced when the bar diameters increases from 4mm to 8mm. Thus, beyond bar diameters of 10 mm, the gain in stiffness begins to decrease. This must be considered in the design of twinwalls.

7.4.1.3 Variation of Concrete Strain

A. Results

The variations of the strain at failure along the depth of the concrete biscuits and core for types FA-1 to FA-7 are shown in Figure 7.12.

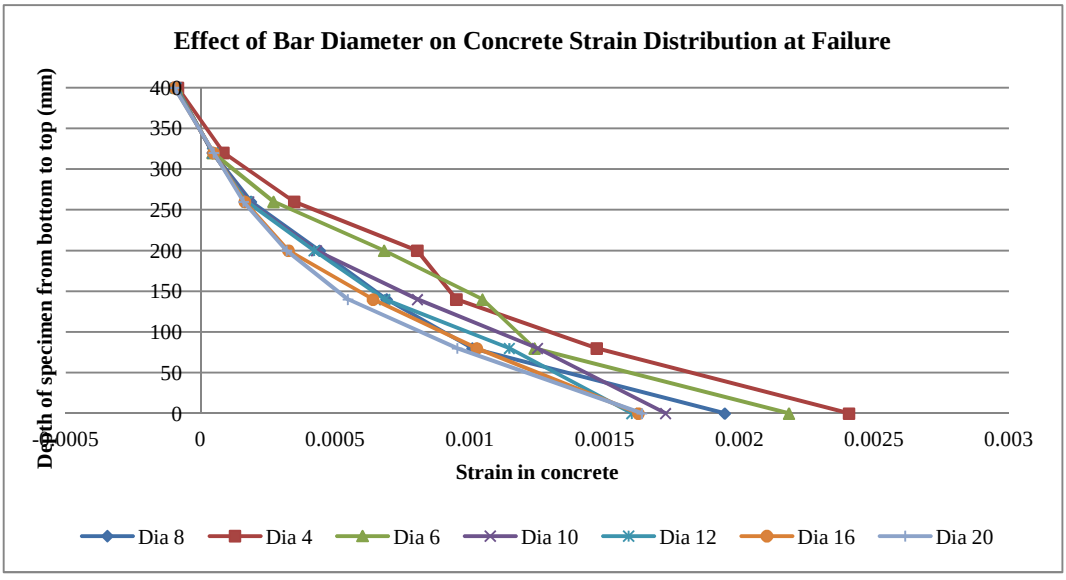

Figure 7.12 - Effect of Dowel Bar Diameter on Variation of Concrete Strain at Failure

B. Discussion

From Figure 7.12, it is observed that the neutral axis lies in the top biscuit at failure in all specimens. Additionally, the strain in the top biscuit is significantly less than that observed in the bottom biscuit. This confirms that more flexural cracks occur in the bottom biscuit resulting in an increase in the strain. The results therefore suggest that the behaviour of the twinwall is very similar to that of a monolithic section, irrespective of the dowel bar diameter.

It is also noted that for smaller bar diameters below 8 mm, the variation of the strain along the depth of the specimen is non-uniform. As the bar diameter increases, the strain profile exhibits more uniformity. This indicates that the distribution of forces between the top and bottom biscuit and thus, the degree of composite action increases as the dowel bar diameter increases. Hence, dowel bar diameters of 8 mm or more is recommended to maximise the degree of composite action in twinwalls.

7.4.1.4 Behaviour at Failure

A. Results

The behaviour of the FE specimen at failure is presented in respect of the vertical deflection and stress in steel lattice bars. The regions highlighted in red represent the areas of maximum deflection (vertical deflection at failure) and yielding of the steel (stresses in lattice bars).

Dowel Bar Diameter, Double Truss		
Type	**Vertical Deflection at Failure**	**Stresses in Lattice Bars**
FA-1 (Dia 4)	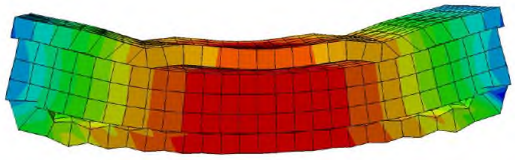	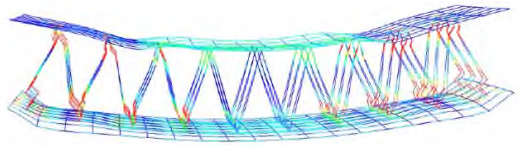
FA-2 (Dia 6)	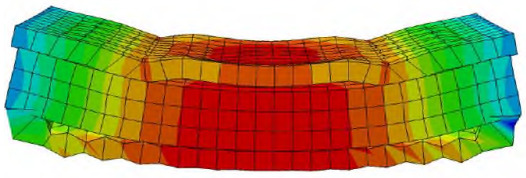	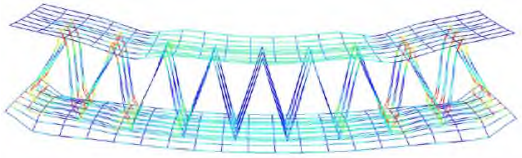
FA-3 (Dia 8)	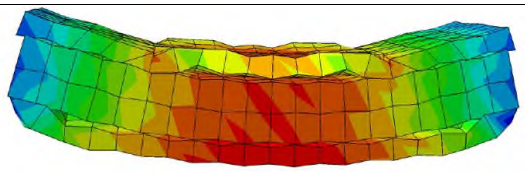	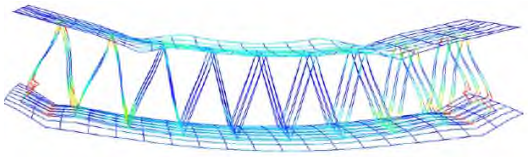
FA-4 (Dia 10)	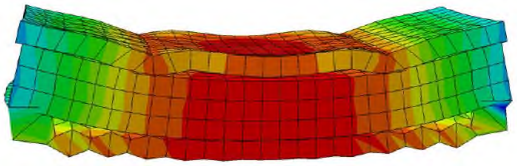	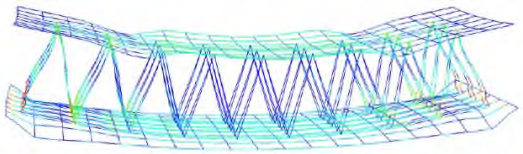
FA-5 (Dia 12)	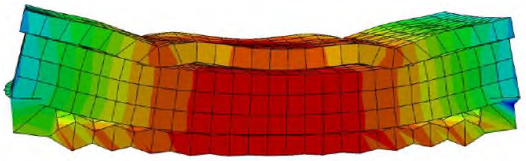	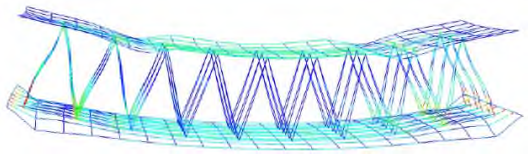
FA-6 (Dia 16)	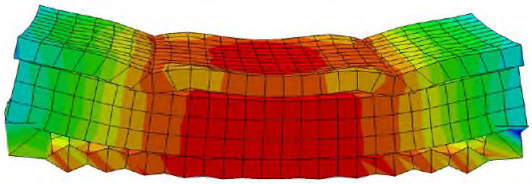	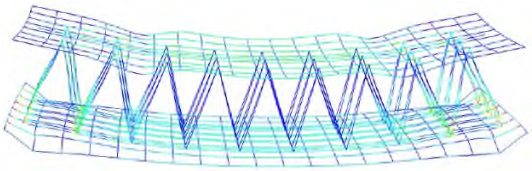
FA-7 (Dia 20)	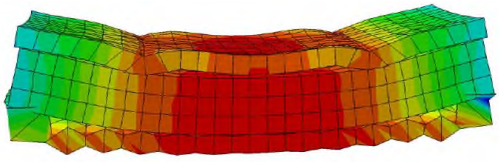	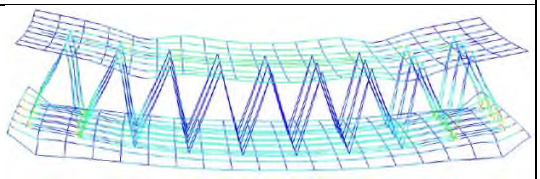

Table 7.8 – General Behaviour: Dowel Bar Diameter – Type FA-1 to FA-7

B. Discussion

From Table 7.8, it is observed that the deformed shapes for all specimens are similar with maximum deflection (highlighted in red) occurring midspan. This is a typical behaviour of specimens subject to four point bending tests.

The deformed shapes of the specimens also show that slip occurs at the interfaces between the Inner Core and the top and bottom Biscuits. Results show that as the diameter of the lattice bar increases, slip at the concrete interfaces decreases.

The stresses in the lattice bars also provide valuable information on the behaviour of the test specimens. As the bar diameters increase, the number of dowel bars reaching their yield stress decreases. An interesting observation is that most of the dowel bars, irrespective of their diameters, do not reach their yield stress. This suggests that the failure of the specimens is not due to the yielding of the diagonal bars, i.e. dowel action. Thus, the failure mechanism of the test specimens may have been primarily due to the interface shear failure occurring at the biscuit interface and the flexural failure. Hence, the failure mode does not seem to be influenced by the dowel bar diameter.

7.4.2 Type of Connector: Single truss v/s. Double truss

The diameters of the dowel bars, were varied to 4mm, 6mm, 8mm, 10mm, 12mm, 16mm and 20mm in the single truss and the results were compared with those obtained for the double truss. Results are discussed in terms of the load and midspan deflection at failure, load-deflection profile and variation of concrete strain at midspan.

7.4.2.1 Load and Deflection at Failure

A. Results

The load and deflection recorded at failure for types FB-1 to FB-7 (single truss) and FA-1 to FA-7 (double truss) are summarised in Table 7.9. The variation of the load and deflection at failure with the dowel bar diameters for both the single and double trusses is also presented in Figures 7.13-7.14

Dowel Bar Diameter	Type	Single Truss Connector		Type	Double Truss	
		Failure	Maximum		Failure	Maximum
4	FB-1	184.13	7.69	FA-1	192.44	8.07
6	FB-2	194.98	5.71	FA-2	198.90	6.13
8	FB-3	203.48	4.73	FA-3	207.63	5.17
10	FB-4	205.03	4.40	FA-4	208.72	4.77
12	FB-5	206.68	4.25	FA-5	210.31	4.51
16	FB-6	206.77	4.03	FA-6	211.02	4.19
20	FB-7	207.65	3.98	FA-7	211.15	4.40

Table 7.9 – Load and Deflection at Failure: Connector Type

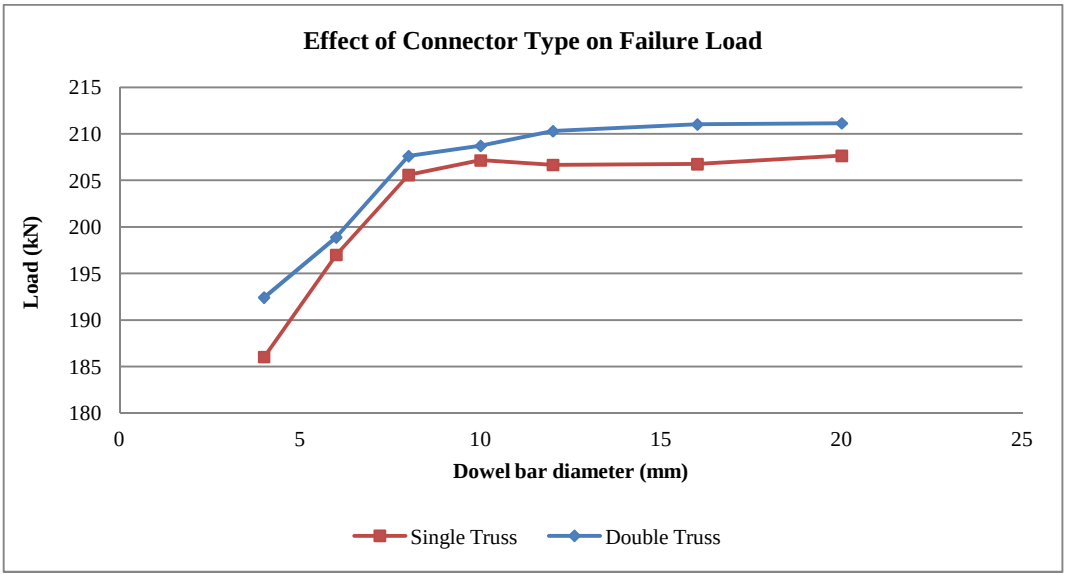

Figure 7.13 - Effect of Connector Type on Failure Load

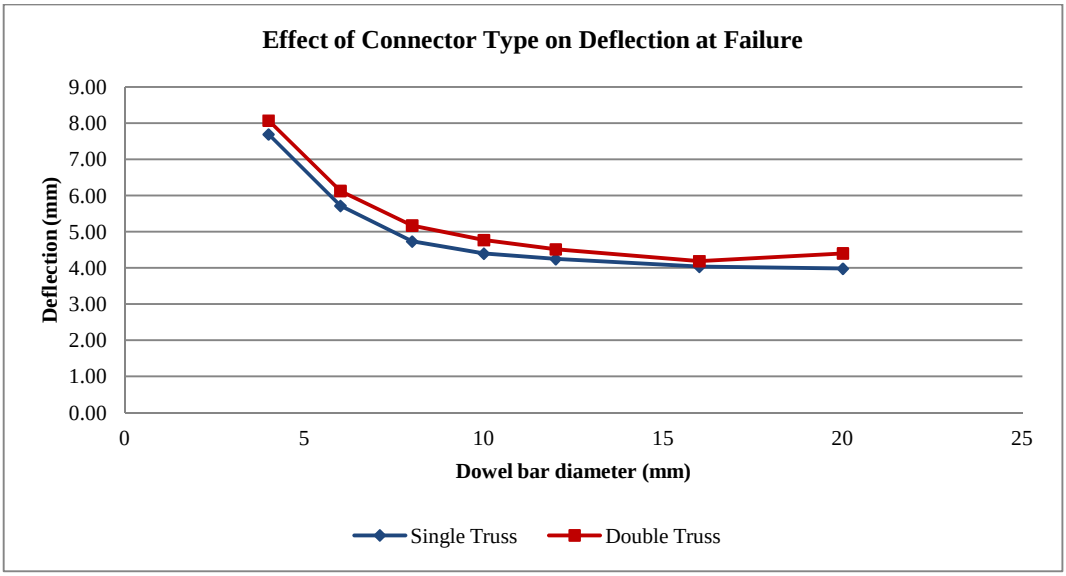

Figure 7.14 - Effect of Connector Type on Deflection at Failure

B. Discussion

From Table 7.9, it can be observed that as the dowel bar diameter increases, the failure load also increases irrespective of the type of connector used. Figure 7.13 shows that this increase is non-linear for both connectors. Results indicate that the failure load increases significantly in the 4mm-8mm diameter region. In the 8mm-12mm region, the increase in failure load begins to decline and beyond the 12 mm diameter, there is a small change in the failure load.

It is also noted that the failure loads for the single truss connectors are less than those of the double truss connectors for all dowel bar diameters. The difference between the failure loads of the single and double trusses is small for dowel bar diameters up to 12mm. Beyond bar diameters of 12mm, the difference between the failure loads for both connector types is more significant. Thus, the double truss is more effective at transferring the forces in twinwalls in comparison with the single truss.

Table 7.9 also shows that as the dowel bar diameter increases, the deflection at failure decreases for both connector types. This is expected since an increase in the bar diameter leads to a rise in the overall stiffness of the test specimens which reduces the deflection. From Figure 7.14, it is observed that the deflection reduces non-linearly as the bar diameter increases. It is also noted that at dowel bar diameters beyond 16 mm, there is almost no change in the deflection at midspan. This indicates that when greater bar diameters are used, the concrete fails by cracking prior to the steel. Hence, to ensure that twinwalls are designed as being under-reinforced for a more economical design, the diameter of the dowel bars must be limited to a maximum of 12 mm.

The results also show that the deflections observed in the double truss are slightly less than those in the single truss. This confirms that the double truss lead to a slight increase in the stiffness of the test specimens and therefore lead to more composite action. It is therefore recommended that double trusses with a maximum dowel bar diameter of 12 mm should be used in twinwalls for optimum structural performance and efficiency.

7.4.2.2 Load-Deflection Profile

A. Results

The deflection at midspan of the bottom biscuit at failure for types FA-1 to FA-7 and FB-1 to FB-7 are plotted for each load increment as shown in Figures 7.15-7.16.

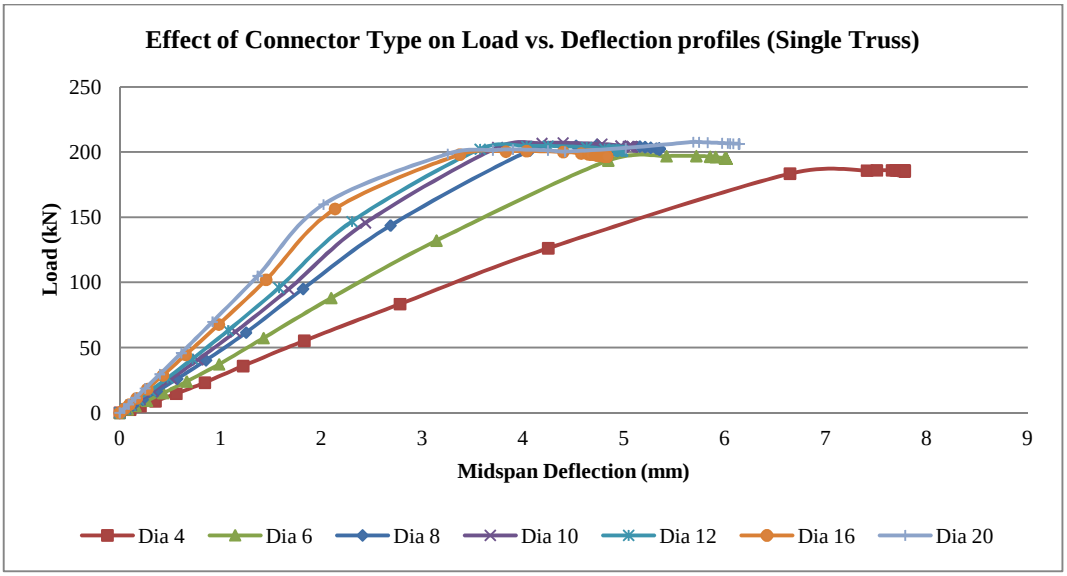

Figure 7.15 - Effect of Connector Type on Load-Deflection profiles: Single Truss

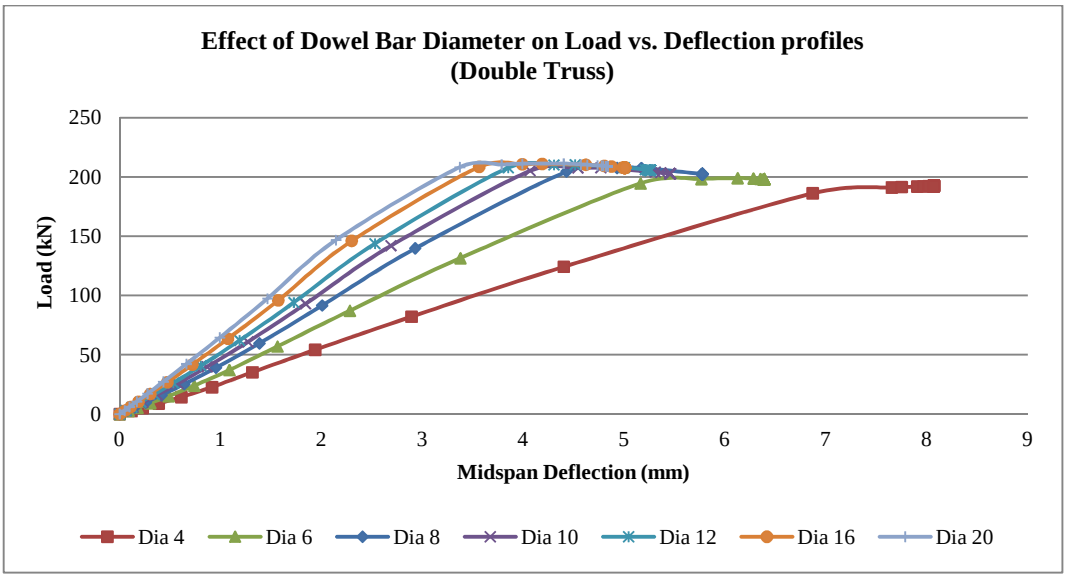

Figure 7.16 - Effect of Connector Type on Load-Deflection profiles: Double Truss

B. Discussion

From Figures 7.15-7.16, it is observed that the load-deflection profiles for the single and double trusses show similar trends. At smaller dowel bar diameters of 4mm and 6mm, the load-deflection profile is almost linear until failure. However, as the bar diameter increases, the load-deflection profiles seem to occur in three main stages.

Initially, the deformations remain elastic up to around 50-60% of the total failure load. Beyond this stage, the specimens exhibit slightly non-linear behaviour. A few ‘kinks’ are also observed in the load-deflection profiles which are representative of the formation of cracks in the bottom biscuits resulting in sudden increases in deformations.

The load-deflection profiles also show that when the bar diameter increases, the stiffness of the specimens increases irrespective of the type of connector used. The increase in stiffness is more pronounced when the bar diameters increases from 4mm to 8mm. Thus, beyond bar diameters of 10 mm, the gain in stiffness begins to decrease.

The behaviour of the single and double trusses is therefore very similar in terms of their deformations. Though the double trusses is slightly better at transferring forces from the top to the bottom biscuits, the use of single trusses also a viable option for use as shear connectors in twinwalls.

7.4.2.3 Variation of Concrete Strain

A. Results

The variations of the strain at failure along the depth of the concrete biscuits and core for the single and double trusses with varying diameters are shown in Figures 7.17-7.18. A comparison of the strains at failure between the single and double trusses is also shown in Figure 7.19.

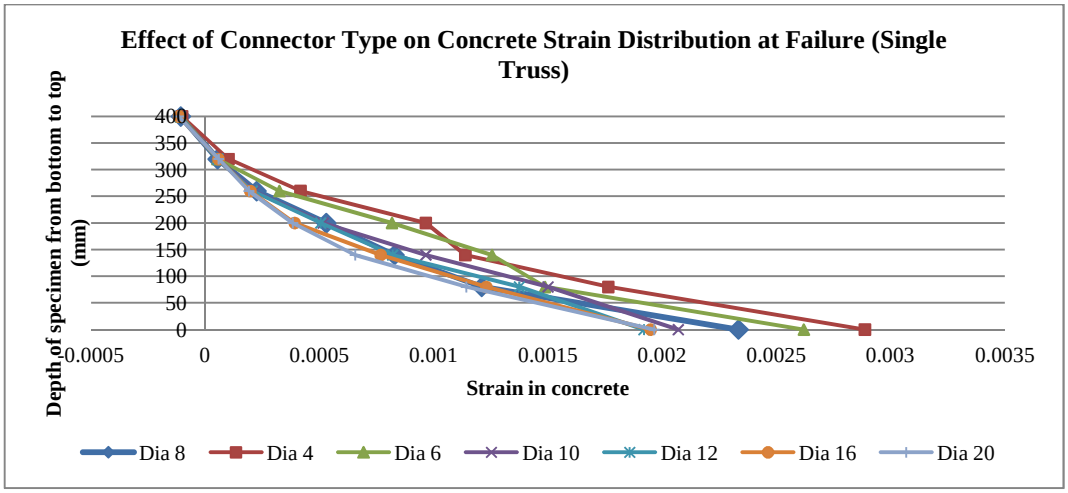

Figure 7.17 - Effect of Connector Type on Variation of Concrete Strain at Failure: Single Truss

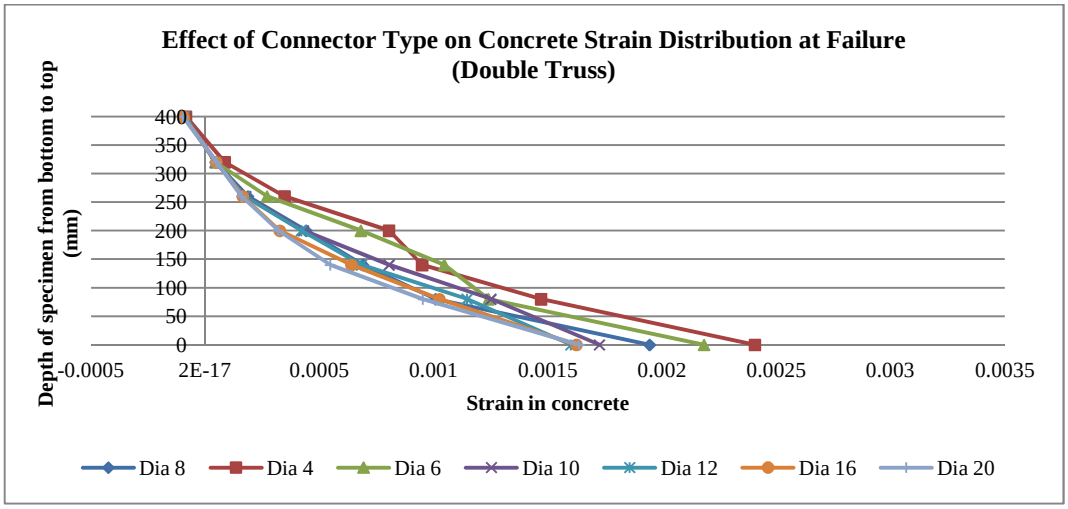

Figure 7.18 - Effect of Connector Type on Variation of Concrete Strain at Failure: Double Truss

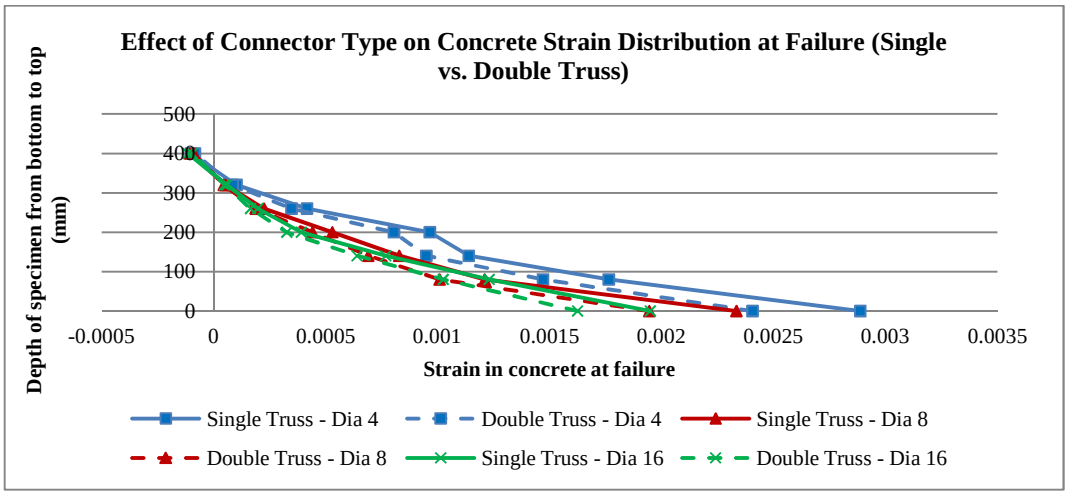

Figure 7.19 - Effect of Connector Type on Variation of Concrete Strain at Failure: Single vs. Double Truss

B. Discussion

From Figures 7.17-7.18, it is observed that the neutral axes for both the single and double trusses lie in the top biscuit at failure in all specimens. Additionally, the strain in the top biscuit is significantly less than that observed in the bottom biscuit. This confirms that more flexural cracks occur in the bottom biscuit resulting in an increase in the strain. The results therefore suggest that the behaviour of the twinwall is very similar to that of a monolithic section, irrespective of the dowel bar diameter.

For both connector types, for smaller bar diameters below 8 mm, the variation of the strain along the depth of the specimen is non-uniform. As the bar diameter increases, the strain profile exhibits more uniformity. This indicates that the distribution of forces between the top and bottom biscuit and thus, the degree of composite action increases as the dowel bar diameter increases. Hence, dowel bar diameters of 8 mm or more is recommended to maximise the degree of composite action in twinwalls.

Figure 7.19 shows that the strains developing in the single truss specimens at all dowel bar diameters are higher than those in double truss specimens. This confirms that the connector type affects the distribution of forces as well as the formation of the flexural cracks in the specimens. Thus, the single and double trusses seem to have an effect on the overall behaviour of the test specimens.

7.4.2.4 Behaviour at Failure

A. Results

The behaviour of the FE specimens at failure is presented in respect of the vertical deflection and stress in steel lattice bars. The regions highlighted in red represent the areas of maximum deflection (vertical deflection at failure) and yielding of the steel (stresses in lattice bars). The results for the double trusses were provided in Table 7.8 and those for the single trusses are given in Table 7.10 below.

Dowel Bar Diameter, Single Truss		
Type	**Vertical Deflection at Failure**	**Stresses in Lattice Bars**
FB-1 (Dia 4)	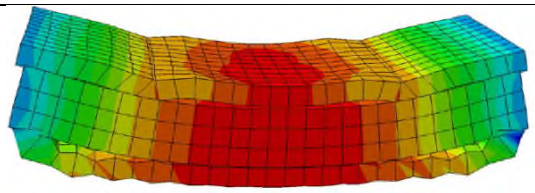	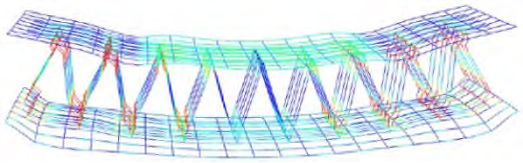
FB-2 (Dia 6)	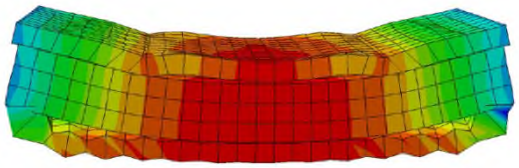	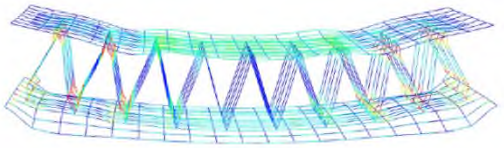
FB-3 (Dia 8)		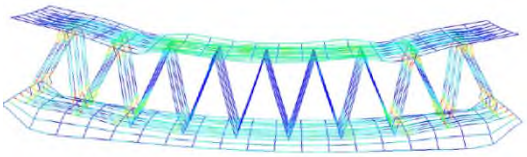
FB-4 (Dia 10)		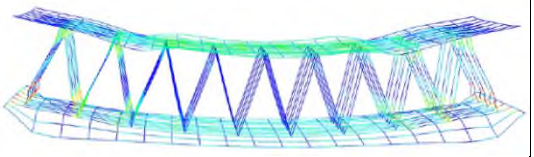

FB-5 (Dia 12)	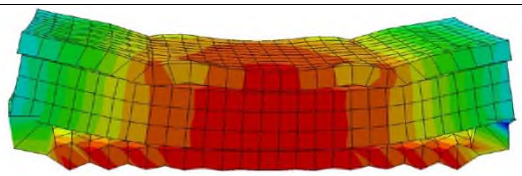	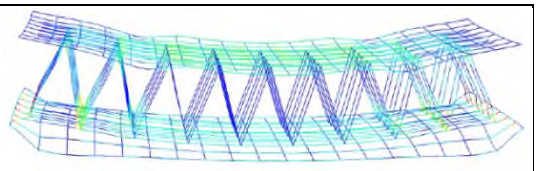
FB-6 (Dia 16)	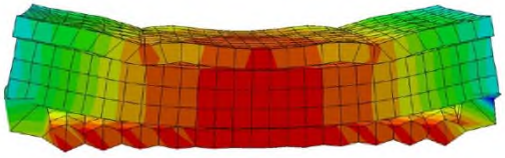	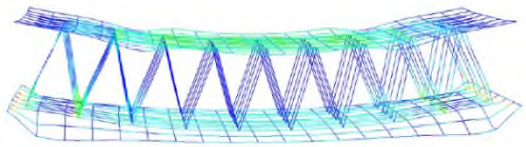
FB-7 (Dia 20)	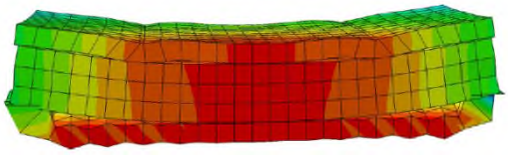	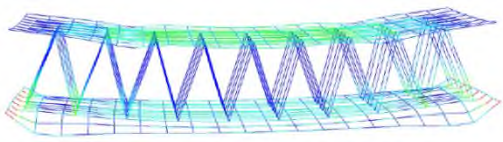

Table 7.10 – General Behaviour: Dowel Bar Diameter – Type FB-1 to FB-7

B. Discussion

From Table 7.10, it is observed that the deformed shapes for all specimens are similar with maximum deflection (highlighted in red) occurring midspan. This is a typical behaviour of specimens subject to four point bending tests.

The deformed shapes of the specimens also show that slip occurs at the interfaces between the core and the top and bottom biscuits. Results show that as the diameter of the lattice bar increases, slip at the concrete interfaces decreases.

The stresses in the lattice bar show that as the bar diameters increase, the number of dowel bars reaching their yield stress decreases. An interesting observation is that most of the dowel bars, irrespective of their diameters, do not reach their yield stress. This suggests that the failure of the specimens is not due to the yielding of the diagonal bars,

i.e. dowel action. Thus, the failure mechanism of the test specimens may have been primarily due to the interface shear failure occurring at the biscuit interface and the flexural failure of the test specimen.

The behaviour of both the single and double trusses is similar in terms of their deformations and steel stresses. Hence, it is recommended that further research is carried out on the potential use of single trusses in lieu of double trusses in twinwall applications.

7.4.3 Thickness of Twinwall

The overall thickness of the twinwall was varied in terms of the height of the lattice girder only. The lattice heights were varied to 320mm, 280mm, 240mm, 200mm and 160mm resulting in overall twinwall thicknesses of 400mm, 360mm, 320mm, 280mm and 240mm respectively. Results are discussed in terms of the load and midspan deflection at failure, load-deflection profile and variation of concrete strain at midspan.

7.4.3.1 Load and Deflection at Failure

A. Results

The load and deflection recorded at failure for types FC-1 to FC-5 are summarised in Table 7.11. The variation of the load and deflection at failure with the thickness of the specimens is also presented in Figures 7.20-7.21.

Type	Girder Height	Thickness (mm)			Overall Thickness	Ultimate Strength	Maximum Deflection
		Biscuit 1	Core	Biscuit 2			
FC-1	320	80	240	80	400	207.63	5.17
FC-2	280	80	200	80	360	201.23	7.00
FC-3	240	80	160	80	320	187.17	10.45
FC-4	200	80	120	80	280	184.00	14.07
FC-5	160	80	80	80	240	155.40	18.49

Table 7.11 – Load and Deflection at Failure: Thickness

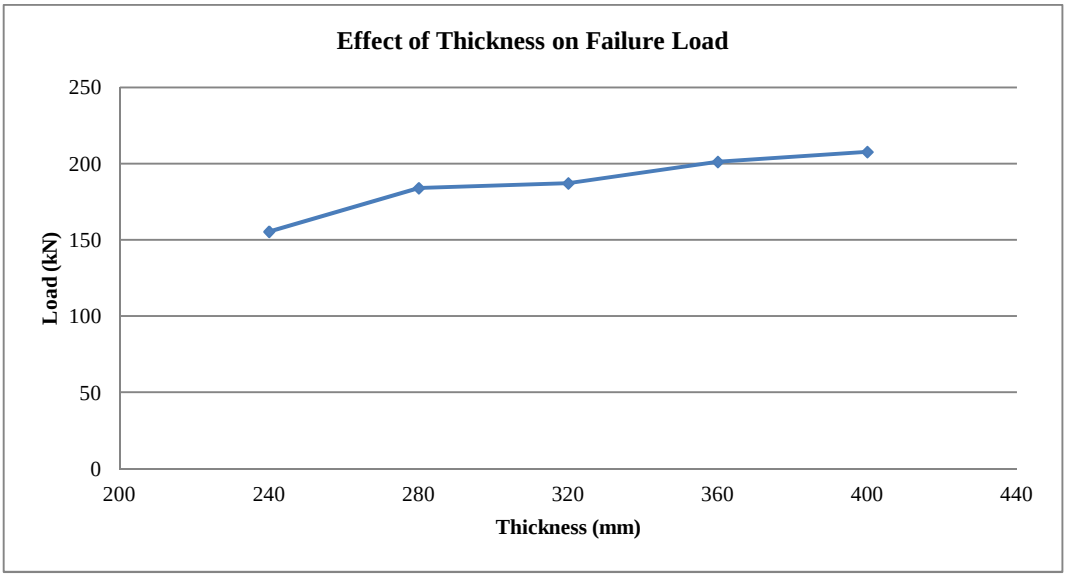

Figure 7.20 - Effect of Thickness on Failure Load

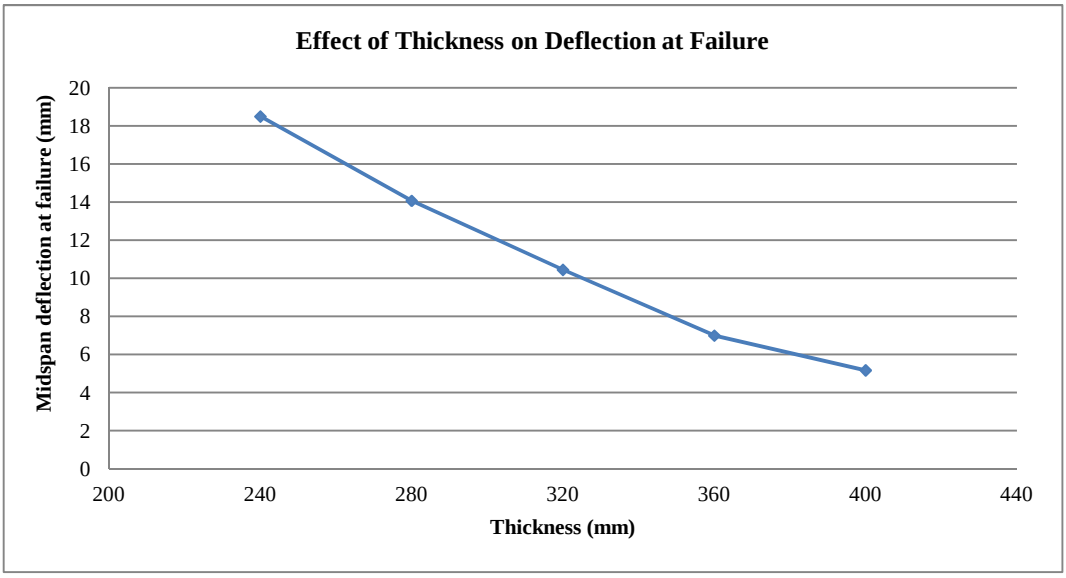

Figure 7.21 - Effect of Thickness on Deflection at Failure

B. Discussion

From Table 7.11, it can be observed that as the thickness of the specimen increases, the failure load also increases. Figure 7.20 shows that the increase in failure load is not linear. The maximum gain in failure load occurs when the thickness increases from 240mm to 280mm. From thicknesses of 280mm to 320mm, the gain in failure load/strength is almost constant and beyond thicknesses of 320mm, the strength of the specimens increases.

Table 7.11 also shows that as the thickness increases, the deflection at failure decreases. This is expected since an increase in the thickness leads to a rise in the overall stiffness of the test specimens which reduces the deflection. From Figure 7.21, it is observed that the deflection reduces almost linearly as the thickness increases.

It must be noted at smaller thicknesses of 240mm and 280mm, the deflection is quite high which may be concern when designing for serviceability limit state. Thus, thicknesses of 240mm and 280mm may not be suitable for use in water retaining structures where deflection and cracking are paramount to design.

7.4.3.2 Load-Deflection Profile

A. Results

The deflection at midspan of the bottom biscuit at failure for types FC-1 to FC-5 are plotted for each load increment as shown in Figures 7.22.

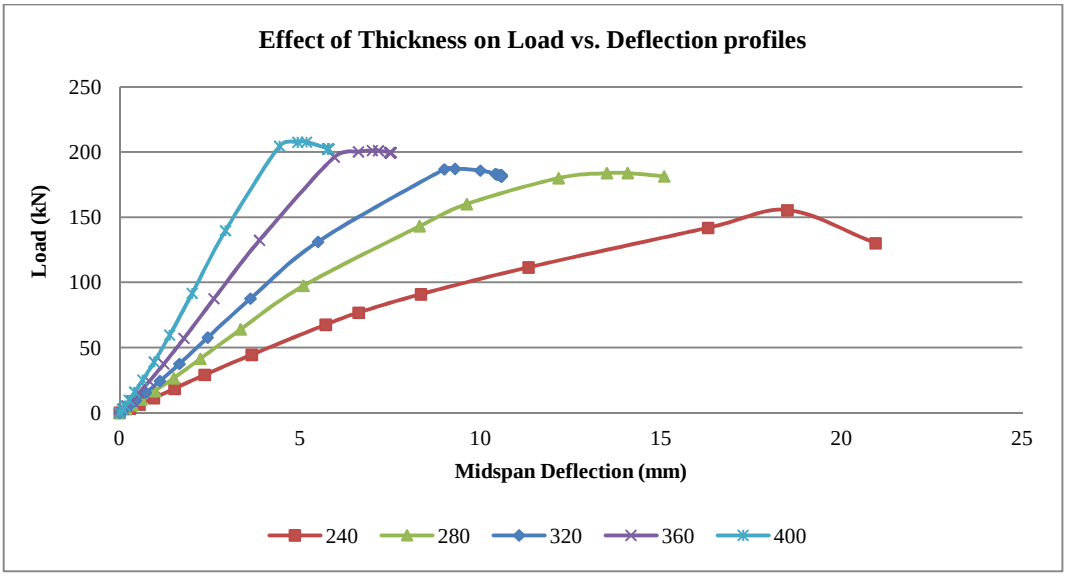

Figure 7.22 - Effect of Thickness on Load-Deflection profiles

B. Discussion

From Figure 7.22, it can be seen that the load-deflection profiles are similar for all thicknesses. Initially, the deformations remain elastic up to around 50-60% of the total failure load. Beyond this stage, the specimens exhibit slightly non-linear behaviour. This behaviour is more noticeable for smaller thicknesses which suggest that more diagonal bars are mobilised and therefore yield, resulting in a non-linear profile.

The load-deflection profiles also show that when the thickness increases, the stiffness of the specimens increases. The increase in stiffness seems to be rather equal for all thicknesses which suggest that an almost linear relationship exists between the thickness and stiffness.

7.4.3.3 Variation of Concrete Strain

A. Results

The variations of the strain at failure along the depth of the concrete biscuits and core for the single and double trusses with varying diameters are shown in Figure 7.23.

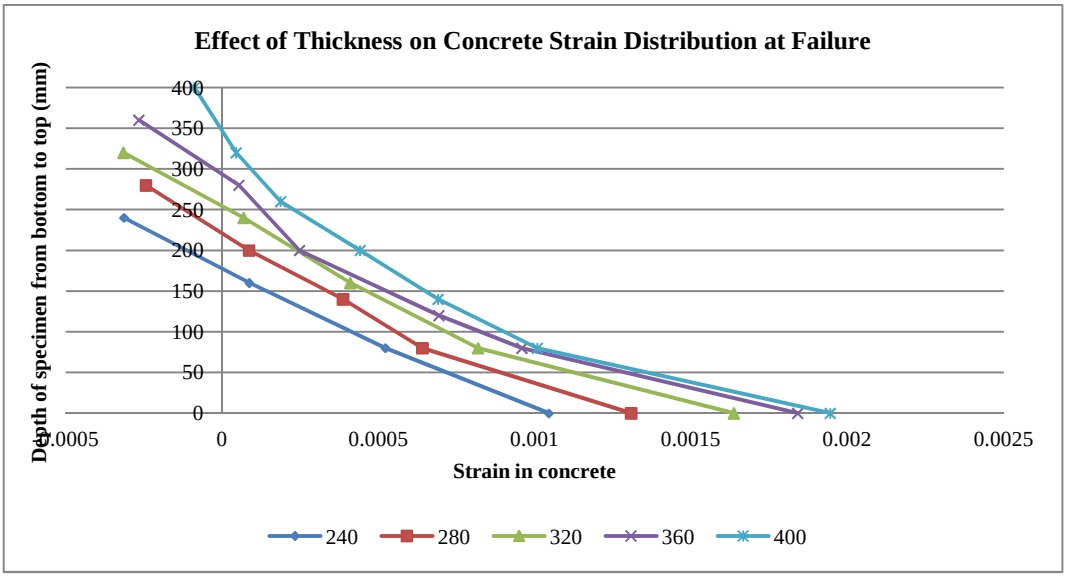

Figure 7.23 - Effect of Thickness on Variation of Concrete Strain at Failure

B. Discussion

From Figure 7.23, it is observed that the neutral axis lies in the top biscuit at failure in all specimens. Additionally, the strain in the top biscuit is significantly less than that observed in the bottom biscuit. This confirms that more flexural cracks occur in the bottom biscuit resulting in an increase in the strain. The results therefore suggest that the behaviour of the twinwall is very similar to that of a monolithic section, irrespective of the thicknesses of the specimens.

It is also noted that for smaller thicknesses of 240mm and 280mm, the variation of the strain along the depth of the specimen is more uniform. As the thickness increases, the strain profile becomes less uniform. This indicates that the distribution of forces between the top and bottom biscuit and the degree of composite action increases as the thickness decreases.

7.4.3.4 Behaviour at Failure

A. Results

The behaviour of the FE specimens at failure is presented in respect of the vertical deflection and stress in steel lattice bars. The regions highlighted in red represent the areas of maximum deflection (vertical deflection at failure) and yielding of the steel (stresses in lattice bars).

Thickness of Twinwall		
Type	**Vertical Deflection at Failure**	**Stresses in Lattice Bars**
FC-1 (240)	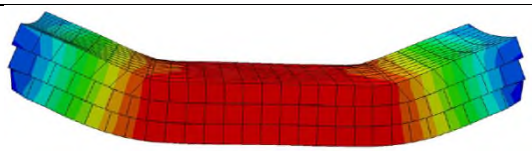	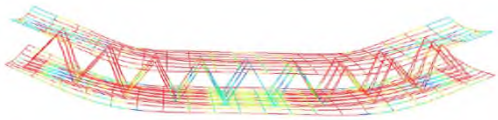
FC-2 (280)		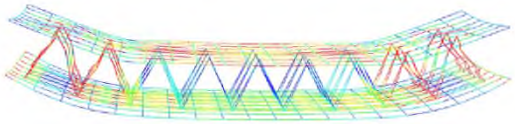
FC-3 (320)		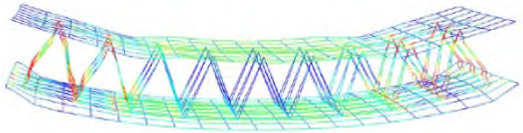

FC-4 (360)	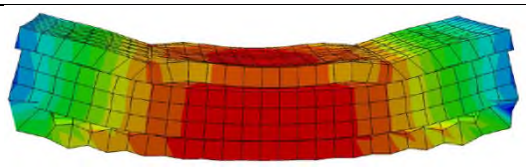	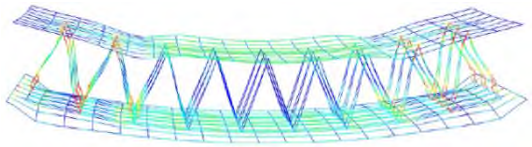
FC-5 (400)	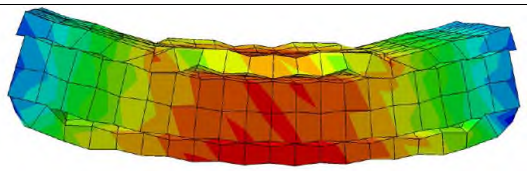	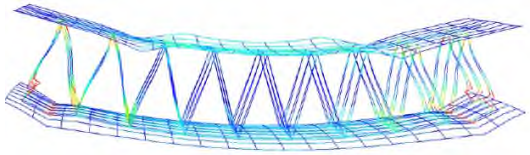

Table 7.12 – General Behaviour: Thickness – Type FB-1 to FB-7

B. Discussion

From Table 7.12, it is observed that the deformed shapes for all specimens are similar with maximum deflection (highlighted in red) occurring midspan. This is a typical behaviour of specimens subject to four point bending tests. The deformed shapes of the specimens also show that slip occurs at the interfaces between the Inner Core and the top and bottom Biscuits. The deformed shapes of the specimens also show that specimens with lower thicknesses seem to deform more uniformly than those with higher thicknesses. This confirms that as the thickness of the specimens increases, the degree of composite action decreases.

The stresses in the lattice bars also provide important information on the behaviour of the test specimens. It can be seen that as the thickness of the specimens increases, the number of dowel bars reaching their yield stress decreases. For thicknesses of 240mm and 280mm, most of the diagonal bars are mobilised. This reduces significantly as the thickness increases beyond 280mm. This indicates that in specimens with lower thicknesses, the failure is primarily due to yielding of the diagonal dowel bars. For

higher thicknesses, the failure mechanism may mostly be a function of failure occurring at the biscuit interface and the flexural failure of the test specimen.

7.5 Overview of FE Analysis

7.5.1 Validation of FE Model

The FE model was validated against the results from the experiment carried out for types A3-E3.

It was observed that the differences between the experimental and FE failure loads ranged from 5.6% and 10.1%. The load-deflection profiles for the experimental and FE results followed a similar trend but the FE specimens were slightly stiffer than the experimental ones. The deformed shapes and stress in the steel bars also confirmed that the experimental and FE specimens behaved in a similar manner.

The FE model developed using the ABAQUS software was therefore deemed as being suitable to investigate the structural behaviour of twinwall specimens.

7.5.2 Effect of Dowel Bar Diameter

The dowel bar diameters were varied to 4mm, 6mm, 8mm, 10mm, 12mm, 16mm and 20mm.

The failure loads observed confirmed that increasing the diameter of the dowel bar beyond 12mm did not lead to significant increases in overall strength of the twinwall specimens.

As the dowel bar diameter increased, the deflection at failure decreased but at dowel bar diameters beyond 16 mm, there was almost no change in the deflection at midspan. Thus, it is recommended that to ensure that twinwalls an efficient and more economical design, the diameter of the dowel bars must be limited to a maximum of 12 mm in twinwalls.

The load-deflection profiles also showed that when the bar diameter increased the stiffness of the specimens increased. The strain profiles confirmed that as the dowel bar diameter increases, the degree of composite action also increases. Hence, dowel bar diameters of 8 mm or more is recommended to maximise the degree of composite action in twinwalls.

The deformed shapes and the stresses in the steel indicated that the failure mechanism of the test specimens may have been primarily due to the interface shear failure occurring at the biscuit interface and the flexural failure. Hence, the failure mode did not seem to be influenced by the dowel bar diameter.

7.5.3 Effect of Type of Connector

Single and double trusses with bar diameters of 4mm, 6mm, 8mm, 10mm, 12mm, 16mm and 20mm were analysed.

The failure loads observed confirmed that the double trusses were more effective at transferring the forces in twinwalls in comparison with the single truss. The deflections in the double truss were slightly less than those in the single truss.

The load-deflection profiles also showed that when the bar diameter increased, the stiffness of the specimens increased irrespective of the type of connector used. This confirms that the behaviour of the single and double trusses is very similar in terms of their deformations and that single trusses can potentially be used in twinwalls.

The strains developing in the single truss specimens at all dowel bar diameters were higher than those in double truss specimens. This suggests that the type of connector used seems to have an effect on the overall behaviour of the test specimens.

The behaviour of both the single and double trusses was similar in terms of their deformations and steel stresses. Thus, the potential use of single trusses instead of double trusses should be explored further.

7.5.4 Effect of Thickness of Twinwall

The overall thicknesses of the specimens were varied to 240mm, 280mm, 320mm, 360mm and 400mm by varying the height of the lattice girder.

As the thickness of the specimen increased, the failure load increases but the deflection decreased. In 240mm and 280mm thick specimens, the deflection was quite high which may be concern when designing for serviceability limit state.

The load-deflection profiles also showed that when the thickness increases, the stiffness of the specimens increased almost linearly. As the thickness increased, the strain profile became less uniform. This indicates that the degree of composite action increases as the thickness decreases.

The deformed shape and stresses in the lattice bars showed that for thicknesses of 240mm and 280mm, most of the diagonal bars were mobilised. As the thickness increased, the number of dowel bars mobilised reduced. This suggests that in specimens with lower thicknesses, the failure is primarily due to yielding of the diagonal dowel bars and for higher thicknesses, the failure mechanism is mostly due to failure occurring at the biscuit interface and the flexural failure.

Chapter 8

Conclusions and Recommendations

8.1 Conclusions

The aim of this research was to investigate the structural behaviour of twinwall panels. The following conclusions can be drawn from the experimental, theoretical and FE work carried out on twinwall panels.

8.1.1 Assessment of Interface Shear Strength

Push-out tests in accordance with Annex B of EC4 were carried out on large scale and small scale twinwall specimens. Results confirmed that a modified version of the pus-out tests can be carried out on small scale specimens to investigate the structural behaviour of twinwalls.

Modified push-out tests were carried out on small scale twinwall panels to determine the factors affecting the interface shear strength of twinwalls. The longitudinal/interface shear occurring at the interface between the precast concrete biscuits and the in-situ

concrete core in twinwalls is influenced by the surface roughness of the concrete interfaces, the concrete strength, the embedment depth of the lattice shear connectors and the dowel bar diameter.

As the roughness of the surface at the biscuit/core interface increases, the longitudinal shear strength of the twinwalls increases. The interface shear strength is not affected by the strength of the concrete in the core but is significantly influenced by strength of the concrete in the biscuits.

It is also observed that the interface shear connector is fully anchored at an embedment depth of 20 mm which is greater than the embedment depth of 16.5 mm determined from Clause 6.3.3 of Eurocode 4. The interface shear strength decreases at embedment depth of 15mm. Hence, EC4 can be used to determine the minimum embedment depth of the lattice girder in twinwalls.

Variations in the surface roughness of the interfaces, the concrete strength, the embedment depth of the lattice shear connectors and the dowel bar diameter also influence the stiffness of the twinwall test specimens.

The load-deflection profiles confirmed that the push-out test specimens primarily deform in three main stages. Before the first crack is formed, a linear behaviour is observed. The first crack occurs at the core/biscuit interface. The specimens then deform in a non-linear manner until failure. Almost all specimens fail by yielding in the form of necking or fracture of the steel lattice bars at the core/biscuit interface.

The experimental results were also compared with the prediction of Clause 6.2.5 of Eurocode 2. It was observed that the recommendations made EC2 provides conservative estimates of the interface shear strength in twinwalls, provided that the lattice shear connectors are fully anchored in the concrete biscuits.

EC2 suggests that the inclination angle,α of the dowel, in this case, the leg of the lattice girder, is in the range of $45^0 \leq \alpha \leq 90^0$. Results confirmed that there was a negligible difference between the EC2 theoretical values obtained for the minimum of 45^0 and the actual inclination angle of the lattice leg of 38^0. Hence, the validity of the EC2 interface shear equation ($45^0 \leq \alpha \leq 90^0$) can be extended to take into account a smaller angle of inclination of $\alpha = 38^0$.

8.1.2 Assessment of Flexural Strength

Four point bending tests were carried out on twinwall panels to investigate the factors affecting the flexural strength and degree of composite action in twinwalls. The lattice shear connector, the depth of the lattice shear connector and the concrete core influence the flexural failure load, stiffness and degree of composite action of the twinwall test specimens.

The lattice shear connector significantly increases the failure load, stiffness and degree of composite action in the twinwall test specimens. The failure load more than doubles and the top and bottom deflections decreased significantly when the lattice connector is used. The degree of composite action in the test specimens where the lattice connectors are used is approximately 7% greater than those with no lattice connector. This confirms

that the presence of the lattice girder contributes towards the degree of composite action in the test specimens.

Increasing the lattice depth from 60 mm to 80 mm significantly increases the failure load, stiffness and degree of composite action of the test specimens. Varying the depth of the lattice does not seem to affect the overall failure mechanism of the test specimens.

The introduction of a concrete core between the top and bottom biscuit more than doubles the failure load of the test specimens. The concrete core also leads to a rise in the stiffness and degree of composite action.

Casting the test specimen in three stages increases the failure load by 3% in comparison with the test specimen cast as a single solid section. This confirms that the behaviour of twinwall panels is very similar to that of fully monolithic sections. Additionally, the degree of composite action increases when the concrete core is used but is not affected by the casting procedure of the test specimens.

All twinwall test specimens behave in a partially composite manner. At early stages of loading, the load-deflection profiles of the specimens lie close to the fully composite limit. As the load increases, the load-deflection profiles exhibit non-linear behaviour and shift towards the non-composite limit.

Results also confirm that lattice bars are subject to compression and tension. This suggests the lattice bars transfer forces from the top to the bottom biscuits and hence act as effective shear connectors in twinwall panels.

8.1.3 FE Analysis

Finite Element Analysis was developed using the ABAQUS software. The FE model was validated against the results from the experiment carried out for types A2-E2 specimens. It is observed that the differences between the experimental and FE failure loads range from 5.6% and 10.1%. The load-deflection profiles, deformed shapes and stresses in the steel bars also confirm that the experimental and FE specimens behaved in a similar manner. Hence, the FE model developed using the ABAQUS software was therefore deemed as being suitable to investigate the structural behaviour of twinwall specimens.

The dowel bar diameters were varied to 4mm, 6mm, 8mm, 10mm, 12mm, 16mm and 20mm. As the dowel bar diameter increases, the failure load increases but the deflection at failure decreases. The load-deflection profiles also show that when the bar diameter increases, the stiffness of the specimens increases. The strain profiles confirm that as the dowel bar diameter increases, the degree of composite action also increases. The deformed shapes and the stresses in the steel indicate that the failure mechanism of the test specimens may have been primarily due to the interface shear failure occurring at the biscuit interface and the flexural failure.

Single and double trusses with bar diameters of 4mm, 6mm, 8mm, 10mm, 12mm, 16mm and 20mm were modelled and investigated. Results confirm that both the single and double trusses behave in a similar manner but the double truss connectors are more effective in transferring the forces in the specimens. Single truss connectors can therefore be used as an alternative to double truss (3D lattice) in twinwalls.

The overall thicknesses of the specimens were varied to 240mm, 280mm, 320mm, 360mm and 400mm by varying the height of the lattice girder. As the thickness of the specimen increases, the failure load increases but the deflection decreases. Results also confirm that the degree of composite action increases as the thickness decreases. The stresses in the steel bars indicate that in specimens with lower thicknesses, the failure is primarily due to yielding of the diagonal dowel bars and for higher thicknesses, the failure mechanism is mostly due to failure occurring at the biscuit interface and the flexural failure.

8.2 Recommendations for Design of Twinwalls

Based on the results from the experimental, theoretical and numerical (FE) investigation of the structural behaviour of twinwalls, the load transfer mechanism in twinwalls is dependent on three main structural actions (1) Flexural capacity, (2) Shear capacity and (3) Interface shear capacity.

The flexural capacity is provided through tension in the embedded reinforcement and compression in the precast biscuits and the core and embedded reinforcement in the opposite face. The vertical shear is resisted by the lattice girders, and the forces between the in-situ core and precast biscuits are transferred by longitudinal (interface) shear.

Based on the above, the following generic flowchart is recommended for the preliminary design of twinwalls:

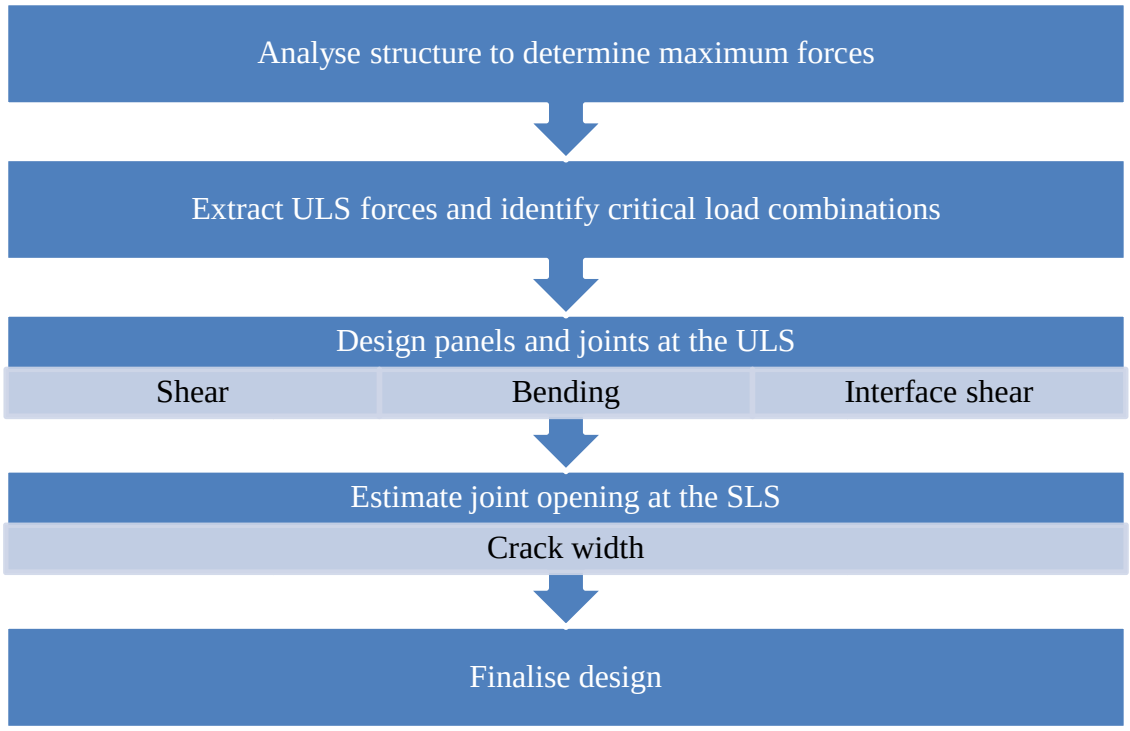

Figure 8.1 - Design Procedure for Twinwalls

Thus, twinwalls must be designed for ultimate limit state (ULS) and serviceability limit state (SLS). Based on the findings of this research and the recommendations made by EC2 and EC4, the approach shown in Figure 8.2 can be used for the design of twinwalls in water retaining structures.

The design life and durability of the twinwalls must first be assessed to confirm the necessary cover required. The ultimate flexural, shear and interface shear requirements can then be used to determine the area of longitudinal and transverse reinforcement, the amount of shear reinforcement (i.e. lattice reinforcement), and adequacy of the longitudinal shear capacity at the core/precast biscuit interfaces.

Design Life and Durability

- Specify Design Life
- Determine Exposure Conditions (*EC2-1: Table 4.1)*
- Determine Cover Requirements (*NA to EC2-1: Table NA.3)*

Ultimate Flexural Capacity

- $\mathbf{A_{s,ult,req} < A_{s,ult,provided}}$ *(EC2-1: Table 2.1N)*
- Determine worst case (bottom joint) moment, M_{ult}
- Determine reinforcement area required: $A_{s,ult,req}=M/[(f_{sy}/\gamma_s)z]$

Ultimate Shear Capacity

- $\mathbf{V_{Ed} < V_{Rd,c}}$
- Determine shear resistance: $V_{Rd,c}=[C_{Rd,c}k(100\rho_1 f_{ck})^{1/3}+k_1\sigma_{cp}]b_w d \geq V_{Rd,c}=(v_{min}+k_1\sigma_{cp})b_w d$ *(EC2-1: Eq. 6.2a)*
- Determine applied shear: $V_{Ed} \leq 0.5 b_w d v f_{cd}$ *(EC2-1: Eq. 6.5)*
- If $V_{Ed} > V_{Rd,c}$ therefore, shear reinforcement necessary.

Shear interface Requirements

- $\mathbf{v_{Edi} \leq v_{Rdi}}$ *(EC2-1: Cl. 6.2.5)*
- $v_{Edi}=\beta V_{Ed}/(z_{bi})$
- $v_{Rdi}=cf_{ctd}+\mu\sigma_n+\rho f_{yd}(\mu \sin\alpha+\cos\alpha) \leq 0.5 v f_{cd}$

Lattice Capacity

- $\mathbf{P_{applied} < P_{Rd}}$ *(EC4-1: Cl 6.3.3)*
- P_{Rd} is the lesser of $(0.8fu\ \pi d^2/4)/y_v$ and $(0.29\alpha d2\sqrt{(f_{ck}E_{cm})})/y_v$

Crack Width Requirement

- $\mathbf{w_{k,\ actual} < w_{k,\ allowable}}$
- Determine maximum allowable crack width, w_{k1} *(EC2-3: Cl.7.3.1)*
- Determine actual crack width, $w_k=s_{r,max}(\varepsilon_{sm}-\varepsilon_{cm})$ *(EC2-Eq. 7.8)*
- Provide minimum crack control reinforcement: $A_{smin}\sigma_s=k_c k f_{ct,eff} A_{ct}$

Figure 8.2 - Design of Twinwalls to EC2

On the basis of the results obtained from the experimental, theoretical and numerical investigated; the following specific recommendations to the design of twinwalls are made:

1. Results from the push-out tests confirm the EC2 ‘smooth’ surface roughness should be used to provide conservative estimates of the interface shear resistance of twinwalls. This corresponds to the coefficient of cohesion, c = 0.2 and the coefficient of friction, $\mu = 0.6$ in Clause 6.2.5 of EC2.

2. Push-out tests have confirmed that the tensile strength of the concrete should be based on the strength of the biscuits rather than the core. It is recommended that the lowest strength of the precast concrete biscuits is used to determine the interface shear strength in twinwalls in Clause 6.2.5 of EC2.

3. The angle of inclination in typical lattice girders used in twinwall is less than 45^o (typically 38^o for 80 mm deep lattice girders). Result showed that the EC2 theoretical values obtained by using the actual angle of inclination $\alpha = 38^0$ and the EC2 limit of $\alpha = 45^0$ are almost equal. Thus, it is recommended that the validity of Clause 6.2.5 of EC2 ($45^0 \leq \alpha \leq 90^0$) should be extended to take into account a smaller angle of inclination of $\alpha = 38^0$.

4. It must be ensured that the embedment depth of the lattice girders is greater than the critical embedment depth determined from Clause 6.3.3 of Eurocode 4.

5. Results from the flexural tests confirm that the degree of composite action occurring in twinwalls is similar to that of fully monolithic members. Thus, no further allowances or factors of safety are required for the design of twinwalls in respect of the degree of composite action.

6. The FE analysis confirmed that the diameter of the dowel bar (i.e. diagonal lattice bar) must be limited to a minimum of 8 mm and a maximum of 12mm to ensure optimum structural performance and economy of design.

Though the current research primarily investigates the effect of parameters affecting the ultimate behaviour of twinwalls, particular attention must also be given to the performance of twinwalls during serviceability limit state. Hence, the allowable crack width must be compared with the actual crack width occurring in twinwalls as shown in Figure 8.2. In addition to these checks, it must be ensured any joints within the twinwalls are designed to allow transfer of forces between the various twinwall elements.

In water retaining structures, the horizontal joints occur at the bottom of the walls at the junction with the base slab. In these locations, it is therefore recommended that the in-situ concrete (core) is allowed to flow beneath the walls in order to provide a bedding joint suitable for transfer of compressive and shear forces. Additionally, continuity reinforcement should also be provided at horizontal joints with splice bars lapped with the embedded biscuit reinforcement.

8.3 Recommendations for Future Work

Further research is required to address the other gaps in the knowledge and understanding of the structural behaviour of twinwalls.

- Tests are required in order to improve the reliability of the results. This is particularly applicable to the push-out tests. As discussed, Clause 6.2.5 of EC2 classifies the roughness of the substrate surface as very smooth, smooth and rough. This classification is clearly inaccurate since it is reliant upon the subjective assessment of the technician. Hence, classification of the roughness of the surfaces needs to be undertaken via experimental testing. It is also necessary to investigate the influence of other surface preparation methods on the interface shear strength as well as to identify the variability of the roughness degree obtained using the same preparation method used.

- It was previously mentioned that the use of twinwall panels needs to be extended to water retaining structures. Though an understanding of the structural behaviour of the twinwalls has been provided in this study, the durability of the twinwalls has not been investigated. Hence, more research is required in this field.

- Another aspect that needs to be evaluated is the thermal properties of twinwalls. Since the biscuits and the core are made of concrete, more research is required on their inherent thermal properties.

- The current study has also confirmed that the concrete core does not influence the shear or the flexural strength of the twinwall panels. Hence, more research needs to be carried out to determine the materials which could act as fillers for the void between the precast biscuits.

- Twinwall panels are primarily made up of 3-D lattice girders. As confirmed by the FE analysis, single trusses can potentially be used as an alternative to the 3-D double trusses. Thus, the effect of varying the type of connectors in the twinwall panels needs to be established. Variations of the type of material, the orientation and angle of inclination can be of particular interest.

References

ACI Committee 318. 2005. Building Code Requirements for Structural Concrete (ACI 318-05) and Commentary (ACI 318R-05). American Concrete Institute.

Al-deen, S., Ranzi, G., & Vrcelj, Z. (2011). Shrinkage effects on the flexural stiffness of composite beams with solid concrete slabs: An experimental study. Engineering Structures, 33(4), 1302-1315.

Allen, D. E. (1970, December). Probabilistic study of reinforced concrete in bending. In ACI Journal Proceedings (Vol. 67, No. 12). ACI.

American Institute of Steel Construction (AISC). (1999). Load and resistance factor design specification for structural steel buildings. Chicago.

Arya, C. (2009). Design of structural elements: Concrete, steelwork, masonry and timber designs to British standards and Eurocodes. CRC Press.

Attard, M. M., Minh, N. G., & Foster, S. J. (1996). Finite element analysis of out-of-plane buckling of reinforced concrete walls. Computers & structures,61(6), 1037-1042

Aziz, R.J, (2010). Shear Capacity of Concrete Prisms With Interface Joints. Journal of Engineering. 16 (2), pp.5084-5097

Benayoune, A., Samad, A.A., Trikha, D.N., Ali, A.A. and Ellinna, S.H.M. (2008). Flexural behaviour of pre-cast concrete sandwich composite panel–Experimental and theoretical investigations. Construction and Building Materials, 22(4), 580-592.

Benayoune, A., Samad, A. A., Ali, A. A., & Trikha, D. N. (2007). Response of pre-cast reinforced composite sandwich panels to axial loading. Construction and Building materials, 21(3), 677-685.

Benayoune, A., Samad, A.A.A., Trikha, D.N., Ali, A.A.A. and Ashrabov, A.A. (2006). Structural behaviour of eccentrically loaded precast sandwich panels. Construction and Building Materials, 20(9), 713-724.

British Precast (2009). Precast Concrete in Civil Engineering. Surrey: The Concrete Centre

British Standard Institute. (2009). BS EN 1994-1-1: 2004, Eurocode 4: Design of composite steel and concrete structures — Part 1-1: General rules and rules for buildings. London: BSI Group.

British Standard Institute. (2009). BS EN 1990:2002+A1:2005: Eurocode. Basis of structural design. London: BSI Group.

British Standard Institute. (2005). BS 5400-5:2005: Steel, concrete and composite bridges. Code of practice for design of composite bridges. London: BSI Group.

British Standard Institute. (2004). BS EN 1992-1-1: 2004, Eurocode 2: General – Common rules for building and civil engineering structures. London: BSI Group.

British Standard (1997) B. S. 8110-1: 1997: Structural use of concrete–Part 1. London: BSI Group.

Bush, T. D., & Stine, G. L. (1994). Flexural behavior of composite precast concrete sandwich panels with continuous truss connectors. PCI journal, 39(2).

Bush, T. D., & Zhiqi, W. (1998). Flexural analysis of prestressed concrete sandwich panels with truss connectors. PCI journal, 43(5), 76-86.

Bryson, J. O., Skoda, L. F., & Watstein, D. (1965). Flexural Behavior of Prestressed Split Beam Composite Concrete Sections. PCI Journal, 10(2), 77-91.

Cise, D., & Lakes, R. S. (1997). Moisture ingression in honeycomb core sandwich panels. Journal of materials engineering and performance, 6(6), 732-736.

Choi, D. U., Jirsa, J. O., & Fowler, D. W. (1999). Shear Transfer Across Interface Between New and Existing Concretes Using Large Powder-Driven Nails. ACI Structural Journal, 96(2).

Chaudhari, S. V., & Chakrabarti, M. A. (2012). Modeling of concrete for nonlinear analysis Using Finite Element Code ABAQUS. International Journal of Computer Applications, 44(7), 14-18.

Concrete Centre (2006). Concise Eurocode 2: For the design of in-situ concrete framed buildings to BS-EN 1992-1-1: 2004 and its UK National Annex: 2005. Surrey: The Concrete Centre.

Einea, A., Salmon, D. C., Tadros, M. K., & Culp, T. (1994). A new structurally and thermally efficient precast sandwich panel system. PCI journal, 39(4).

Ernst, S., Bridge, R.Q. and Wheeler, A. (2010). Correlation of Beam Tests with Pushout Tests in Steel-Concrete Composite Beams. Journal of Structural Engineering. ACSE. 183-192.

Gohnert, M. (2003). Horizontal shear transfer across a roughened surface.Cement and Concrete Composites, 25(3), 379-385.

Goodchild, C. H., & Glass, J. (2004). Best Practice Guidance for Hybrid Concrete Construction. The Concrete Centre, Camberley.

Hanson, N. W. (1960). Precast-Prestressed Concrete Bridges 2: Horizontal Shear Connections. Portland Cement Association, Research and Development Laboratories.

Haskett, M., Oehlers, D.J., Mohamed Ali, M.S. and Sharma, S.K. (2010). The shear friction aggregate interlock resistance across sliding planes in concrete. Magazine of Concrete Research. 62 (12), 907–924.

Hawkins, N. M. (1973). The strength of stud shear connectors. Institution of Engineers (Australia) Civ Eng Trans, (1).

Hendy, C.R. and Smith, D.A. (2007). Designer's Guide to EN 1992-2. London: Thomas Telford Publishing.

Hicks, S. J., & McConnel, R. E. (1996). The shear resistance of headed studs used with profiled steel sheeting. Composite construction in steel and concrete III ASCE. 325-338)

Hindo, K. R. (1990). In-Place Bond Testing and Surface Preparation of Concrete. Concrete International, 12 (4), 46-48.

Hoigard, K.R., Kritzler, R.W. and Mulholland, G.R. (1993). Structural analysis of stone clad precast concrete building panels. International journal of rock mechanics and mining sciences & geomechanics abstracts. Pergamon. 30 (7), 1567-1573.

Hu, H. T., & Schnobrich, W. C. (1990). Nonlinear analysis of cracked reinforced concrete. ACI Structural Journal, 87(2).

Jayas, B. S., & Hosain, M. U. (1988). Behaviour of headed studs in composite beams: push-out tests. Canadian Journal of Civil Engineering, 15(2), 240-253.

Johnson, R.P. and Anderson, D. (2004). Designer's Guide to EN 1994-1-1. London: Thomas Telford Publishing.

Johnson, R. P., & Oehlers, D. J. (1981, December). Analysis and design for longitudinal shear in composite T-beams. In ICE Proceedings (Vol. 71, No. 4, pp. 989-1021). Thomas Telford.

Júlio, E.N.B.S., Branco, F.A.B. and Silva, V. D. (2004). Concrete-to-Concrete Bond Strength. Influence of the Roughness of the Substrate Surface. Construction and Building Materials, 18 (9), 675-681.

Júlio, E. N. B. S., Dias-da-Costa, D., Branco, F. A. B., & Alfaiate, J. M. V. (2010). Accuracy of design code expressions for estimating longitudinal shear strength of strengthening concrete overlays. Engineering Structures, 32(8), 2387-2393.

Kabir, M. Z. (2005). Structural Performance of 3-D Sandwich Panels Under Shear and Flexural Loading. Scientia Iranica, 12(4), 402-408

Kang, J. (2015). Composite and non-composite behaviors of foam-insulated concrete sandwich panels. Composites Part B: Engineering, 68, 153-161.

Kim, B. Wright, H.D, Cairns, R. and Bradford, M.A. (1999). The numerical simulation of shear connection. Mechanics of Structures and Materials. Bradford: Bridge & Foster. 341-344.

Kuhn, J. M., & Buckner, C. D. (1986). Effect of concrete placement on shear strength of headed studs. Journal of Structural Engineering, 112(8), 1965-1971.

Lam, D. and El-Lobody, E. (2005). Behavior of Headed Stud Shear Connectors in Composite Beam. Journal of Structural Engineering 131 (1). ASCE. 96-107.

Laing O'Rourke. (2010). Precast Twinwall Design Guide. Laing O'Rourke.

Lee, B. J., & Pessiki, S. (2007). Design and analysis of precast, prestressed concrete, three-wythe sandwich wall panels. PCI journal, 52(4), 70-83.

Lee, B. J., & Pessiki, S. (2008). Experimental evaluation of precast, prestressed concrete, three-wythe sandwich wall panels. PCI journal, 53(2), 95-115.

Lee, A. J., Kelly, H., Jagoda, R., Rosenfeld, A., Stubee, E., Colaco, J., ... & van Burik, H. (2006). Affordable, safe housing based on expanded polystyrene (EPS) foam and a cementitious coating. Journal of materials science, 41(21), 6908-6916.

Liew, J.Y.R. and Sohel, K.M.A. (2009). Lightweight steel–concrete–steel sandwich system with J-hook connectors. Engineering Structures, 31(5), 1166-1178.

Mattock, A.H. and Hawkins, N.M. (1972). Shear Transfer in reinforced concrete recent research. Precast Concrete Institute. March-April, 55-75.

Maximos, H. N., Pong, W. A., Tadros, M. K., & Martin, L. D. (2007). Behavior and design of composite precast prestressed concrete sandwich panels with NU-tie. Final Report.

MC90, C. E. B. F. I. P. (1993). Design of Concrete Structures. CEB-FIP Model Code 1990.

Mousa, M. A., & Uddin, N. (2012). Structural behavior and modeling of full-scale composite structural insulated wall panels. Engineering Structures, 41, 320-334.

Naito, C.J., Hoemann, J.M., Bewick, B.T. and Hammons, I. (2009). Evaluation of shear tie connectors for use in insulated concrete sandwich panels. United States: Air Force Research Laboratory.

Obaidat, Y. T., Heyden, S., & Dahlblom, O. (2010). The effect of CFRP and CFRP/concrete interface models when modelling retrofitted RC beams with FEM. Composite Structures, 92(6), 1391-1398.

Oehlers, D.J. and Bradford, M.A. (1995). Elementary Behaviour of Composite Steel and Concrete Structural Members. Oxford: Butterworth-Heinman.

Ollgaard, J. G., Slutter, R. G., & Fisher, J. W. (1971). Shear strength of stud connectors in lightweight and normal-weight concrete. AISC Engineering Journal, 8(2), 55-64

Paik, J. K., Thayamballi, A. K., & Kim, G. S. (1999). The strength characteristics of aluminum honeycomb sandwich panels. Thin-walled structures, 35(3), 205-231.

Pessiki, S., & Mlynarczyk, A. (2003). Experimental evaluation of the composite behavior of precast concrete sandwich wall panels. PCI journal, 48(2), 54-71.

Pfeifer, D. W., & Hanson, J. A. (1965). Precast Concrete Wall Panels: Flexural Stiffness of Sandwich Panels. ACI Special Publication, 11.

Pokharel, N., & Mahendran, M. (2004). Finite element analysis and design of sandwich panels subject to local buckling effects. Thin-walled structures, 42(4), 589-611.

Pong, W. A., Girgis, A. M., & Tadros, M. K. (2005). SP-230-2: Proposed GFRP Connectors in Sandwich Panels. ACI SPECIAL PUBLICATIONS, 230(1), 21.

Reinecke, R., & Zilch, K. (2002, January). Capacity of Shear Joints in Applications of High Performance Concrete in Strengthening and Retrofitting of old Concrete Structures. In IABSE Symposium Report (Vol. 86, No. 5, pp. 30-38). International Association for Bridge and Structural Engineering.

.Revesz, S. (1953, February). Behavior of Compressive T-Bemas with Prestressed and Unprestressed Reinforcement. In ACI Journal Proceedings(Vol. 49, No. 2). ACI.

Rezaifar, O., Kabir, M. Z., Taribakhsh, M., & Tehranian, A. (2008). Dynamic behaviour of 3D-panel single-storey system using shaking table testing.Engineering Structures, 30(2), 318-337

Rizkalla, S. H., Hassan, T. K., & Lucier, G. (2009). FRP shear transfer mechanism for precast, prestressed concrete sandwich load-bearing panels.ACI Special Publication, 265.

Salmon, D. C., Einea, A., Tadros, M. K., & Culp, T. D. (1997). Full scale testing of precast concrete sandwich panels. ACI Structural Journal, 94(4).

Scudamore, R. J., & Cantwell, W. J. (2002). The effect of moisture and loading rate on the interfacial fracture properties of sandwich structures. Polymer composites, 23(3), 406-417.

Simulia, D. (2011). ABAQUS 6.11 analysis user's manual. Abaqus, 6, 22-6.

Slutter, R. G., & Driscoll Jr, G. C. (1963). Flexural strength of steel and concrete composite beams. Journal of the Structural Division, ASCE, Vol. 91, No. ST2

Stoll, F., Campbell, S., Day, S., & Sheppard, M. (2004). High-performance, low-cost infusion cores for structural sandwich panels. Proceedings of SAMPE.

Swartz, S. E., Rosenbraugh, V. H., & Berman, M. Y. (1974, January). Buckling tests on rectangular concrete panels. In ACI Journal Proceedings (Vol. 71, No. 1). ACI.

Teraszkiewicz, J. S. (1965). Tests on stud shear connectors. Road Research Laboratory.

Thames Water (2013). Beckton Update: January 2013. London: Thames Water.
Whittle, R. and Taylor, H. (2009). Design of Hybrid Concrete Buildings - A guide to the design of buildings combining in-situ and precast concrete. Surrey: Concrete Centre.

Topkaya, C., Yura, J. A., & Williamson, E. B. (2004). Composite shear stud strength at early concrete ages. Journal of Structural Engineering, 130(6), 952-960.

Wahalathantri, B. L., Thambiratnam, D. P., Chan, T. H. T., & Fawzia, S. (2011, April). A material model for flexural crack simulation in reinforced concrete elements using ABAQUS. In Proceedings of the First International Conference on Engineering, Designing and Developing the Built Environment for Sustainable Wellbeing (pp. 260-264). Queensland University of Technology.

Yukio, A. and Sato, Ryoichi. (1983, December). *Studies on Deformation and Crack of Reinforced Concrete Flexural Members under Low Temperature*, Concrete Library International, (2), 16.